



Technische Universität München
TUM School of Medicine and Health

Optimization of an Advanced Therapy Medicinal Product (Recellularized Tracheal Scaffold) To Enhance Engraftment and Clinical Functionality

Sarah Khalid Al Ageel

Vollständiger Abdruck der von der TUM School of Medicine and Health der Technischen
Universität München zur Erlangung eines
Doctor of Philosophy (Ph.D.)
genehmigten Dissertation.

Vorsitz: Prof. Dr. Manuel Spitschan

Betreuer: Prof. Dr. Hans-Günther Machens

Prüfer der Dissertation:

1. Prof. Dr. Rainer Burgkart
2. Prof. Dr. Arndt F. Schilling

Die Dissertation wurde am 29.09.2023 bei der Fakultät für Medizin der Technischen
Universität München eingereicht und durch die TUM School of Medicine and Health am
20.12.2023 angenommen.

ABSTRACT

Laboratory-based tracheal engineering represents a prominent therapeutic avenue under active investigation, offering potential solutions for replacing non-reconstructible damaged tracheal segments. Individuals afflicted with untreatable long segmental tracheal defects often endure a diminished quality of life and heightened mortality rates. However, as with all engineered constructs, successful transplantation of the trachea necessitates the prompt and robust establishment of vascularization thereby, surpassing the critical point at which graft necrosis initiates. In our research, we employed the chorioallantoic membrane (CAM) model as an in-vivo animal model to demonstrate that the genetic modification of mesenchymal stromal cells to transiently overexpress specific growth factors such as vascular endothelial growth factor (VEGF) and basic fibroblast growth factor (bFGF) yields significant improvements in vascularization within tracheal biopsies in comparison to conventional protocols. This innovative strategy is designed to furnish the requisite vascular support capable of mitigating tissue necrosis following transplantation. Consequently, it holds promise for enhancing the longevity and engraftment potential of in-situ organs.

ZUSAMMENFASSUNG

Das Tracheal-Engineering im Labor stellt einen wichtigen therapeutischen Weg dar, der derzeit aktiv untersucht wird und potenzielle Lösungen für den Ersatz nicht rekonstruierbarer beschädigter Trachealsegmente bietet. Menschen mit unbehandelbaren langen Trachealsegmentdefekten leiden häufig unter einer verminderten Lebensqualität und einer erhöhten Sterblichkeitsrate. Wie bei allen künstlichen Konstrukten ist jedoch für eine erfolgreiche Transplantation der Trachea eine rasche und robuste Vaskularisierung erforderlich, die den kritischen Punkt, an dem eine Transplantatnekrose einsetzt, übersteigt. In unserer Forschung haben wir das Modell der Chorioallantoismembran (CAM) als In-vivo-Tiermodell verwendet. Mit diesem Ansatz konnten wir zeigen, dass die genetische Veränderung von mesenchymalen Stromazellen zur vorübergehenden Überexpression von Wachstumsfaktoren wie dem vaskulären endothelialen Wachstumsfaktor (VEGF) und dem basischen Fibroblasten-Wachstumsfaktor (bFGF) im Vergleich zu herkömmlichen Protokollen zu einer signifikanten Verbesserung der Vaskularisierung in Trachealbiopsien führt. Diese innovative Strategie zielt darauf ab, die erforderliche vaskuläre Unterstützung zu liefern, um die Gewebenekrose nach der Transplantation abzuschwächen. Sie ist daher vielversprechend, um die Langlebigkeit und das Transplantationspotenzial von In-situ-Organen zu erhöhen.

DEDICATION AND ACKNOWLEDGEMENTS

First and foremost, I would like to thank my family, whose unwavering support has made this journey possible. I would like to thank most of all, my father who has been my rock and my idol, and my mother, who has made it her life mission to make me strong. I would like to thank my brothers and my sisters who were there whenever I needed them, and I would also like to thank my husband who has taken time away from his own life, just to be here and make sure that I am able to make the best out of the opportunity that has been granted to me. Without you, this would not be possible.

I would like to thank Herr Prof. Dr. med. Hans-Günther Machens for hosting me in his laboratory, and for continuing this journey with me even after the cancellation of the TETRA project. Thank you, Professor. I would like to thank Frau Ursula Hopfner and Frau Manuela Kirsch for their companionship, their assistance, and their friendship. You also are a large and very happy part of my journey and my success. In addition, I would like to acknowledge, and thank my colleague and friend, Xiaobin Cong for everything he has done, and all the assistance he has lent me.

I would also especially like to thank both Frau Raphaela Blum and Frau Bettina Scratch for their unfaltering support and kindness. You both helped me get through some of the most challenging times. I would like to acknowledge my friends here in Germany, my family away from home, who have been there every day pushing me to continue.

I would like to thank my government and my hospital, who have unwaveringly continued to support me despite the many challenges that I have faced throughout my journey here. Whenever I called, you answered, and whenever I needed, you gave. Thank you.

I would also like to acknowledge two very important people in my life, Dr. Nadia Awni Sakati and Girnasah Alrasheed. Girnasa, you pulled me back, and helped me become strong to face almost anything, for that I will be eternally grateful. Dr. Sakati, you are my idol, and the reason I embarked on this journey in the first place. You are my source of inspiration. If only I could become even a fraction of the person you are, and achieve a marginal amount of what you have achieved, I would be eternally grateful.

Lastly, to the light of my life Khalid. It is to you that I dedicate all of my work.

TABLE OF CONTENTS

ABSTRACT.....	ii
ZUSAMMENFASSUNG.....	ii
DEDICATION AND ACKNOWLEDGEMENTS	iii
TABLE OF CONTENTS	iv
LIST OF FIGURES.....	vi
LIST OF TABLES.....	viii
LIST OF ABBREVIATIONS.....	ix
1. CHAPTER I: THE TRACHEA.....	1
1.1. INTRODUCTION.....	1
1.2. BACKGROUND.....	3
1.2.1. FORM AND FUNCTION.....	3
1.2.1.1. THE ANATOMICAL STRUCTURE OF THE TRACHEA.....	3
1.2.1.2. THE TRACHEAL BLOOD SUPPLY	4
1.2.1.3. NERVES.....	5
1.2.1.4. HISTOLOGICALLY.....	6
1.2.1.5. PHYSIOLOGICAL FUNCTION	8
1.2.2. TRACHEAL MALFUNCTION: INDICATIONS FOR TRACHEAL REPLACEMENT	9
1.2.2.1. TRACHEAL DAMAGE AND DISEASE	9
1.2.2.2. DISEASE BURDEN	10
1.2.2.3. MALFUNCTIONING TRACHEA: TREATMENT APPROACHES	10
1.2.2.4. APPROACHES TO TREATING OR REPLACING LONG SEGMENTAL DEFECTS.....	12
1.2.3. TISSUE ENGINEERING: TRACHEA.....	13
1.2.3.1. COMPONENTS OF A TISSUE ENGINEERED TRACHEA.....	13
1.2.3.2. STATE OF THE ART: DECELLULARIZED TISSUE ENGINEERED TRACHEA	15
1.2.3.3. TRACHEAL ENGINEERING: CHALLENGES	21
1.3. THESIS SUMMARY & GENERAL HYPOTHESIS.....	22
2. CHAPTER II: MATERIALS & METHODS.....	27
2.1. REAGENTS & MATERIALS.....	27
2.2. CELLULAR PROCUREMENT.....	29
2.3. CHARACTERISATION OF CELLS (MSCs and DFs)	37
2.4. CELLULAR QUALITY ASSESSMENT MEASURES (HEALTH, CONFLUENCY, AND FUNCTION)	42
2.5. DECELLULARIZED TRACHEAL SCAFFOLDS.....	43
2.6. COCULTURES	48
2.7. IN VITRO PRE-VASCULARISATION	49

2.8.	PROTEIN AND CYTOKINE EXPRESSION QUANTIFICATION.....	51
2.9.	THREE-DIMENSIONAL SEEDING (3D).....	53
2.10.	IN-OVO IMPLANTATION	56
2.11.	EXPERIMENTAL SET-UP OF MANUFACTURING SIMULATION PROCESS.....	57
2.12.	STAINING	67
2.13.	ISOLATION OF SINGLE CELLS FROM TRACHEA.....	68
2.14.	FINAL PROTOCOL MANUFACTURING: 3D VISUALISATION	72
2.15.	IMAGING	74
2.16.	STATISTICAL ANALYSIS	77
3.	CHAPTER III: RESULTS	78
3.1.	GENERATION OF BASIC PRODUCTS.....	78
3.2.	COCULTURE OF DERMAL FIBROBLASTS WITH BONE MARROW DERIVED MSCS	89
3.3.	GENETIC MODIFICATION OF CELLS: NUCLEOFECTION.....	92
3.4.	3D SCREENING EXPERIMENTS WITH INEGRA® MATRIX	96
3.5.	EXPRESSION OF ANGIOGENESIS FACTORS: SCREENING EXPERIMENTS	116
3.6.	3D TESTING OF TRACHEAL BIOPSIES: IDENTIFICATION OF FINAL PROTOCOL.....	119
3.7.	3D IMPLANTATION OF TRACHEAL BIOPSIES: IDENTIFICATION OF FINAL PROTOCOL.....	123
4.	CHAPTER VI: DISCUSSION	132
4.1.	VASCULARISATION	132
4.2.	CELLS AND SCAFFOLDS	133
4.3.	2D COCULTURE OF MSCS AND DERMAL FIBROBLASTS	139
4.4.	GENETIC MODIFICATION	140
4.5.	SCREENING STUDIES	141
4.6.	TRACHEAL STUDIES.....	149
5.	THE CONCLUSION	157
	BIBLIOGRAPHY	159

LIST OF FIGURES

FIGURE 1: ANTERIOR VIEW OF THE STRUCTURE OF THE TRACHEA.....	3
FIGURE 2.THE TRACHEAL SEGMENTED BLOOD SUPPLY.....	5
FIGURE 3. ANATOMY AND HISTOLOGY OF THE TRACHEAL WALL.....	7
FIGURE 4.THE PROCESS OF TRACHEAL RESECTION AND END TO END ANASTOMOSIS	11
FIGURE 5.EXAMPLES OF DIFFERENT STRATEGIES FOR TRACHEAL REPLACEMENT	12
FIGURE 6. CLINICAL EVENTS THAT CHILD UNDERWENT UNTIL THE FOURTH YEAR FOLLOW-UP	18
FIGURE 7.PROCESS OF ISOLATING PRIMARY HUMAN MESENCHYMAL STROMAL CELLS FROM BONE MARROW.	30
FIGURE 8. PROCESS OF MSC CELL EXPANSION USING CULTIVATION MEDIAS	34
FIGURE 9. OVERVIEW OF GENERAL PROCESS OF TRACHEAL HANDLING PRIOR TO MANUFACTURING.....	43
FIGURE 10.TRACHEAL CHARACTERISATION: METRICS.....	44
FIGURE 11.TRACHEAL BIOPSIES: HANDLING & CUTTING.....	45
FIGURE 12.IN-OVO CHORIOALLANTOIC MEMBRANE ASSAY.	57
FIGURE 13.MANUFACTURING PROCESS OF SCREENING EXPERIMENTS.....	58
FIGURE 14.PROCESS OF GENERATING COCULTURE 1 SEEDED SCAFFOLD.	61
FIGURE 15.PROCESS OF GENERATING COCULTURE 1 ALGINATE ENCAPSULATED SCAFFOLD.....	62
FIGURE 16.PROCESS OF GENERATING COCULTURE 2 SEEDED SCAFFOLD.	63
FIGURE 17.PROCESS OF GENERATING COCULTURE 2 ENCAPSULATED SEEDED SCAFFOLDS.....	64
FIGURE 18.PROCESS OF GENERATING COCULTURE 3 SEEDED SCAFFOLD	65
FIGURE 19.PROCESS OF GENERATING COCULTURE 3 ENCAPSULATED AND SEEDED SCAFFOLDS	66
FIGURE 20. GRAPHICAL REPRESENTATION OF THE TET MANUFACTURING STEPS.....	72
FIGURE 21.MICROCT IMAGE ANALYSIS STEPS	76
FIGURE 22.ILLUSTRATION OF THE IMPACT OF HPL VERSUS FBS CULTIVATION ON THE ISOLATION AND MORPHOLOGY OF HUMAN BONE MARROW-DERIVED MESENCHYMAL STEM/STROMAL CELLS (MSCS) ...	78
FIGURE 23.MSC GROWTH KINETICS.....	79
FIGURE 24.REPRESENTATION OF FLOW CYTOMETRY PANEL ASSESSING MSCS FOR COMMON MARKERS.	81
FIGURE 25.TRI-LINEAGE DIFFERENTIATION OF HUMAN MESENCHYMAL STROMAL CELLS (MSCS)	82
FIGURE 26.HUMAN DERMAL FIBROBLASTS MORPHOLOGY AND GROWTH KINETICS	83
FIGURE 27.REPRESENTATION OF FLOW CYTOMETRY PANEL ASSESSING DFS FOR COMMON MSC MARKERS. ...	84
FIGURE 28.TRI-LINEAGE DIFFERENTIATION OF HUMAN DERMAL FIBROBLASTS.....	85
FIGURE 29.MEASUREMENT METRICS OF DECELLULARIZED PORCINE TRACHEA.....	86
FIGURE 30.SCANNING ELECTRON MICROSCOPY IMAGES OF POST-STERILISED SCAFFOLDS.....	87
FIGURE 31. POST-STERILISATION CULTIVATION OF TRACHEA.....	88
FIGURE 32.THE IMPACT OF CO-CULTIVATING DFS WITH MSCS AT VARYING RATIOS	89
FIGURE 33. THE IMPACT OF CO-CULTIVATING DF WITH MSCS AT VARYING RATIOS.	90
FIGURE 34.COCULTURE OF DFS AND MSCS AT 50:50 RATIO	90
FIGURE 35.TRANSFECTION STUDIES: ASSESSED PARAMETERS POST PMAX-GFP NUCLEOFECTION.....	92
FIGURE 36.ALAMAR BLUE METABOLIC ASSAY RESULTS	93
FIGURE 37.CELL CYTOTOXICITY STUDIESTS.....	94
FIGURE 38.CELL CHARACTERISATION ASSAYS.....	95
FIGURE 39.COMPARISON OF NATURAL SECRETIONS OF HUMAN BONE-MARROW DERIVED MSCS	96
FIGURE 40.ENUMERATION OF CAM ASSAY BLOOD VESSELS. COMPARISON BETWEEN PROTOCOLS 1 & 2	97
FIGURE 41.VEGF RELEASE UNDER DIFFERENT CONDITIONS.....	98
FIGURE 42.ENUMERATION CAM ASSAY BLOOD VESSELS: COMPARISON BETWEEN PROTOCOLS 1 & 3.....	99
FIGURE 43.VEGF AND BFGF RELEASE UNDER DIFFERENT CONDITIONS.	100
FIGURE 44.ENUMERATION OF CAM ASSAY BLOOD VESSELS: COMPARISON BETWEEN PROTOCOLS 2 & 4	101
FIGURE 45.VEGF AND BFGF EXPRESSION UNDER DIFFERENT CONDITIONS	102
FIGURE 46.ENUMERATION OF CAM ASSAY BLOOD VESSELS: COMPARISON BETWEEN PROTOCOLS 1 , 3 & 5	103
FIGURE 47.VEGF AND BFGF EXPRESSION UNDER DIFFERENT CONDITIONS	105
FIGURE 48.ENUMERATION OF CAM ASSAY BLOOD VESSELS: COMPARISON BETWEEN PROTOCOLS 1,7 & 9 ...	106

FIGURE 49.VEGF AND BFGF EXPRESSION UNDER DIFFERENT CONDITIONS.	107
FIGURE 50.ENUMERATION OF CAM ASSAY BLOOD VESSELS: COMPARISON BETWEEN PROTOCOLS 1 ,11 & 13.	108
FIGURE 51.VEGF AND BFGF EXPRESSION UNDER DIFFERENT CONDITIONS	109
FIGURE 52.ENUMERATION OF CAM ASSAY BLOOD VESSELS: COMPARISON BETWEEN PROTOCOLS 1 ,12 & 14.	110
FIGURE 53.VEGF AND BFGF EXPRESSION UNDER DIFFERENT CONDITIONS	111
FIGURE 54.ENUMERATION OF CAM ASSAY BLOOD VESSELS: COMPARISON BETWEEN PROTOCOLS 1,17 & 19	112
FIGURE 55. VEGF AND BFGF EXPRESSION UNDER DIFFERENT CONDITIONS	113
FIGURE 56.ENUMERATION OF CAM ASSAY BLOOD VESSELS: COMPARISON BETWEEN PROTOCOLS 1,18 & 20	114
FIGURE 57.HEAT MAP: ENGINEERING PROTOCOLS ANGIOGENESIS GROWTH FACTOR RELEASE.	116
FIGURE 58.ANGIOGENIC PROTEOME PROFILE: INDIVIDUAL FACTORS	118
FIGURE 59.TRACHEAL BIOPSIES VEGF AND BFGF EXPRESSION LEVELS	119
FIGURE 60.SINGLE CELL PROTOCOLS: CELLULAR OUTPUTS.	120
FIGURE 61.FLOW CYTOMETRY ANALYSIS OF SINGLE CELLS ISOLATED FROM SEEDED TRACHEA PRIOR TO IMPLANTATION	121
FIGURE 62.STATISTICAL ANALYSIS OF SURFACE MARKER EXPRESSION OF ISOLATED SEEDED CELLS	122
FIGURE 63.ENUMERATION OF CAM ASSAY BLOOD VESSELS: COMPARISON BETWEEN PROTOCOLS 1,2,3, AND 4.	123
FIGURE 64.MICROCT IMAGE ANALYSIS STEPS	124
FIGURE 65.MICROCT IMAGING AND QUANTIFICATION WITH ANGIOTOOL®: EXPERIMENT 1	125
FIGURE 66.MICROCT IMAGING AND QUANTIFICATION WITH ANGIOTOOL®: EXPERIMENT 2	127
FIGURE 67.MICROCT IMAGING AND QUANTIFICATION WITH ANGIOTOOL®: EXPERIMENT 3	129
FIGURE 68.STATISTICAL ANALYSIS OF MICROCT IMAGING AND QUANTIFICATION WITH ANGIOTOOL®	131

LIST OF TABLES

TABLE 1. DONOR INCLUSION AND EXCLUSION CRITERIA.	29
TABLE 2. FLOW CYTOMETRY STAINING PANEL.	40
TABELLE 3.RATIO OF SEEDED DERMAL FIBROBLASTS TO MSCS	48
TABELLE 4.ANGIOGENESIS ARRAY CYTOKINE TABLE	53
TABELLE 5. OVERVIEW OF SCREENING CONDITIONS: PROTOCOLS AND IMPLANTS	59
TABELLE 6.FINAL PROTOCOLS SCREENED WITH TRACHEAL BIOPSIES	73

LIST OF ABBREVIATIONS

Ab/am: antibiotics /antimycotics

Abs: antibodies

Ags: Antigens

Alpha-MEM: Alpha Dulbecco's Modified Eagle Medium

ATMP: Advanced Therapeutic Medicinal Product

bFGF: Fibroblast Growth Factor -Basic

bm-MSCs: Bone marrow-derived mesenchymal stromal/stem cells

CAM Assay: Chorioallantoic Membrane Assay

CD: Cluster of differentiation

CM: Complete media

cPDL: Cumulative population doubling time

DFs: Dermal Fibroblasts

DMEM: Dulbecco's Modified Eagle Medium

DMSO: Dimethylsulfoxide

DS: Decellularized Scaffolds

DT: Decellularized Trachea

ECs: Endothelial cells.

ECM: Extracellular Matrix

ELISA: Enzyme-linked immunosorbent assay

Em: Emission

EMA: European Medicines Agency

ET-OH: Ethanol

EU: European Union

Ex: Excitation

FBS: Foetal Bovine Serum

FCS: Foetal Calf Serum

FTTLs: full-thickness tracheal lesions

GAG: Glycosaminoglycan

GFP: Green fluorescent protein

GMP: Good Manufacturing Practice

GRO: Growth related oncogene

H&E Stain: Haematoxylin and Eosin Stain

H₂O: Water

HAS: Human Serum Albumin

HDF: Human Dermal Fibroblasts

HEPES buffered saline solution (BSS): (N-2-hydroxyethylpiperazine-N'-2-ethanesulfonic acid)
Buffered saline solution

HLA: Human Leukocyte Antigen

hPL: Human Platelet Lysate

h-MSCs: Human Mesenchymal Stromal/Stem Cells

HUVECs: Human Umbilical Vein Endothelial Cells

IL-6: Interleukin 6

IL-8: Interleukin 8

IM: Integra[®] Matrix

ISCT: International Society of Cell Therapy and Gene Therapy

LDH Assay: Lactate dehydrogenase assay

LSD: Long Segmental Defects

LSTD: Long Segmental Tracheal Defects

MCP-1: Monocyte chemoattractant protein-1

MSCs: Mesenchymal Stromal/Stem Cells

NaCl: Sodium Chloride

NET: Neutrophil Extracellular Traps

PDL: Population Doubling Level

PDT: Population Doubling Time

Post-op: Post-operative

PSD: Partial Surface Dehydration

QC: Quality Control

RANTES: regulated upon activation, normal T-cell expressed and secreted, CCL

RBCs: Red Blood Cells

RCF: Centrifugal force or G-force

RPM: Rounds per minute- speed of rotational bowl

RT: Room Temperature

TE: Tissue Engineering/ Tissue Engineered

TEFs: Trachea-oesophageal fistulas

TET: Tissue engineered trachea

TETB: Tissue engineered tracheal biopsy

TETG: Tissue engineered tracheal graph

TIMP-2: Tissue inhibitor of metalloproteinase-2

THY-1: Thymocyte differentiation antigen-1, CD90

VEGF: Vascular Endothelial Growth Factor

WBCs: White blood cells

1. CHAPTER I: THE TRACHEA

1.1. INTRODUCTION

Tissue engineering offers a promising avenue for the generation of tracheal constructs, particularly in the context of addressing complex and large segmental tracheal defects. This approach holds substantial potential for developing replacement structures for various organs, including the trachea. The primary objective of tissue-engineered trachea construction is to faithfully replicate the structural and functional attributes of the native trachea[1]. This goal is achieved through the synergistic application of cells, biomaterials, and bioengineering techniques.

Nonetheless, the clinical demand for functional large segmental tracheal grafts (LSTG) to serve as replacement organs in cases of intractable advanced structural tracheal disorders persists as an unfulfilled requirement[2, 3]. This need becomes evident when the extent of tracheal damage exceeds 50% in adults, and 30% in children [4]. Patients with tracheal stenosis, lesions, or obstructions due to damage or congenital defects, smaller than 50% of the trachea length in adults, or 30% of the tracheal length in children, are typically treated with primary resection followed by end-to-end anastomosis[5-9]. With longer or larger defects however, or defects resulting from multiple resections due to recurrent disease, this approach is not feasible[6, 10, 11].

Regrettably, patients confronted with substantial segmental loss often grapple with significantly elevated morbidity and mortality rates [12]. As a result, an interest in providing a replacement construct as a viable means of subsistence has been generated as early as the late 1890s[13]. Since its inception, numerous endeavors have been perused in both human and animal models, employing diverse approaches and a wide spectrum of materials. These approaches encompass composite strategies e.g., solid prosthesis integrated with Fascia Lata grafts or Polypropylene enriched with collagen and stem cells) [13, 14], autologous tissue reconstruction methods (e.g., utilizing intestinal or esophageal tubes as tracheal substitutes) [15], and various materials; including porous prostheses (e.g., silicone prostheses) [13, 16], solid prosthesis, biological prosthesis including: allografts[14-16], homografts, xenografts, and autografts (e.g. an aortic graft or the forearm free fasciocutaneous flap) [17]. Recent advancements have even delved into the realm of tracheal stem cell regeneration [13, 18, 19]. In 2004, Grillo categorized tracheal replacement approaches into five main categories: non-viable tissues, foreign materials, autologous tissues, tissue engineering, and tracheal transplantation [20, 21].

Regardless of the approach pursued, the overarching aim of tracheal replacement has consistently revolved around the creation of a construct capable of serving as a stable and enduring conduit for respiration. The key attributes of such a construct encompass the capacity to restore the homeostatic barrier between the trachea and its surrounding environment, ensuring an appropriate lumen for ventilation, lateral rigidity, and longitudinal elasticity[22]. It further entails an impermeable inner lining of ciliated columnar epithelium[22], functioning as a barrier against infection, scar formation, and aiding in the clearance of inhaled agents, while regulating lung fluid balance and smooth muscle formation to mitigate recurrent infections[18, 23]. Adequate cartilage content is essential to maintain tracheal strength, mechanics, biocompatibility, and prevent tracheal collapse. Additionally, the

construct must accommodate normal head and neck function, possess growth potential in pediatric patients, and critically, facilitate sufficient vascularization[24]. However, despite the multifaceted efforts, challenges persist, including complications related to infection, tracheal collapse, granulation formation, dislodgement, and, most significantly, inadequate vascularization.

Vascularization, defined as the establishment of de novo primitive vascular networks through the differentiation of precursor cells or angioblasts into endothelial cells, stands as one of the most formidable challenges in graft engineering and implantation. Delays in vascularization frequently lead to tissue necrosis, granulation formation, and stenosis of the transplant[25], culminating in the imperilment of graft survival and ultimately, graft failure[26]. The trachea, as an organ, possess particular vascularization challenges due to the absence of a distinct primary vascular blood supply. Instead, it predominantly relies on a network of small blood vessels, often referred to as segmented vasculature [27], or tracheal-esophageal branches, which emanate from the tracheal vasculature to deliver vital blood, nutrients, and oxygen to its cellular constituents [26]. Consequently, the resection of tracheal segments disrupts the segment's blood supply, and even the swift transplantation of the segment can lead to the subsequent demise of the resected graft [27].

In light of these challenges, the development of innovative methodologies to induce vascularization in tissue-engineered tracheas holds the promise of enhancing vasculature development, thereby improving blood supply and subsequently enhancing tissue development, fortifying strength, and reducing the need for subsequent healthcare interventions.

1.2. BACKGROUND

1.2.1. FORM AND FUNCTION

1.2.1.1. THE ANATOMICAL STRUCTURE OF THE TRACHEA

Originating at the inferior edge of the larynx, and located in the middle of the thoracic cavity, the trachea is a midline, hollow organ that is tubular in shape. Superiorly, it is connected at level C6 by the cricotracheal ligament to the cricothyroid cartilage and is composed of soft tissue that is supported by 16-22 stacked, and C-shaped hyaline cartilage rings which form the anterior and lateral walls of the trachea [28, 29]. These cartilage rings not only provide structural integrity but are also interconnected by a delicate membrane (known as the annular ligament) [28, 30-32] (Figure 1.). Posteriorly, the hyaline cartilage rings are connected to the trachealis muscle, a structure composed of flat longitudinal smooth muscle fibers embedded within a fibro-elastic inter-cartilaginous and membranous connective tissue which connects the inferior part of the upper cartilage to the superior edge of the cartilage below [28]. Thus, lending the trachea its semi-flexibility and an overall D-shaped appearance [28, 33, 34].

Positioned anterior to the esophagus, the trachea connects to the primary bronchus, which subsequently bifurcates into the right and left mainstem bronchi [28, 31]. The region where these structures converge is known as the carina [28, 29, 31] and exhibits a broader morphology in the proximal region than the distal one [31].

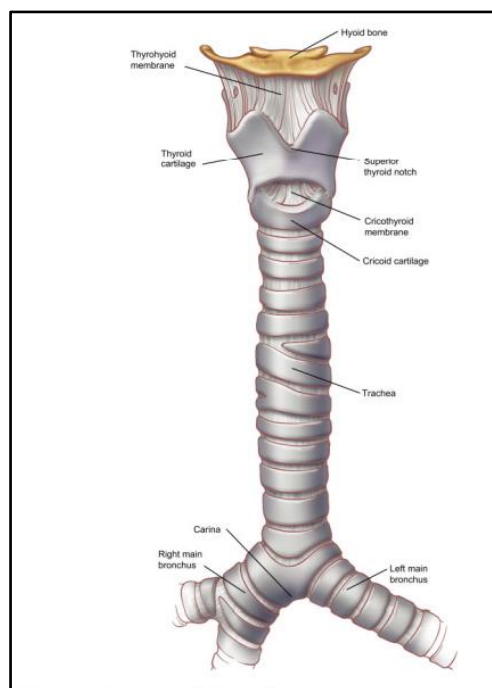


Figure 1: Anterior view of the Structure of the Trachea. Image adapted from *Surgical Anatomy of the Trachea* [28]

Regarding the shape and the morphometry of the human trachea, there is apparent sexual dimorphism, which is particularly pronounced in adults [35]. In children under 3 months of age, the trachea measures approximately 5cm in length [63]. This length disparity is further differentiated by gender, with measurements typically falling between 10-13 cm in males and slightly less in females [27, 32, 34]. In terms of diameter, the trachea of an adult male typically measures between 24 to 26 mm, while that of a female range from 22 to 24 mm [30, 31].

In addition to these size differences, there appears to be a correlation between tracheal shape and gender, with males often displaying a more U-shaped trachea, while females tend to exhibit tracheas that vary between elliptical and C-shaped configurations [35]. Multiple studies have confirmed these distinctions in both size and shape based on gender. For instance, an in vivo and in vitro morphometric study conducted in 2009 by Kirolos K, et al., employing high-resolution CT scans, revealed significant differences in mean tracheal length, antero-posterior and transverse diameters, as well as tracheal volume between men and women, with men generally exhibiting larger measurements [33].

Although the trachea is a hollow organ that would normally not be classified as complex as per se the kidney, the trachea is quite complex with regards to its vascular structure.

1.2.1.2. THE TRACHEAL BLOOD SUPPLY

The trachea is unique in that its blood supply comes from a network of small blood vessels, as it lacks a distinct, major arterial supply[27]. Instead, it receives blood supply from laterally segmental branches, with multiple small vessels distributed along its length[28, 29, 32, 36].

Tracheoesophageal branches of the inferior thyroid artery and bronchial arteries primarily supply blood to the trachea. The inferior thyroid artery, a branch of the thyrocervical trunk, sends branches to the proximal part of the trachea[28, 29, 32, 36]. Bronchial arteries, arising from the proximal descending aorta and/or its major branches, on the other hand, contribute to the vascularization of the distal part of the trachea, crania, and the bronchi[28, 29, 32, 36]. The vessels of the bronchial arteries segmentally branch superiorly and inferiorly across several tracheal rings before entering the trachea. Thereby, creating a lateral longitudinal anastomosis from which transverse inter-cartilaginous arteries both insert and course through (anteriorly or posteriorly) the space between the tracheal rings[28, 29, 32, 36] (**Figure 2.**).

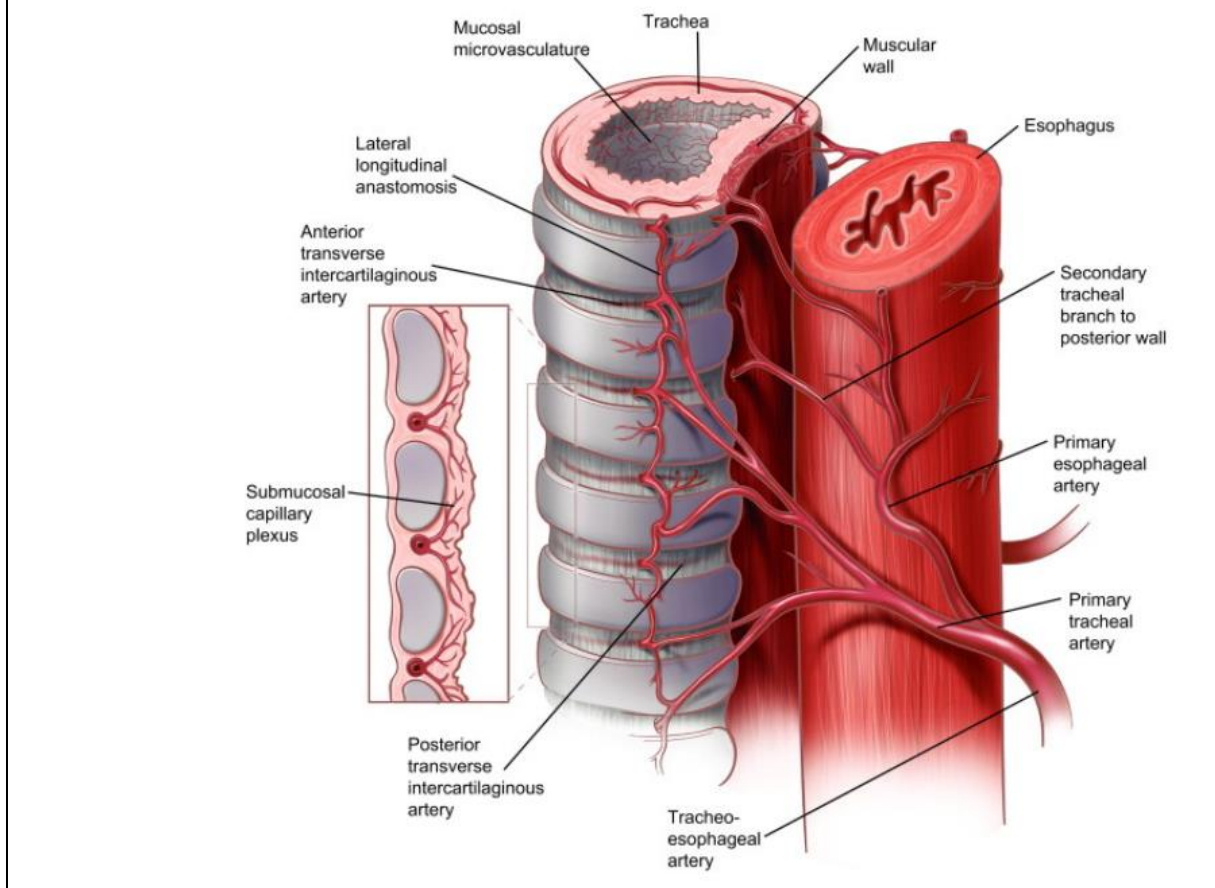


Figure 2. The Tracheal Segmented Blood Supply. Adapted from *Surgical anatomy of the Trachea*[28]

These arteries terminate in a submucosal plexus of blood vessels that provides nourishment to the tracheal cartilage, while the secondary branches of the tracheoesophageal arteries provide nourishment to the membranous part of the trachea[32]. These vessels are crucial for maintaining the health and function of the respiratory epithelium.

1.2.1.3. NERVES

The trachea receives parasympathetic innervation from the vagus nerve (CNX)[37], which plays a crucial role in regulating airway function. The vagus nerves exit the skull and travel alongside the common carotid arteries before reaching the superior mediastinum[32]. The right recurrent laryngeal nerve follows a path beneath the right subclavian artery, while the left recurrent laryngeal nerve branches underneath the aortic arch. These nerves provide parasympathetic, somatic, and motor innervation to the trachea and enter the larynx through the inferior constrictor muscles. Damage to these nerves during surgery can lead to vocal cord paralysis and voice-related issues. Additionally, sympathetic innervation of the trachea is provided by the middle cervical ganglia[32]. Parasympathetic innervation of the trachea is responsible for regulating airway smooth muscle tone, glandular secretion in the airways, and vascular tone in the lungs and bronchi[38]. Two distinct parasympathetic pathways project to the airways, with opposing effects on airway smooth muscle but cooperative effects on mucus secretion[38]. Notably, different regions of the airway mucosa are innervated by afferent

nerves arising from different vagal ganglia, with proximal areas receiving input from the jugular vagal ganglia and distal regions from the nodose ganglia[39].

1.2.1.4.HISTOLOGICALLY

The tracheal tissue, also known as the tracheal wall, consists of several distinct layers:

Inner Mucosa: This is the innermost layer, referred to as the laminal mucosa. It is composed of pseudostratified columnar epithelium, which contains specialized kinocilia that move foreign materials and irritants upward to help expel them. Additionally, mucin-producing goblet cells are present in this layer, contributing to the secretion of mucus. The mucus serves to trap debris from the air and maintain the moisture of the ciliated layer. Ducts within the mucosal layer connect to the mucous gland ducts located in the submucosal layer [28, 29, 32, 36, 40, 41].

Submucosa: Situated below the mucosal layer, the submucosal layer contains various components, including fatty and endothelial cells[42], nervous tissue, and blood vessels [32, 42]. It also houses elastin and collagen fibers, which enhance the elasticity and structural support of the trachea. Smooth muscles within this layer enable the trachea to change its diameter during the inhalation and exhalation processes [32, 40, 42]. **Hyaline Cartilage Layer:** Surrounding and supporting the submucosal layer is the hyaline cartilage layer. This layer comprises chondrocytes, and cells within lacunae inside the cartilage that occur singularly or in clusters called isogenous groups, contributing to its structural integrity and support [40, 42] (Figure 3.).It is surrounded by the perichondrium which is a layer of dense irregular connective tissue[41] that merges with submucosa and can be divided into two layers: fibroblasts that produce type I collagen on the outer surface of the perichondrium (outer fibrous layer) and another inner chondrogenic layer that contains fibroblast-like cells,. These cells can initiate matrix production (type II collagen), differentiate into chondroblasts, and develop into immature chondrocytes

Trachealis Muscle Layer: Located in the posterior wall of the trachea, this layer is connected to the endpoints of the C-shaped cartilage rings. It is primarily composed of muscle tissue and plays a vital role in the contraction and regulation of the tracheal diameter. This is crucial for processes like coughing and clearing irritants from the airway[32, 40, 42].

Adventitia: The outermost layer of the tracheal wall is known as the adventitia. It serves as the connecting layer that attaches the trachea to the surrounding soft tissues. Composed mainly of loose connective tissue, the adventitia provides structural support and stability to the trachea [32, 42]

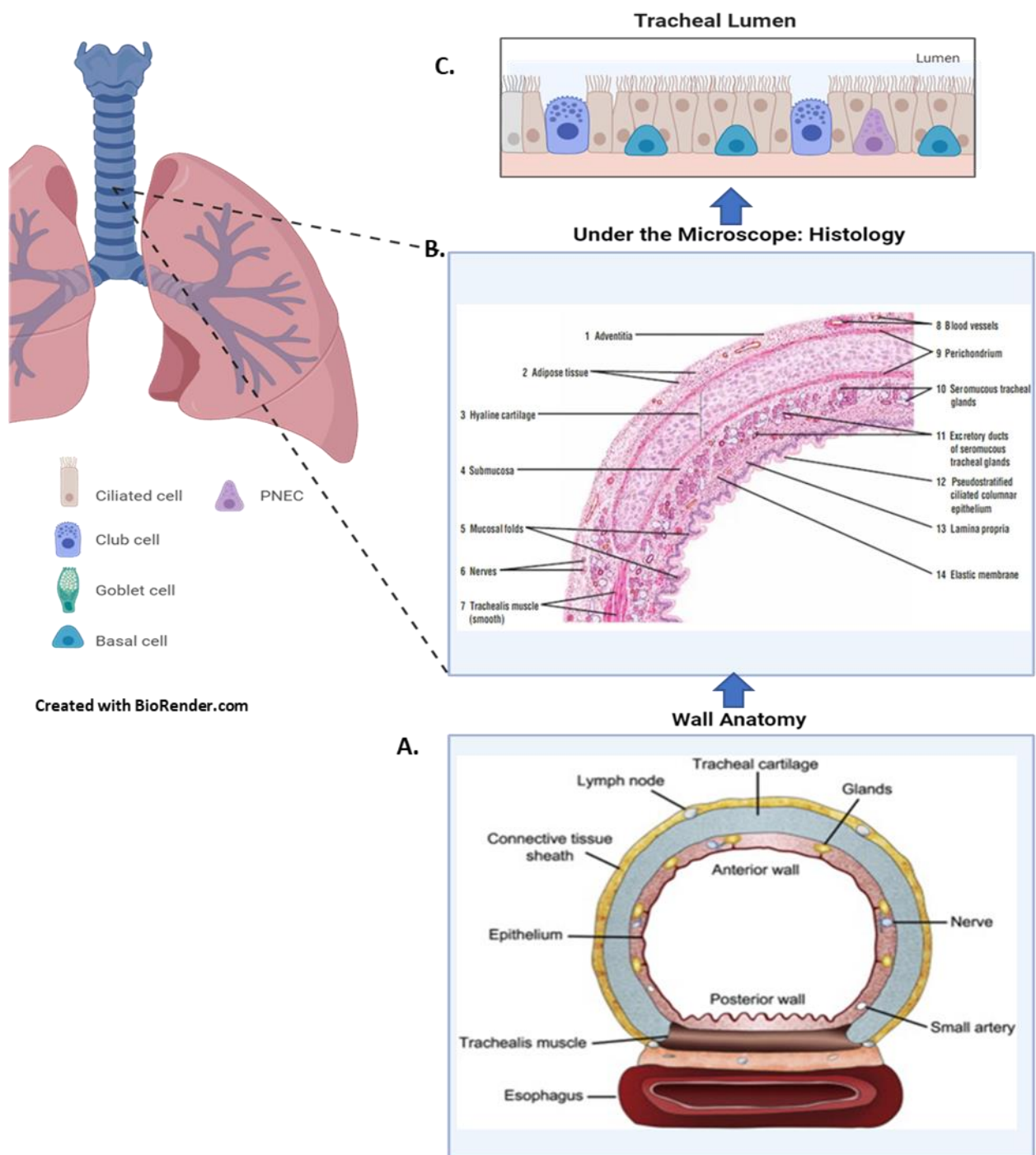


Figure 3. Anatomy and Histology of the Tracheal Wall.

A. Wall anatomy of the trachea. Image adapted from Lawrence D, et.al.2015 [33]. **B.** Histological Transverse Section of the tracheal wall (Hematoxylin & Eosin stain) adapted from DiFiore's atlas of histology,2008 [41]. **C.** Cells of the tracheal Lumen.

1.2.1.5. PHYSIOLOGICAL FUNCTION

The trachea plays a crucial role in the respiratory system as a conduit for the exchange of oxygen and other gases during inhalation and exhalation [28, 29, 31]. It serves as a vital link between the external environment and the lung tissue, facilitating breathing by expanding during inhalation. Any obstruction or narrowing of the trachea can lead to significant breathing difficulties with severe consequences for patients [28, 29, 31]. In addition to its role in gas exchange, the trachea also contributes to the exchange of heat and moisture and aids in the removal of particulate matter from the respiratory system [2].

The efficiency of air transport through the trachea is reliant on its inner diameter. According to the Hagen-Poiseuille law, flow resistance in a tube is inversely proportional to the fourth power of its radius in laminar flow. Elevated flow rates leading to turbulence further increase resistance, with various factors such as mucosal swelling, airway muscle constriction, tumors, and the use of endotracheal tubes significantly exacerbating airflow resistance. For example, a 50% reduction in the tracheal inner diameter can result in a 16-fold increase in resistance, and under turbulent flow conditions, this increase can reach up to 32-fold [2]. Structurally, the trachea consists of a composite arrangement of longitudinal muscle, C-shaped cartilage rings, and specialized respiratory mucosa. It serves as a conduit connecting the larynx to the bronchi, facilitating respiration while aiding in the removal of secretions from the trachea and bronchi [20]. The trachea is uniquely adaptable to withstand both internal and external mechanical forces, exhibiting remarkable flexibility and the ability to maintain lateral rigidity during positive and negative pressure changes during breathing and other physiological processes [20]. This structural design combines lateral rigidity and longitudinal flexibility, which are essential for regulating tracheal lumen diameter, preventing collapse, and providing support during the inhalation and exhalation phases [43, 44]. Typically, the trachea features approximately two cartilage rings per centimeter, with each ring averaging 4 mm in height. The tracheal wall is about 3 mm thick, and its average external diameter measures 2.3 cm in the coronal plane and 1.8 cm in the sagittal plane. While the tracheal lumen is circular at birth, it often assumes an ovoid shape as a child matures into an adult, although a persistent circular shape is considered a normal adult variant. Changes in intraluminal pressure during respiration, ventilation, and maneuvers like the Valsalva maneuver can alter the tracheal lumen diameter [26]. Coughing can narrow the tracheal lumen by contracting the trachealis muscle, leading to the approximation of the cartilaginous C-shaped rings. Aging or the presence of obstructive airway diseases may result in a reduction in the lateral diameter and an increase in the anteroposterior (AP) diameter, causing the characteristic "saber sheath" tracheal configuration. In cases of chronic obstructive pulmonary disease, softening of the cartilage rings can lead to AP narrowing, particularly when the posterior wall thickens, potentially causing luminal obstruction during expiration or coughing [26].

1.2.2. TRACHEAL MALFUNCTION: INDICATIONS FOR TRACHEAL REPLACEMENT

1.2.2.1. TRACHEAL DAMAGE AND DISEASE

Tracheal damage can manifest in various forms, including disruption, malformation, tracheal stenosis, or neoplastic disease. It can result from a wide spectrum of underlying etiologies, spanning from: inflammation or infection, to congenital defects, the presence of malignancy (i.e. squamous cell carcinoma or adenoid cystic carcinoma [45]), blunt-force trauma, to iatrogenic factors like extended intubation or failure or complications of previously performed surgery (i.e. for benign diseases or congenital defects), and tracheoesophageal fistula [4, 34, 46]. Patients afflicted with extensive tracheal defects often experience a significantly compromised quality of life and face elevated mortality risks [4, 33, 34, 47]. Tracheal defects typically manifest as tracheal stenosis, tracheomalacia, and/or tracheoesophageal fistulas and can be categorized into one of two broad groups: Congenital or Acquired[33, 34, 47].

Tracheal Stenosis (TS) represents the narrowing of the tracheal lumen, which can range from mild to severe in its manifestation[42, 48]. In adults, TS is predominantly acquired and can be attributed to various factors, including trauma, malignancy, tracheostomy, inflammation, and prolonged endotracheal intubation[48-50]. In contrast, TS in children is primarily congenital in origin but can also develop as an acquired condition [49, 51]. Severe congenital tracheal stenosis, particularly in neonates and infants, poses a significant medical challenge and is a leading cause of mortality in this population. It is characterized by severe respiratory distress, frequent hospitalizations, the necessity for endotracheal intubation, ventilator support, and recurrent respiratory tract infections[52] [48] . A study conducted in 2002 on 20 patients with TS who underwent surgical ablation revealed that chronic inflammation played a pivotal role in the pathogenesis of TS. This chronic inflammation led to fibrosis, resulting in the thickening of the mucosal layer within the tracheal wall and the subsequent development of tracheal stenosis[50]. Histological examination of surgically removed sections of narrowed trachea demonstrated that plasma cells were the predominant leukocyte type within the inflammatory infiltrates. In most TS samples, the epithelial surface remained intact and featured cilia. However, when the tracheal lumen was entirely obliterated, cilia were notably absent. The mucosal cells and glands within the tracheal wall were generally well preserved in TS samples[50].The necessity to remove segments affected by TS was frequently linked to prior tracheal surgeries, which were associated with tracheal lumen closure and cartilage ring ossification [50].

Tracheomalacia is characterized by the weakening or damage to the tracheal cartilage, leading to collapse [41]. It can be congenital (present from birth) or acquired later in life, often resulting in tracheal stenosis [52]. Common symptoms of tracheomalacia include stridor, wheezing, dyspnea, and fatigue upon exertion [52, 53]. Diagnosis involves tests like chest X-rays, CT scans, airway fluoroscopy, direct laryngoscopy, and bronchoscopy [53, 54]. Treatment varies based on severity and may include specialized care, medications, respiratory support, or surgery [52-54]. Tracheomalacia is relatively rare.

In patients suffering from chronic obstructive pulmonary disease (COPD), tracheobronchomalacia occurs in 7-15% [52]. Primary congenital tracheomalacia however, affects at least 1 in 2,100 children [52, 55].

Tracheoesophageal fistula describes the presence of one or more holes, or an irregular connection between the oesophagus and the trachea and form most often before birth as a congenital abnormality and only rarely as a result of post-thoracic surgery complication or a complication of

prolonged invasive mechanical ventilation (MV) [53]. In the past three years, during the COVID-19 pandemic, an exceptional rise in the occurrence of full thickness tracheal lesions (FTTLs) and Tracheoesophageal fistulas (TEFs) in COVID-19 patients undergoing ventilation was observed, although the underlying causes remain unclear [53].

1.2.2.2. DISEASE BURDEN

Tracheal disorders, including injuries, stenosis, and diseases, pose significant medical challenges, associated with notable morbidity and mortality rates [3, 4]. Conditions like tracheostomies, tracheal injuries, and diseases leading to stenosis carry substantial morbidity and mortality burdens [4, 47], placing a considerable strain on healthcare systems [47]. These cases often necessitate multiple hospital visits and ongoing acute clinical interventions [47].

In recent years, respiratory diseases, including those affecting the trachea, have surged as a leading cause of disability and death, with a global increase in affected individuals [34, 49, 50]. Notably, the COVID-19 pandemic has further exacerbated the prevalence of respiratory diseases and associated complex tracheal conditions [54]. Tracheal stenosis is a significant concern, with 20% to 30% of tracheostomy patients developing some degree of stenosis, and a subset experiencing debilitating symptoms requiring invasive procedures [3, 47]. Prolonged invasive mechanical ventilation or intubation can lead to severe outcomes like full-thickness tracheal lesions (FTTLs) and tracheoesophageal fistulas (TEFs), though these complications are generally rare (0.3%-30%) under normal circumstances [54]. Various factors, including trauma, inflammation, malignancies, and congenital defects, contribute to tracheal alterations, necessitating interventions like tracheal resection or reconstruction [51, 55]. However, long-segmental tracheal disease poses unique challenges, with limited effective treatment options [56].

Tracheal and main bronchi disorders represent an unmet medical need in respiratory medicine, driven by factors like prolonged intubation and tracheostomy rates, particularly in COVID-19 patients [34]. While several approaches have been explored for replacing long-segmental tracheal defects, a definitive solution for restoring a functional respiratory system remains elusive [34]. In short, tracheal afflictions carry significant morbidity and mortality risks, with the COVID-19 pandemic amplifying the challenges associated with complex tracheal diseases. The limited treatment options for these conditions underscore the need for innovative approaches in respiratory medicine.

1.2.2.3. MALFUNCTIONING TRACHEA: TREATMENT APPROACHES

Common approaches to maintain tracheal airway include methods like stenting, bouginage, or suboptimal laser treatments [1, 34, 41]. However, when these approaches are ineffective or inapplicable, the choice of treatment depends on the size of the tracheal defect. Pediatric patients with defects smaller than 30% of their tracheal size (around 2 cm) and adults with defects smaller than 50% of their tracheal size (approximately 5-6 cm) may undergo segmental resection followed by direct end-to-end anastomosis or tracheoplasty [1, 34, 44, 48, 57]. Larger or longer defects carry a higher risk of complications [57].

For congenital Tracheal Stenosis (TS), the primary treatment is surgical intervention, particularly sliding tracheoplasty. However, the long-term outcomes of this procedure are challenging, with

mortality rates ranging from 16% to 36% and reintervention rates of up to 44% [47]. Furthermore, despite the progress in surgical methods, there persist challenges in the surgical process itself, as well as issues related to operation complexity, respiratory management, and postoperative care [47]. Therefore, if the tracheal defects are above the cut-off line (i.e. > 30% or > 50%), then they are considered major tracheal defects [34] or long segmental tracheal defects (LSTD) [4], for which, direct end-to-end anastomosis is not possible and alternative approaches must be considered, primarily, in the form of palliative care [34] or tracheal reconstruction and/or replacement [4].

Tracheal reconstruction is a complex surgical procedure indicated for primary tracheal neoplasms (squamous cell carcinoma, adenoid cystic carcinoma), thyroid cancer, extensive tracheoesophageal fistulas, unsuccessful previous surgery for benign tracheal diseases (re-stenosis, long-term stenosis that has been dilated or been non-surgically repaired), and, rarely, congenital tracheal stenosis [4]. However, primary tracheal resection with direct end-to-end anastomosis after release of the surrounding anatomical structures is insufficient when the length of trachea resected is greater than 50% in adults or 30% in children (Figure.4) [4].

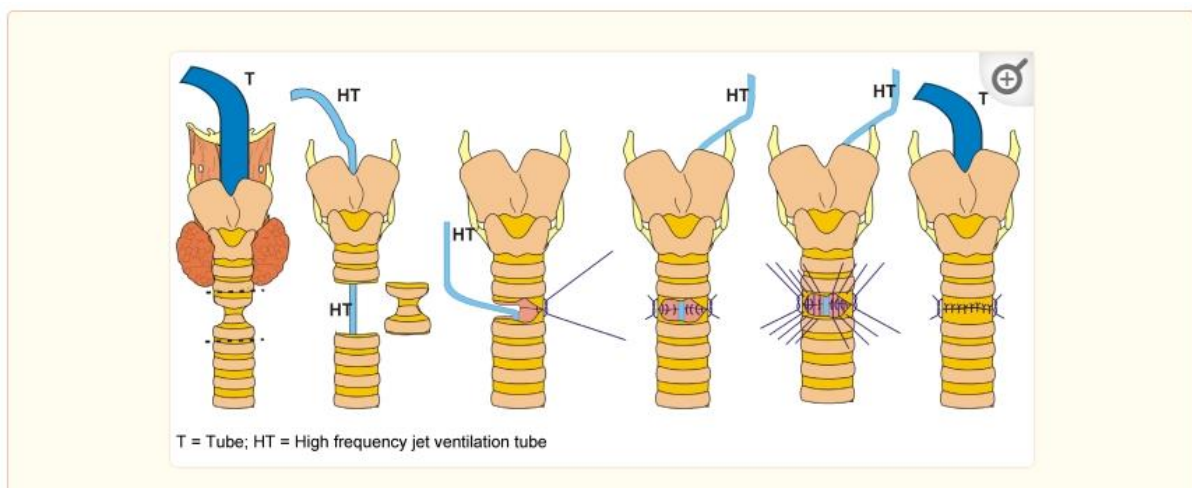


Figure 4. The process of tracheal resection and end to end anastomosis. Image adapted from Friedel G, et. Al .2003 [2]

Despite numerous attempts, obtaining suitable tracheal replacements or reconstructing the trachea for long segmental defects (LSD) still remains one of the greatest challenges of thoracic surgery [4, 56, 57]. Several attempts have been made to restore function to patients suffering from long circumferential tracheal defects, or long segmental tracheal defects (LSTD). Generally, these attempts can be classified into two main categories: tissue engineering attempts (TE) and non-tissue engineering attempts (non-TE). Non-TE attempts comprise approaches that are based on allogenic replacement, autologous restructuring, or the use of synthetic prostheses that are directly transplanted in vivo. In contrast, TE approaches depend on in vitro manufacturing of replacement constructs prior to in vivo transplantation (Figure 5.) [33, 34, 57].

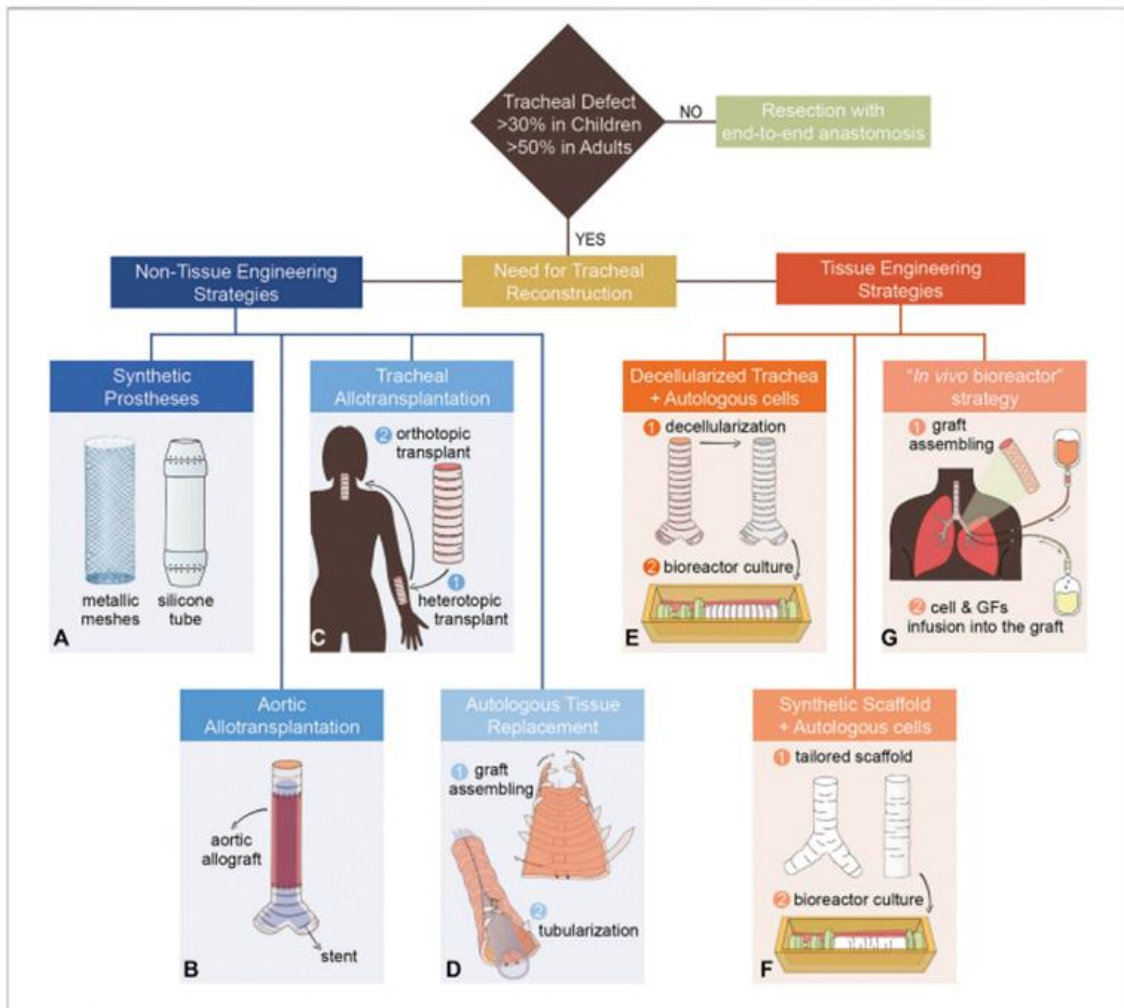


Figure 5. Examples of different strategies for tracheal replacement. Figure adapted from Adamo D, et. al 2022[34]

1.2.2.4. APPROACHES TO TREATING OR REPLACING LONG SEGMENTAL DEFECTS

Long segmental tracheal defects (LSTD) pose a substantial challenge in clinical medicine. Conventional treatment methods have faced limitations, prompting exploration into alternative approaches for LSTD management. These approaches encompass autologous reconstruction, allogeneic transplantation, reconstructed allografts, non-viable prosthetics, and tissue-engineered tracheas [57] [4].

Allogenic Replacement – Allografts

Allogenic tracheal transplantation, initiated by Rose and colleagues in 1979, aimed to address long airway defects [14]. Earlier attempts faced significant hurdles, including immunological responses leading to rejection, sluggish revascularization resulting in necrosis, liquefaction, graft stenosis, and fibrosis [58]. More recently, big advances have been made. However, despite these advances, challenges persist due to donor scarcity and the need for post-transplant immunosuppression therapy [47, 55, 62]. Allogenic tracheal transplantation remains an option for specific cases but is not universally applicable [57]. The scarcity of matching donor tracheas and the need for

immunosuppression underscore the continued relevance of tissue engineering in addressing inoperable tracheal pathologies [47, 55, 62].

Recent investigations into aortic allografts as an LSTD substitute have also shown promise; however, their long-term clinical efficacy and risk of complications, such as calcification and degeneration, require further assessment [57]. Although feasible, allograft transplantation carries inherent risks, such as contamination and disease transmission [59]. The American Association of Tissue Banks (AATB) reported a low infection rate of 0.014% in allogeneic tissue transplantation [59]. To mitigate this risk, allograft sterilization techniques, primarily utilizing radiation, are employed [59].

Autologous Restructuring - Autologous Tissue Biocomposite or Composite

One crucial aspect of autologous restructured biocomposites is the formation of cartilage rings for tracheal support. Some reproducible and effective techniques, such as the use of aortic homografts or vascularized autografts, have been reported [60]. Toenail grafts offer applicability in tracheal reconstruction due to their anatomical and physiological similarities to the respiratory tract, maintaining flexibility and lumen patency [60].

Replacement with Synthetic Prosthetic

Synthetic materials, despite several attempts, have generally yielded unfavorable outcomes for reconstructing long segmental tracheal defects. These materials suffer from limited biocompatibility, granulation formation, lack of flexibility, failure to engraft properly, and susceptibility to infections [5, 48]. Over the past half-century, various synthetic materials have been evaluated for tracheal scaffold production, but immunological complications and bacterial infections have hindered their success [61]. Additionally, these materials lack essential organ-specific biomechanical properties, such as flexibility, strength to prevent collapse, and the ability to form airtight seals [61].

Tissue Engineering

Numerous attempts have been made to engineer replacement tracheal constructs using diverse cell types, scaffolds, and processing methodologies. Notably, a decellularized human cadaveric trachea has achieved clinical translation success [5]. The complexity of the trachea makes it challenging to fabricate an implant that accurately replicates both morphological and mechanical tissue features. As a result, there is a growing trend toward using decellularized matrices and autologous cells as fundamental components in trachea engineering [62]. To date, no ideal treatment exists for patients with long segmental airway disorders. Tissue engineering has emerged as a promising alternative for tracheal replacement [15].

1.2.3. TISSUE ENGINEERING: TRACHEA

1.2.3.1. COMPONENTS OF A TISSUE ENGINEERED TRACHEA

Tissue engineering (TE) represents an interdisciplinary approach that amalgamates elements from medicine, life sciences, and engineering disciplines, aimed at creating biological substitutes capable of fully restoring both the structure and functionality of damaged tissues or organs [60]. The primary impetus behind TE is to address the global shortage of organs available for transplantation, a critical issue arising from the substantial incongruity between the high demand for organ transplants and the limited supply of suitable donor organs [60, 61]. The concept of cultivating lab-grown organs in vitro

holds great potential as a viable solution to address this organ scarcity. Among the various applications of TE, tissue-engineered tracheas (TETs) have emerged as a promising option, particularly for patients facing inoperable tracheal pathologies with no accessible donor organs [47, 55, 60]. Consequently, TETs represent a viable solution to bridge the deficit in available tracheal donor tissues [47].

The core principles underpinning organ engineering encompass four primary components: the selection of appropriate cell types, the utilization of suitable scaffolds, the incorporation of specialized media and additives, and the deployment of bioreactors to facilitate tissue development [60]. These components collaborate in creating lab-grown organs or tissues. Tissue engineering relies on fundamental components delineated by Langer and Vacanti in 1993[63], which include:

Cell Types: One of the pivotal facets of tissue engineering is the careful selection of the most appropriate cell types. Cells serve as the foundational building blocks for engineered tissues, and the choice of cell source holds paramount importance. In the context of tracheal tissue engineering, researchers have explored a broad spectrum of cell types, encompassing various types of stem cells with diverse potencies and origins, such as adipose-derived Mesenchymal Stem/Stromal Cells MSCs and bone marrow-derived MSCs, along with progenitor cells sourced from the pericardium, pleura, and trachea itself. However, the identification of the ideal cell source or a synergistic combination remains an ongoing area of research[64]. Mesenchymal stem cells, particularly those derived from bone marrow and adipose tissue, have gained widespread acceptance due to their availability, capacity for expansion in culture, and potential for multilineage differentiation [55].

Scaffolds: Scaffolds play a pivotal role in tissue engineering, serving as a foundational element in tissue construct formation. The selection of an appropriate scaffold is a crucial decision influenced by multiple factors, including the specific tissue to be engineered and the intended purpose of the construct. Scaffold characteristics profoundly influence cell adhesion and overall tissue development. Additionally, scaffolds are instrumental in preserving the structural integrity of the engineered construct, ensuring proper integration into surrounding tissues, resistance to mechanical stresses, and maintaining functionality. The choice of scaffold necessitates meticulous consideration, encompassing factors such as scaffold type and its compatibility with the chosen cell seeding method. Typically, scaffolds fall into two primary categories: biological and synthetic [60, 62]. Biological scaffolds have historically been sourced from various origins, encompassing autologous, allogeneic, and xenogeneic sources [60]. In the context of tissue-engineered tracheas (TETs), common scaffold choices include decellularized donor tracheas [2, 47]. The type of scaffold employed significantly shapes the selection of cell seeding techniques, with complex micro-architectures requiring more dynamic methods for cell incorporation due to potential hindrances in passive incorporation, such as the "drip technique" [63]. It is crucial to investigate the attributes of decellularized tracheal scaffolds and their compatibility with specific seeding methodologies.

Several critical factors merit consideration when evaluating scaffolds. Firstly, the scaffold should exhibit non-toxicity towards both the incorporated cells and the host organism. It should also facilitate adequate nutrient provision to every cell within the construct. Additionally, mechanical properties are a vital concern, as certain scaffolds with inadequate mechanics, like fibrin gels or hydrogels, exhibit limited utility in the context of tissue engineered trachea. Compatibility between the scaffold and the chosen seeding technique is crucial to avert damage to the seeded cells, such as apoptosis or cell lysis, thereby ensuring reproducible results in the tissue-engineering process [63].

Decellularized scaffolds, or decellularized matrices (dECM) represent a scaffold material with low immunogenicity achieved by removing cells from tissues through physical or chemical methods. dECM comprises a complex network of interrelated macromolecules and exhibits intricate components. It retains many intrinsic tissue components, including collagen, elastin, proteoglycans, hyaluronic acid,

and growth factors [42, 63]. Over the past two decades, dECM, with its intricate composition, structural similarity to natural tissues, excellent biocompatibility, and low immunogenicity, has garnered significant attention in biomaterial research. Its applications span a broad range of biomaterials, encompassing decellularized pericardium, blood vessels, corneas, bone, and its utilization as a coating for 3D-printed polycaprolactone (PCL) tubes [43, 65-67].

Media Additives: Specialized media and additives are essential for supporting cell growth and development during tissue engineering. These components supply the necessary nutrients to sustain cell viability and promote tissue maturation. Different media additives can result in different outcomes for the same cells. In the context of mesenchymal stem cells (MSCs) for example, there is significant variability in cell isolation techniques and expansion conditions, with little attention paid to the distinct variations of growth factors and other supplements utilised [68]. Consideration should be given to the culture media and supplements used in research to ensure reproducible results and minimize clinical complications [65].

Bioreactors: Bioreactors represent dynamic systems designed to create a conducive environment for tissue growth and maturation. By providing controlled conditions and mechanical stimulation, bioreactors play a crucial role in the development of functional engineered tissues. Successful re-epithelialization of decellularized tracheal scaffolds for example, remains a challenge in tracheal graft success, and understanding the hydrodynamic environment within bioreactors is essential for achieving viable tracheal grafts [67].

Tissue engineering holds immense promise in addressing tracheal pathologies and alleviating the scarcity of donor tracheas for transplantation. The strategic integration of suitable cell types, scaffolds, and bioreactors offers the potential to produce functional tissue-engineered tracheas, emphasizing its significance in the realm of regenerative medicine [62]. While progress has been made in allogeneic tracheal transplantation, tissue engineering remains a promising avenue for addressing tracheal conditions that may otherwise be inoperable or face a lack of donor organs [48, 56, 61]. These tissue-engineered tracheas must adhere to specific criteria outlined by Belsey [22] and Grillo [44], encompassing lateral rigidity, longitudinal flexibility, airtightness, integration into adjacent tissues, the presence of a ciliated respiratory epithelium, and minimal reliance on immunosuppressants [43]. As research continues to advance, tissue engineering offers hope for individuals confronting challenging tracheal conditions and may hold the key to future clinical solutions.

1.2.3.2.STATE OF THE ART: DECELLULARIZED TISSUE ENGINEERED TRACHEA

1.2.3.2.1. Pre-Clinical Animal Trials:

Numerous studies and research groups have demonstrated the potential and efficacy of utilizing decellularized scaffolds for tracheal reconstruction and engineering. Pre-clinical trials have encompassed a variety of animal species, including pigs [69], dogs, rabbits [43, 48] [70], and rats [43, 71]. These studies exhibit differences in cell sources and methodologies. In rabbit studies, one investigation focused on a novel procedure for rapid partial tracheal decellularization, yielding low-immunogenic cartilage [71]. Canine trials involved assessing in vivo biocompatibility by recellularizing canine tracheal scaffolds with epithelial and endothelial progenitor cells, resulting in tissue preservation and proliferation without fibrotic tissue formation [69]. An optimized decellularization protocol for canine tracheas was developed, meeting stringent criteria for scaffold quality [69].

Researchers have also employed decellularized tracheal scaffolds in other animal models, including mice and rats [73, 74]. In the porcine model, in vitro regeneration of decellularized pig oesophagus was achieved using human amniotic stem cells [75]. Investigations have explored various techniques for porcine tracheal scaffold decellularization, including mechanical agitation, freeze-thaw cycles, and chemical treatments [73]. Structural integrity and preservation methods for swine tracheal scaffolds were examined in a separate study [76]. Another research endeavour investigated the in vivo regeneration potential of decellularized pig tracheas, facilitating the creation of tissue-engineered airway transplants in pigs [77]. Collectively, trials involving pigs and decellularized tracheal scaffolds have yielded encouraging results, encouraging the exploration of diverse decellularization and regeneration strategies. These animal-based investigations are pivotal for advancing tissue engineering and regenerative medicine, offering promising avenues for clinical applications.

1.2.3.2.2. HUMAN TRIALS

To date, in literature there have been three documented cases of humans transplanted with tissue engineered tracheal transplants that are based on decellularized scaffolds. All three transplants had all taken place due to lack of other alternatives and the TET were attempted for compassionate use. Two of the cases survived, while the third case passed-away.

I. CASE I (ADULT PATIENT):

The inaugural tracheal tissue engineering transplant (TET) occurred in 2008 by Macchiarini et al. In this procedure, a 30-year-old female afflicted with end-stage bronchomalacia of the left main bronchus received a decellularized cadaveric donor trachea. This tracheal scaffold was augmented with autologous epithelial cells sourced from bronchoscopic biopsy samples of the right main bronchial mucosa. Additionally, it was infused with autologous, expanded bone marrow mesenchymal stem-cell-derived chondrocytes [71]. Subsequently, the TET construct underwent controlled cultivation within a rotational bioreactor, with the decellularized trachea undergoing re-population via micro-syringe infusion. The scaffold rotation, at 90-degree intervals every 30 minutes, ensured comprehensive cellular adherence to the tracheal surfaces [71]. The total duration of bioreactor culture spanned four days. Following resection of the left main bronchus, the TET graft underwent tailored shaping and end-to-end anastomosis.

According to the report by Macchiarini et al. in 2008, the procedure resulted in the prompt restoration of bilateral ventilation, with the patient's left lung being adequately ventilated. Subsequently, the patient underwent a ten-day stay in the intensive care unit (ICU), followed by transfer to the general ward, and ultimate discharge without complications after an additional ten days. At the four-month mark, the graft displayed normal appearance and function, obviating the need for immunosuppression [71].

In 2014, a five-year follow-up study was published in *The Lancet* by Gonfiotti et al., chronicling the outcomes of Macchiarini et al.'s 2008 transplant. Following the initial procedure, the patient underwent regular multidetector Computed Tomography (CT) scans and bronchio-assessments every three months. Furthermore, mucosal biopsy sampling was conducted biannually, complemented by continuous monitoring encompassing respiratory function, cough reflex, quality of life, and screening for recipient antibodies against donor human leukocyte antigen (HLA) [72]. One year into the monitoring, the sole notable development was the emergence of progressive cicatricial stenosis within the native trachea, in proximity to the TET anastomosis, necessitating recurring endoluminal stenting.

However, the TET graft remained resilient, open, recellularized, vascularized, and proficient in mucus clearance. The patient maintained normal lung function and a healthy cough reflex. There was no occurrence of teratoma formation in the seeded stem cells, and no detection of anti-donor antibodies. The patient's life returned to normalcy, with sporadic bronchoscopic interventions involving stenting constituting the sole medical interventions [72].

Subsequently, concerns regarding the ethicality and authenticity of Macchiarini's work began to emerge, with revelations in 2018 suggesting falsified findings [73].

In 2019, The Lancet issued an update on the aforementioned patient's status, indicating that she had undergone a left pneumonectomy [74]. Molins provided an account of the patient's post-transplant progress, contrasting with the accounts by Macchiarini et al. and Gonfiotti et al. Postoperatively, the patient required stenting of the transplanted bronchus three weeks after surgery due to homograft collapse [74]. Nine months later, the patient sought follow-up care at a different medical institution, beyond which no information was available [73]. However, in 2014, she presented with total atelectasis of the left lung, 80% bronchial collapse, acute respiratory failure, and reported multiple stenting procedures during her absence from the Department of Thoracic Surgery at the Thoracic Surgery Hospital Clinic, Barcelona University. This starkly contrasted the statements made in Gonfiotti et al.'s 5-year follow-up paper, which had indicated a return to normalcy in the patient's life, revealing a substantial decline in her health. The patient experienced recurrent bronchial obstruction, retained only 20% of expected lung function, endured multiple lung infections necessitating intervention, and ultimately underwent a transsternal left lung pneumonectomy in July 2019. Thankfully, the recovery post-pneumonectomy transpired without complications, and as of 30 months post-operation, the patient had fully recuperated without any further medical incidents [74]. In February 2023, The Lancet issued a letter of concern regarding the 5-year follow-up paper pertaining to the transplant.

In conclusion, this case underscores the exigency for more resilient tracheal grafts that are less susceptible to collapse, thus mitigating the necessity for frequent medical interventions. The vulnerabilities observed in the implanted graft can be attributed to various aspects of TET construction and subsequent implantation.

II. **CASE II (PAEDIATRIC PATIENT):**

In 2010, the second case unfolded involving a stem-cell-based, tissue-engineered tracheal replacement procedure performed in a paediatric patient. Subsequently, in 2012, a comprehensive two-year follow-up study was published in The Lancet [71]. The technique used, presents great potential for the use of tissue-engineered tracheal grafts as a treatment methodology for large segmental tracheal defects (LSTD) through the utilization of tissue-engineered tracheal grafts. In this particular case, Elliott M. et al. documented the intervention for a 12-year-old male afflicted with long-segmental congenital tracheal stenosis and pulmonary sling. The therapeutic approach involved the transplantation of a tissue-engineered decellularized cadaveric trachea that had been repopulated with autologous bone marrow Mesenchymal stem cells, a procedure carried out on compassionate grounds [71]. Initially, the child's compromised airway was supported with metallic stents. However, due to stent failure, an alternative approach was adopted, entailing the use of a decellularized cadaveric trachea repopulated with autologous bone marrow Mesenchymal stem cells, collected after brief treatment with granulocyte colony-stimulating erythropoietin (GCSF). This tissue-engineered tracheal construct also

featured patches of autologous epithelium and topical application of human recombinant erythropoietin [71].

The two-year post-operative evaluation yielded insights into the advantages, disadvantages, and challenges associated with this technique. Notably, challenges included the formation of NET (Neutrophil Extracellular Trap) pockets [71]. Subsequently, a four-year follow-up study, reported by Hamilton N.J. et al. in the American Journal of Transplantation, provided an extensive examination of the child's progress since the initial 2010 transplant [2]. This comprehensive analysis incorporated clinical notes, serial tracheoscopy images, lung function assessments, blood sample analyses to investigate the presence of anti-HLA antibodies, scrutiny of epithelial morphology, evaluation of T cell activity, ki67, and cleavage caspase 3 activity. Additionally, computational fluid dynamic simulations were utilized to assess airflow parameters [2].

During the first-year post-transplantation, the child underwent a series of medical interventions, primarily related to graft instability and its propensity for collapse (Figure 6.).

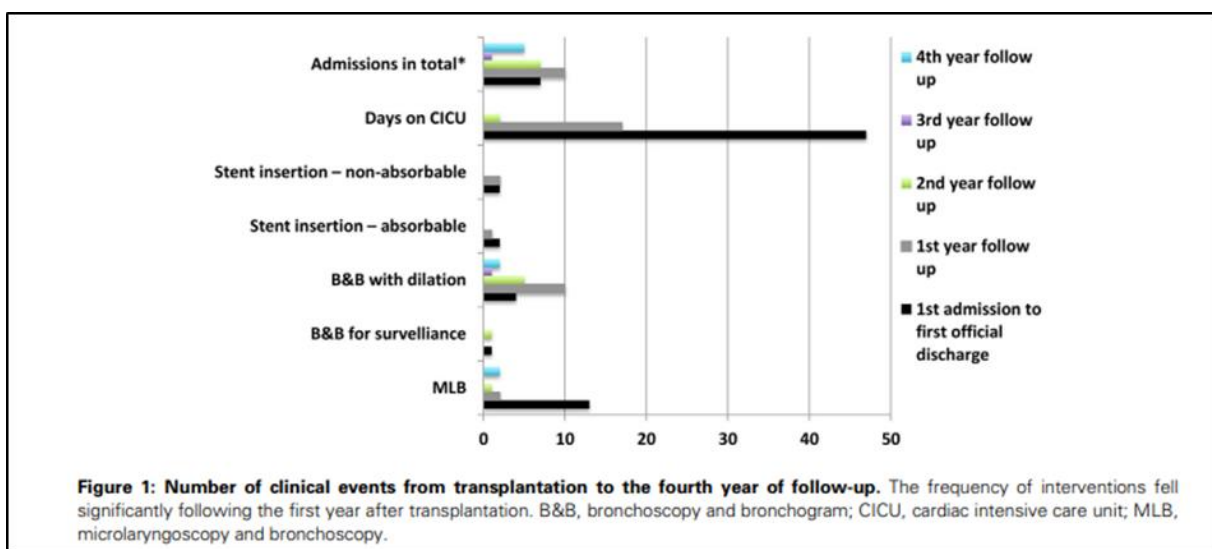


Figure 6. Clinical Events That Child Underwent Until the Fourth Year Follow-Up. Adapted from Hamilton NJ, et.al [3]

These interventions encompassed an eight-day hospitalization period, 25 postoperative procedures to manage secretions and granulation tissue, and the implantation of two bioabsorbable tracheal stents to address malacia of the transplanted trachea. Furthermore, respiratory support was required on four occasions during the initial phase [2]. In August 2010, the child was discharged but necessitated several return visits for additional stent insertions, including one bioabsorbable and two self-expanding nitinol stents. These interventions were necessitated by issues such as retained secretions, granulation of tissue, and the presence of a malacic segment in the distal transplanted trachea [2]. Over the course of the first year of follow-up, there were two additional ICU admissions. After six months post-op, the child's airway had stabilized sufficiently to enable his return to school. During the second year of follow-up, one ICU admission was recorded. In late 2013, the need for repeated interventions

decreased until the emergence of an infection and stenosis within the tracheal stents and the left bronchus necessitated intervention [2]. Nevertheless, beyond the first year, the frequency of interventions declined, and the four-year follow-up indicated that the child had resumed school and maintained an overall good clinical condition [2].

Histological examination of the implant, performed via endoscopy and histocytology, revealed complete mucosal lining regeneration after 15 months, with a differentiated respiratory layer exhibiting no abnormal immune activity. Computational fluid dynamic analysis disclosed a growth restriction within the area of in-stent stenosis. These findings underscored the need for further optimization of tissue-engineered tracheal constructs before formalizing this approach as an established therapeutic modality. However, these observations did not detract from the long-term feasibility of employing decellularized tissue-engineered tracheas as a viable treatment methodology for LSTD in children. Subsequent research should concentrate on developing bioengineered tracheal replacements characterized by reduced morbidity, improved biomechanical attributes, and cost-effectiveness [2].

Several challenges were encountered throughout this case study, including graft malacia, elevated manufacturing and treatment costs, heightened morbidity, particularly within the first-year post-transplant, which necessitated numerous hospital interventions and incurred substantial treatment costs. Furthermore, the imperative to enhance tracheal biomechanics and stability was evident [2]. It is noteworthy that the transplantation of the tissue-engineered tracheal graft was pursued on compassionate grounds as a last-resort measure when conventional therapies had exhausted their utility. This urgent procedure ultimately allowed the child to progress in life, resuming educational activities despite formidable obstacles encountered until graft stabilization was achieved [51]. While this case illustrates the validity of deploying tissue-engineered tracheal constructs under compassionate circumstances in paediatric patients, it remains evident that numerous challenges persist, and the long-term efficacy of this approach necessitates further investigation

CASE III:

In 2017, the third case was documented by Elliott M. et al., showcasing the transplantation of a decellularized cadaveric trachea in a 15-year-old girl. This procedure was coupled with the introduction of autologous bone marrow-derived mesenchymal stromal cells and epithelial cells, conducted on compassionate grounds [72]. The patient had been born with a single left lung and, at the age of 2 months, underwent a tracheoplasty with lateral costal cartilage graft repair. However, this procedure was followed by an inability to extubate and persistent malacia, necessitating the placement of balloon-expandable stainless-steel stents [71]. Subsequently, recurrent stenosis occurred, despite serial balloon dilations, leading to a pericardial patch tracheoplasty at 4 years of age [71]. Unfortunately, the patient faced ongoing challenges, including the formation of recurrent granulation tissue and re-stenosis along the repaired trachea. Initially, conservative management was pursued, but the situation ultimately culminated in the need for a tracheostomy [71]. On the same night as the tracheostomy, the child became reliant on bilevel positive airway pressure (BiPAP) ventilation [71]. Eleven years later, at the age of 15, the patient experienced a respiratory arrest at home, necessitating successful resuscitation. Her clinical condition deteriorated, placing her at risk of further respiratory arrests. Consequently, the consideration of tracheal replacement therapy emerged as a compassionate intervention due to the absence of viable conventional therapeutic options [71].

The procedure involved the use of an allogenic human cadaveric donor trachea, which was decellularized under Good Manufacturing Practice (GMP) compliant conditions. Subsequently, the trachea was ex vivo seeded with expanded bone marrow-derived mesenchymal stromal cells (MSCs) and nasal-derived epithelial cells. The manufacturing process of the tissue-engineered trachea (TET)

adhered to all European regulations governing the production of advanced therapeutic medicinal products (ATMPs) [71]. Following incubation in a static bioreactor, the TET was prepared for implantation. During the implantation process, both proximal and distal ends of the replacement trachea were anastomosed and assessed for air leaks before bypass removal [71]. Due to insufficient omentum resulting from previous surgeries, the possibility of an omentum wrap for pre-vascularization of the tracheal construct was not feasible [71]. Postoperative antibiotics were administered to mitigate the risk of infection [71].

Following the surgery, the trachea was examined and found to be patent, with an intact anastomosed graft. A partially prolapsed trachealis was observed, which improved with positive airway pressure support [71]. Post-surgery, the patient received ventilator support with minimal settings through the tracheostomy. Within 24 hours, the tracheostomy was downsized to an uncuffed fenestrated tube [71]. The patient displayed the ability to consume pureed foods and speak full sentences [71]. Over time, she continued to make progress, with a reduction in ventilator support and the implementation of non-invasive positive pressure ventilation. The patient demonstrated the capacity to walk distances greater than 100 meters, a feat that was previously unattainable. After 13 days, she was discharged from intensive care to her local care center, where she could tolerate up to one hour without intermittent positive airway support. However, on the 15th day post-surgery, the patient experienced ventilatory compromise due to the progression of narrowing within the tracheal graft [71]. An acute extrinsic compressive event was suspected, possibly involving an intrathoracic hemorrhage [71], and regrettably, the patient passed away.

In the course of this investigation, each stage of the reconstructive procedure adhered to the stringent standards mandated by Good Manufacturing Practice (GMP) [71, 72]. Specifically, the donor trachea underwent decellularization utilizing reagents purposefully formulated to comply with GMP criteria. Concurrently, the expansion of autologous bone marrow cells and epithelial cells was conducted within a licensed cell therapy facility. Subsequent to this, the cultured cells were methodically seeded onto the decellularized matrix within a specialized bioreactor, as comprehensively elucidated by Elliott et al. in their 2017 publication [71, 72]. Regrettably, notwithstanding the initially promising outcomes, an acute tracheal obstruction of the posterior wall emerged two weeks post-transplantation, culminating in the untimely passing of the young patient. Faced with this tragic outcome, the authors strongly recommended the incorporation of stents during the initial postoperative months. Furthermore, they emphasized the inherent complexities entailed in the translation of a tissue-engineered reconstructive approach from the controlled preclinical setting to the multifaceted clinical arena, alluding to the inherent limitations of in vivo models in replicating the intricate intricacies of real-world clinical scenarios [71, 72].

In summary, these three cases collectively underscore the potential and challenges associated with tracheal tissue engineering transplants (TETs) in both adult and pediatric patients. **Case I**, involving an adult patient, showcased the implantation of a decellularized cadaveric donor trachea augmented with autologous epithelial cells and bone marrow-derived mesenchymal stem-cell-derived chondrocytes. While initially promising, the case later raised ethical concerns, highlighting the need for more robust and resilient tracheal grafts. **Case II**, involving a pediatric patient, demonstrated the potential of tissue-engineered tracheal grafts for treating large segmental tracheal defects. Despite initial challenges and numerous interventions, the patient's long-term clinical condition improved, emphasizing the value of TETs in compassionate cases. **Case III**, also involving a pediatric patient, highlighted the complexities of tracheal replacement therapy. While the initial procedure showed promise, the patient faced significant complications, ultimately resulting in her unfortunate demise. This case emphasized the importance of careful patient selection and ongoing monitoring in TET procedures.

In all cases, adherence to Good Manufacturing Practice (GMP) standards was critical for the success of the procedures. However, challenges such as graft collapse and complications post-transplantation underscore the need for continued research and refinement of TET techniques to improve patient outcomes. Additionally, the translation of tissue-engineered reconstructive approaches from preclinical settings to clinical practice remains a complex endeavor, necessitating further investigation and consideration of real-world clinical scenarios.

1.2.3.3. TRACHEAL ENGINEERING: CHALLENGES

In the pursuit of tissue engineering solutions for tracheal reconstruction, numerous intricate challenges emerge. As non-communicable diseases become increasingly prevalent and our population continues to age, the demand for functional tracheas is on the rise. However, realizing the potential of tissue engineering in this domain requires a deep understanding of the multifaceted hurdles it presents.

Scientifically, our tools for studying graft development and interactions within the human body are limited, which hampers our progress [73]. Additionally, tracking the behavior of implanted stem cells and their progeny in vivo is currently beyond our capabilities [73]. Bridging the gap between ex vivo incubation and in vivo integration is another crucial area of exploration [74]. Controlling the biomechanical properties of tissue-engineered constructs is essential for their success [74].

Ensuring successful re-epithelialization is vital for preventing complications like stenosis and infections [59]. Vascularization within the graft must be carefully managed to support tissue survival and reduce infection risks [58]. Moreover, recreating a functional blood supply through anastomosis remains a formidable challenge [3]. Enhancing cell retention efficiency and promoting cartilage regeneration are continuous concerns [58]. Also, translational and manufacturing challenges involve tailoring protocols to individual patient needs, making standardization a complex endeavor [10]. For instance, Developing Good Manufacturing Practice (GMP)-compatible bioreactors, or single use bioreactors are pivotal for consistent production [10].

On the operational and implantation front, ensuring graft stability is paramount for maintaining airway patency [58]. The integration of the engineered construct with the surrounding environment remains a mystery [73, 75]. Timely and adequate vascularization is necessary for graft survival and infection prevention [58]. Managing post-operative complications such as scarring, stenosis, and immune rejection is an ongoing challenge [74]. Predicting long-term benefits and understanding patient-specific responses are elusive goals [74]. Additionally, assessing graft growth in pediatric patients poses a unique set of challenges [51]. Evaluating the impact on quality of life and comparing costs are also essential considerations [2]. The lack of safe and effective in vivo monitoring tools further complicates research and development [3].

In addition, the shadow of the Macchiarini scientific misconduct investigations have cast doubt on the field, potentially slowing progress in tracheal reconstruction techniques that hold promise as treatments for previously unsolvable conditions.

When seeking the ideal tracheal substitute, issues emerge with allogeneic implants, which face challenges related to immunological responses, inadequate revascularization, tissue necrosis, graft stenosis, and fibrosis [67]. TET grafts confront hurdles associated with antigenicity, long-term viability,

tumorigenic risks, maintenance of neovascularization, biomechanical properties, and graft-native tissue interface stenosis [67]. Decellularized TET grafts have their own set of challenges, including cell adherence, mechanical support, revascularization, and immunological responses [55]. Choosing the right cell source, type, differentiation stimuli, and scaffold is imperative for successful graft development [55]. Prompt neovascularization is crucial to graft survival and function [61].

In conclusion, tissue engineering for tracheal reconstruction is a complex field but not without promise. Addressing these multifaceted challenges is vital for progress, and considering patient-specific factors is essential. Ethical research practices and rigorous standards are paramount, especially in light of past controversies such as the Macchiarini scandal. Adequate vascularization of tissue engineered constructs specifically the trachea, remains a hurdle to its full translation into the clinic.

1.3. THESIS SUMMARY & GENERAL HYPOTHESIS

The research project titled “Optimization of an Advanced Therapy Medicinal Product (Recellularized Tracheal Scaffold) To Enhance Engraftment and Clinical Functionality” revolves around enhancing vascularisation of a lab grown tissue engineered tracheal construct, with the future aim of the generation of a viable tissue-engineered trachea as a substitute for patients suffering from structural airway diseases (such as large segment stenosis) that are otherwise untreatable by the current standards of care and are subject to high risks of mortality.

The project’s rudimentary concept of tracheal construction is based on Elliot’s et al. [3] concept of tracheal construction and on a former project funded by the European Commission within the Horizon 2020 Research framework program called TETRA (Tissue Engineered Trachea), which focused on around the manufacturing of safe and efficacious clinical grade transplantable tracheas under Good Manufacturing Practice (GMP) conditions. The primary TETRA methodology of tracheal construction was founded on the utilization of a decellularized cadaveric donor tracheal scaffold, seeded with autologous, expanded, mesenchymal stromal cells (MSCs) that were incubated in a bioreactor and subsequently implanted into the recipient. Prior attempts at tissue engineered tracheal transplants utilizing the same, or a similar approach as the TETRA trial have had somewhat clinically satisfactory results. However, they were faced with prolonged duration of maturation and integration of tracheal tissue in vivo, multiple therapeutic visits, and at times, surgical interventions and stenting. Therefore, efforts needed to be made to further develop and optimize the tissue engineered tracheal protocol and manufacturing process, and to provide a final product that is well integrated post-transplant and requires minimal healthcare intervention.

One of the largest impediments to successfully generate functional and long-lasting tissue constructs and implants is sufficient and/or prompt vascularization of the generated construct. Delays in vascularization often lead to the endangerment of the transplants’ cell survival and can ultimately result in graft failure. Thus, the main focus of this PhD project is to further optimize the development of the tissue engineered trachea by enhancing its vascularization capacity while also taking into consideration various translational requirements. Several strategies are to be implemented, some of which include: genetic modification of hBM-MSCs and hDF to overexpress the vascularization factors VEGF and bFGF and the substitution of Foetal Bovine Serum (FBS) with human Platelet Lysate (hPL) in the culture media.

Vascular Endothelial Growth Factor (VEGF) and basic Fibroblast Growth Factor (bFGF) are growth factors that are well known to play a prominent role in vasculogenesis and angiogenesis. They are also a valuable resource for therapeutic angiogenesis approaches[73]. Several studies have indicated that FGF and VEGF have a synergistic effect[74, 75], and that their overexpression has positive results as observed in the rat and rabbit limb ischemia model[76],and with both wound [77] and fracture healing[78]. Also, controlled direct injection of bFGF has shown to significantly promote the growth of tracheal cartilage in the rabbit model[79]. Delayed or insufficient revascularization subsequently results in tissue necrosis characterized by liquefaction and can also lead to graft stenosis and fibrosis [58]. Therefore, it is reasonable to believe that, by enhancing the secretion of both factors into the forming tracheal tissue, enhanced neo-vascularisation of the internally developing tracheal tissue can be achieved (**Hypothesis Number 1**).

Mesenchymal Stromal Cells (MSCs), previously known as 'mesenchymal stem cells'[80], are a heterogeneous population of self-renewing, multipotent cells, with the ability to differentiate into cell types of mesodermal origin such as: chondrocytes, adipocytes, and osteocytes [81, 82]. They can be found in many tissues in the body including: the bone marrow[83], adipose tissue[83], the placenta[84, 85], nervous tissue, umbilical cord[83], and the dental pulp[86]. They have several important features that include their ability to evade and modulate the immune response[87], home to sites of disease or injury, and to secrete bioactive factors[80] that promote tissue repair through paracrine activity of the secreted proteins/ peptides and hormones, transfer of mitochondria to injured cells, and the transfer of exosomes or microvesicles containing RNA and other molecules[87]. MSCs also play a role in aiding the formation of blood vessels[88]. In a xenograft hind limb ischemia model, MSCs engineered to overexpress VEGF strongly induced the migration of endothelial cells and enhanced blood flow resolution[89].

Studies have revealed, that the co-culturing of MSCs with other cell types may have a synergistic effect on the function of the cells. Bone marrow-derived MSCs (BM-MSCs) co-cultured with keratinocytes in a fibroblast-embedded collagen gel showed that epidermal development is strongly influenced by the percentage of co-cultured BM-MSCs[90]. In 2015, a study performed by Fitzpatrick et al., co-cultured MSCs isolated from cord blood and adipose tissue with hepatocytes from donor organs deemed unfit for transplantation resulting in an improved function and viability of the cells. In addition, the co-culture of MSCs with fibroblasts influences dermal fibroblast response to injury and augments fibroblast functions that are critical to wound healing[91, 92]; while fibroblasts on the other hand, have been found to aid in the increase of MSC proliferation[93].

Fibroblasts, another heterogeneous population of cells, are a member of the family of connective tissue cells and are present in almost all human tissues. Fibroblasts play a principal role in the production and refashioning of the Extra Cellular Matrix (ECM) [94]of which different cellular components such as: cartilage cells, fibroblasts, and bone cells are both related and inter-convertible[95]. Similarly, to MSCs, fibroblasts have the ability to secrete paracrine factors that can influence other cells. Fibroblasts play a major role in: maintaining the robustness of skin and tissue homeostasis[96], in protection against infection[97, 98], in wound healing and aging[98-100], and in aiding in angiogenesis[101-103]. Due to their many features, both MSCs and fibroblasts have been an attractive cell source for tissue engineering, particularly, tracheal tissue engineering[25, 104-106]. Therefore, we hypothesize, that the co-culturing MSCs and Fibroblasts may supplant the need for

utilizing genetic modification tools to enhance angiogenesis stimulating factors VEGF or bFGF. Alternatively, if one or both are genetically enhanced and co-cultured, then that may lead to further secretion of both factors into the forming tracheal tissue, and subsequent further augmentation of neo-vascularisation of the internally developing tracheal tissue (**Hypothesis Number 2**).

Notably, to achieve a suitable dose for manufacturing of products intended for clinical application, many regenerative cell types such as mesenchymal progenitor cells, require propagation and cellular expansion due to their low frequency of occurrence [107].

Foetal Bovine Serum (FBS) and/or other supplements containing animal derivatives are currently the standard cell culture media supplement for the expansion of different cell types such as MSCs and fibroblasts[108-110]. However, the use of FBS and other supplements with animal derivatives is strongly discouraged by regulatory authorities, as such supplementation presents various issues in terms of lack of standardization during preparation resulting in batch-to-batch variability (and ultimately leading to discrepancy in cell culture performance), xenogeneity, risks related to transmission of diseases[111], concerns in regards to procurement methods and animal welfare, and general global availability. This has resulted in an urgent need for suitable human alternatives for the manufacture of clinical cell therapeutic products and has become even more important within the context of the exponentially growing field of regenerative therapies. Several studies have been employed on proving the efficacy of using human derivatives such as human Platelet Lysate (hPL) and other lysate preparations (e.g. Platelet, Rich Plasma, PRP) as a substitute for regular growth serums of xenogeneic origin like FBS[112-115].

hPL is cell-free and highly enriched in thrombocytic growth factors while exhibiting low contents of plasma proteins such as immunoglobulins, albumin, and fibrinogen[116]. Investigations have indicated that culturing cells with hPL results in an increase in proliferation, a decrease in population doubling time while maintaining clonogenicity, characteristic immunophenotype, *in vitro* lineage differentiation capacity, and other specific cell characteristics such as: *in vitro* T cell immunosuppressive capability. MSCs and fibroblasts have also presented an increase in Colony Forming Unit–Fibroblast (CFU-F) size. More importantly, hPL has proven to maintain cell functionality without an increase in genomic instability[117]. Some of the different cell types that have displayed increased cell survival and expansion potential when being cultured in human platelet lysate and/or other lysate preparations include: periodontal ligament cells[118], tendon cells[119], osteoblast-like cells[120], skin fibroblasts[121], chondrocytes[122], endothelial cells[123], in addition to multipotent cells such as adipose-derived stem cells and mesenchymal stromal cells[107, 124, 125].

In order to enhance the secretion of bFGF and VEGF and thus, achieve angiogenic augmentation in the tracheal construct, hBM-MSCs and human dermal fibroblasts (hDF) will be genetically modified via electroporation to transiently overexpress bFGF and VEGF as described Zhang, Z. & Slobodianski, A, 2011[126]. Upon transfection, cells will be seeded onto human/porcine decellularized tracheal scaffolds, incubated, analysed, and successively tested in an *in vivo* setting. However, genetic modification of cells via means of transfection such as electroporation often leads to high low cell viability post transfection. In most protocols, high transfection efficiency coincides with low cell survival and vice versa[127-131]. This poses a great challenge when designing protocols that require high amounts of transient factor delivery for regenerative purposes as most of the cells do not survive the modification procedures. For successful genetic modification, quality control, seeding onto the

tracheal scaffold, and achieving enhanced vascular development in an *in vivo* environment, a substantial quantity of viable, metabolically active transfected cells is essential.

Given all the different attributes of hPL in maintaining cell functionality, genomic stability, and increasing expansion rates while decreasing cell population doubling time, we postulate that culturing cells with hPL throughout the transfection procedure may result in better outcomes in terms of cell count, viability and transfection rates. Also, given that hPL is an improved derivative of PRP [132, 133] and that PRP has proven to have positive results in propagating angiogenesis and cellular differentiation towards mesodermal lineages [134-136], one may hypothesize that culturing the cells with hPL throughout the manufacturing procedure (including seeding onto tracheal scaffold and incubation in the bioreactor), and then subsequently implanting the seeded scaffold in an *in vivo* setting may result in enhanced angiogenesis and/or tissue development within the tracheal construct when compared to culturing them with FBS. **(Hypothesis Number 3).**

Cellularization or recellularization of grafts remains a significant challenge in tissue engineering for clinical applications. This challenge involves ensuring that cells can effectively infiltrate and adhere to the scaffold, achieve even distribution, and survive the necessary incubation period. This incubation period is critical for enabling blood vessel growth and nutrient supply, which in turn allows for the development of more advanced and functional tissues [63, 137, 138]. Adequate cell seeding has been established as a crucial factor in achieving functional tissues [139]. Various seeding techniques have been explored to enhance cell engraftment. These techniques can be broadly categorized as dynamic or static. Dynamic seeding methods aim to promote cell attachment through mechanical means, while static methods, such as direct seeding, rely on gravity for cell attachment [140]. Another approach is cell encapsulation, which is a quasi-static seeding technique where cells are embedded within a biomaterial like alginate to protect them during the seeding process [140]. Alginate, a hydrogel known for its biocompatibility, biodegradability, and pro-angiogenic properties, is commonly used for cell encapsulation [140].

Despite extensive research on decellularization protocols, *in vivo* decellularized scaffolds have encountered challenges related to airway stenosis due to compromised cartilage [8, 13]. Attempts at recellularization have not yielded successful outcomes, casting doubt on the feasibility of this approach in recent clinical studies [56]. Alginate stands out as the predominant biomaterial for cell microencapsulation and is the primary choice for clinical applications. It is an encapsulation matrix that has been approved for human use by the U.S. Food and Drug Administration (FDA) [141-143]. Alginate-based biomaterials have found wide application in tissue engineering and regenerative medicine due to their favourable characteristics, including biocompatibility, biodegradability, and the ability to form hydrogels [144-147]. Alginate has been employed in various applications, such as drug and gene delivery, cancer theranostics, antimicrobial agents, wound healing, and as carriers for tissue engineering [144]. Its properties make it particularly suitable for bone tissue engineering and bioprinting, as it possesses features like gelling ability, biocompatibility, and mechanical strength [147]. Alginate-based scaffolds have also been used for drug delivery in tissue engineering, including the fabrication of 3D scaffolds like sponges, foams, microspheres, and injectables [146]. Additionally, alginate hydrogels can be customized to enhance their performance as 3D microenvironments for cells [148]. Therefore, we hypothesized that by encapsulating the hBM-MSCs and the hDF with alginate, then seeding the cells onto trachea previously soaked with calcium buffer, the alginate would solidify and retain the seeded cells, thereby bypassing cell run-off, maintaining a higher seeding density, and ultimately improving the overall construct's performance. **(Hypothesis Number 4).**

Thus, taking into consideration the above, four main hypotheses will be implemented to further optimize the development of the tissue engineered tracheal construct:

Hypothesis 1: By transiently genetically altering human dermal fibroblasts and/or bone marrow derived MSCs to produce higher concentrations of bFGF and/or VEGF and seeding them onto the trachea, we may be able to enhance the formation of the inner tracheal vasculature; and thereby increase the likelihood of graft survival and integration.

Hypothesis 2: By culturing MSCs and human dermal fibroblasts in hPL we can find an adequate, and GMP compliant, replacement for FBS that will expand cells quickly, and maintain them enough to be able to achieve higher numbers of viable and robust cells. Thus, surmounting challenges related to critical time point definitions due to the duration required for cellular expansion with FBS and possible further cellular, vascular, and tissue development in comparison to the original protocol received from the TETRA project “**Reference Protocol**”.

Hypothesis 3: By co-culturing bone marrow derived human mesenchymal stromal cells with human dermal cells, we will achieve a synergistic effect that may lead to an enhancement of factor secretion from both cell types, and thus, further development in the tracheal tissue engineering protocol.

Hypothesis 4: By encapsulating the cells in an alginate hydrogel and seeding the hydrogel onto trachea soaked in calcium buffer, we would be able to retain all the seeded cells, and would also lead to an enhancement of grow factor and/or paracrine factor secretion of the cells. Thus, leading to better engineering outcomes.

Either one, or a combination of the prior hypotheses, followed by subsequent incubation, and transplant in an *in vivo* setting will result in an enhancement of the formation of the inner tracheal vasculature; and thereby increase the likelihood of graft survival and integration.

THESIS SCOPE AND OBJECTIVES

Primary Objective:

To identify, study, and subsequently translate opportunities of optimizing the Tissue Engineered Trachea for autologous use, focusing on vascularization and ultimately aiming at aiding in tissue integration and engraftment

Secondary Objectives:

1. To investigate the effect of hPL replacement of FBS with regards to the tissue engineering process
2. To investigate the impact of transient genetic modification on the vascularisation of the trachea
3. To develop a protocol that would aid in the vascularisation of trachea or tissues of similar structure.

2. CHAPTER II: MATERIALS & METHODS

2.1. REAGENTS & MATERIALS

2.1.1. MEDIA PREPARATIONS

For parallel testing of the effects of the media additives on the cells different media preparations were made

MEDIA FOR BONE MARROW-DERIVED MSC CULTIVATION:

Complete Media 1 (CM1): 500 ml Alpha MEM Eagle w/o L-glutamine (PAN - Biotech, Germany) prepared with 10% Fetal Bovine Serum (FBS) (Gibco™, ThermoFischer Scientific, Germany) + 1% L-glutamine (Capricorn Scientific, Germany) + 1% antibiotic/antimycotic (ab/am) X100 (Capricorn Scientific, Germany)

Complete Media 2 (CM2): 500 ml Alpha MEM Eagle w/o L-glutamine (PAN - Biotech, Germany) prepared with 5% hPL (University Hospital Ulm, Institute for Clinical Transfusion Medicine and Immunogenetics, Germany) + 1% ab/am (Capricorn Scientific, Germany) + 1IU/ml of Heparin-Natrium-25000 (Catalogue #PZN-3029843, Ratiopharm, Germany).

Washing Media 1 (WM1): 500 ml Alpha MEM Eagle w/o L-glutamine (PAN - Biotech, Germany) prepared with 1% L-glutamine (Capricorn Scientific, Germany) + 1% ab/am (Capricorn Scientific, Germany)

MEDIA FOR DERMAL DERIVED FIBROBLAST CULTIVATION:

Complete Media 3 (CM3): 500ml DMEM w: 4.5 g/L Glucose and w: st. Glutamine (PAN - Biotech, Germany) prepared with 10% FBS (Gibco™, ThermoFischer Scientific, Germany) + 1% am/am (Capricorn Scientific, Germany)

Complete Media 4 (CM4): 500 ml DEMM w: 4.5 g/L Glucose and w: st. Glutamine (PAN - Biotech, Germany) prepared with 5% hPL (University Hospital Ulm, Institute for Clinical Transfusion Medicine and Immunogenetics, Germany) +1% ab/am (Capricorn Scientific, Germany) + 1IU/ml of Heparin-Natrium-25000 (Catalogue #PZN-3029843, Ratiopharm, Germany).

Washing Media 2 (WM2): 500 ml DEMM w: 4.5 g/L Glucose and w: st. Glutamine (PAN - Biotech, Germany) prepared with 1% ab/am (Capricorn Scientific, Germany).

Dermal Fibroblast Media (DFM): 500 ml of Dermal fibroblast Media (Promocell, Germany) + supplement (Promocell, Germany) + 1% ab/am (Capricorn Scientific, Germany).

MEDIA FOR 3T3 Mouse cells:

Complete Media 8 (CM8): 500ml DMEM w: 4.5 g/L Glucose and w: st. Glutamine (PAN - Biotech, Germany) prepared with 10% FCS + 1% am/am (Capricorn Scientific, Germany).

DIFFERENTIATION MEDIA:

Osteogenic Differentiation Media (ODM): 90ml of StemPro™ Osteocyte/Chondrocyte Differentiation Basal Medium (Gibco™, ThermoFischer Scientific, Germany) + 10 ml of StemPro™ Osteogenesis Supplement (Gibco™, ThermoFischer Scientific, Germany) + 0.5% ab/am (Capricorn Scientific, Germany).

Chondrogenic Differentiation Media (CDM): 90ml of StemPro™ Osteocyte/Chondrocyte Differentiation Basal Medium (Gibco™, ThermoFischer Scientific, Germany) + 10 ml of StemPro™ chondrogenesis Supplement (Gibco™, ThermoFischer Scientific, Germany) + 0.5% ab/am (Capricorn Scientific, Germany).

Adipogenic Differentiation Media (ADM): 90ml of StemPro™ Adipocyte Differentiation Base Medium ((Gibco™, ThermoFischer Scientific, Germany) + 10 ml of StemPro™ Adipogenesis Supplement + + 0.5% ab/am (Capricorn Scientific, Germany).

COCULTURE MEDIA (CocM):

Coculture Media 1 (CocM 1): 50:50 ratio of (CM1): 500 ml Alpha MEM Eagle w/o L-glutamine (PAN - Biotech, Germany) prepared with 10% Fetal Bovine Serum (FBS) (Gibco™, ThermoFischer Scientific, Germany) + 1% L-glutamine (Capricorn Scientific, Germany) + 1% antibiotic/antimycotic (ab/am) X100 (Capricorn Scientific, Germany) & **(CM3):** 500ml DMEM w: 4.5 g/L Glucose and w: st. Glutamine (PAN - Biotech, Germany) prepared with 10% FBS (Gibco™, ThermoFischer Scientific, Germany) + 1% am /am (Capricorn Scientific, Germany)

Coculture Media 2 (CocM 2): 50:50 ratio of (CM2): 500 ml Alpha MEM Eagle w/o L-glutamine (PAN - Biotech, Germany) prepared with 5% hPL (University Hospital Ulm, Institute for Clinical Transfusion Medicine and Immunogenetics, Germany) + 1% ab/am (Capricorn Scientific, Germany) + 1IU/ml of Heparin-Natrium-25000 (Catalogue #PZN-3029843, Ratiopharm, Germany) & **(CM4):** 500 ml DEMM w: 4.5 g/L Glucose and w: st. Glutamine (PAN - Biotech, Germany) prepared with 5% hPL (University Hospital Ulm, Institute for Clinical Transfusion Medicine and Immunogenetics, Germany) +1% ab/am (Capricorn Scientific, Germany) + 1IU/ml of Heparin-Natrium-25000 (Catalogue #PZN-3029843, Ratiopharm, Germany).

2.2. CELLULAR PROCUREMENT

2.2.1. Donor Cell Inclusion and Exclusion Criteria

	Tissue Type	Inclusion Criteria	Exclusion Criteria
1	Human Bone Marrow	Age: 18-45	Age: ≤18 years and ≥ 45 years
2		Healthy patients with no disease that may result in marring bone marrow functions and/or patients in remission	Leukemia, Bone Marrow Failure, other disease impacting bone marrow integrity.
3		Infectious Disease Negative (ex. HIV I/II, HCV, HBV, HAV, and Syphilis)	Patients positive for infectious diseases
1	Human Dermal Fibroblasts	Age: 18-45	Age: ≤18 years and ≥ 45 years
2		Preferably healthy patients and/or patients with no known conditions to affect skin in any aspect	Diabetes- Autoimmune diseases- cancers affecting skin- and other skin related afflictions
3		Infectious Disease Negative (ex. HIV I/II, HCV, HBV, HAV, and Syphilis)	Patients positive for infectious diseases

Table 1. Donor Inclusion and Exclusion Criteria.

Number of participants:

Bone Marrow: a minimum of 8 donations were obtained from otherwise healthy patients as described above with the required ethical approval and consent forms (ethical vote # 329/10, ethics committee, University Hospital Frankfurt am Main).

Human Dermal Fibroblasts: 6 donor fibroblasts from 6 different donors were purchased for these experiments.

2.2.2. ISOLATION, EXPANSION, AND CRYOPRESERVATION OF CELLS

2.2.3. ISOLATION AND CULTIVATION OF PRIMARY HUMAN BONE MARROW-DERIVED MESENCHYMAL STROMAL CELLS (MSCS)

Human bone marrow filters and samples were obtained from bone marrow donations made by healthy individuals under the required ethical approval

Filters containing bone marrow (BM) residue from leftover healthy BM donations, were flushed using sterile DPBS w/o: Ca and Mg (PAN – Biotech, Germany). After washing the filters 3-4 times with DPBS w/o: Ca and Mg (PAN – Biotech, Germany) and collecting the diluted BM in 50ml falcon tubes (CELLSTAR®, Greiner Bio-One GmbH, Germany), 10-15ml of Lymphoprep was pipetted into the bottom of tube (under the bone marrow diluted with PBS) resulting in an overlay of bone marrow over the

Lymphoprep. The tubes were then centrifuged (Rotanda 460R, Hettich, Germany) 400G/RCF for 30 minutes at 20C° (without brakes) to allow for density gradient separation of the bone marrow (Figure 7.). Ensuing centrifugation, four layers were observed: the dark-red, red blood cell (RBC) layer, followed by the clear lymphoprep layer, then milk-white buffy-coat layer (containing all the white blood cells -WBCs), and finally a yellow transparent layer of plasma. The buffy-coat layer was carefully collected into another tube using a serological pipette and was washed x 2 with washing media 1 (WM1) consisting of 500 ml Alpha MEM Eagle w/o L-glutamine (PAN - Biotech, Germany) prepared with 1% L-glutamine (Capricorn Scientific, Germany) + 1% ab/am (Capricorn Scientific, Germany) and centrifuged (Rotanda 460R, Hettich, Germany) each time at 1200rpm for 5 minutes, at 20C° (without brakes). After washing, the cells were re-suspended in 10ml of WM1 and promptly counted by taking 10 µL of the cell suspension and placing it into an Eppendorf tube with 140 µL of Türk's solution (cell suspension to Türk's solution dilution ratio 1:15). Türk's solution is a hematological stain that allows for white blood cell count by destroying red blood cells and platelets and staining the nuclei of white blood cells. The solution was mixed and allowed to stand for 2-3 minutes before mixing again and counting using a C-Chip hemocytometer (NanoEnTek Inc.,Korea).

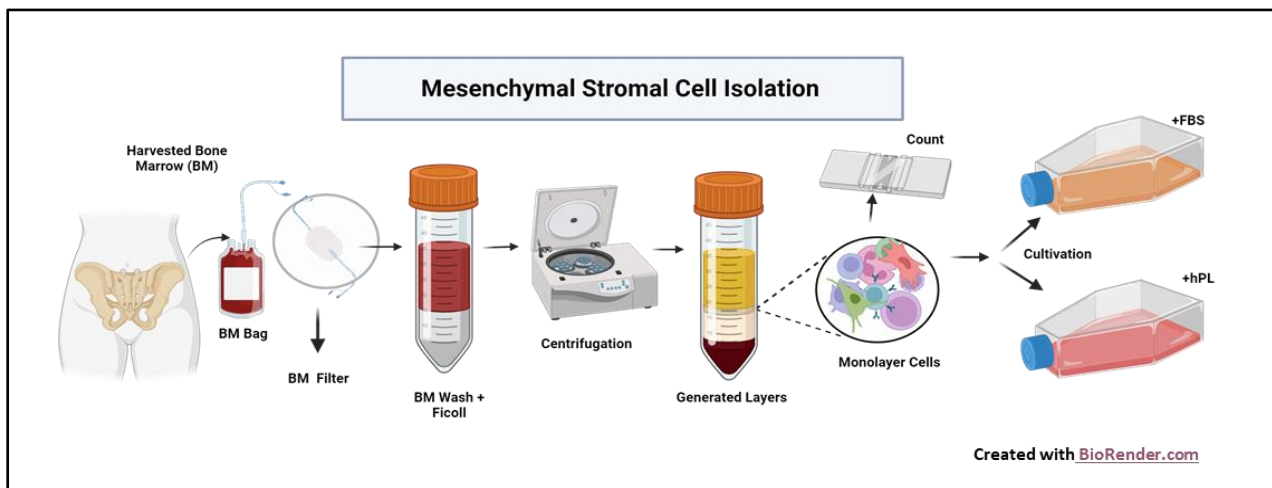


Figure 7. Figure. Process of Isolating Primary Human Mesenchymal Stromal Cells from Bone Marrow.

Harvested Bone marrow (normally from the upper iliac crest) is placed into bone marrow bags for infusion. The bone marrow (BM) passes through a filter, and the filter is what is used for MSC collection. Wash generated from filter is placed in a tube with lymphoprep/ficoll and centrifuged. The buffy layer (monolayer containing WBS) is collected, counted, and plated accordingly.

Cells in the four upper corners of the were counted and averaged and the total cell count in the suspension was accessed according to the following equation:

$$\begin{aligned}
 \textit{Total cell count} &= \textit{average of four corners} \times \textit{volume of cell suspension} \\
 &\times \textit{dilution factor} \times 10^4
 \end{aligned}$$

If further dilution was required to be able to count the cells, then the total cell count was assessed as follows:

Total cell count

$$= \text{average of four corners} \times \text{volume of cell suspension} \\ \times \text{dilution factor} \times 10^4$$

After counting, the cells were promptly split in half, into two 50ml tubes (CELLSTAR®, Greiner Bio-One GmbH, Germany), spun down at 1200 rpm for 5 minutes at 20C° (with brakes) , WM1 was decanted and one tube was re-suspended in Complete Media 1 (CM1) containing: 500 ml Alpha MEM Eagle w/o L-glutamine (PAN - Biotech, Germany) prepared with 10% Fetal Bovine Serum (FBS) (Gibco™, ThermoFischer Scientific, Germany) + 1% L-glutamine (Capricorn Scientific, Germany) + 1% antibiotic/antimycotic (ab/am) X100 (Capricorn Scientific, Germany); while the other was resuspended in Complete Media 2 (CM2) containing: 500 ml Alpha MEM Eagle w/o L-glutamine (PAN - Biotech, Germany) prepared with 5% hPL (*University Hospital Ulm, Institute for Clinical Transfusion Medicine and Immunogenetics, Germany*) + 1% ab/am (Capricorn Scientific, Germany) + 1IU/ml of heparin at a concentration of 12000 . The tubes containing cells suspended in different media, were further spilt in equal volumes to seed T-175 flasks (details) with a seeding density between at a minimum of 100,000 cells per cm²-240,000 cells per cm² per flask. Number of flasks to seed and the required volume per flask was based on the following equations:

Number of cells for a required cell conc. (per cm²) w. specific flask size =

$$\text{Size of flask} \times \text{required seeding density per cm}^2 \left(\text{ex. } 6000 \frac{\text{cells}}{\text{cm}^2} \right)$$

Number of Flasks to seed =

$$\text{Total number of cells in suspension} \div \text{Number of cells required for a cell conc.}$$

Flasks seeded with cells that were suspended in CM1, each contained 20ml of CM1; while those corresponding seeded with the cell suspension in CM2, each contained 20ml of CM2. All flasks were placed in cell incubators at 37 ° C +/- 2 ° C, 5% CO² +/- 1%, and passive humidification. After 24 hours, a media change was made for all flasks. Then, the media was changed every 2-3 days for CM1, and every 5-7 days for CM2. Ensuing expansions were carried out accordingly.

2.2.4. COUNTING AND EXPANSION OF CELLS

2.2.4.1. Automated Cell Counting - CASY® Counter

An automated multi-parameter cell counter, the CASY® counter (Innovatis, OLS OMNI Life Science, Germany) relies on the pulsation of an electric field throughout a column of passing cells and particles with a defined pore size. This in turn, generates a high resistance signal that varies according to their size and conductivity. Dying cells generate much lower resistance and signal due to their disrupted cell membranes. Based on an equation that calculates the Integral (which is directly proportional to the cell size and differs between debris, dead, and live cells), the CASY® (Innovatis, OLS OMNI Life Science, Germany) provides precise information on the viability

percentage, the total cell count /ml (number of live/dead cells), the amount of viable cells/ml and amount of cell debris (among others).

To calculate the total number of viable cells in a cell suspension, 100µl of the cell suspension was placed in a defined volume of 10mls of CASY[®]ton, the obtained result from the CASY[®] counter (Innovatis, OLS OMNI Life Science, Germany) was then multiplied with the original volume of the cell suspension according to the below formula:

Total Number of Viable Cells in Cell suspension

$$= \text{Number of viable } \frac{\text{cells}}{\text{ml}} \times \text{the volume of the original cell suspension}$$

2.2.4.2. Manual Cell Counting -Trypan Blue (Sigma-Aldrich, USA)

When warranted, manual counting of cells to obtain the total cell number, and percentage, of viable cells was performed via Trypan blue staining of cells. Dead or dying cells allow the dye to seep into the cellular cytoplasm, thus, allowing for cells to be stained blue. Living and healthy cells with an intact cellular membrane however, retain non-stained and luminescent characteristics under brightfield microscopy. Trypan blue was prepared by diluting 1:2 in 0.9% NaCl (Carl Roth, Germany) Or used directly Trypan Blue Solution 0,4% (Sigma-Aldrich, USA)

For manual counting:

Cell suspensions were diluted 1:2 with Trypan blue solution and 10µl of the stained cell suspension was taken and injected into Neubauer chamber. Cells of the four Neubauer chamber quadrat were counted (live cells unstained, dead cells blue) and the cell number/ml and viability were calculated according to the following equations:

$$\text{Cell } \frac{\text{number}}{\text{ml}} = \text{average of 4 quadrat – corners} \times 2 \times 10^4$$

Total Number of Vible Cells

$$= \text{average of 4 quadrat corners (unstained cell counts)} \times \text{cell susp. vol.} \\ \times \text{trypan blue dil. factor (2)} \times 10^4$$

Total Number of Dead Cells

$$= \text{average of 4 quadrat corners (stained cell counts)} \times \text{cell susp. vol.} \\ \times \text{trypan blue dil. factor (2)} \times 10^4$$

$$\text{Viability \%} = \frac{\text{Total N. of viable cells}}{\text{Total N. of cells (dead \& alive)}} \times 100$$

2.2.5. THAWING OF CELLS

Cryopreserved cells either purchased or obtained were thawed in complete media containing a 10% serum additive. Cryopreserved MSCs designated for cultivation with 5% hPL (University of Ulm, Germany) were thawed using 10% hPL as a serum additive to aid in cell

recovery post-thaw. Cryopreserved cells held in liquid nitrogen (LN2) at -196 C° were warmed in a water bath at 37C° until a small amount of ice was left in the vial.

With primary MSC isolations at passage 0, the contents of the vials were quickly removed and resuspended in a 15ml falcon tube with **WM1** of which 100µl was taken for counting with the CASY® Counter (Innovatis, OLS OMNI Life Science, Germany). The remaining cell suspension was split into two tubes concurring to the calculated number of flasks and their corresponding media, and then centrifuged (Rotanda 460R, Hettich, Germany) at 1200 rpm for 5 minutes at 20C°. After which, the supernatant was discarded and the cells were plated accordingly.

Otherwise, all other thawed cells were directly plated in a T-75 (Greiner Bio-One, Germany) with prewarmed complete media. The following day, a media change was made for all conditions.

2.2.6. EXPANSION OF PRIMARY BONE-MARROW DERIVED MSCS

Cultivated cells were examined microscopically every two days under a brightfield microscope (Zeiss, Germany). Upon achieving 80%-90% confluency, cells were detached using Trypsin 0.25 %/EDTA 0.02 % in DPBS, w/o: Ca and Mg (PAN – Biotech, Germany). The cells were first washed with DPBS (PAN – Biotech, Germany), and then 5ml, 3ml, or 1ml of trypsin (PAN – Biotech, Germany) was added to a T-175, T-75, or T-25 flask respectively. The flasks were then incubated for 5 minutes at 37 ° C +/- 2 ° C, 5% CO² +/- 1%, with passive humidification. Afterwards, they were washed with WM1. MSCs are well known to be a heterogenous population of cells. When they are expanded in vitro, their cell population is a mix of stem cells, progenitor cells, and differentiated cells [137]. Therefore, in order to maintain this heterogeneity and avoid the concentration of one cell type in an expansion lineage, all harvested cells were pooled into one 50ml tube (CELLSTAR®, Greiner Bio-One GmbH, Germany) and promptly counted using the CASY® Counter (Innovatis, OLS OMNI Life Science, Germany). Calculations were made to seed the flasks at a density of either 6000 cells/cm² or 3000 cell/cm² depending on the initial post-isolation or post-thaw cell counts. The first seeding after isolation was designated P0, and subsequent harvests and seedings were designated accordingly. Cellular growth kinetic were monitored throughout the expansion process, and parameters assessed included:

- Cellular Morphology
- Confluency
- Total Cells Counts
- Cell viability
- Population doubling Time and Population doubling levels.

The expansion procedure of MSCs was the same for the two types of media steps: **CM1** & **CM2**, and followed the same steps (Figure.8)

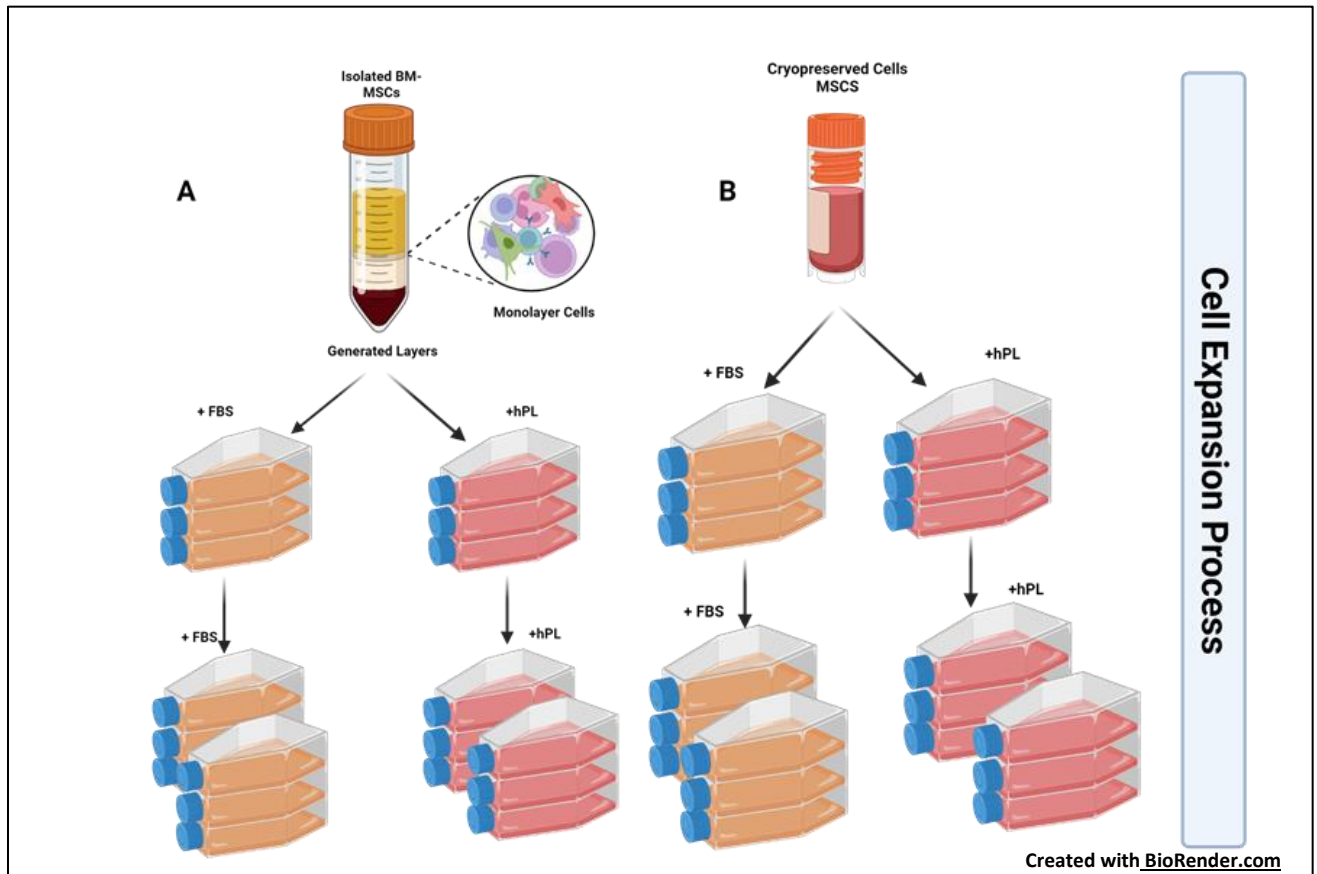


Figure 8. Process of MSC cell expansion using cultivation medias. A. Process of expanding cells after isolation from BM using CM1 + FBS and CM2 +hPL. **B.** Process of expanding cells post-thaw using CM1 + FBS and CM2 +hPL.

2.2.7. PROPAGATION OF HUMAN DERMAL FIBROBLAST

Primary human dermal fibroblasts (HDF) were purchased at passage number (0 or 1) from (Promo-cell, Germany) with the following characteristics: healthy individuals with no known underlying disease, of an age group between 18- 59 years of age (n=6), 4 males and 3 females. Dermal fibroblasts were isolated from various locations in the body.

After thawing the vials with HDF, the cells were directly plated onto a T-75 flask with dermal fibroblast media (DFM) and placed into an incubator at 37 °C +/- 2 °C, 5% CO² +/- 1%, with passive humidification. The next day, a media change was made. Cells were monitored till they reached a confluency of 90-100% after which they were trypsinized using Trypsin 0.25 %/EDTA 0.02 % in DPBS, w/o: Ca and Mg (PAN – Biotech, Germany) for 5 minutes in an incubator. Trypsinization was stopped using WM2 and the cells were counted, centrifuged (Rotanda 460R, Hettich, Germany) at 1200 rpm for 5 minutes at 20C° (without brakes), then resuspended in **CM3** and **CM4** to be further expanded similarly to MSC expansion.

2.2.8. CRYOPRESERVATION OF CELLS:

MSC and NHD cryopreservation was performed by suspending cells in CM + 10% Dimethyl sulfoxide (DMSO) + 10% Human Serum Albumin (HAS). The cells were then placed in Mr. Frosty containers (Thermo Scientific, USA) which are designed to achieve a cooling rate of $-1^{\circ}\text{C}/\text{minute}$ after being placed in a -80°C freezer. The next day, the samples were moved for storage in a liquid nitrogen vapor phased container until further use.

2.1.8. CELL AGE AND GROWTH KINETICS:

Cell age is indeed a critical quality control parameter with direct implications for cell performance and, consequently, the outcomes of any study [138, 139]. Traditionally, the passage number of cells has been employed as a surrogate measure of cell age. However, it has become increasingly evident that the passage number alone does not provide an accurate representation of a cell's true age or condition. To more accurately assess cell age, the growth kinetics of mesenchymal stem cells (MSCs) and dermal fibroblasts (DF) have been monitored.

A. Counting and Expansion of Cells:

Cell counts and viability % were obtained using the automated CASY[®] counter (Innovatis, OLS OMNI Life Science, Germany) (unless stated otherwise) and the total number of cells, cell recovery, and the population doubling time (PDT), the population doubling level (PDL), and the cumulative population doubling level (cPD) were estimated according to formulas provided by Spohn, G. et.al.[140] and Agostini, F. et.al [128]

using the following equations:

Cell Recovery or MSC Yield:

MSC cell recovery after primary seeding of bone-marrow onto flasks, was denoted as the amount of adherent fibroblast-like cells to flasks surfaces. It was calculated as follows:

$$\% \text{ of Recovered Cells} = \frac{\text{Total cells counted after first trypsinization}}{\text{Total cells initially seeded onto flasks}} \times 100$$

Where the total cells initially seeded onto flasks signifies the total number of seeded cells at the initial plating of bone-marrow and the total cells counted after trypsinization indicates the cells collected after the first passage.

Cell Population Doubling Time (PDT):

Defined as the duration required for cell population to double in size [141]. PDT for exponential growth cultures was calculated as follows:

$$PDT = \ln(2) \div \text{growth rate} \quad [140]$$

Where "ln" is natural logarithm and the growth rate is calculated by:

$$\text{Growth Rate} = \frac{N(t)}{N(0)} \div t \quad [140]$$

$N(t)$ is cells at time t , $N(0)$ is cells at time 0, and t is time in culture.

$$PDT = t \times \ln(2) \div \ln\left(\frac{N(t)}{N(0)}\right) \quad [140]$$

Or

$$PDT = \text{culture time} \times \ln(2) \div \ln\left(\frac{\text{cell number}_{\text{harvest}}}{\text{cell number}_{\text{seeded}}}\right) \quad [128, 140]$$

Cell Population Doubling Level (PDL) & Cumulative Population Doubling Level (cPDL):

The population doubling level describes the total number of times cells in a specific population have doubled since their initial isolation. The more the cells replicate, the higher the likelihood that they will undergo change in phenotype and in function.

For the first passage, the population doubling number was calculated as:

$$N = N^0 \times 2^n \quad [140]$$

N =final cell number, N_0 = initial cell number, n = the number of generations, and:

$$n = 3.322(\log N - \log N^0) \quad [140]$$

For the cumulative population doubling level (**cPDL**) or the population doubling levels following the primary population doubling calculation however, the following equation was used:

$$cPDL = 3.322 \times (\log(\text{cell number}_{\text{harvest}}) - \log(\text{cell number}_{\text{seeded}})) + X \quad [140]$$

X = the population doubling level of previous passage.

2.1.9. CULTIVATION OF 3T3 Cells

Mouse embryonic fibroblast cell line 3T3 was thawed, resuspended in CM1, and incubated at 37 ° C +/- 2 ° C, 5% CO₂ +/- 1%, and passive humidification. The next day, the media was changed to fresh media, and the cells were split every 3 days.

2.3. CHARACTERISATION OF CELLS (MSCs and DFs)

2.3.1. Flow Cytometry Cell Immunophenotyping

As part of the International Society for Cellular Therapy and Gene Therapy's (ISCT) minimum criteria for the identification of human bone marrow-derived MSCs [82], MSC cell expression of the following panel of cell surface markers was examined using the Human MSC Analysis Kit (BD Stemflow™, BD Biosciences, USA): Positive Markers CD90 FITC, CD105 PerCp-Cy5.5, CD73 APC, Negative Markers CD34 PE, CD 11b PE, CD19 PE, CD45 PE, HLA DR PE. In addition to these markers, CD44 PE (BD Stemflow™, BD Biosciences, USA), CD146 PE-CY™7 (BD Pharmingen™, BD Biosciences, USA), CD271 V450 (BD Horizon™ BD Biosciences, USA), and CD106 BV510 (BD OptiBuild™, BD Biosciences, USA).

The process of flow cytometry analysis began with the harvest of adherent cells from flasks using a mild dissociation agent, Accutase (PromoCell, Germany) for 3 minutes. Then, the reaction was stopped using washing media (depending on the cell type), and the cells were spun down at 1200g, for 5 minutes at 20C. The supernatant was discarded, and the cells were resuspended in complete media (with serum) and counted using the CASY® Counter (Innovatis, OLS OMNI Life Science, Germany).

Then, (unless the availability of cells was a limiting factor) a minimum of 1×10^6 cells were counted for each staining procedure. After cells were counted, and the required volume was collected, the cells were spun down once again at 1200g, 20C, for 5 minutes, the supernatant discarded and they were subsequently resuspended in BD Pharmingen™ Stain Buffer (BD Biosciences, USA). Staining of the cells was performed in accordance to the below panel (Table.2).

Panel	Tube #	Marker	Clone	Conjugate Fluorophore	Excitation Laser (nm)	Emission Bandpass	Company	Comments	
Compensation Single Stains	1	CD 90	5E10	FITC	FL-1	525/10	BD Stemflow™, BD Biosciences, USA	Positive Single Stains Mouse Anti-Human + Viability	
		DRAQ7™ Dye	-	Viability	FL-7 Or FL-8	725/20	Invitrogen™ ThermoFisher SCIENTIFIC, USA		
	2	CD 105	266	PerCp-Cy5.5	FL-4	695/30	BD Stemflow™, BD Biosciences, USA		
		DRAQ7™ Dye	-	Viability	FL-7 Or FL-8	725/20	Invitrogen™ ThermoFisher SCIENTIFIC, USA		
	3	CD 73	AD2	APC	FL-6	660/20	BD Stemflow™, BD Biosciences, USA		
		DRAQ7™ Dye	-	Viability	FL-7 Or FL-8	725/20	Invitrogen™ ThermoFisher SCIENTIFIC, USA		
	4	DRAQ7™ Dye	-	Viability	FL-7 Or FL-8	725/20	Invitrogen™ ThermoFisher SCIENTIFIC, USA	Only Viability	
	5	CD 271	C40-1457	V450	FL-9	450/40	BD Horizon™ BD Biosciences, USA	Positive Single Stains Mouse Anti-Human + Viability	
		DRAQ7™ Dye	-	Viability	FL-7 Or FL-8	725/20	Invitrogen™ ThermoFisher SCIENTIFIC, USA		
	6	CD 146	P1H12	PE-CY™7	FL-5	755LP	BD Pharmingen™, BD Biosciences, USA		
		DRAQ7™ Dye	-	Viability	FL-7 Or FL-8	725/20	Invitrogen™ ThermoFisher SCIENTIFIC, USA		
	7	CD 106	51-10C9	BV 510	FL-10	550/40	BD OptiBuild™, BD Biosciences, USA		
		DRAQ7™ Dye	-	Viability	FL-7 Or FL-8	725/20	Invitrogen™ ThermoFisher SCIENTIFIC, USA		
	8	CD 44	G44-26	PE	FL-2	575/30	BD Stemflow™, BD Biosciences, USA		
		DRAQ7™ Dye	-	Viability	FL-7 Or FL-8	725/20	Invitrogen™ ThermoFisher SCIENTIFIC, USA		
	9	Blank	-	-	-	-	-	Exclusion of Auto Fluorescence	
	Sample Reads Master Mix 1		CD 90	5E10	FITC	FL-1	525/10	BD Stemflow™, BD Biosciences, USA	Human MSC Analysis Kit Positive cocktail Mouse Anti-Human
			CD 105	266	PerCp-Cy5.5	FL-4	695/30	BD Stemflow™, BD Biosciences, USA	
CD 73			AD2	APC	FL-6	660/20	BD Stemflow™, BD Biosciences, USA		

	10	CD34	581	PE	FL-2	575/30	BD Stemflow™, BD Biosciences, USA	Human MSC Analysis Kit Negative Cocktail Mouse Anti-Human
		CD11b	ICRF44	PE	FL-2	575/30	BD Stemflow™, BD Biosciences, USA	
		CD19	HIB19	PE	FL-2	575/30	BD Stemflow™, BD Biosciences, USA	
		CD45	H130	PE	FL-2	575/30	BD Stemflow™, BD Biosciences, USA	
		HLA-DR	G46-6	PE	FL-2	575/30	BD Stemflow™, BD Biosciences, USA	
		DRAQ-7	-	Viability	FL-7 Or FL-8	725/20	Invitrogen™ ThermoFisher SCIENTIFIC, USA	Viability
Sample Reads Master Mix 2	11	mIgG1, κ FITC	X40	FITC	FL-1	525/10	BD Stemflow™, BD Biosciences, USA	Isotype Positive Control + Viability
		mIgG1, κ PerCP-Cy5.5	X40	PerCP-Cy5.5	FL-4	695/30	BD Stemflow™, BD Biosciences, USA	
		mIgG1, κ APC	X40	APC	FL-6	660/20	BD Stemflow™, BD Biosciences, USA	
		mIgG1, κ PE	X40	PE	FL-2	575/30	BD Stemflow™, BD Biosciences, USA	Isotype Negative Control + Viability
		mIgG2a, κ PE	G155-178	PE	FL-2	575/30	BD Stemflow™, BD Biosciences, USA	
		DRAQ7™ Dye	-	Viability	FL-7 Or FL-8	725/20	Invitrogen™ ThermoFisher SCIENTIFIC, USA	Viability
Sample Reads Master Mix 3	12	CD 271	C40-1457	V450	FL-9	450/40	BD Horizon™ BD Biosciences, USA	Single Stains + Viability
		CD 146	P1H12	PE-CY™7	FL-5	755LP	BD Pharmingen™, BD Biosciences, USA	
		CD 106	51-10C9	BV 510	FL-10	550/40	BD OptiBuild™, BD Biosciences, USA	
		DRAQ7™ Dye	-	Viability	FL-7 Or FL-8	725/20	Invitrogen™ ThermoFisher SCIENTIFIC, USA	
Sample Reads Master Mix 4	13	IgG1, κ PE-Cy™7	MOPC-21	PE-CY™7	FL-5	755LP	BD Pharmingen™, USA	Isotype Control
		IgG1, κ V450	MOPC-21	V450	FL-9	450/40	BD Horizon™ BD Biosciences, USA	Isotype Control
		DRAQ7™ Dye	-	Viability	FL-7 Or FL-8	725/20	Invitrogen™ ThermoFisher SCIENTIFIC, USA	Viability

Single Stain + Viability	14	CD 44	G44-26	PE	FL-2	575/30	BD Stemflow™, BD Biosciences, USA	Single Stain Human MSC Analysis Kit
		DRAQ7™ Dye	-	Viability	FL-7 Or FL-8	725/20	Invitrogen™ ThermoFisher SCIENTIFIC, USA	Viability
Single Stain Isotype Control + Viability	15	IgG2b, κ PE CD44	27-35	PE	FL-2	575/30	BD Stemflow™, BD Biosciences, USA	Isotype Control Human MSC Analysis Kit
		DRAQ7™ Dye	-	Viability	FL-7 Or FL-8	725/20	Invitrogen™ ThermoFisher SCIENTIFIC, USA	Viability
Unstained	16	Blank	-	-	-	-	-	Autofluorescence exclusion

Table 2. Flow Cytometry Staining Panel.

Staining of cell surface antigens began with the addition of afore mentioned stains to V-bottom 96 well plates according to the prescribed panel in table number (Table.2).

Viability dye DRAQ-7 (Invitrogen™, ThermoFisher SCIENTIFIC, USA) is also added to the wells to assess cellular status, and 100 µl of cells is added to each well, mixed gently and incubated for 30 minutes at RT in the dark, to allow for proper binding with Antibodies (Abs).

In order to be able to enumerate the number of cells expressing a specific marker, counting beads (Beckman Coulter, USA) with a known concentration/volume were added to the cell suspension at 1:1 volume directly, prior to reading on the Navios (Beckman Coulter, USA).

Excitation and emission of stained cells was detected using the Navios (BECKMAN COULTER, USA) and the Analysis of samples was performed using the Kalusa Analysis software (BECKMAN COULTER, USA).

Gating strategy was based on known location of BM MSCs from literature and all GPF related experiments were read on FL-7 at Ex/Em bandpass of 725/20

2.3.2. Tri-Lineage Differentiation

Tri-lineage differentiation studies were conducted for two reasons:

- A. Identification of cells
- B. Differentiation studies; the impact of different factors such as: transfection, change in media additive during expansion, and cell encapsulation on the ability of cells to differentiate into chondrocytes, adipocytes, and osteocytes.

A. Cell Identification:

MSCs are multipotent cells with the ability to differentiate into three main types of cells:

Osteoblasts, Chondrocytes, and Adipocytes. As part of the ISCT minimal requirements of MSC identification, the ability of isolated primary human MSCs to differentiate into the three lineages must be confirmed[82] . The ability of DF to differentiate was also accessed. To access the tri-lineage differentiation ability of cells, the StemPro™'s Osteogenic (kit# A1007201), Chondrogenic (kit#

A100710), and Adipogenic (kit# A1007001) Differentiation Kits (*Gibco™, ThermoFischer Scientific, Germany*) were used according to manufacturer's instructions (with slight modifications). In short:

For Osteogenic Differentiation:

Osteogenic Differentiation Media (ODM) Preparation: 90ml of *StemPro™ Osteocyte/Chondrocyte Differentiation Basal Medium (Gibco™, ThermoFischer Scientific, Germany)* + 10 ml of *StemPro™ Osteogenesis Supplement (Gibco™, ThermoFischer Scientific, Germany)* + 0.5% *ab/am (Capricorn Scientific, Germany)*.

When cells in culture flasks reached a confluency of 80%, they were harvested using Trypsin/EDTA (PAN – Biotech, Germany), counted, and plated in triplicates using a 12-well plate (CELLSTAR®, greiner BIO-ONE, G) at a density of 1×10^4 cells/cm² with CM. After 3 days, the media was changed to begin the process of differentiation. ODM was changed every 3-4 days for **14-21 days**. After 14 days of cultivation, the cells were fixed in 3.5-3.7% formaldehyde (Fischar, Germany) for 30 minutes, rinsed twice with distilled water and subsequently stained with 2% Alizarin Red S solution (pH 4.2) for 2-3 minutes). After staining, the cells were washed three times with distilled water and subsequently visualized and images were captured using a light microscope (Zeiss, Germany).

For Adipogenic Differentiation:

Adipogenic Media Preparation: 90ml of *StemPro™ Adipocyte Differentiation Base Medium (Gibco™, ThermoFischer Scientific, Germany)* + 10 ml of *StemPro™ Adipogenesis Supplement + + 0.5% ab/am (Capricorn Scientific, Germany)*.

Adipogenic differentiation followed the same protocol as that of osteogenic differentiation with the exception of that CM was replaced with ADM rather than ODM. After 7-14 days, the cells were fixed with 3.5-3.7% formaldehyde (Fischar, Germany) for 5 minutes at RT, rinsed with distilled water, then covered with Oil Red O working solution (Sigma-Aldrich, USA) for 10-15 minutes (with shaking), washed, and subsequently imaged.

For Chondrogenic Differentiation:

Chondrogenic Media Preparation: 90ml of *StemPro™ Osteocyte/Chondrocyte Differentiation Basal Medium (Gibco™, ThermoFischer Scientific, Germany)* + 10 ml of *StemPro™ Chondrogenesis Supplement (Gibco™, ThermoFischer Scientific, Germany)* + 0.5% *ab/am (Capricorn Scientific, Germany)*.

For chondrogenic differentiation, the cells were also harvested at 80% confluency, but were plated in 12-well plates (CELLSTAR®, greiner BIO-ONE, Austria) at a density of 1×10^6 cells per well or 0.256×10^6 cells/cm² and the induction began after 2-4 hours of plating. Cultures were fed every 2-3 days. After 14 -21 days, cultures were fixed with 3.5-3.7% formaldehyde (Fischar, Germany) for 30 minutes, rinsed, with DPBS w/o: Ca and Mg (PAN – Biotech, Germany) and stained with 1% Alcian Blue (Ruth, Germany) prepared in 3% Acetic Acid for 30 minutes, washed with water, counter stained Nuclear Fast Red Stain, washed again, and the imaged using a bright field microscope (Zeiss, Germany).

2.4. CELLULAR QUALITY ASSESSMENT MEASURES (HEALTH, CONFLUENCY, AND FUNCTION)

2.4.1. Morphological and Confluency Examination

Healthy mesenchymal stromal cells retain a fibroblast-like morphology with an elongated spindle-like shape [142]. As cells begin to age, they acquire an enlarged fried-egg-like morphology [143]. Both morphology and confluency of cell cultures were monitored closely using Brightfield microscopy (Zeiss, Germany). Morphology and confluences were registered in accordance to below images.

2.4.2. Cell Metabolic Health and Activity- Alamar Blue metabolic assay

The proliferative ability of cells and their metabolic condition, are an indication of their overall health. The Alamar blue assay detects the cells' proliferation capacity, and their metabolic activity [144], through the mitochondrial reduction of a fluorometric redox indicator resazurin (7-hydroxy-3H-phenoxazin-3-one 10-oxide), a blue-coloured non-fluorescent compound, into a highly fluorescent compound called resorufin (7-hydroxy-3H-phenoxazin-3-one), which can be quantified via optical density (OD) readings[144]. Therefore, in order to assess the cellular metabolic/proliferative condition, upon trypsinization, cells were plated in triplicates in 96-well plates (CELLSTAR®, Greiner Bio-One GmbH, Germany) at a seeding density of 10×10^3 cells /well and incubated at $37^\circ\text{C} \pm 2^\circ\text{C}$, 5% $\text{CO}_2 \pm 1\%$, and passive humidification. After 48 hours, the media was removed, and replaced with new media containing a 1:10 concentration of Alamar blue solution (*0.15mg Resazurin sodium salt (Sigma-Aldrich, USA) in 1ml of DPBS w/o: Ca and Mg (PAN – Biotech, Germany)*), and then incubated $37^\circ\text{C} \pm 2^\circ\text{C}$, 5% $\text{CO}_2 \pm 1\%$, with passive humidification for 1.5 hours. For seeded scaffolds however, this incubation period was extended to 4 hours; after which, the resulting fluorescence was read using a microplate reader at an excitation (Ex) of 560nm; and an emission (Em) of 590nm. All sample results were normalised against blanks.

2.4.3. Cell Cytotoxicity - Lactate Dehydrogenase Assay

Lactate dehydrogenase (LDH) is a cytoplasmic enzyme that plays a key role in anaerobic metabolism. It catalyses the conversion of lactate to pyruvate during glycolysis and is released upon cellular damage[145]. As a result, it is often used as measure to monitor cells for cytotoxicity. Therefore, in order to validate the Alamar blue assay results, and to further assess cellular condition and overall health, the LDH assay was paired with each alamar blue experiment and was conducted at in key points throughout various experiments. In short, prior to removing the culture media from cultivated cells/scaffolds to conduct the Alamar blue assay, 100µl of each condition was removed for the LDH assay. The assay was conducted using the LDH Cytotoxicity detection kit (Kit#11644793001, Roche/Sigma-Aldrich, USA) from which 100µl of reagent mix (2,5µl Catalyst + 112,5µl dye solution /sample) (Cytotoxicity detection kit# 11644793001, Roche, Sigma-Aldrich, USA) was added to the 100µl of sample in a new 96-well plate (CELLSTAR®, Greiner Bio-One GmbH, Germany) and incubated in the dark for 30 minutes. After incubation, the plate was measured using a microplate reader at an optical density of 490nm and a reference of 600nm. All results were normalised against blanks.

2.5. DECELLULARIZED TRACHEAL SCAFFOLDS

Cryopreserved and decellularized porcine tracheal scaffolds were purchased from the Griffin Institute (London, UK) under clean but non-sterile conditions. Received tracheas were cryopreserved in glycerine, in 50ml tubes (CELLSTAR®, Greiner Bio-One GmbH, Germany) containing two-halves per one donor trachea. Upon arrival they were maintained at -80C° until utilisation.

2.5.1. Thawing, Handling, and Sterilisation of Decellularized Scaffolds

Prior to starting the manufacturing process, cryopreserved tracheas were thawed overnight at 4C°. The following day, all tracheas were measured, and then washed before beginning the sterilisation process. The entire thawing, handling, and sterilisation procedure is an eight-day process (Figure.).

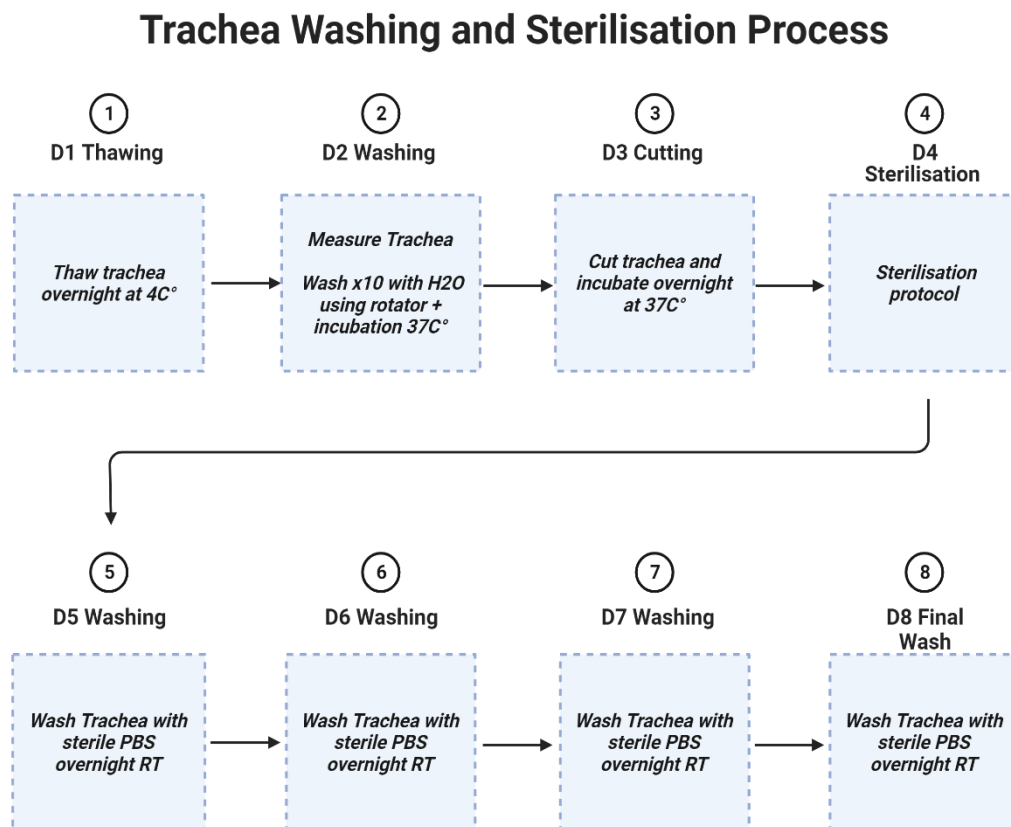


Figure 9. Overview of General Process of Tracheal Handling Prior to Manufacturing. D1- D8 denote the different days in which various steps are undertaken to ensure tracheal sterility. RT= room temperature.

2.5.1.1. Measurement of Trachea:

The first step in handling tracheas after thawing, is measurement. All tracheas to be subsequently used in experimentations and/or manufacturing process were precisely measured as part of their

characterisation procedure. Measured parameters as indicated in (Figure.) Included: height, length, width, and radius and were taken at different points of the tracheal segments in order to get a more accurate idea of the size of the received decellularized porcine trachea which would in turn, allow for an estimation of the number of biopsies that could be generated using a 6mm punch biopsy puncher (Acu-Punch, Acuderm inc., USA) and the number of cells required for seeding.

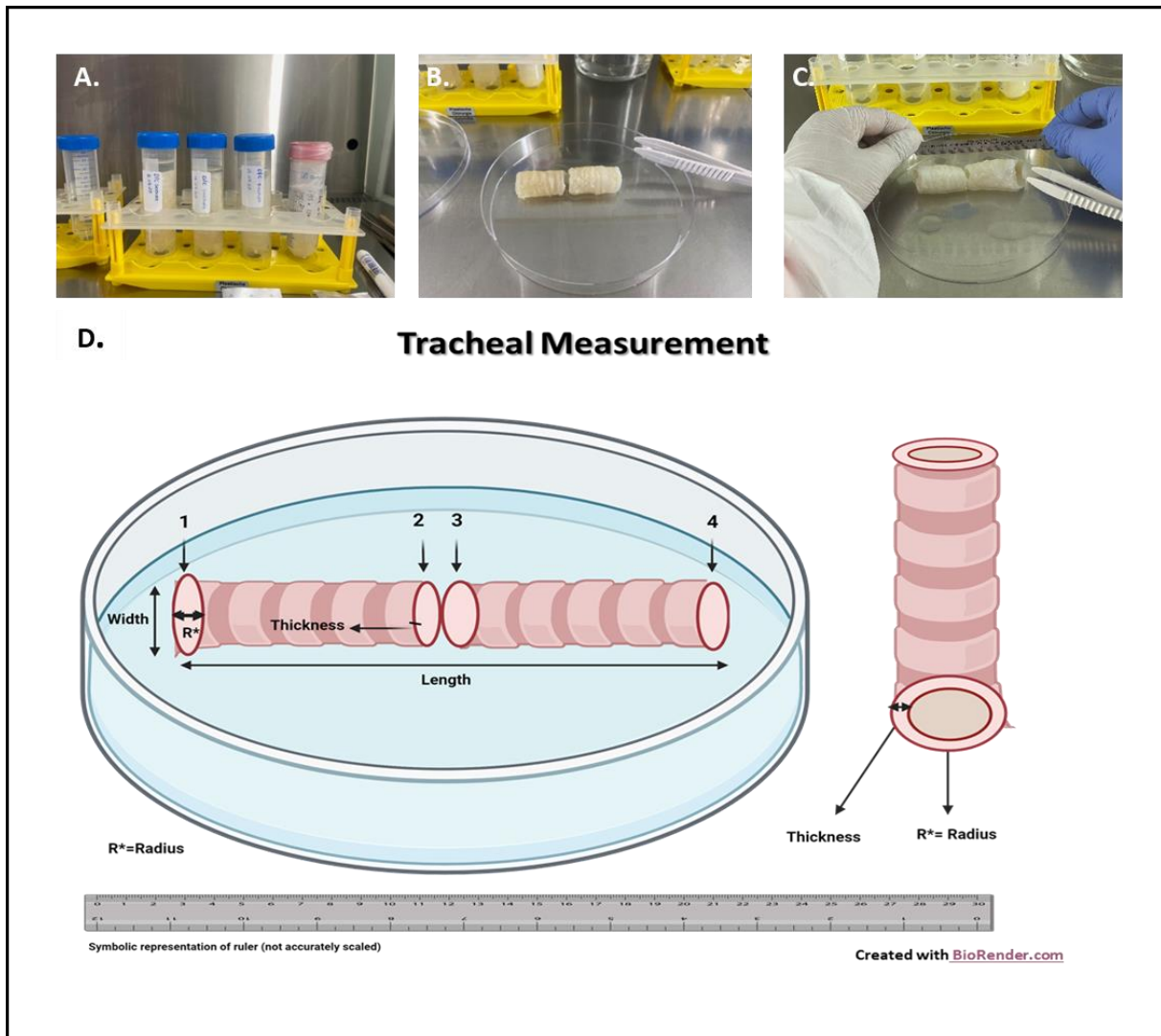


Figure 10. Tracheal Characterisation: Metrics. **A.** Post-Thawed Trachea in 50ml falcon tubes. **B.** Two pieces of a single trachea. **C.** Image of trachea measurement. **D.** Outline of measurement parameters (as part of the manufacturing and characterisation process). Numbers 1,2,3,4 indicated points of measurement.

2.5.1.2. Washing of Trachea:

The second step in handling trachea is washing. Prior to sterilisation, all tracheas underwent an extensive washing procedure to eliminate residue glycerine which can seep into the ECM of the decellularized scaffolds. Each trachea was washed X10 times (intercepted with a period of incubation) in pre-warmed, ultra-pure, and sterile water (H₂O). In short, after measurement, each trachea was placed into a 50ml flacon tube (CELLSTAR®, Greiner Bio-One GmbH, Germany) with pre-warmed (37°C) sterile water and placed into a MACSmix™ tube rotator (MACs, Miltenyi Biotec, Germany) for 10 minutes. After 10 minutes, the trachea was moved into another 50ml tube (CELLSTAR®, Greiner Bio-One GmbH, Germany) with newly-warmed, sterile H₂O and was placed back onto the rotator for another 10 minutes. After repeating this step for X5 times, with the 6th wash, the rotator was placed into the incubator at at 37 ° C +/- 2 ° C, 5% CO₂ +/- 1%, and passive humidification for 2 hours in order to allow for proper seeping of glycerine from the pores of the decellularized scaffolds into the surrounding washing solution. After the two-hour incubation period, the trachea underwent X5 more washes using the same methodology previously mentioned.

2.5.1.3. Cutting of Trachea:

The third step in handling trachea, is cutting and overnight incubation. After washing, the decellularized tracheas were cut to produce uniform 6mm punch biopsies (Acu-Punch, Acuderm inc., USA) containing both cartilage and intra-cartilaginous matrix. The trachealis muscle portion of the trachea was excluded (Figure.). Then, the punch biopsies were placed into another 50ml tube (CELLSTAR®, Greiner Bio-One GmbH, Germany) containing sterile water and placed onto the MACSmix™ tube rotator overnight in an incubator at 37 ° C +/- 2 ° C, 5% CO₂ +/- 1%, and passive humidification.

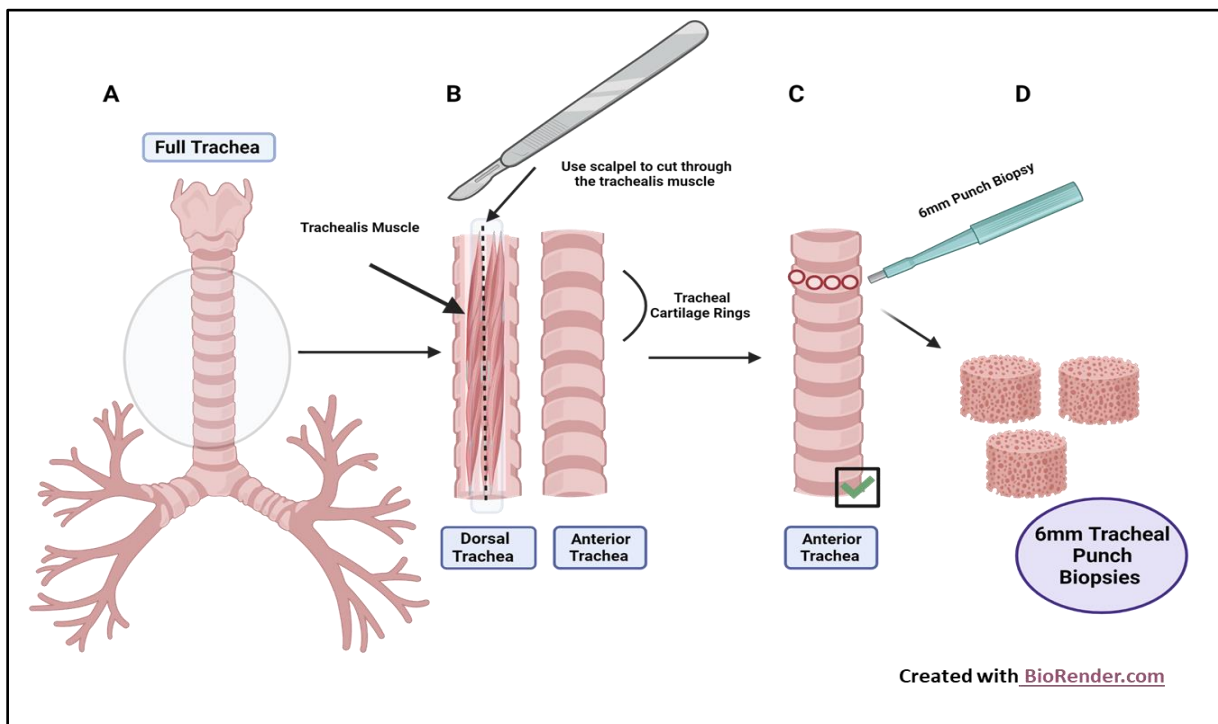


Figure 11. Tracheal Biopsies: Handling & Cutting. A. Original trachea anatomy. B. The dorsal part of the trachea containing the trachealis muscle is cut with a scalpel. Thereby, allowing for subsequent punching of equally sized tracheal probes. C&D. A 6mm diameter puncher biopsy is used to generate 6mm tracheal punch biopsies.

2.5.1.4. Sterilization of Trachea

Decellularization protocols are generally effective in sterilizing most of the tissue they are applied to, depending on the specific components of the decellularization process. Nevertheless, some highly resilient bacteria may persist. Exposure to detergents, such as Triton-X, typically proves efficacious in eradicating the majority of bacteria within the tissue. However, additional sterility measures are routinely implemented to ensure the complete elimination of any remaining bacteria or particularly resilient strains. In certain instances, recalcitrant bacteria, such as various types of Gram-negative aerobic bacteria like *Pseudomonas aeruginosa*, necessitate supplementary sterility steps. In the case at hand, the cryopreserved decellularized trachea acquired from NSBT, UK, was found to harbour *Pseudomonas aeruginosa*, *Stenotrophomonas maltophilia*, *Escherichia coli*, and *Citrobacter braakii*. To decontaminate these tracheal samples for subsequent processing, four distinct sterilization protocols were assessed and employed.

Protocol 1:

After washing and cutting steps have taken place, trachea was sterilized by placing biopsies (n=15) in a 50ml falcon tube (CELLSTAR®, Greiner Bio-One GmbH, Germany) with PBS and 1% ab/am (Capricorn Scientific, Germany), for four hours with continuous agitation using the MACSmix™ tube rotator (MACs, Miltenyi Biotec, Germany) and in an incubator at 37 ° C +/- 2 ° C, 5% CO² +/- 1%, and passive humidification. Rotation was stopped every hour and PBS was changed to fresh PBS with 1% ab/am (Capricorn Scientific, Germany). After which, the tracheal biopsies were placed into a fresh 50 ml falcon tube with sterile PBS and stored at 4C° until use.

Protocol 2:

With protocol 2, after the washing and cutting steps, tracheal biopsies (n=15) were first placed into a 50ml falcon tube (CELLSTAR®, Greiner Bio-One GmbH, Germany) with 96% ethanol (PCR grade) and 2% Peracetic Acid (PAA) solution as described by Hennessy RS, et.al and Dohmen PM, et. al. [146, 147] for four hours at RT with continuous agitation using the MACSmix™ tube rotator (MACs, Miltenyi Biotec, Germany). Followed by a four-day wash protocol in which biopsies were placed in sterile PBS, on a plate shaker at RT, and the PBS was changed every 24 hours. After the fourth day, biopsies were moved to a new 50 ml falcon tube with PBS + 1%ab/am (Capricorn Scientific, Germany) and stored at 4C° until use.

Protocol 3:

Protocol 3 used a two-step sterilisation procedure adapted from a paper by Fidalgo C, et.al. [148]. In short, after the washing and cutting steps, the tracheal biopsies (n=15) were:

Step one: placed in a 50ml falcon tube (CELLSTAR®, Greiner Bio-One GmbH, Germany) with PBS + 1% ab/am (Capricorn Scientific, Germany), placed onto the MACSmix™ tube rotator (MACs, Miltenyi Biotec, Germany), and into the incubator at 37 ° C +/- 2 ° C, 5% CO² +/- 1%, and passive humidification for 24 hours. Following incubation with PBS + ab/am (Capricorn Scientific, Germany), tracheal biopsies were washed twice with sterile PBS (first for 30 mins on a shaker, and the second overnight).

Step two: step one was followed by treatment with 0.1% (v/v) PAA (2ml/cm²) as described by Fidalgo C, et.al. [148]. PAA solution was prepared in PBS and the pH was adjusted to 7.3 with sodium hydroxide and subsequently filtered using a 0.22µm pore-sized filter as recommended. The solution was used within one hour of preparation and tracheal biopsies were placed with the solution on a rotator for 3 hours.

After treatment with PAA, the biopsies underwent 3 washing procedures with sterile PBS (two for 30 minutes, and a third overnight). After washing, the biopsies were placed in a new 50 ml falcon tube with sterile PBS + 1% ab/am (Capricorn Scientific, Germany) and stored at 4C° until use.

Protocol 4:

After washing and cutting steps, extremely contaminated biopsies (n=15) with *pseudomonas aeruginosa*, *Stenotrophomonas maltophilia*, *Escherichia coli*, and *Citrobacter braakii* were treated with 1% Triton-X (Triton™, 9036-19-5, Sigma-Aldrich, Saint Louis, MO, USA) in PBS on the MACSmix™ tube rotator (MACs, Miltenyi Biotec, Germany) for four hours at RT. After four hours, the biopsies were placed onto a plate shaker and were washed for four days in sterile PBS + 1% ab/am (Capricorn Scientific, Germany) at RT. After every 24 hours, the PBS in the tubes was changed to fresh PBS + 1% ab/am (Capricorn Scientific, Germany).

2.5.1.5. Sterility

To access the success or failure of the sterilisation protocols, X3 Scaffolds from each sterilisation protocol was placed in complete culture media one (CM1) containing: Alpha MEM Eagle w/o L-glutamine (PAN - Biotech, Germany) prepared with 10% Fetal Bovine Serum (FBS) (*Gibco™*, *ThermoFischer Scientific, Germany*) + 1% L-glutamine (Capricorn Scientific, Germany) + 1% antibiotic/antimycotic (ab/am) X100 (Capricorn Scientific, Germany) and were left in the incubator for 5 days. After 5 days, the media was assessed for turbidity and bacterial content.

Scaffold/Cell Biocompatibility

In order to access the biocompatibility potential of the scaffolds treated with different sterilisation protocols, n=3 scaffolds of each of the sterilisation protocols, were seeded with 3T3 mouse embryonic fibroblast cells and placed into 24-well culture plates (CELLSTAR®, greiner BIO-ONE, Germany). After a week of incubation at 37 ° C +/- 2 ° C, 5% CO² +/- 1%, with passive humidification, the scaffolds and the cells were assessed for:

- A. Metabolic function (Alamar blue assay) (Sigma Aldrich, USA)
- B. Cell cytotoxicity (LDH assay) (Cytotoxicity detection kit# 11644793001, Roche, Sigma-Aldrich, USA)

C. Cell Viability with Live/Dead Staining

In order to generally visualize seeding success and the number of cells that were alive versus the number of dead cells after a week of static incubation in at 37 ° C +/- 2 ° C, 5% CO² +/- 1%, and passive humidification (incubator conditions). Seeded scaffolds were stained with a fluorescent based red/blue vitality dye. In which 2 drops of NucBlue®Live and propidium iodide (each) were added per ml of medium to label the cells on the scaffolds. NucBlue®Live stains the cellular nucleus blue and indicates the presence of live cells, while the propidium iodide (mechanism) stains the nucleuses of dead cells read. The scaffolds were incubated for 30 mins at 37C° +/- 2 ° C, 5% CO² +/- 1%, and passive humidification, then washed X1 with PBS and fixed with 3.7% of Formaldehyde. Following fixation, the scaffolds were imaged using a fluorescent microscope (Zeiss model, Germany) with Nuc-Blu live: Ex

360 nm; Em 460nm and blue fluorescence = viable cells. While PI: Ex 535nm; Em 617 nm and violet or red fluorescence = dead cells.

2.6. COCULTURES

h-MSCs and HDF have different growth speeds and growth ratios. Some studies have claimed a synergism between the two cell types, while others have claimed that they are two faces of the same cell type that are otherwise indistinguishable [149-151], and others have claimed that they are two distinct cell populations with similar features[152-154] . Therefore, in order to gain some insight into the co-activities of human MSCs and human DFs when cultured together, and to be able to determine their applicability as a coculture for tracheal seeding, a direct seeding coculture experiment was performed. Depending on the

2.6.1. MSC AND FIBROBLAST CO-CULTURE: EXPERIMENTAL SET-UP

Human mesenchymal stem cells (MSCs) derived from bone marrow, procured from five distinct donors (n=5), and human dermal fibroblasts (DF), also from five different donors (n=5), were subject to expansion procedures utilizing two distinct culture media formulations, denoted as CM1 and CM2. Subsequently, these cells were subjected to staining with Mitotracker™ dyes, followed by trypsinization, and subsequent seeding into 12-well culture plates (CELLSTAR®, Greiner Bio-One GmbH, Germany). The seeding process involved various combinations and different cell ratio compositions, each executed in triplicate to ensure robust data acquisition and analysis, as outlined in Table 2. This seeding protocol resulted in a final cell seeding density of 2×10^5 cells per well.

For the ensuing co-culture conditions, once the cells were successfully introduced into the co-culture environment, they underwent cultivation in two distinct co-culture media formulations, termed CocM1 (designated for cells that had been expanded with foetal bovine serum in their media) and CocM2 (reserved for cells that were expanded with human platelet lysate in their culture media).

	Ratio F:M	Fibroblasts	MSCs	Total
1	25:75	0.5×10^5	1.5×10^5	2×10^5
2	50:50	1×10^5	1×10^5	2×10^5
3	75:25	1.5×10^5	0.5×10^5	2×10^5

Tabelle 3. Ratio of seeded Dermal fibroblasts to MSCs (F:M). MSC:DF were calculated to form a final seeding density of 2×10^5 cells/well.

The functional impact of the coculture studies was analyzed by examining the effect of the different co-culture ratios on the expression VEGF and bFGF in their surrounding media.

2.6.2. MITOTRACKER® STAINING

Mitotracker® dyes stain mitochondria within live cells with fluorescent dyes via passive diffusion utilizing the mitochondrial membrane potential (membrane-potential-dependent dyes)[155]. The Mitotracker® dyes accumulate within the mitochondria Membrane-potential-dependent dyes

In order to visually differentiate between the HDF and MSCs used in the coculture studies. Human dermal fibroblasts were stained red using Mitotracker® Red CMXRos (Catalogue #M-7512, Invitrogen-Thermo Fisher Scientific, USA) and human bone marrow-derived MSCs were stained green using Mitotracker® Green FM (Catalogue #M-7514, Invitrogen -Thermo Fisher Scientific, USA) in accordance to the manufacturer's recommendations.

A. Mitotracker® Red CMXRos

Shortly, a 1mM stock solution of Mitotracker® Red CMXRos was prepared by dissolving 50µg of Mitotracker® Red CMXRos in 94µl of Dimethyl sulfoxide (DMSO). Then, minimum of 4 hours prior to trypsinization, cells designated for labelling with Mitotracker® Red CMXRos were treated to a media change containing a 1:2000 dilution of stock Mitotracker® Red CMXRos in cell culture media and incubated at 37 ° C +/- 2 ° C, 5% CO² +/- 1%, and passive humidification. Afterwards, cells labelled with Mitotracker® Red CMXRos were read at an Excitation wavelength of :579nm and an Emission of:599nm using an inverted fluorescence microscope

B. Mitotracker® Green FM

Shortly, a 1mM stock solution of Mitotracker® Green FM was prepared by dissolving 50µg of Mitotracker® Green FM in 74µl of Dimethyl sulfoxide (DMSO). Then, minimum of 4 hours prior to trypsinization, cells designated for labelling with Mitotracker® Green FM were treated to a media change containing a 1:10000 dilution of stock Mitotracker® Green FM in cell culture media and incubated at 37 ° C +/- 2 ° C, 5% CO² +/- 1%, and passive humidification. Afterwards, cells labelled with Mitotracker® Green FM were read at an Excitation wavelength of :490nm and an Emission of:516 nm using an inverted fluorescence microscope

2.7. IN VITRO PRE-VASCULARISATION

2.7.1. TRANSIENT GENETIC MODIFICATION OF CELLS

2.7.1.1. Genetic Modification of Cells – Electroporation/Nucleofection

Nucleofection represents a method of physical transfection wherein plasmid DNA is delivered directly into the cell nucleus through the application of an electrical pulse that induces membrane permeabilization. This technique falls under the broader category of electroporation and relies on the precise interplay of specialized solutions and defined electric parameters to facilitate augmented gene expression [126]. Generally, electroporation stands as an invaluable technique for the transfection of substantial DNA fragments and the attainment of robust transfection efficiencies in established cell lines. Nevertheless, its utility becomes constrained when applied to primary cells and stem cells,

primarily due to the manifestation of heightened post-transfection cytotoxicity. The Amaxa/Lonza Nucleofection® technology represents an optimization of these transfection methods, offering better outcomes by incorporating unique electrical parameters that are pre-programmed for various cell types of interest. In the present investigation, we employed the Amaxa/Lonza Nucleofector®2b device (Lonza, Switzerland) to genetically modify human dermal fibroblasts and human bone marrow-derived MSCs (h-bm derived MSCs) to transiently overexpress human vascular endothelial growth factor (VEGF) and fibroblast growth factor beta (bFGF) using; a GMP compatible protocol adapted from Zhang Z & Slobodianski A, et. al, 2011 [126] and Zhang Z, et.al. 2017 [156]. The bacterial plasmids encoding for vascular endothelial growth factor (VEGF) and fibroblast growth factor beta (bFGF) were both constructed by drawing upon the pmaxGFP® plasmid backbones developed by Lonza [126] to form a pmax-VEGF plasmid, and a pmax- bFGF plasmid, both designed to meet requirements mandated for prospective clinical applications. The pmax (VEGF and bFGF) plasmids used in this study, were obtained from TUMCells (TUMCells, Germany); a German-based Good Manufacturing Practice (GMP) compliant facility, and were manufactured and Quality Controlled (QC) accordingly.

Cells designated for transfection were expanded to a maximum of 4 passages. Prior to the nucleofection procedure, the cells were monitored till they reached a confluency of 70% (within the exponential growth phase). Upon reaching this confluency threshold, and displaying healthy conditions, they were harvested, quantified, split into half, and resuspended in complete media (CM) in 50ml falcon tubes (CELLSTAR®, Greiner Bio-One GmbH, Germany). Each tube was subsequently centrifuged at 1200 rpm (290g) (Rotanda 460R, Hettich, Germany) for 5 minutes at 20C° and resuspended in 300µl of suspension buffer consisting of a mixture of FBS (Gibco™, ThermoFischer Scientific, Germany) and DPBS w/o: Ca and Mg (PAN – Biotech, Germany) to which plasmid DNA was promptly added to, at a concentration of 8µg (corresponds to 8 µl for a DNA Concentration of 1 mg / ml) of plasmid DNA for every 2x10⁶ cells. Then, the DNA/cell suspension was quickly transferred into an electroporation cuvette (Cuvettes Plus™ Electroporation Cuvettes, BTX™ (Gap size 4mm), Germany) and electroporated using the U-24 protocol on the Nucleofector®2b device (Lonza, Switzerland) (the appearance of a small film of white foam was an indication of the success of a procedure). Pre-warmed CM was quickly transferred to the cells and the cells were promptly plated after a small sample was taken for counting. Nucleofection procedures with pmax-bFGF (TUMCells, Germany) and / or pmax-VEGF (TUMCells, Germany) were carried out separately, and the outputs were added together afterward for a pmax-bFGF and pmax-VEGF/cell expressing mixture. Nucleofection procedures with GFP were carried out the same way, with the exception of using pmax-GFP plasmids instead of the VEGF and/or bFGF plasmids.

2.7.1.2. Assessment of Cell Viability, Cell Recovery, and Transfection Yields:

A. In 2D Preliminary Experiments Using GFP:

Cell Viability: Cell viability was calculated as:

$$\frac{\text{the number of surviving cells post transfection}}{\text{total number of cells (pre-transfection)}} \times 100$$

% of GFP+ Cells: The % of GFP+ cells were calculated after 24 hours of cell cultivation in T-75 flasks according to flow cytometry machine Navios (Model number, Beckman

Coulter, USA) reading on FL-1 at an Ex/Em 525/40, and analysis using the Kaluza Software (version, Beckman Coulter, USA).

Yield of Transfection (Y): was calculated as

Cell Recovery

For each micro-electroporated sample (m), cell recovery (CR) was determined using the equation

$$CR (\%) m = (CA_m/CA_c) \times 100,$$

where CA is the number of cells alive and c is the non-electroporated control.

Yield of transfection (Y) was calculated using the equation

$$Y (\%) m = (GFP+ \times CA_m) / CT_c \text{ where } CT \text{ is the number of total cells.}$$

B. For 3D Scaffolds seeding:

Cell Viability: The post-transfection cell viability was accessed using the CASY® counter (Innovatis, OLS OMNI Life Science, Germany). Directly after cells were transfected and prior to seeding, they were resuspended in CM and a sample was taken for enumeration.

2.8. PROTEIN AND CYTOKINE EXPRESSION QUANTIFICATION

The detection and quantification of specific proteins related to angiogenesis and the differentiation of human bone marrow-derived mesenchymal stromal cells and human dermal fibroblasts into osteocytes, adipocytes, and chondrocytes was detected by means of enzyme-linked immunosorbent assays (ELISAs). Sandwich ELISAs were performed in accordance to manufacturer's recommendations and all reagents and buffers were prepared as per kit-accompanying protocols. In short, 96-well plates (CELLSTAR®, Greiner Bio-One GmbH, Germany) we coated with capture antibody and incubated overnight at Room Temperature (RT). The next day, the plates were washed X3 with Wash Buffer, blocked for an hour at RT with 300µl Reagent Diluent, washed again X3 with Wash Buffer, and then the samples and the prepared standards were added at 100µl per-well and allowed to incubate at RT for two hours. After the 2-hour incubation period, the plates were washed again, and a 100µl of Detection Antibody was added for an incubation period of 2 hours at RT. This was followed with the addition of 100µl of Streptavidin-HRP (Horseradish Peroxidase) for 20 minutes in the dark at RT, washing X3, and the addition of 100µl of Substrate Solution to each well for another 20 minutes at RT in the dark. The ensuing reaction was stopped after 20 minutes through the addition of 50µl of Stop Solution and the optical density of each well was determined using the microplate reader at wavelength of 450nm. Growth factor concentrations were read using a via the MikroWin 2000 software.

2.8.1. Quantification of Basic Fibroblast Growth Factor (bFGF)

Basic fibroblast growth factor or basic fibroblast growth factor 2 is a growth factor and signalling protein that is encoded by the FGF2 gene and plays a major role in angiogenesis[157].

In order to detect the amount of bFGF released by cell culture(s)/seeded scaffold(s) into the supernatants under different conditions, 150-200µl of media was taken and cryopreserved at -80C°. This was performed after a week of incubation for the coculture studies (section), and on implantation day (after 5-7 days incubation post manufacturing) for the screening experiments (section 2.10). All other samples were used fresh on designated days according to the requirements of the experiment. For the detection of bFGF, the Human FGF basic/FGF2/bFGF DuoSet ELISA (catalogue# DY233, R&D systems, USA) was used according to manufacturer's instructions and as mentioned previously under section 2.6. None of the samples used were diluted.

2.8.2. Quantification of Vascular Endothelial Growth Factor (VEGF)

Vascular endothelial growth factor or vascular endothelial growth factor-A (VEGF or VEGF-A), also known as permeability factor (VPF) is one of the most critical regulators of angiogenesis and vasculogenesis [158]. In order to detect the amount of VEGF released by cell culture(s)/seeded scaffold(s) into the supernatants under different conditions, 150-200µl of media was taken and cryopreserved at -80C° until the VEGF detection assay was performed. For the detection of VEGF, the Human VEGF DuoSet ELISA (catalogue# DY293B, R&D systems, USA) was used according to manufacturer's instructions and as mentioned previously under section 2.6. All VEGF Elisa's were performed with previously cryopreserved samples.

2.8.3. ASSESSMENT OF ANGIOGENESIS POTENTIAL

ANGIOGENESIS ARRAYS: ANALYSIS OF ANGIOGENIC PROTEOME PROFILE

To detect the presence of various cytokines associated with the angiogenic process and evaluate the angiogenic capacity of the cell/scaffold secretome under various conditions, we conducted angiogenesis array analyses; Human Angiogenesis Antibody Array - Membrane (43 Targets) (catalogue # ab193655, Abcam, UK)

Human Angiogenesis Antibody Array - Membrane (43 Targets) (catalogue # ab193655, Abcam, UK)

The human angiogenesis antibody array (Abcam, UK) is a semi-quantitative assay that provides high content screening using similar principles to Elisa and is able to detect a variety of targets at a sensitivity of 25 to 250,000 pg/mL and a range of 10,000-fold. In this assay, media collected from the culture supernatant of each condition of the five (n=5) screening manufacturing procedures described in section 2.10 was collected on day 8, prior to scaffold implantation, and stored in -80C° until the angiogenesis arrays were performed. Assessment of the 43 target proteins (Table 4.) took place in accordance to the manufacturer's recommendation with no sample dilution. All buffers and required reagents were prepared as recommended by the manufacturer's protocol. In short, membranes were placed up right in an 8-well tray and blocked with 2 ml 1x blocking buffer at room temperature (RT) for 30 minutes. Then, the buffer was aspirated and 1 ml of the undiluted sample was pipetted into each well and incubated overnight at 2-8C°. The next day, the samples were washed by placing the membranes into clean containers, adding 20-30ml of Wash Buffer I per membrane, and washing at RT with gentle shaking (large volume wash). Afterwards, the membranes were returned to the 8 well trays for 3 more washings (2ml of 1X Wash Buffer I into each well for 5 minutes at RT). When the 3 washes

with 1X Wash Buffer I were finished, two subsequent washes were made with 1X Wash Buffer II using the same methodology. Then, 1 ml of 1x Biotinylated Antibody Cocktail was pipetted into each well and the plates were incubated at 2-8°C overnight. The next day, the membranes were washed again, and 2 ml of 1X HRP-Conjugated Streptavidin was added with a 2-hour incubation period at RT. The membranes were washed again as previously mentioned and then placed face-up onto a sheet of blotting paper lying on the benchtop. Excess buffer was removed via blotting, the membranes were transferred onto a plastic sheet, and 500µl of a mixture of equal volume (1:1) of Detection buffer C and Detection Buffer D was pipetted onto each membrane and incubated for 2 minutes at RT. After 2 minutes, another plastic sheet was placed on top and the membranes were transferred to the Chemidoc machine and images of the membranes were captured using a series of exposures till images with low background and strong positive signal spots that do not bleed into one another were achieved.

	Target		Target		Target		Target		Target
1	Angiogenin	11	GRO alpha	21	IL-4	31	PDGF-BB	41	uPAR
2	Angiopoietin-1	12	GRO beta	22	IL-6	32	PECAM-1 (CD31)	42	VEGF-A
3	Angiopoirtin-2	13	GRO gamma	23	IL-8 (CXCL8)	33	PLGF	43	VEGFR2
4	Angiostatin	14	I-309 (TCA-3/CCL1)	24	I-TAC (CXCL11)	34	RANTES (CCL5)		VEGFR3
5	bFGF	15	IFN-gamma	25	Leptin	35	TGF beta 1		VEGF-D
6	EGF	16	IGF-1	26	MCP-1 (CCL2)	36	Thrombopoietin (TPO)		
7	ENA-78 (CXCL5)	17	IL-10	27	MCP-3 (MARC/CCL7)	37	Tie-2		
8	Endostatin	18	IL-1alpha (IL-1 F1)	28	MCP-4 (CCL13)	38	TIMP-1		
9	GCSF	19	IL-1 beta (IL-1 F2)	29	MMP-1	39	TIMP-2		
10	GM-CSF	20	IL-2	30	MMP-9	40	TNF alpha		

Tabelle 4. Angiogenesis Array Cytokine Table. Cytokines Assessed by Human Angiogenesis Antibody Array - Membrane (catalogue # ab193655, Abcam, UK).

2.9. THREE-DIMENSIONAL SEEDING (3D)

2.9.1. CELL ENCAPSULATION WITH ALGINATE HYDROGEL

2.9.1.1. Preparation of Alginate and Other Requirements

2X wash buffer:

Sterile, filtered Wash Buffer 2 (2X Wash Buffer) was prepared by dissolving 300mM of Sodium Chloride (NaCl 17,53 g/l) (0,876g in 50 ml) in 50mM HEPES (4-(2-hydroxyethyl)-1-piperazineethanesulfonic acid) (11,91 g/l) (0,595g in 50ml) and adjusting to pH 7.4. All purchased form (Karl Roth GmbH& Co. KG, Karlsruhe, Germany).

1X wash buffer:

Sterile, filtered Wash Buffer 1 (1X Wash Buffer) was prepared by dissolving 150mM of Sodium Chloride (NaCl 8,77 g/l) (0.877g in 100ml) in 25 mM HEPES (4-(2-hydroxyethyl)-1-piperazineethanesulfonic acid) (5,96g/l) (0,596g for 100ml) and adjusting to pH 7.4. All purchased form (Karl Roth GmbH& Co. KG, Karlsruhe, Germany).

Preparation of Calcium Buffer

Sterile, filtered Calcium Buffer was prepared by dissolving 100mM of Calcium chloride dihydrate (CaCl₂·2 H₂O 14.7 g/l) (2.94g in 200ml) in 25mM HEPES (4-(2-hydroxyethyl)-1-

piperazineethanesulfonic acid) (5.96 g/l) (1.192g in 200ml) and adjusting to pH 7.4. purchased from (Karl Roth GmbH & Co. KG, Karlsruhe, Germany).

Preparation of 4% alginate:

4 % Sodium alginate (Sigma Alderich, USA) was prepared by diluting 4 grams of Alginate, into 100ml of sterile water. Serialisation of alginate was performed using a benchtop autoclave (Systec VX-95, Systec, Germany).

Preparation of 2% Alginate:

2% alginate was prepared by diluting previously prepared sterile 4% alginate (sigma-aldrich) 1:2 with 2X wash buffer (sterile, filtered: 300mM Sodiumchloride (NaCl 8.77 g/l) (2.94 g for 200 ml) and 50mM HEPES (11,91 g/l) (0.595g for 50ml), PH-wert 7.4 -Karl Roth GmbH &Co. KG (Karlsruhe, Deutschland)).

2.9.1.2. Encapsulation:

Once the desired cell count was achieved in the cell suspension, it was spun down at 1200 rpm for 5 minutes. Then, the supernatant was discarded, and the cells were resuspended in 2% alginate (in a calculated volume of to allow 20 µl cell suspension of required concentration per disk). The disks (which were first submerged in PBS+ 1%ab/am) were dehydrated by pressing down on them using sterile gloves + sterile gauze. Then, they were placed in 24 well plates with one disk per well. The cell suspension containing alginate was then dropped onto the scaffolds and they were allowed to expand to full size. After the scaffolds absorbed the alginate media, 500µl of calcium buffer (sterile, filtered: 100nM Calciumchloride (NaCl, 8.77g/l) (0.877g for 100ml), 55 mM Tri-sodium/citrate dihydrate (C₆H₅Na₃O₇), pH-wert 7,4- Karl roth GmbH & Co. KG (Karlsruhe, Deutschland)) was dropped gently onto the scaffolds and left for 3-5 minutes. This which the alginate's instant gelation. Then the calcium was replaced with culture media and placed into the incubator.

2.9.2. CALCULATION OF CELL TO SCAFFOLD SEEDING DENSITY

Seeding densities were initially calculated based on a concentration of 1.5×10^5 cells/cm² with the assumption of uniform scaffold size. Therefore, in order to obtain the accurate seeding density per scaffold, the area of a 6mm punch biopsy was calculated based on the area of a cylinder as follows:

$$Area_{scaffold} = 2\pi rh + 2\pi r^2$$

Where r = radius, and h= height.

2.9.3. DIRECT CELL SEEDING OF TWO DIFFERENT SCAFFOLDS: INTEGRA® MATRIX AND DECELLULARIZED TRACHEA

2.9.3.1. Integra® Matrix (IM)

INTEGRA® Dermal Regeneration Template Single Layer, is an advanced 3D porous matrix consisting of bovine tendon collagen and chondroitin-6-sulfate and is used for dermal regeneration and more

recently, for cartilage regeneration. The IM was used in screening experiments as a substitute scaffold prior to tracheal trials due to limitations in tracheal quantity.

In order to mimic the approximate size and condition of the tracheal punch-biopsies, the IM sheet was cut into 6mm round-disks using a 6mm punch biopsy (Acu-Punch, Acuderm inc., USA), and then placed into sterile DPBS w/o: Ca and Mg (PAN – Biotech, Germany) and maintained at 4C° until use.

Direct, and passive seeding of IM was achieved by placing the disks on sterile gauze and covering them with another piece of sterile gauze and gently pressing on them to dry them out. Once the matrix dried out, it was placed into a 24-well plate (CELLSTAR®, greiner BIO-ONE, Germany) (one scaffold per well), and seeded with a 20µl droplet of media containing the required cell concentration. The seeded IM scaffolds were then placed into the incubator at 37 ° C +/- 2 ° C, 5% CO² +/- 1%, and passive humidification for 1 hour prior to the addition of the relevant CM.

2.9.3.2. Decellularized Trachea (DT)

All tracheas underwent a sterilisation process and were cut into 6mm punch biopsies prior to use. Direct, and passive seeding of trachea was performed after partial surface dehydration (PSD) of the trachea as described by Al Belushi, H. 2020 [159]. In short, prior to seeding of tracheal biopsies, they were first placed into 24 well plates (CELLSTAR®, greiner BIO-ONE, Austria) and conditioned with the designated media (as per specific seeding protocol) for 1-3 hours. Then, they were placed into an incubator at 37 ° C +/- 2 ° C, 5% CO² +/- 1%, and passive humidification for 1-2 hours in order to eliminate excess moisture and improve seeding efficiency. After PSD, the cells were seeded onto the DT by pipetting a 20µl cell suspension drop per biopsy.

2.9.3.3. Direct Seeding

Direct, and passive seeding of scaffolds describes the drying of scaffolds first (either DT or IM) as depicted earlier under section 2.9.3.1 and 2.9.3.2. (direct seeding of two different scaffolds). In short, the scaffolds were first dried out for better absorption, then they were rehydrated with the cell suspension. Afterwards, they were then placed into the incubator at 37 ° C +/- 2 ° C, 5% CO² +/- 1%, and passive humidification for 1 hour. At which point, the appropriate media was added. Subsequently, the scaffolds were left in the incubator for about 5 days until implantation and testing.

2.9.3.4. Cell Encapsulation

Prior to seeding the scaffolds with alginate encapsulated cells, the scaffolds were first dried in 24 well plates (CELLSTAR®, greiner BIO-ONE, Austria) as depicted earlier under section 2.9.3.1 and 2.9.3.2. (direct seeding of two different scaffolds). Then, cell suspensions containing complete media were centrifuged (Rotanda 460R, Hettich, Germany) at 1200rpm for 5 minutes, at 20C° upon which, the media was discarded and the cells were resuspended in 2% alginate (section 2.9). The Alginate/cell suspension volume was calculated according to the number of scaffolds multiplied by a 20µl drop of alginate cell suspension/scaffold. After the scaffolds were seeded with the encapsulated cell suspension, 300-400 µl of calcium buffer was placed on top of the scaffolds for a duration of 3 minutes

(enough to cover the scaffolds). Then the calcium was removed, and it was replaced with the relevant complete media (CM).

2.10. IN-OVO IMPLANTATION

In-Ovo Chorioallantoic Membrane Assay

2.10.1. Animal welfare and compliance:

In compliance with Directive 2010/63/EU of the European Parliament, embryonic chicks were kept in experimental conditions until embryonic day 15, after which, all chicks were euthanized in accordance with the German Animal Welfare Law.

2.10.2. Chorioallantoic Membrane Assay (CAM)

The in-ovo chorioallantoic membrane (CAM) assay offers an established, in-vivo, method that can provide a comprehensive and quick platform to screen for the applicability of the modifications made under our tissue engineering protocol [160-162].

The protocol used was adapted from Schmitd LB, et.al & Sys GML, et.al [163, 164]. Inactivated, fertilised, and specified pathogen-free (SPF) eggs we purchased from (VALO BioMedia GmbH, Germany). Three to seven days prior to the arrival of the eggs, the egg incubator (Hatchmaster, Germany) was set to a temperature of 37.8°C and a minimal humidity of 60%. Upon arrival, purchased eggs were placed in a room with a fixed temperature of 17°C for minimum of 24 hours and a maximum of 5 days. The day before beginning the CAM assay, the eggs were moved to room temperature (between 20-24 °C) for 12-24 hours to allow them to adjust. The day the eggs were placed into the egg incubator was designated as embryonic **day 0**. For the **first 3 days**, the eggs were rotated at 2-hour intervals to prevent the adherence of the developing embryo to the shell. **On day 3**, the rotation was stopped and the eggs were marked for opening. **At day 7**, the CAM membrane was dropped by creating two small holes at a 90° angle (one placed at the tip of the blunt edge of the egg and the other placed next to highly vascularised area of the CAM a minimum of 2 cm away from the developing embryo) and sucking the air out using a small Pasteur pipette bulb (Figure. Image D.). Then, a small window was opened using the Drumel and covered with 3M™ Tegaderm™ (praxisgroup24, Germany). **On embryonic day 8**, after a 24-hour period to allow the chick embryos to adjust to initial opening of the shell, the window was enlarged, and the engineered biopsies were implanted. The opened windows were once again covered with 3M™ Tegaderm™ (praxisgroup24, Germany) and they were allowed to remain in the egg incubators at a humidity of +/- 70°C till embryonic day 15. On day 15, prior to termination, the scaffolds were first imaged in-ovo, then 300µl was pipetted onto the CAM. After which, scissors were used quickly to cut the egg shell in half beginning from the hole made at the blunt end. The chick embryo was then promptly euthanised in accordance with the German Animal Welfare Law.

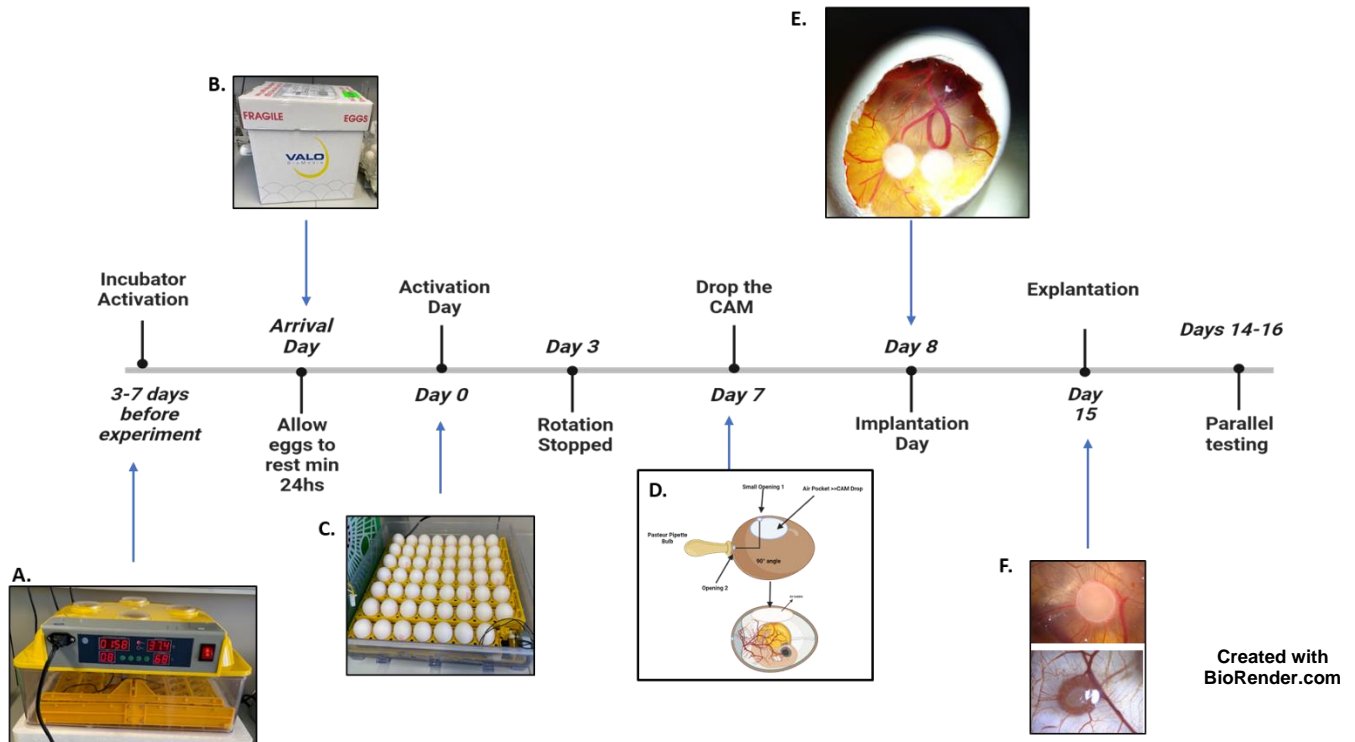


Figure 12. In-Ovo Chorioallantoic Membrane Assay. **A.** Egg incubator adjusting to 60% humidity and 37.8°C. **B.** Eggs allowed to settle for a minimum of 24 hours prior to activation. **C.** Activation Day: day the eggs are placed into the incubator and designated as day 0. **D.** Day 7 post activation: the CAM is dropped by creating two small holes at a 90° angle; one in the middle of the blunt head of the egg and the other next to a well vascularised area (at least 2 cm away from embryo), and then using a Pasteur pipette bulb to suck the air and drop the CAM. **E.** Day 8 (24 hours after opening) engineered scaffold(s) are placed onto the CAM. **F.** Day 15: Imaging and Explantation. **First**, the scaffolds are imaged in ovo, then the membrane is extracted and imaged again in vitro.

2.11. EXPERIMENTAL SET-UP OF MANUFACTURING SIMULATION PROCESS

2.11.1. MULTI-PARAMETRIC SCREENING PROCEDURE

In order to screen for the “optimal” protocol that would be the most conducive towards enhanced vascularisation, a manufacturing process depicted in (Figure) was performed five (n=5) times, and the results of these process were used in the development of the final testing protocol. Twenty-four, 24 different conditions consisting of varying combinations (Table.) were tested and implanted with blanks correlating to the conditions in-ovo.

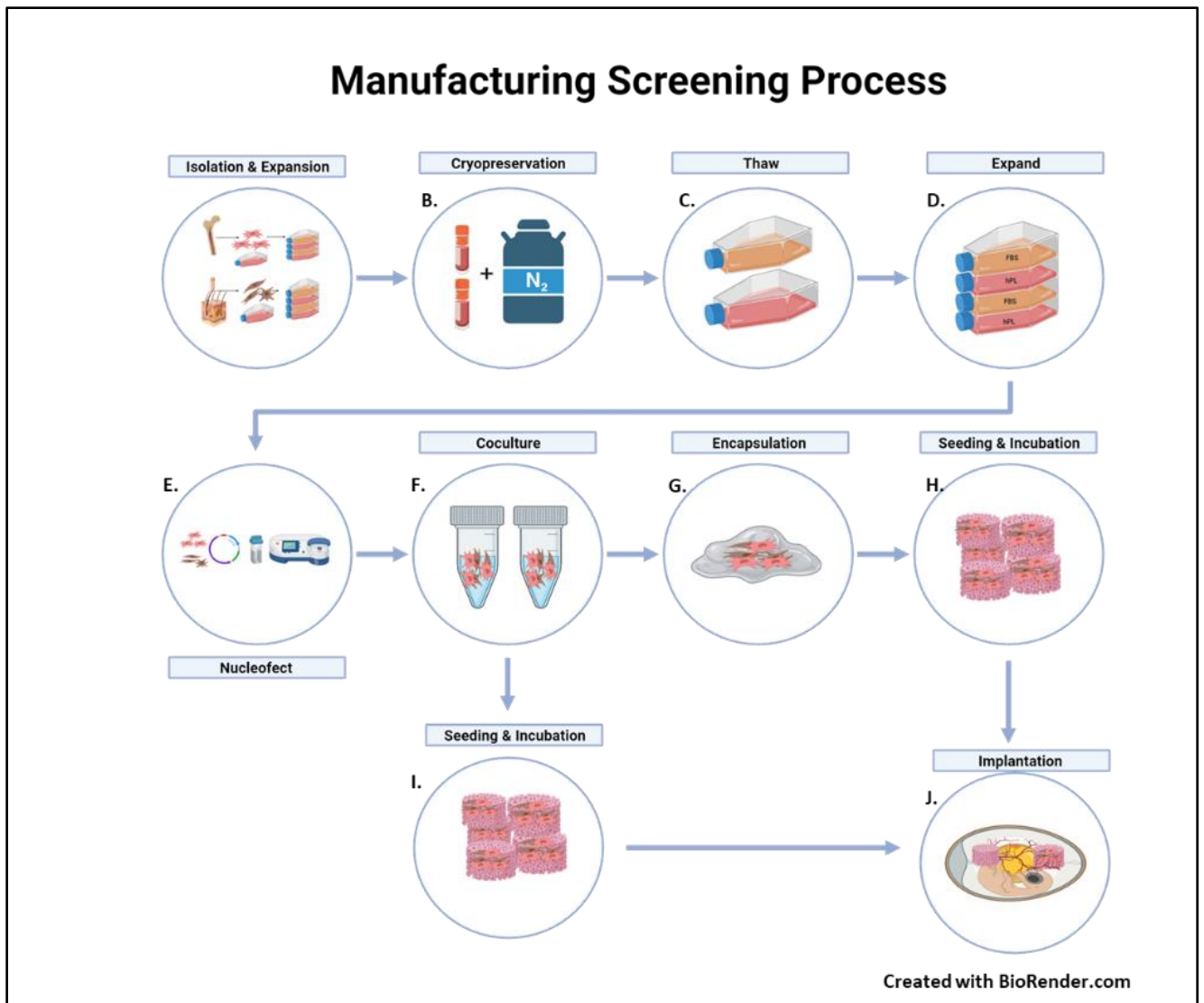


Figure 13. Manufacturing Process of Screening Experiments. **A.** Primary isolation/thaw and 1st expansion of human MSCs and DF (**n=5**). **B.** Cryopreservation of cells until time of use. **C.** Thaw of cells using two different media additives (FBS and hPL). **D.** Expansion of cells with two different media additives. Genetic modification using the 2B Nucleofector Device. **F.** Coculture of cells using different combinations and different ratios. **G.** Encapsulating some cell combinations with alginate. **H.** Seeding the encapsulated cells onto 6mm biopsies. **I.** Seeding the rest of the cells (non-encapsulated) directly onto 6mm biopsies. **J.** Implantation of the scaffolds in ovo onto the CAM.

2.11.2. SCREENED CONDITIONS

#	Protocol	In Ovo Implants	#	Protocol	In Ovo Implants
1	Protocol 1	TET 1+ Blank + FBS	13	Protocol 13	Coculture 2+ Blank +FBS
2	Protocol 2	TET 1+ Blank + hPL	14	Protocol 14	Coculture 2+ Blank +hPL
3	Protocol 3	TET 1 A + Blank A + FBS	15	Protocol 15	Coculture 2 A +Blank A +FBS
4	Protocol 4	TET 1 A + Blank A +hPL	16	Protocol 16	Coculture 2 A+ Blank A +hPL
5	Protocol 5	TET 2 + Blank +FBS	17	Protocol 17	Coculture 3 + Blank +FBS
6	Protocol 6	TET 2 + Blank +hPL	18	Protocol 18	Coculture 3+ Blank +hPL
7	Protocol 7	TET 2 A +Blank A +FBS	19	Protocol 19	Coculture 3 A + Blank A +FBS
8	Protocol 8	TET 2 A +Blank A + hPL	20	Protocol 20	Coculture 3 A + Blank A + hPL
9	Protocol 9	Coculture 1 +Blank + FBS	21	Control 1	Blank Scaffold + CM 1
10	Protocol 10	Coculture 1 +Blank + hPL	22	Control 2	Blank Scaffold + CM2
11	Protocol 11	Coculture 1 A + Blank A + FBS	23	Control 3	Blank Scaffold + Cocul. Media 1*
12	Protocol 12	Coculture 1 A + Blank A + hPL	24	Control 4	Blank Scaffold + Cocul. Media 2**

Tabelle 5. Overview of Screening Conditions: Protocols and Implants. * Coculture Media 1 ** Coculture Media 2.

2.11.2.1. PROTOCOL/CONDITION DESCRIPTION (S):

Blank: describes the addition of a blank unseeded scaffold (soaked in media)

Blank A: describes the addition of a blank seeded scaffold that has been coated with alginate and soaked in media

Protocol 1 (TET 1 + FBS): is an acronym for tissue engineered trachea protocol 1 which describes the use of expanded human bone marrow-derived MSCs, cultivated in media with FBS as an added supplement (derived from the protocol described by Elliot et.al. and TETRA), and seeded at a concentration of $1.5 \cdot 10^5$ cells/cm² using direct seeding methodology and maintained under static conditions with CM1 until implantation. >>> **Standard/Reference Protocol.**

Protocol 2 (TET 1) + hPL: is an acronym for tissue engineered trachea protocol 2 which describes the use of expanded human bone marrow-derived MSCs, cultivated in media with hPL rather than FBS as an added supplement (derived from the protocol described by Elliot et.al. and TETRA, with **modification1**), and seeded at a concentration of $1.5 \cdot 10^5$ cells/cm² using direct seeding methodology and maintained under static conditions with CM2 until implantation. >>> **Modification 1: Change in media supplement for better cell expansion.**

Protocol 3 (TET 1 A + FBS): is an acronym for tissue engineered trachea protocol 3 which describes the use of expanded human bone marrow-derived MSCs, cultivated in media with FBS (added supplement), and seeded onto 6 mm scaffolds at a concentration of $1.5 \cdot 10^5$ cells/cm² after encapsulating the cells with alginate. Seeding methodology was direct seeding and the scaffolds were maintained under static conditions with CM1 until implantation. >>>**Modification 2: Encapsulation of cells for enhanced cell seeding retention.**

Protocol 4 (TET 1 A + hPL): is an acronym for tissue engineered trachea protocol 4 which describes the use of expanded human bone marrow-derived MSCs, cultivated in media with *hPL* (added supplement), and seeded onto 6 mm scaffolds at a concentration of $1.5 \cdot 10^5$ cells/cm² after encapsulating the cells with alginate. Seeding methodology was direct seeding and the scaffolds were maintained under static conditions with CM2 until implantation. >>>**Modification 3: Change in media supplement and encapsulation.**

Protocol 5 (TET 2 + FBS): is an acronym for tissue engineered trachea protocol 5 which describes the use of expanded human bone marrow-derived MSCs, cultivated in media with FBS as an added supplement (derived from the protocol described by Elliot et.al. and the original TETRA protocol), and seeded at a concentration of $7.5 \cdot 10^5$ cells/cm² (five times the amount recommended by TETRA) using a direct seeding methodology and maintained under static conditions with CM1 until implantation >>>**Modification 4: 5x Increase in cell seeding concentration.**

Protocol 6 (TET 2 + hPL): is an acronym for tissue engineered trachea protocol 6 which describes the use of expanded human bone marrow-derived MSCs, cultivated in media with *hPL* as an added supplement (derived from the protocol described by Elliot et.al. and the original TETRA protocol), and seeded at a concentration of $7.5 \cdot 10^5$ cells/cm² (five times the amount recommended by TETRA) using a direct seeding methodology and maintained under static conditions with CM2 >>> **Modification 5: 5x Increase in cell seeding concentration and change in media supplement.**

Protocol 7 (TET 2 A + FBS): is an acronym for tissue engineered trachea protocol 7 which describes the use of expanded human bone marrow-derived MSCs, cultivated in media with FBS (as an added supplement), and seeded onto 6 mm scaffolds at a concentration of $7.5 \cdot 10^5$ cells/cm² (five times the amount recommended by TETRA) after encapsulating the cells with alginate. Employed seeding methodology consisted of direct seeding and the scaffolds were maintained under static conditions with CM1 until implantation. >>>**Modification 6: 5X Increase in cell seeding concentration and alginate encapsulation.**

Protocol 8 (TET 2 A + hPL): is an acronym for tissue engineered trachea protocol 8 which describes the use of expanded human bone marrow-derived MSCs, cultivated in media with *hPL* (as an added supplement), and seeded onto 6 mm scaffolds at a concentration of $7.5 \cdot 10^5$ cells/cm² (five times the amount recommended by TETRA) after encapsulating the cells with alginate. Employed seeding methodology consisted of direct seeding and the scaffolds were maintained under static conditions

with CM2 until implantation. >>>**Modification 7: 5X Increase in cell seeding concentration, change in media supplement, and alginate encapsulation.**

Protocol 9 (Coculture 1 + FBS): is an acronym for tissue engineered trachea protocol 9 which describes the use of both expanded human bone marrow-derived MSCs and human dermal fibroblasts (HDFs), cultivated in media with FBS (as an added supplement), combined into one tube (Figure 14.) at a ratio of 50:50, and seeded onto 6 mm scaffolds at a concentration of 1.5×10^5 cells/cm². Employed seeding methodology consisted of direct seeding and the scaffolds were maintained under static conditions with **CocM1** until implantation. >>>**Modification 8: Coculture with HDF.**

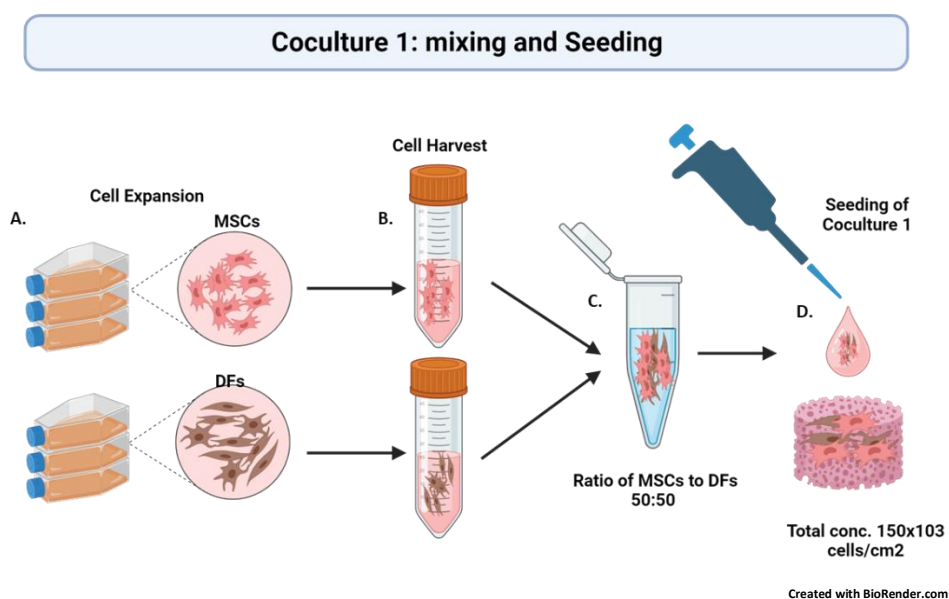


Figure 14. Process of Generating Coculture 1 seeded scaffold. **A.** Expansion of MSCs and HDFs. **B.** Trypsinization and counting of cells. **C.** Mixing of cells in an Eppendorf tube at a ratio of 50:50. **D.** Direct seeding of scaffolds at a seeding density of 1.5×10^5 cells/cm².

Protocol 10 (Coculture 1 + hPL): is an acronym for tissue engineered trachea protocol 10 which describes the use of both expanded human bone marrow-derived MSCs and human dermal fibroblasts (HDFs), cultivated in media with hPL (as an added supplement), combined into one tube (Figure 14.) at a ratio of 50:50, and seeded onto 6 mm scaffolds at a concentration of 1.5×10^5 cells/cm². Employed seeding methodology consisted of direct seeding and the scaffolds were maintained under static conditions with CocM2 until implantation. >>>**Modification 8: Change in media supplement and coculture with HDF.**

Protocol 11 (Coculture 1 A + FBS): is an acronym for tissue engineered trachea protocol 11 which describes the use of both expanded human bone marrow-derived MSCs and human dermal fibroblasts (HDFs), cultivated in media with FBS (as an added supplement), combined into one tube (Figure 15.) at a ratio of 50:50, and seeded onto 6 mm scaffolds at a concentration of 1.5×10^5 cells/cm² after

cellular encapsulation with alginate (FIGURE). Employed seeding methodology consisted of direct seeding and the scaffolds were maintained under static conditions with CocM1 until implantation. >>>**Modification 8: Coculture with HDF and alginate encapsulation.**

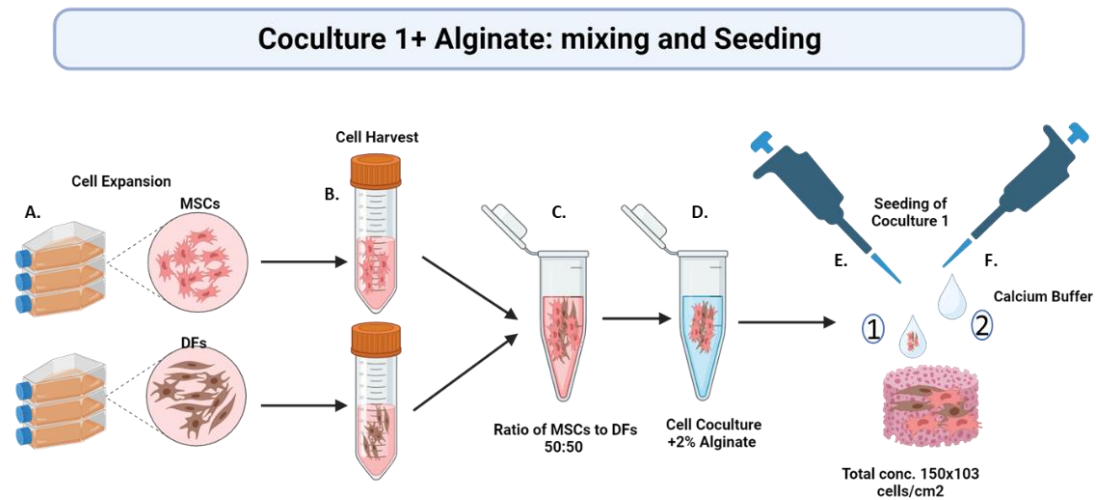


Figure 15. Process of Generating Coculture 1 Alginate Encapsulated Scaffold. A. Expansion of MSCs and HDFs. B. Trypsinization and counting of cells. C. Mixing of cells in an Eppendorf tube at a ratio of 50:50. D. Encapsulation of cells with Alginate. E. First, direct seeding of cells immersed in alginate at a seeding density of 1.5×10^5 cells/cm². F. Second, addition of calcium buffer.

Protocol 12 (Coculture 1 A + hPL): is an acronym for tissue engineered trachea protocol 12 which describes the use of both expanded human bone marrow-derived MSCs and human dermal fibroblasts (HDFs), cultivated in media with hPL (as an added supplement), combined into one tube (Figure 15.) at a ratio of 50:50, and seeded onto 6 mm scaffolds at a concentration of 1.5×10^5 cells/cm² after cellular encapsulation with alginate (FIGURE). Employed seeding methodology consisted of direct seeding and the scaffolds were maintained under static conditions with CocM2 until implantation. >>>**Modification 8: Change in media supplement, coculture with HDF, and alginate encapsulation.**

Protocol 13 (Coculture 2 + FBS): is an acronym for tissue engineered trachea protocol 13 which describes the use of both expanded non-transfected human bone marrow-derived MSCs and transfected MSCs (nucleofected with VEGF and bFGF 1:1), cultivated in media with FBS (as an added supplement), combined into one tube (Figure) at a ratio of 50:50, and seeded onto 6 mm scaffolds at a concentration of 1.5×10^5 cells/cm². Employed seeding methodology consisted of direct seeding and the scaffolds were maintained under static conditions with CM1 until implantation. >>>**Modification 8: Coculture with transfected MSCs.**

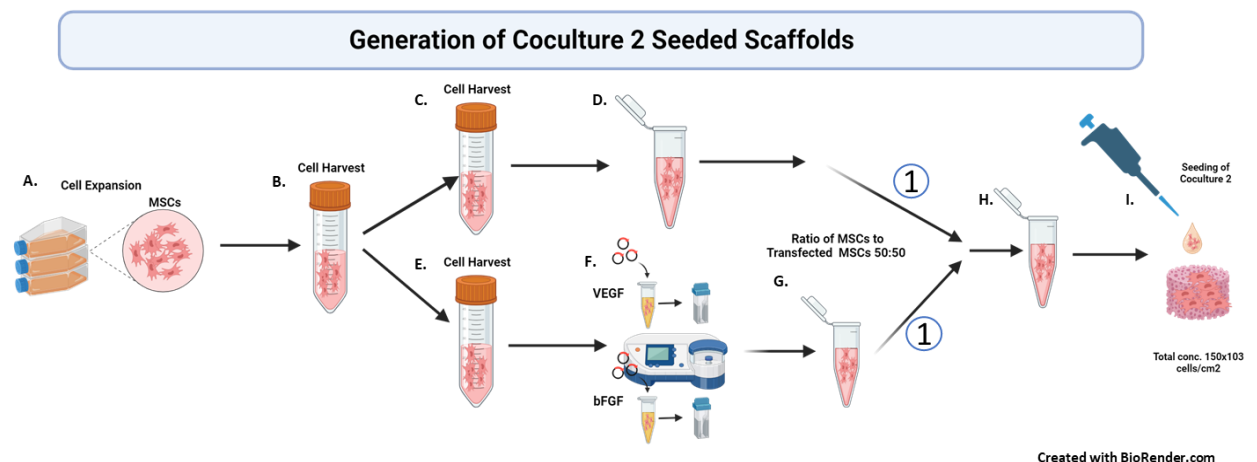


Figure 16. Process of Generating Coculture 2 Seeded Scaffold. A. Expansion of MSCs. B. Trypsinization and counting. C. Splitting of cells into the required amount for direct seeding. D. Preparation of cells for Direct Seeding. E. Splitting of cells for transfection. F. Transient genetic modification of MSCs to over express bFGF and VEGF. G. Mixing of pmax-bFGF nucleofected MSCs and pmax-VEGF nucleofected MSCs into one tube. H. Generation of Coculture 3: (1) addition of non-transfected MSCs at a seeding density of 0.75×10^5 cells/cm² (2) addition of VEGF and bFGF transfected MSCs at a seeding density of 0.75×10^5 cells/cm². I. Direct seeding of coculture 2 onto scaffolds at a total seeding density of 1.5×10^5 cells/cm².

Protocol 14 (Coculture 2 + hPL): is an acronym for tissue engineered trachea protocol 14 which describes the use of both expanded non-transfected human bone marrow-derived MSCs and transfected MSCs (nucleofected with VEGF and bFGF 1:1), cultivated in media with hPL (as an added supplement), combined into one tube (Figure 16.) at a ratio of 50:50, and seeded onto 6 mm scaffolds at a concentration of 1.5×10^5 cells/cm². Employed seeding methodology consisted of direct seeding and the scaffolds were maintained under static conditions with CM2 until implantation. >>>**Modification 8: Change in media supplement and coculture with transfected MSCs.**

Protocol 15 (Coculture 2 A + FBS): is an acronym for tissue engineered trachea protocol 15 which describes the use of both expanded non-transfected human bone marrow-derived MSCs and transfected MSCs (nucleofected with VEGF and bFGF 1:1), cultivated in media with FBS (as an added supplement), combined into one tube (Figure 17.) at a ratio of 50:50, and seeded onto 6 mm scaffolds at a concentration of 1.5×10^5 cells/cm² after cellular encapsulation with alginate. Employed seeding methodology consisted of direct seeding and the scaffolds were maintained under static conditions with CM1 until implantation >>>**Modification 8: Coculture with transfected MSCs and alginate encapsulation.**

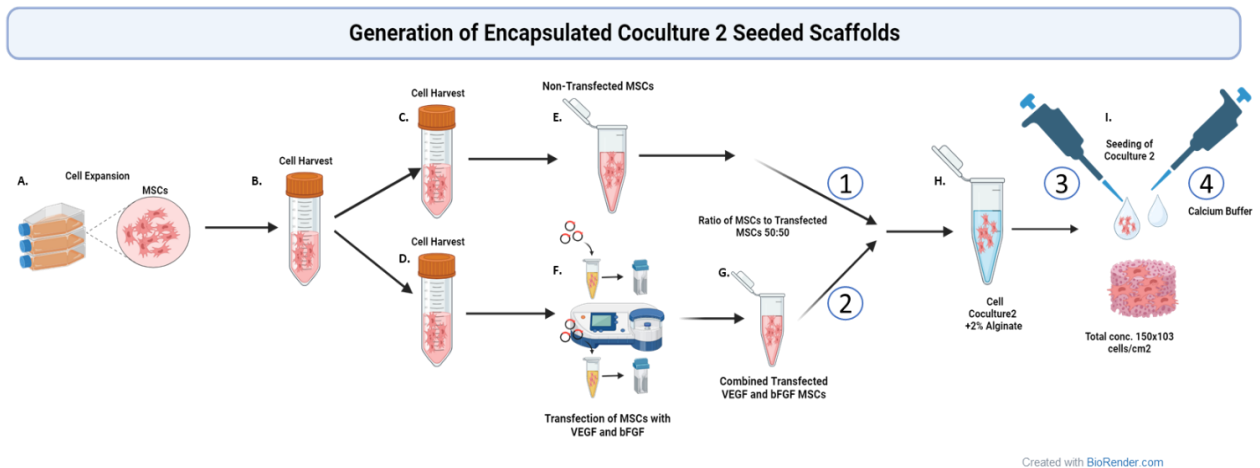


Figure 17. Process of Generating Coculture 2 Encapsulated Seeded Scaffolds. A. Expansion of MSCs. B. Trypsinization and counting of cells. C. Splitting of cells into the required amount for direct seeding. D. Splitting of cells for transfection. E. Preparation of cells for Direct Seeding. F. Transient genetic modification of MSCs to over express bFGF and VEGF. G. Mixing of pmax-bFGF nucleofected MSCs and pmax-VEGF nucleofected MSCs into one tube. H. Mixing of: (1) non-transfected MSCs at a seeding density of 0.75×10^5 cells/cm² & (2) VEGF and bFGF transfected MSCs at a seeding density of 0.75×10^5 cells/cm² and then encapsulating with alginate. I. Seeding Process: (3) direct seeding of cells immersed in alginate at a seeding density of 1.5×10^5 cells/cm² (4) addition of calcium buffer.

Protocol 16 (Coculture 2 A + hPL): is an acronym for tissue engineered trachea protocol 16 which describes the use of both expanded non-transfected human bone marrow-derived MSCs and transfected MSCs (nucleofected with VEGF and bFGF 1:1), cultivated in media with hPL (as an added supplement), combined into one tube at a ratio of 50:50, and seeded onto 6 mm scaffolds at a concentration of 1.5×10^5 cells/cm² after cellular encapsulation with alginate (Figure 17.). Employed seeding methodology consisted of direct seeding and the scaffolds were maintained under static conditions with CM2 until implantation. >>>**Modification 8: Change in media supplement, coculture with transfected MSCs, and alginate encapsulation.**

Protocol 17 (Coculture 3 + FBS): is an acronym for tissue engineered trachea protocol 17 which describes the use of both expanded non-transfected human bone marrow-derived MSCs and transfected **HDFs** (nucleofected with VEGF and bFGF 1:1), cultivated in media with FBS (as an added supplement), combined into one tube (Figure 18.) at a ratio of 50:50, and seeded onto 6 mm scaffolds at a concentration of 1.5×10^5 cells/cm². Employed seeding methodology consisted of direct seeding and the scaffolds were maintained under static conditions with CocM1 until implantation. >>>**Modification 8: Coculture with transfected HDF.**

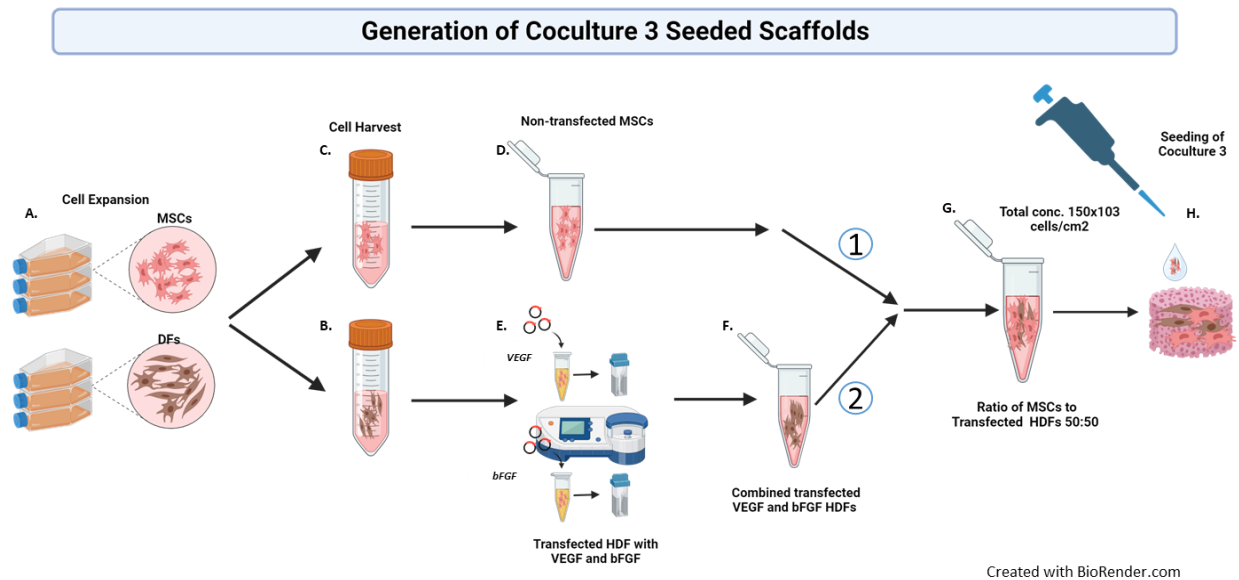


Figure 18. Process of Generating Coculture 3 Seeded Scaffold. **A.** Expansion of MSCs and HDFs. **B.** Trypsinization and counting of HDFs. **C.** Trypsinization and counting of MSCs. **Preparation of cells for Direct Seeding.** **E.** Transient genetic modification of MSCs to over express bFGF and VEGF. **F.** Mixing of pmax-bFGF nucleofected MSCs and pmax-VEGF nucleofected MSCs into one tube. **G.** Generation of Coculture3: **(1)** addition of non-transfected MSCs at a seeding density of 0.75×10^5 cells/cm² **(2)** addition of VEGF and bFGF transfected HDFs at a seeding density of 0.75×10^5 cells/cm². **H.** Direct seeding of coculture 3 onto scaffolds at a total seeding density of 1.5×10^5 cells/cm².

Protocol 18 (Coculture 3 + hPL): is an acronym for tissue engineered trachea protocol 18 which describes the use of both expanded non-transfected human bone marrow-derived MSCs and transfected *HDFs* (nucleofected with VEGF and bFGF 1:1), cultivated in media with hPL (as an added supplement), combined into one tube at a ratio of 50:50, and seeded onto 6 mm scaffolds at a concentration of 1.5×10^5 cells/cm². Employed seeding methodology consisted of direct seeding and the scaffolds were maintained under static conditions with CocM2 until implantation. >>>**Modification 8: Change in media supplement and coculture with transfected HDF.**

Protocol 19 (Coculture 3 A + FBS): is an acronym for tissue engineered trachea protocol 19 which describes the use of both expanded non-transfected human bone marrow-derived MSCs and transfected *HDFs* (nucleofected with VEGF and bFGF 1:1), cultivated in media with FBS (as an added supplement), combined into one tube (Figure) at a ratio of 50:50, and seeded onto 6 mm scaffolds at a concentration of 1.5×10^5 cells/cm² after cellular encapsulation with alginate (Figure 19.). Employed seeding methodology consisted of direct seeding and the scaffolds were maintained under static conditions with CocM1 until implantation. >>>**Modification 8: Coculture with transfected HDFs and alginate encapsulation.**

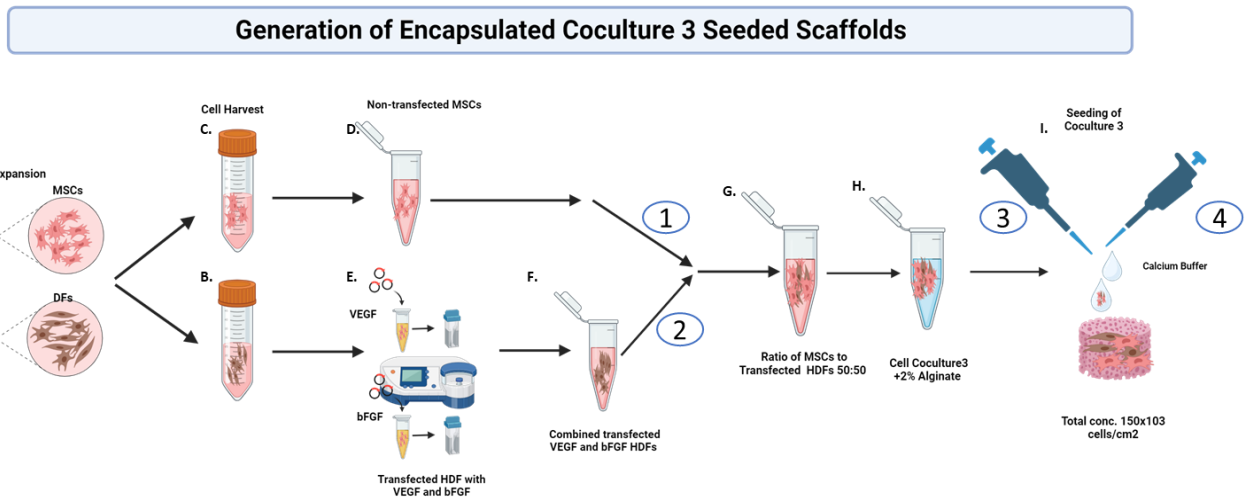


Figure 19. Process of Generating Coculture 3 Encapsulated and Seeded Scaffolds. **A.** Expansion of MSCs and HDFs. **B.** Trypsinization and counting of HDFs. **C.** Trypsinization and counting of MSCs. **Preparation of cells for Direct Seeding.** **E.** Transient genetic modification of MSCs to over express bFGF and VEGF. **F.** Mixing of pmax-bFGF nucleofected MSCs and pmax-VEGF nucleofected MSCs into one tube. **G.** Generation of Coculture3: **(1)** addition of non-transfected MSCs at a seeding density of 0.75×10^5 cells/cm² **(2)** addition of VEGF and bFGF transfected HDFs at a seeding density of 0.75×10^5 cells/cm². **H.** Alginate encapsulation of coculture 3 cells. **I.** Seeding Process: **(3)** direct seeding of cells immersed in alginate at a total seeding density of 1.5×10^5 cells/cm² **(4)** addition of calcium buffer.

Protocol 20 (Coculture 3 A + hPL): is an acronym for tissue engineered trachea protocol 20 which describes the use of both expanded non-transfected human bone marrow-derived MSCs and transfected **HDFs** (nucleofected with VEGF and bFGF 1:1), cultivated in media with hPL (as an added supplement), combined into one tube at a ratio of 50:50, and seeded onto 6 mm scaffolds at a concentration of 1.5×10^5 cells/cm² after cellular encapsulation with alginate. Employed seeding methodology consisted of direct seeding and the scaffolds were maintained under static conditions with CocM2 until implantation. >>>**Modification 8: Change in media supplement, coculture with transfected HDFs, and alginate encapsulation.**

Control 1: describes an unseeded scaffold soaked in **(CM1)** Alpha MEM Eagle w/o L-glutamine (PAN - Biotech, Germany) + FBS (Gibco™, ThermoFischer Scientific, Germany) + ab/am and treated as a test scaffold.

Control 2: describes an unseeded scaffold soaked in **(CM2)** Alpha MEM Eagle w/o L-glutamine (PAN - Biotech, Germany), Germany) + hPL + ab/am and treated as a test scaffold.

Control 3: describes an unseeded scaffold soaked in coculture media 1 **(CocM1)** consisting of a 50:50 ratio of **CM1:CM3** (Alpha MEM Eagle w/o L-glutamine (PAN - Biotech, Germany) + prepared with 10% FBS (Gibco™, ThermoFischer Scientific, Germany) + 1% am /am (Capricorn Scientific, Germany) & DMEM w: 4.5 g/L Glucose and w: st. Glutamine (PAN - Biotech, Germany) prepared with 10% FBS (Gibco™, ThermoFischer Scientific, Germany) + 1% am /am (Capricorn Scientific, Germany)).

Control 4 : describes an unseeded scaffold soaked in coculture media 2 **(CocM2)** consisting of a 50:50 ratio of **CM2:CM4** (Alpha MEM Eagle w/o L-glutamine (PAN - Biotech, Germany) + prepared with 10%

FBS (Gibco™, ThermoFischer Scientific, Germany) + 1% am /am (Capricorn Scientific, Germany) & DMEM w: 4.5 g/L Glucose and w: st. Glutamine (PAN - Biotech, Germany) prepared with 10% FBS (Gibco™, ThermoFischer Scientific, Germany) + 1% am /am (Capricorn Scientific, Germany)).

Once the engineered scaffolds were generated they were incubated at 37 ° C +/- 2 ° C, 5% CO² +/- 1%, and passive humidification for 5-7 days. After 5-7 days, they were implanted in ovo onto the CAM next to a large vessel to encourage vascularization. Engineering of the scaffolds took place on the same day as day 1-2 of egg incubation, and were subsequently implanted on embryonic day 8 in accordance to the CAM assay protocol (9.2)

2.12. STAINING

Alcian Blue Staining:

Alcian Blue is for cartilage matrix and proteoglycans staining, it stains both blue.

Preparation of Alcian Blue Solution: *is prepared as 1% Alcian blue (Roth, Germany) + 3% Acetic Acid (Catalogue N. 7437.1, Roth, Germany) or 1gram of Alcian blue + 100 ml of 3% Acetic Acid stored at 2-4C°*

Alizarin Red S Staining:

Alizarin Red stains calcium produced by the cells red/brown.

Preparation of 0.5% Alizarin Red S Solution: *0.5g of Alizarin Red (Catalogue N. A-5533, Sigma-Aldrich, USA) powder was dissolved in 100ml ultrapure water using a magnetic rotator and a shaker. The resulting solution was then adjusted to a pH of 4.2 using 10% ammonium hydroxide and HCL.*

Alizarin Red stains calcium deposits red/orange.

Oil Red O Staining:

Oil red O stains fat vacuoles within cells orange.

Preparation of Oil Red O stain:

Stock solution: *150mg of Oil Red O (Catalogue N. O-0625, Sigma-Aldrich, USA) powder was dissolved in 50ml isopropanol while stirring overnight. The solution was then filtered using a 0.2µm pore-sized filter and stored at 4C°.*

Working solution: *Oil Red O working solution was prepared fresh before use, and consisted of 3 parts Oil Red O stock solution and 2 parts of Ultrapure water.*

Oil Red O stains fat vacuoles in the cells an orange colour that can easily be visualized using brightfield microscopy.

2.13. ISOLATION OF SINGLE CELLS FROM TRACHEA

In order to gain insight on status post seeding onto 3D tracheal matrices and incubation, and prior to implantation, four different protocols were investigated to identify the most suitable approach to isolate single cells from seeded tracheal biopsies for subsequent flow cytometry analysis. End target was set at 90+% of viability and the larger number of cells collected from the biopsies.

PROTOCOL 1:

Protocol one was adapted from an in-house protocol (Experimental Plastic Surgery and Hand Surgery Laboratory, Department of Plastic Surgery and Hand surgery, Klinikum rechts der Isar, TUM, Germany) Seeded scaffolds were treated to an enzyme solution consisting of 1mg collagenase A per 1ml of PBS (0.1%), filtered for sterility with a 0.22µm pore size filter.

Prepared Solutions:

DNase I solution (freshly prepared each time): DNase (100 mg) (DNase I, from bovine pancreas, Catalogue# DN25-100MG, Sigma-Aldrich®, USA) in 0.15M Sodium Chloride (NaCl) (5mg/ml).

DNase I Stock Solution1 (S1): 25 mg in 5ml of 0.15M NaCl (5mg/ml).

DNase I Stock solution 2 (S2): 1ml S1+ 4ml 0.15M NaCl (1mg/ml).

Working Solution (prepared from 5ml of stock solutions):

4.495 ml of Collagenase A; 0.1% =1mg/ml, + 0.005ml DNase I; µg/ml (S2 1:1000), + 0.5ml EDTA; 10mM (Stock 1:10) = 300µl working solution / biopsy

Protocol:

Prior to beginning the dissociation process, the scaffolds were weighed, washed 1X with DPBS w/o: Ca and Mg (PAN – Biotech, Germany), cut into small pieces (as small as possible) using a scalpel, and transferred into 1.5 ml Eppendorf tubes. Then 300µl of Collagenase I working solution was added to each biopsy and incubated at 37C° for 30 minutes in a water bath with 10-minute intervals of vortexing until an emulsion emerged. Afterwards, the reaction was stopped with 300µl of DPBS w/o: Ca and Mg (PAN – Biotech, Germany) + 10% FBS (Gibco™, ThermoFischer Scientific, Germany), and samples were centrifuged at 340g(2.300rpm) using the Eppendorf Minispin (Mini Star, silverline 1,5ml Eppis, VWR,). The supernatant was carefully removed, resuspended in 300µl of DPBS, and filtered through a 100µM pore filter into Eppendorf tubes for removal of biopsy residues. Then, another filtration step was made, and the cell suspension was centrifuged at 340g (1.300rpm) (Rotanda 460R, Hettich, Germany) for 10 minutes at 20C°. The supernatant was subsequently removed, and the pellet was resuspended in 300µl of complete cell culture media. After the samples were resuspended 100µl was taken for counting on the CASY® counter (Innovatis, OLS OMNI Life Science, Germany), and 20µl of the cell suspension was added to another 20µl of 0.2% trypan blue solution (**Sigma-Aldrich, USA**) (of which 10µl was taken) for counting using the Neubauer chamber (C-Chip haemocytometer, DHC-N01, NanoEnTek Inc., Gyeonggi-do, Korea).

PROTOCOL 2:

This protocol was adapted from a paper by Greaney AM, et.al. 2020[165]. Seeded scaffolds were treated to an Accutase working solution. In short:

Prepared Solutions:

DNase I solution (freshly prepared each time): DNase (100 mg) (DNase I, from bovine pancreas, Catalogue# DN25-100MG, Sigma-Aldrich®, USA) in 0.15M Sodium Chloride (NaCl) (5mg/ml).

DNase I Stock Solution1 (S1): 25 mg in 5ml of 0.15M NaCl (5mg/ml).

DNase I Stock solution 2 (S2): 1ml S1+ 4ml 0.15M NaCl (1mg/ml).

Working Solution (prepared form 5ml of stock solutions):

4,495ml Accutase (Accutase Solution 100 ml, PromoCell, Germany) in PBS+ 5mM EDTA 0.005ml + Dnase I; 1µg/ml (S2 1:1000) + 0.5ml EDTA; 10mM (Stock 1:10) = 300µl working solution / biopsy

Protocol:

Prior to beginning the dissociation process, the scaffolds were weighed, washed 1X with DPBS w/o: Ca and Mg (PAN – Biotech, Germany), cut into small pieces (as small as possible) using a scalpel, and transferred into 1.5 ml Eppendorf tubes. Then 300µl of the Accutase working solution was added to each biopsy and incubated for 10 minutes at RT on the tilt shaker, and then placed on the MACSmix™ tube rotator (MACs, Miltenyi Biotec, Germany) in the incubator at 37C° for 5 minutes. After incubation, the samples were shortly vortexed, filtered through a 100µm cell filter for the removal of biopsy residues. The cell suspension was centrifuged once again at 340g (1.300rpm) (Rotanda 460R, Hettich, Germany) for 10 minutes at 20C°. The supernatant was removed, and the pellet was resuspended in 300µl of complete cell culture media. After the samples were resuspended 100µl was taken for counting on the CASY® counter (Innovatis, OLS OMNI Life Science, Germany), and 20µl of the cell suspension was added to another 20µl of 0.2% trypan blue solution (Sigma-Aldrich, USA) (of which 10µl was taken) for counting using the Neubauer chamber (C-Chip haemocytometer, DHC-N01, NanoEnTek Inc., Gyeonggi-do, Korea).

PROTOCOL 3:

This protocol was adapted from a paper by Greaney AM, et.al. 2020[165]. Seeded scaffolds were treated to a Protease XIV working solution. In short:

Prepared Solutions:

Preparation of Protease XIV Stock Solution:

Protease XIV (1g): 20mg in 100ml 10mM sodium acetate (NaAc) + 5mM calcium acetate (CaAc) solution (0.2mg/ml)

10mM Sodium Acetate Trihydrate (NaAc) + 5mM Calcium Acetate CaAc (200ml): 100ml A.dest + 272mg NaAc + 100ml 10mM CaAc.

DNase I solution (freshly prepared each time): DNase (100 mg) (DNase I, from bovine pancreas, Catalogue# DN25-100MG, Sigma-Aldrich®, USA) in 0.15M Sodium Chloride (NaCl) (5mg/ml).

DNase I Stock Solution1 (S1): 25 mg in 5ml of 0.15M NaCl (5mg/ml).

DNase I Stock solution 2 (S2): 1ml S1+ 4ml 0.15M NaCl (1mg/ml).

Working Solution1 (prepared form 5ml of stock solutions):

4.35ml PBS+ 0.1ml Dnase I; 0.1mg/ml (S1 1:50) + 0.05ml Protease XIV; 1% 0.2mg/ml (Stock 1:100) 0.5ml EDTA; 10mM (Stock 1:10). Further dilute 1:8 with washing medium α -MEM with 1%L-Glu, 1%ab/am (without FBS)>> 500µl 1Wks + 3.5ml washing medium=300µl working solution / biopsy

DL-Dithiothreitol (DTT) (1g): must be freshly prepared for every procedure:

(50mg/ml) 25mg of DTT in 500µl distilled water.

Working Solution2 (prepared form 5ml of stock solutions):

3.55ml PBS+ 0.1ml DNase I; 10µg/ml (S2 1:100) +0.1ml EDTA; 2mM (Stock 1:50) + 1.25ml Collagenase 1; 0.25mg/ml (stock 1:4) + 0.05ml DTT; 0.5mg/ml (stock 1:100) =300µl working solution / biopsy

Protocol:

Prior to beginning the dissociation process, the scaffolds were weighed, washed 1X with DPBS w/o: Ca and Mg (PAN – Biotech, Germany), cut into small pieces (as small as possible) using a scalpel, and transferred into 1.5 ml Eppendorf tubes. Then 300µl of the Protease XIV working solution was added to each biopsy and incubated for approximately 17 hours on the MACSmix™ tube rotator (MACs, Miltenyi Biotec, Germany) at 4C°. After incubation, the reaction was stopped with 300µl of complete medium (with FBS), the Eppis were vortexed for 10 seconds, centrifuged at 300g for 5 minutes (Eppendorf Centrifuge, 5415R, Germany) at 4C°, the supernatant was removed, the cell pallet was resuspended with the biopsy pieces in 300µl of washing medium, and centrifuged again (as previous). Afterwards, the biopsies were resuspended in 300µl Working Solution 2 and incubated on the MACSmix™ tube rotator (MACs, Miltenyi Biotec, Germany) at 37C° for 10 minutes. The reaction was stopped once again with 300µl of complete medium (+ FBS), filtered through a 100µm cell filter for the removal of biopsy residues and the samples were transferred to new 1.5ml Eppendorf tubes for centrifugation (Eppendorf Centrifuge, 5415R, Germany) at 300g for 5 minutes and 4C°. After centrifugation, the supernatant was removed and the cells were resuspended in complete cell culture medium with 10% FBS. After the samples were resuspended, 100µl was taken for counting on the CASY® counter (Innovatis, OLS OMNI Life Science, Germany), and 20µl of the cell suspension was added to another 20µl of 0.2% trypan blue solution (Sigma-Aldrich, USA) (of which 10µl was taken) for counting using the Neubauer chamber (C-Chip haemocytometer, DHC-N01, NanoEnTek Inc., Gyeonggi-do, Korea).

PROTOCOL 4:

This protocol was adapted from a paper by Ravindran A, et.al.2018[166]. Seeded scaffolds were treated to a Collagenase type II-based working solution. In short:

Prepared Solutions:

Preparation of the enzyme buffer from stock solutions 200ml:

197ml RPMI Medium + 3ml HEPES 0,015M (Stock 1:66,6)

DNase I solution (freshly prepared each time): DNase (100 mg) (DNase I, from bovine pancreas, Catalogue# DN25-100MG, Sigma-Aldrich®, USA) in 0.15M Sodium Chloride (NaCl) (5mg/ml).

DNase I Stock Solution1 (S1): 25 mg in 5ml of 0.15M NaCl (5mg/ml).

DNase I Stock solution 2 (S2): 1ml S1+ 4ml 0.15M NaCl (1mg/ml).

Working Solution (prepared form 5ml of stock solutions):

3,675ml preheated enzyme buffer +0.625ml collagenase type 2; 0.125mg/ml (stick 1:8) +0,2ml DNase I; 0,2mg/ml (S1 1:25) +0,5ml EDTA; 10mM (Stock 1:10) = 300µl working solution / biopsy

Protocol:

Prior to beginning the dissociation process, the scaffolds were weighed, washed 1X with DPBS w/o: Ca and Mg (PAN – Biotech, Germany), cut into small pieces (as small as possible) using a scalpel, and transferred into 1.5 ml Eppendorf tubes. Then 300µl of the Collagenase type-II working solution was added to each biopsy and incubated in a water bath at 37C° for 45 minutes with vigorous vortexing every 5 minutes. The reaction was stopped after 45 minutes by adding 300µl of cell culture medium with 10% FBS (Gibco™, ThermoFischer Scientific, Germany) and the supernatant was transferred with the biopsy pieces to a 24-well plate (CELLSTAR®, greiner BIO-ONE, Germany) (1 well/Eppi.). Once all the samples had been transferred to the wells they were subjected to mechanical separation by means of pipetting up and down 10X with a 1ml syringe. Afterwards, the supernatant was filtered using a 100µm cell filter into a new 1.5ml Eppendorf tube. The remaining biopsy pieces were returned to the 24 well plate with 300µl medium. The process of mechanical separation was repeated another 3 times with the syringe and filtering and then the samples were pooled and centrifuges at 400g 4°C for 10min using the (Eppendorf centrifuge, 5415R, county). The supernatant was removed and the cell pellet was resuspended in 300µl in complete medium. After the samples were resuspended 100µl was taken for counting on the CASY® counter (Innovatis, OLS OMNI Life Science, Germany), and 20µl of the cell suspension was added to another 20µl of 0.2% trypan blue solution (Sigma-Aldrich, USA) (of which 10µl was taken) for counting using the Neubauer chamber (C-Chip haemocytometer, DHC-N01, NanoEnTek Inc., Gyeonggi-do, Korea).

2.14. FINAL PROTOCOL MANUFACTURING: 3D VISUALISATION

The previous experiments resulted in the design of the final screening experiments which tested four different manufacturing process with different conditions, against the standard or control manufacturing process adapted from Elliot, et.al and the TETRA protocol; and consisting of MSCs expanded in media with FBS seeded directly onto a decellularized trachea under static conditions. The following figure (number) provides an overview of the final 3D screening protocol (n=3).

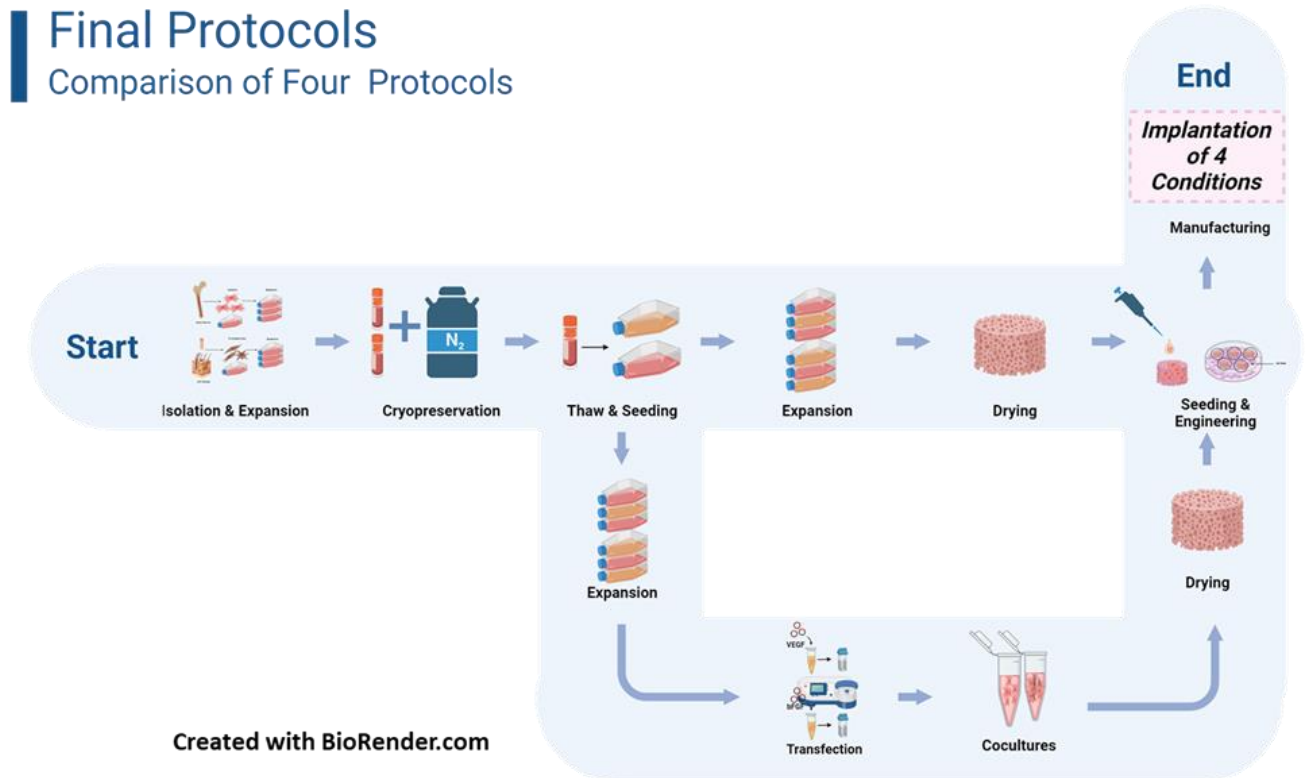


Figure 20. Graphical Representation of the TET Manufacturing Steps.

2.14.1. SCREENING CONDITIONS

#	Protocol	In Ovo Implants
1	Protocol 1	TET 2 +FBS (Standard Reference Protocol)
2	Protocol 2	TET 2 + hPL
3	Protocol 3	Coculture 2 + hPL
4	Protocol 4	Coculture 3 + hPL

Tabelle 6. Final Protocols Screened with Tracheal Biopsies

2.14.2. PROTOCOL/CONDITION DESCRIPTION

Protocol 1 (TET 2 + FBS): is an acronym for tissue engineered trachea protocol 1 which describes the use of expanded human bone marrow-derived MSCs, cultivated in media with FBS as an added supplement (derived from the protocol described by Elliot et.al. and the TETRA protocol), and seeded at a concentration of $7.5 \cdot 10^5 \text{ cells/cm}^2$ (five times the amount recommended by the TETRA Protocol) using a direct seeding methodology and maintained under static conditions with CM1 until implantation >>> **Modification 4: 5x Increase in cell seeding concentration.**

Protocol 2 (TET 2 + hPL): is an acronym for tissue engineered trachea protocol 2 which describes the use of expanded human bone marrow-derived MSCs, cultivated in media with **hPL** as an added supplement (derived from the protocol described by Elliot et.al. and the TETRA protocol), and seeded at a concentration of $7.5 \cdot 10^5 \text{ cells/cm}^2$ (five times the amount recommended by the TETRA protocol) using a direct seeding methodology and maintained under static conditions with CM2 >>> **Modification 5: 5x Increase in cell seeding concentration and change in media supplement.**

Protocol 3 (Coculture 2 + hPL): is an acronym for tissue engineered trachea protocol 3 which describes the use of both expanded non-transfected human bone marrow-derived MSCs and transfected MSCs (nucleofected with VEGF and bFGF 1:1), cultivated in media with hPL (as an added supplement), combined into one tube at a ratio of 50:50, and seeded onto 6 mm scaffolds at a concentration of $7.5 \cdot 10^5 \text{ cells/cm}^2$. Employed seeding methodology consisted of direct seeding and the scaffolds were maintained under static conditions with CM2 until implantation. >>> **Modification 8: Change in media supplement and coculture with transfected MSCs.**

Protocol 4 (Coculture 3 + hPL): is an acronym for tissue engineered trachea protocol 4 which describes the use of both expanded non-transfected human bone marrow-derived MSCs and transfected *HDFs* (nucleofected with VEGF and bFGF 1:1), cultivated in media with hPL (as an added supplement), combined into one tube at a ratio of 50:50, and seeded onto 6 mm scaffolds at a concentration of 7.5×10^5 cells/cm². Employed seeding methodology consisted of direct seeding and the scaffolds were maintained under static conditions with CocM2 until implantation. >>>**Modification 8: Change in media supplement and coculture with transfected *HDF*.**

2.14.3. Experimental Analysis

A. In vitro Analysis

- Single cell Isolation carried as described previously under segment 2.14
- Subsequent staining was carried out:
 - ◆ 2D cells (same cells as those seeded in scaffolds) were stained with compensation panel stains and blank to be used as compensation
 - ◆ Condition 1/Protocol1: MSCS cultivated with FBS (no further manipulation) was used as a reference standard or (positive control)

B. In vivo Analysis

- In vivo analysis encompassed the imaging and quantification of the tracheal biopsy in the CAM.
- MicroCT imagine of stained scaffolds with MicroFil®

2.15. IMAGING

2.15.1. 2D IMAGE PROCUREMENT

2.15.1.1. STEREOMICROSCOPE

All CAM images were obtained using a Zeiss Microscope at a 0.63x 0.65-fold magnification.

2.15.1.2. BRIGHTFIELD MICROSCOPY

Zeiss brightfield Microscope: Inverted phase contrast light microscope system (Axio Vert.A1, Carl Zeiss, Jena, Germany) was used in the procurement of brightfield images.

2.15.1.3. Fluorescence Microscopy

Fluorescent images were captured using an inverted fluorescence microscope platform (Axio Observer Z1, Carl Zeiss, Jena, Germany).

2.15.1.4. ELECTRON MICROSCOPY

Tracheal scaffolds from different sterilization procedures were examined using a scanning electron microscope in collaboration with the Department of Mechanical Engineering, TUM, Garching, Germany. After sterilization, samples were fixed using 3.7% formaldehyde and were dehydrated with a series of steps.

A. Preparation of Reagents:

1xPBS: 100 ml of DPBS w/o: Ca and Mg (PAN – Biotech, Germany) + 900 ml ultrapure water.

50% Ethanol (ET-OH): 50ml ET-OH +50ml ultrapure water.

70% ET-OH: 70ml ET-OH +30 ml ultrapure water.

80% ET-OH: 80ml ET-OH +20ml ultrapure water.

B. Dehydration Steps:

Step 1: the scaffolds were placed twice for 15 minutes in 50% ET-OH at RT.

Step 2: then placed twice for 15 minutes in 70% ET-OH at RT.

Step 3: then twice for 15 minutes in 80% ET-OH at RT.

Step 4: then the biopsies were placed once for 30 minutes in 99% ET-OH at RT.

Step 5: then once more overnight in 99% ET-OH in a cold room.

Critical Drying was achieved by allowing the scaffolds to air-dry overnight

C. Imaging:

After the dehydration steps were achieved, the scaffolds were fixed onto the electron microscopy scanning disk, then they were sprayed with gold, and were scanned and imaged on the JOEL EO scanning electron microscope (JOEL, Germany).

2.15.2. 3D IMAGE PROCUREMENT

Micro-Computed Tomography (MicroCT) Imaging

The in-ovo chorioallantoic membrane (CAM) assay offers an established, in-vivo, method that can provide a comprehensive and quick platform to screen for the applicability of the modifications made in our engineering protocol. However, in order to assess the overall vascular development of our trachea accurately and quantitatively, in-depth, 3D visualisation and analysis of the developing and infiltrating blood vessels is required.

MicroFil[®], an injectable silicone rubber compound is used with micro computed tomography (MicoCT) to provide the required 3D information. Coupled with the CAM assay, it has been an invaluable tool to aid in the screening and study of neovascularisation and blood vessel infiltration into implants [167-174].

After one week in-ovo (inside the CAM), the surrounding vasculature of embedded tracheal biopsies were perfused with Microfil[®] (FlowTech, USA) following the protocol described by Woloszyk et al. [175]. Briefly, the mixture of Microfil[®] (FlowTech, USA) components (at a ratio of 2ml of component+ 2.5 ml of diluent + 0.225ml of reagent MICROFIL[®], FlowTech, USA) was carefully injected into the vasculature depending on volume needed, or until it was no longer possible to inject anymore dye mixture. After, injection, the eggs were paced into the fridge at 4C° overnight. The next day, the eggs were taken out, and the scaffolds were removed from inside the embryonic chick shell, washed with PBS, fixed in 4% paraformaldehyde, and subsequently placed in 70% ethanol until microCT imaging.

Regions of interests were defined initially, by cutting the biopsies uniformly using a 6mm puncher for punch biopsies (Acu-Punch, Acuderm inc., USA), after implantation and staining, the extracted and

stained cam membrane containing the integrated and vascularised biopsies were further defined by using an 8mm puncher for biopsies (Acu-Punch, Acuderm inc., USA) around the implant. For imaging, the fixed punch biopsies were placed in 1.5 ml Eppendorf tubes containing PBS, and imaging of the samples was performed in collaboration with the Department of Experimental Traumatology at the Klinikum rechts der Isar, Munich, Germany, with an isotropic nominal resolution of 9 μ m, at 50 kV, 500 μ A, an exposure of 280 ms, and two-fold frame averaging based on the protocol described by Woloszyk et al.[168], using the Skyscan 1176 in vivo micro-CT scanner from Bruker.

2.15.3. IMAGE ADJUSTMENT

All 2D CAM Assay images were adjusted using Fiji/Image J (Version 1.53t, National Institute of Health “NIH”, USA), Java 1.8.0_341 (32-bit) with uniform recorded Macro Batch adjustment as follows: images were transformed from RGB colour to 8-bit grey-scale images, smoothed, sharpened, and their brightness and contrast adjusted in order to be able to better visualise small blood vessels.

All 3D scaffold infiltration images were first adjusted using Fiji/Image J (Version 1.53t, National Institute of Health “NIH”, USA), Java 1.8.0_341 (32-bit)

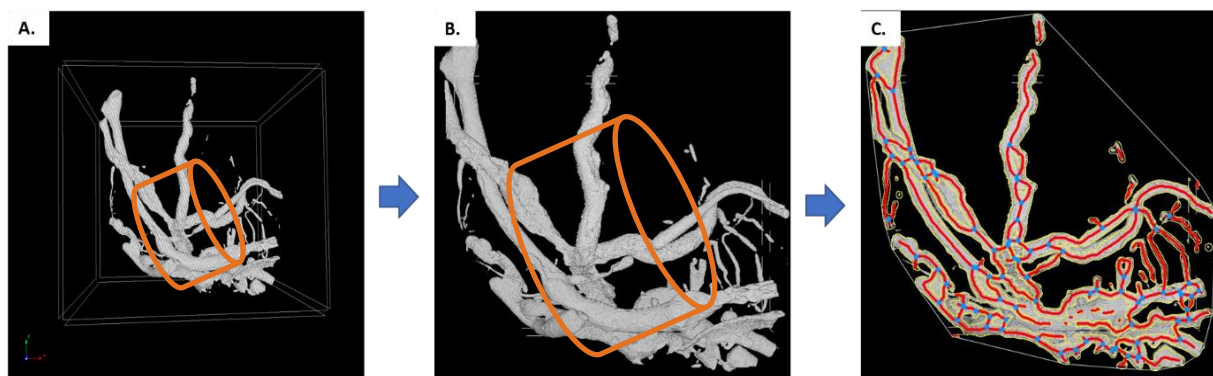


Figure 21. MicroCT Image analysis steps. **A.** Original image with grid. **B.** Image processed with Fiji/Image J Version 1.53t. (removal of the grid and converting image to JPG). **C.** Enumeration using AngioTool 64. Version 0.6a (02.18.14). The orange cylinder is a depiction of what the images would like with Scaffolds

2.15.4. IMAGE ANALYSIS AND ANALYSIS OF VASCULAR NETWORKS

2.15.4.1. Chorioallantoic Membrane Images Quantification Using IKOSA[®] Deep Learning Software (KMLVISION, <https://www.kmlvision.com/>, Austria)

IKOSA: Deep learning software[176]

Image output parameters included the following:

- Total Vessel Area: This refers to the total area covered by detected vessels in Pixel². The value range is ≥ 0 .
- Total Vessel Length: The total vessel length refers to the overall length of all detected vessels in pixels. The value range is ≥ 0 .
- Vessel Mean Thickness: This parameter refers to the mean thickness of the detected vessels in the image in pixels. The value range is ≥ 0 .
- Number of Vessel number of branching Points: These are the points where blood vessels divide into two or more branches. The value range is ≥ 0 .
- Size of Region of Interest

2.15.4.2. MicroCT Images Vessel Quantification

MicroCT image vessel quantification was carried out using AngioTool 64. Version 0.6a (02.18.14)

2.16. STATISTICAL ANALYSIS

Statistical analysis was conducted using GraphPad Prism 9 for windows 64-bit, version 9.5.1 (733), GraphPad Software, San Diego, California USA, www.graphpad.com. All quantitative data in the figures are presented as mean \pm SEM (Standard error of the mean). Indication of statistically significant difference is defined as $p < .05$ (* $p < .05$, ** $p < .01$, *** $p < .001$, and **** $p < .0001$). Generally, for non-paired multiple comparisons, One-way ANOVAs with Tukey test was performed. For paired comparisons between two groups, paired t tests were conducted.

MicroCT:

The results from the MicroCT vascular image quantification (using AngioTool) were statistically measured using an ordinary One-way ANOVA with no matching or pairing with the means of each group was compared to mean of the control group (protocol one) to decipher significance.

CAM Assay:

Results from the CAM Assay vascular image quantification by IKOSA Deep Learning software (KMLVISION, <https://www.kmlvision.com/>, Austria) were statistically measured using:

- Multi group comparison: Ordinary One-way ANOVA (with no matching or pairing with the means of each group was compared to mean of the control group (protocol one) to decipher significance.
- Two group comparison:

3. CHAPTER III: RESULTS

3.1. GENERATION OF BASIC PRODUCTS

3.1.1. Human Mesenchymal Stromal Cell Isolation and Expansion

3.1.1.1. Isolation of MSCs: FBS vs. hPL

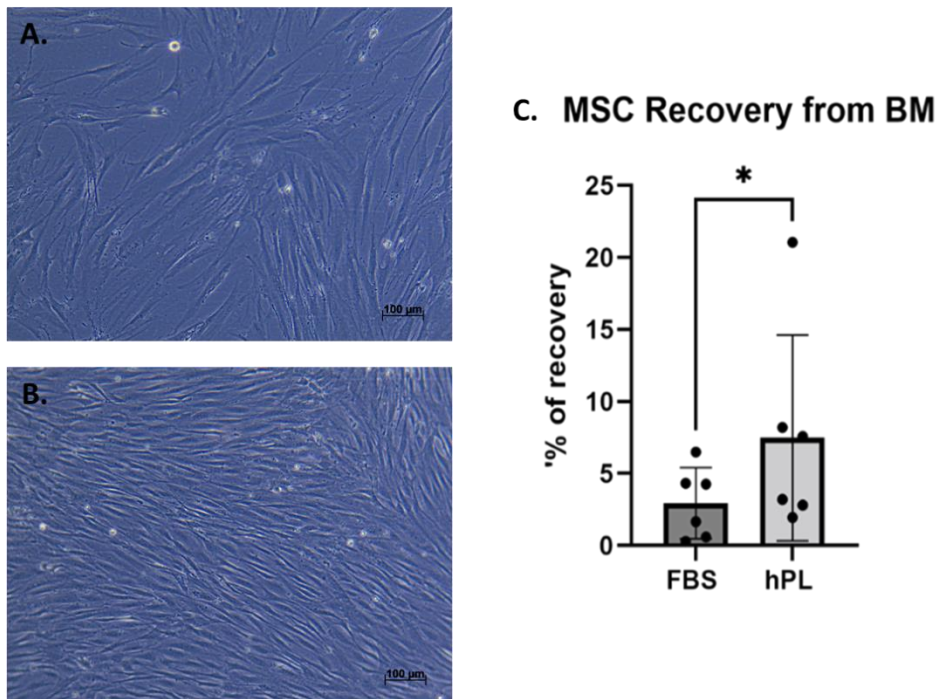


Figure 22. Illustration of the impact of hPL versus FBS cultivation on the isolation and morphology of human bone marrow-derived mesenchymal stem/stromal cells (MSCs). **A.** Image of MSCs cultivated with FBS at P2; image taken at 10x magnification. **B.** Image of the same cells cultivated in the presence of hPL and at the same time point; image taken at 10x magnification. **C.** The amount of MSCs recovered from initial isolation from bone marrow to passage 1 (P1), split into half and cultivated with FBS or hPL.

The provided figure elucidates the differential effects of human platelet lysate (hPL) versus fetal bovine serum (FBS) on the proliferative capacity and morphological attributes of mesenchymal stem/stromal cells (MSCs). Specifically, Figure A portrays MSCs cultured with fetal bovine serum (FBS) at passage 2. This micrograph captures MSCs manifesting a fibroblast-like morphology characterized by a spindle-shaped appearance. Notably, these cells exhibit an incipient transition toward a flatter, ovoid morphology, a distinctive trait commonly associated with prolonged cultivation of MSCs in the presence of FBS, particularly in subsequent passages. Furthermore, it is evident that these cells are larger in size and exhibit a diminished rate of growth compared to their counterparts cultured in the presence of human platelet lysate (hPL). Conversely, Figure B illustrates the same population of MSCs cultured with hPL at the identical time point. In stark contrast, these cells maintain a spindle-shaped, fibroblast-like morphology, and they are characterized by a smaller cellular size. Additionally, the level of cell confluency observed in this culture condition is notably higher when compared to FBS-cultivated MSCs at the same temporal milestone. Figure C presents a comparative analysis elucidating the quantitative disparity in cell recovery, spanning from post-isolation to the first passage, between MSCs cultivated with FBS and those exposed to hPL.

3.1.1.2. MSC Expansion

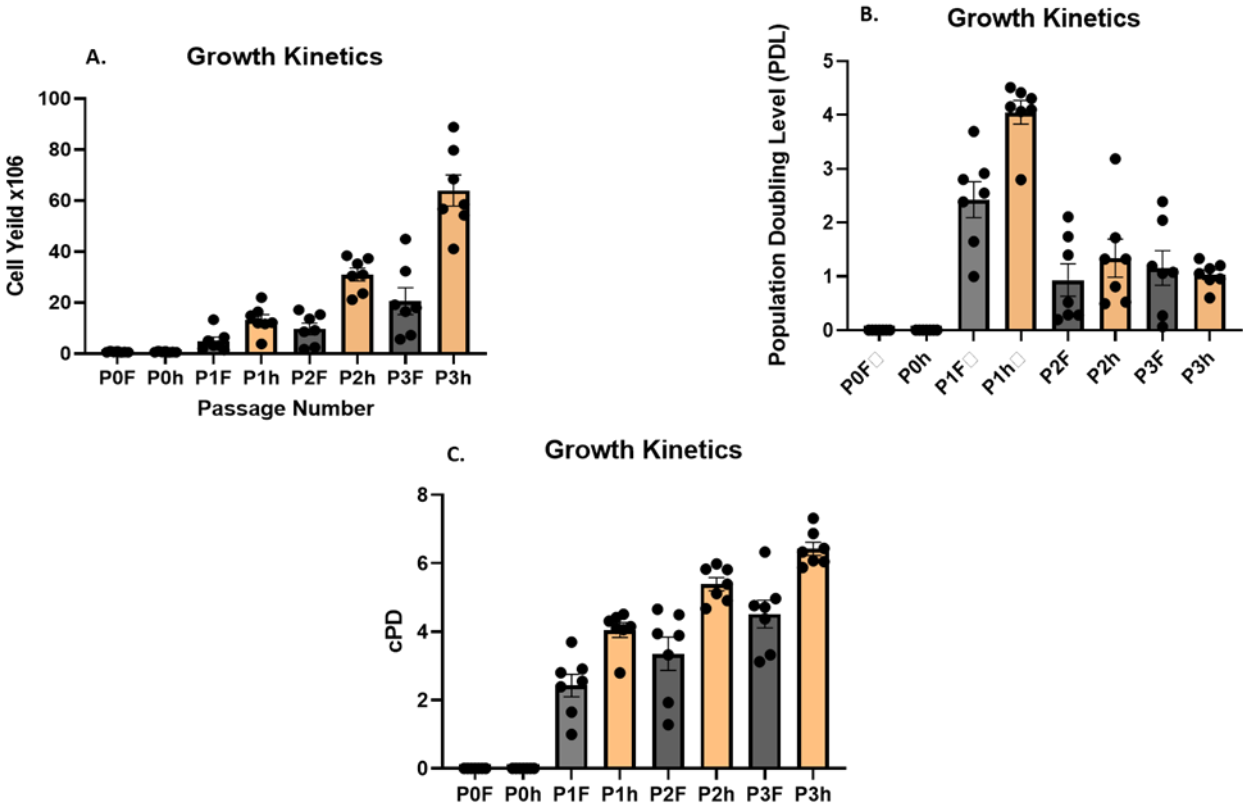


Figure 23. MSC Growth Kinetics. A. Assessment of MSC cellular yield after 3 passages (FBS vs. hPL) n=7. B. Assessment of Population Doubling Level (PDL) after 3 passages (FBS vs. hPL) n=7. C. Assessment of cumulative population doubling (cPD) after 3 passages (FBS vs. hPL) n=7.

The aforementioned diagram delineates the impact of foetal bovine serum (FBS) in comparison to human platelet lysate (hPL) as culture media supplements on the growth kinetics of human bone marrow-derived Mesenchymal Stem Cells (MSCs). Figure A provides an empirical evaluation of the cellular yield across seven distinct donors (n=7) throughout passages 0 to 3, while employing either FBS or hPL as supplementation, wherein the application of hPL exhibits an exponential augmentation in cell proliferation relative to FBS with each successive passage. Contrastingly, Figure B scrutinizes the Population Doubling Level (PDL), defined as the cumulative number of cell population doublings over the course of in vitro culture, within the same MSC population, under contrasting culture supplementation regimens, revealing the zenith of PDL during passage 1. Figure C elucidates the cumulative Population Doublings (cPD) experienced by MSCs cultivated in the presence of either FBS or hPL supplementation[177]. MSCs cultured with hPL manifest a considerably higher aggregate cell count by the culmination of passage 3. However, it is noteworthy that solely a marginally increased number of cumulative population doublings are observed by the conclusion of the aforementioned passage. In summation, the cultivation of MSCs yields more favourable outcomes in terms of cellular quantity, a phenomenon consonant with the extant body of scientific literature[113, 178, 179].

3.1.2. Human Mesenchymal Stromal Cell Characterisation

A. Flow Cytometer Characterisation Panel

Primary human bone marrow-derived MSCs were assessed for their ability express common MSCs markers in accordance to ISCT the minimal criteria for MSC identification [82] as follows:

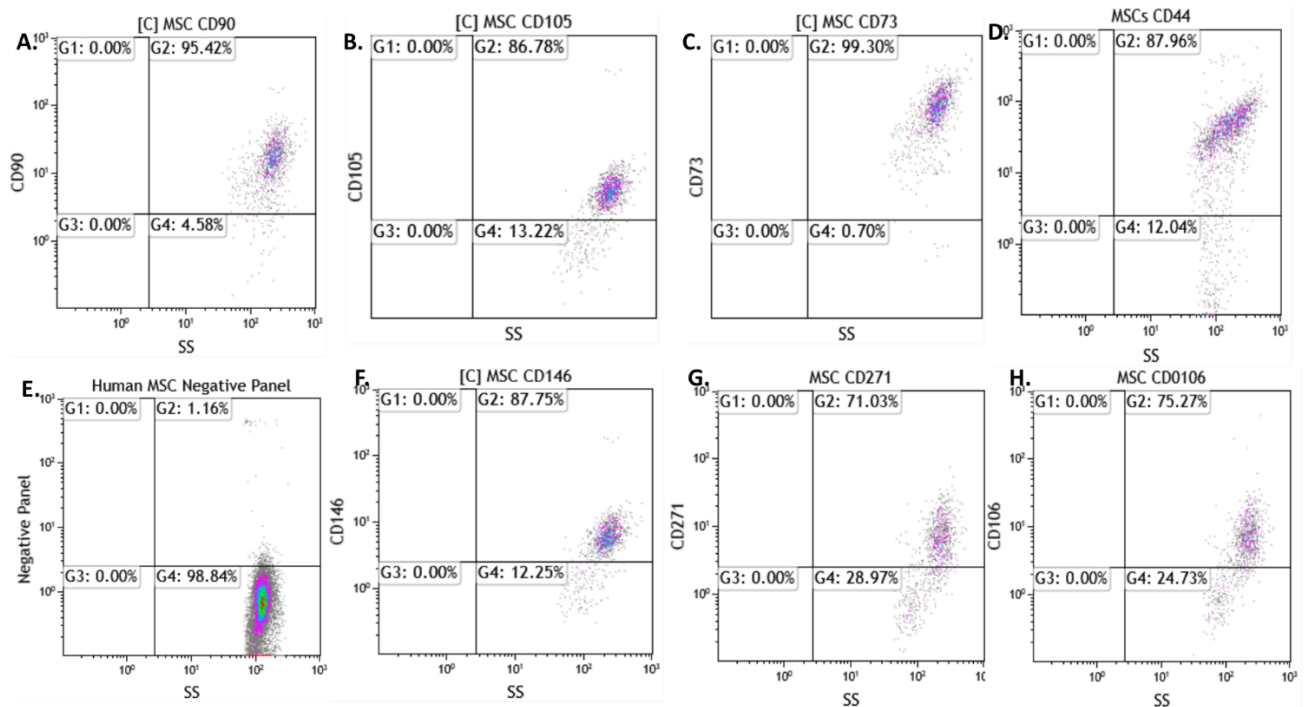


Figure 24. Representation of Flow Cytometry Panel Assessing MSCs for Common Markers. A. MSCs stained for CD90 surface marker expression. **B.** MSCs stained for CD105 surface marker expression. **C.** MSCs stained for CD73 surface marker expression. **D.** MSCs stained for CD44 surface marker expression. **E.** MSCs stained for hematopoietic negative panel surface marker expression. **F.** MSCs stained for CD146 surface marker expression. **G.** MSCs stained for CD271 surface marker expression. **H.** MSCs stained for CD106 surface marker expression.

The depicted figure illustrates a flow cytometry analysis panel conducted on human bone marrow-derived mesenchymal stromal cells (MSCs) with a sample size of n=8. This panel was designed in accordance with the guidelines established by the International Society for Cell Therapy and Gene Therapy (ISCT) for the minimal criteria utilized in the identification of MSCs. The panel encompasses both the mandatory positive markers as specified by ISCT, namely CD90, CD105, and CD73, as well as the requisite negative markers consisting of CD34, CD11b, CD19, CD45, and HLA-DR (presented collectively as the negative panel). In conjunction with the ISCT-mandated markers, additional markers associated with MSCs, including CD44, CD146, CD271, and CD106, were incorporated into the analysis. The results of this analysis are presented as follows: **A.** Demonstrates MSCs expressing positive surface marker CD90 in compliance with ISCT's minimal criteria. **B.** Depicts MSCs displaying positive surface marker CD105 in alignment with ISCT's minimal criteria. **C.** Illustrates MSCs exhibiting positivity for surface marker CD73, consistent with ISCT's minimal criteria. **D.** Reveals MSCs expressing CD44, an MSC-associated marker, in addition to the ISCT minimal criteria markers. **E.** Highlights MSCs exhibiting negativity for the negative panel markers (CD34, CD11b, CD19, CD45, HLA-DR) in accordance with ISCT's minimal criteria. **F.** Demonstrates MSCs expressing positive surface marker CD146, an MSC-associated marker, alongside the ISCT minimal criteria markers. **G.** Depicts MSCs expressing CD271, an MSC-associated marker, in conjunction with the ISCT minimal criteria markers. **H.** Illustrates MSCs expressing CD106, another MSC-associated marker, in addition to the ISCT minimal criteria markers.

B. MSC Tri-lineage Differentiation

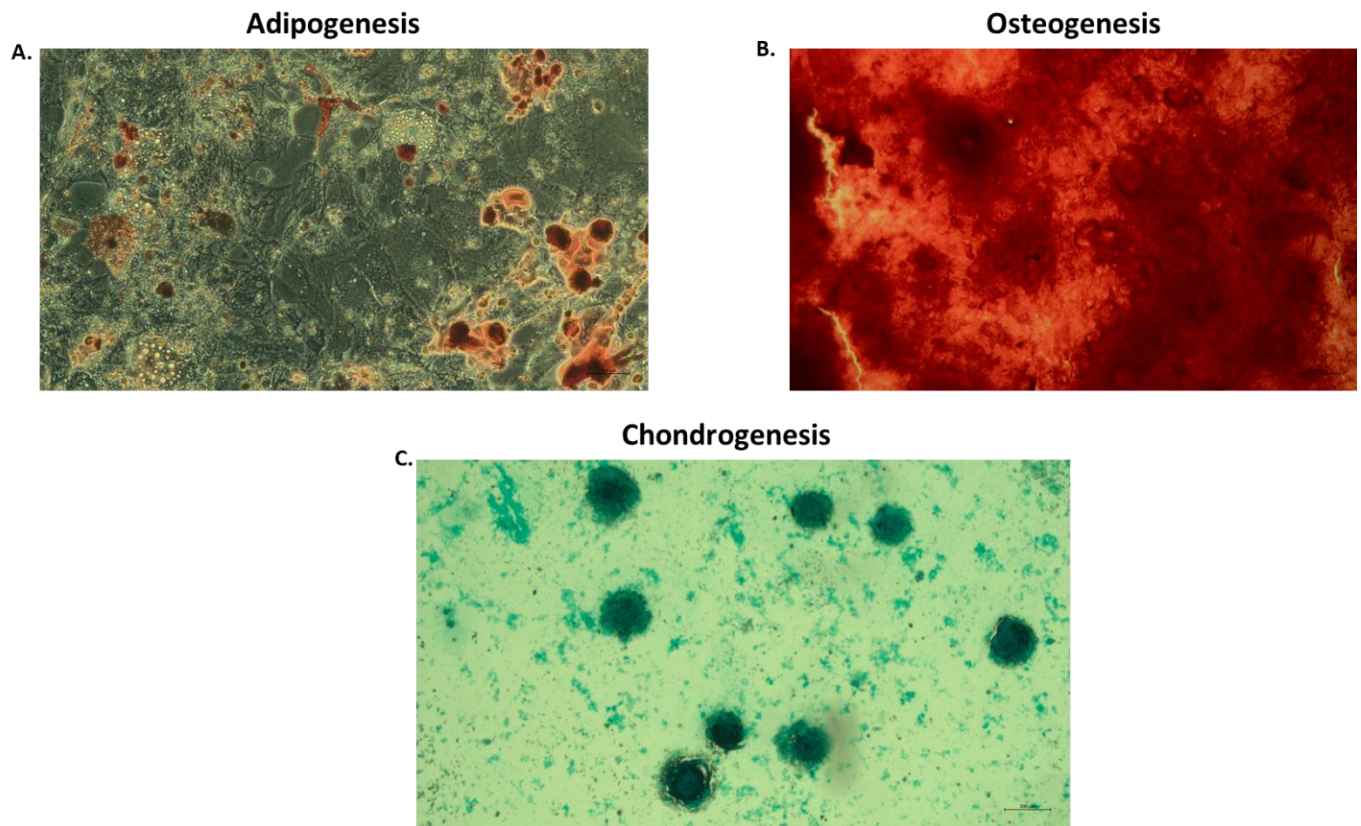


Figure 25. Tri-lineage Differentiation of Human Mesenchymal Stromal Cells (MSCs). **A.** Oil red staining of adipocyte vacuoles taken at x10 magnification. **B.** Alizarin Red staining of osteocyte calcium deposits taken at x5 magnification. **C.** Alcian blue staining of chondrocytes taken at x5 magnification.

The inherent capacity of mesenchymal stromal cells (MSCs) to undergo differentiation into the three principal lineages, namely chondrocytes, osteocytes, and adipocytes, was evaluated and substantiated as an integral component of meeting the minimal criteria prescribed by the International Society for Cell Therapy (ISCT) for MSC identification. A cohort of MSCs (n=8) was subjected to differentiation induction protocols, followed by subsequent staining procedures to verify their multilineage differentiation potential.

3.1.3. Human Dermal Fibroblast Expansion

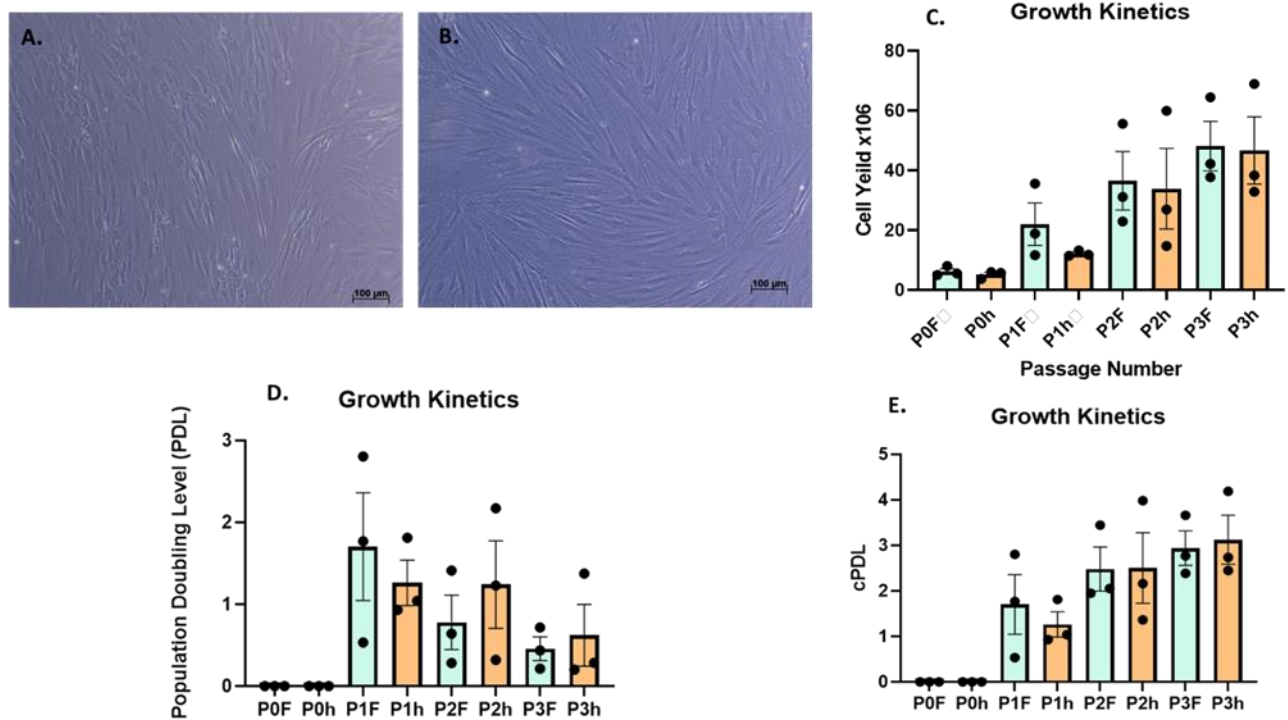


Figure 26. Human Dermal Fibroblasts Morphology and Growth Kinetics. **A and B.** Morphology of DFs cultivated in presence of FBS (A) and in the presence of hPL (B). **C.** Assessment of DFs cellular yield after 3 passages (FBS vs. hPL) n=7. **D.** Assessment of Population Doubling Level (PDL) after 3 passages (FBS vs. hPL) n=7. **E.** Assessment of cumulative population doubling (cPD) after 3 passages (FBS vs. hPL) n=7.

The previous figure serves as an illustration of the influence exerted by Fetal Bovine Serum (FBS) and Human Platelet Lysate (hPL) supplementation on the morphological attributes and growth kinetics of human dermal fibroblasts (hDFs) during their cellular expansion, as determined through a sample size of n=3. Figure A and Figure B, respectively, provide visual representations of hDFs undergoing cultivation in the presence of FBS and hPL at the third passage. In both instances, no appreciable nonconformities are discernible in the cellular morphology, which continues to exhibit the characteristic spindle-shaped, fibroblast-like conformation. Figure C portrays the quantitative depiction of cellular yield from the initial isolation phase through the culmination of the third passage, drawing a comparative analysis between the utilization of FBS and hPL as culture supplements. Figure D on the other hand, delineates the population doubling levels of hDFs over successive passages, spanning from passage 0 to passage 3, in conjunction with the application of both FBS and hPL as culture additives. Concurrently, Figure E presents a comprehensive overview of the cumulative population doubling levels for hDFs subjected to cultivation under the influence of the aforementioned

dual supplements. Overall, no substantial disparities are readily discernible when cultivating hDFs with the two different supplements.

3.1.4. Characterisation of Human Dermal Cells

A. Flow Cytometer Characterisation

The evaluation of human dermal fibroblasts for their potential to exhibit common mesenchymal stromal cell (MSC) markers, along with surface markers not typically found on fibroblasts, was conducted in the following manner:

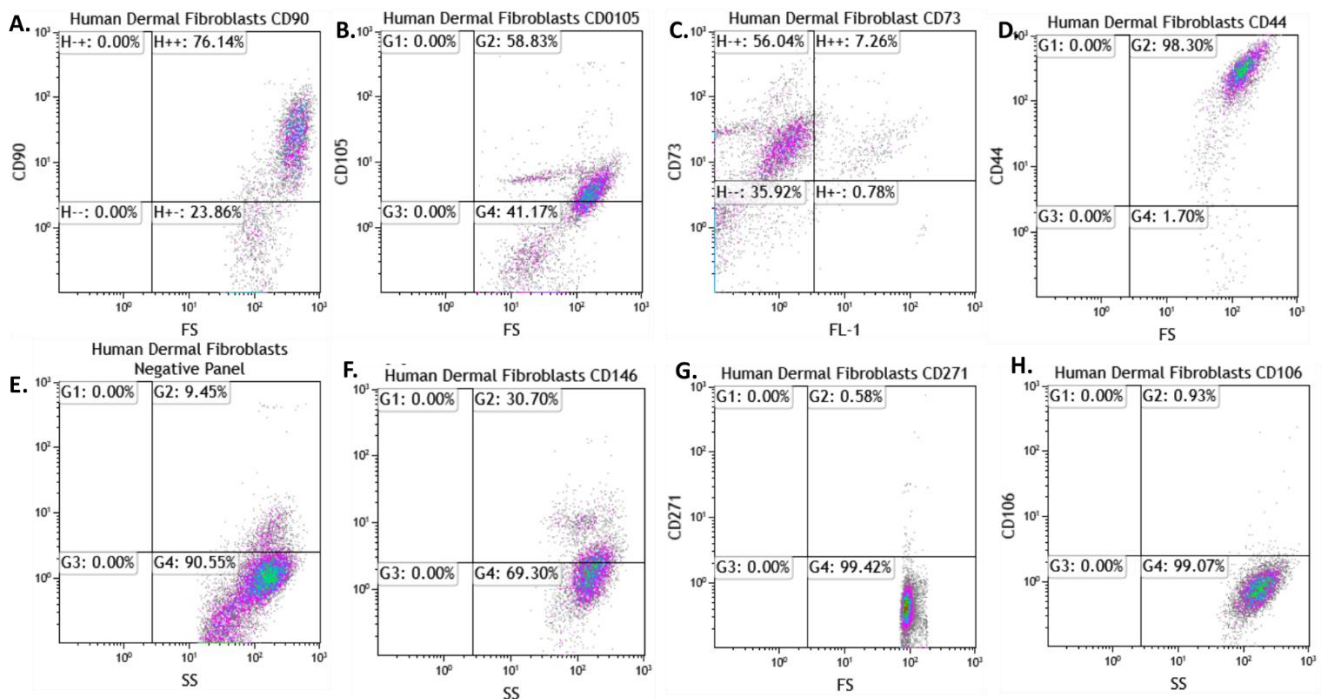


Figure 27. Representation of Flow Cytometry Panel Assessing DFs for Common MSC Markers. A. DFs stained for CD90 surface marker expression. **B.** DFs stained for CD105 surface marker expression. **C.** DFs stained for CD73 surface marker expression. **D.** DFs stained for CD44 surface marker expression. **E.** DFs stained for hematopoietic negative panel surface marker expression. **F.** DFs stained for CD146 surface marker expression. **G.** DFs stained for CD271 surface marker expression. **H.** DFs stained for CD106 surface marker expression.

The presented figure provides a visual representation of a flow cytometry analysis conducted on human dermal-derived fibroblasts (DFs), with a sample size of n=8. This analysis was devised in compliance with the criteria established by the International Society for Cell Therapy and Gene Therapy (ISCT) for the minimal criteria used in the identification of mesenchymal stromal cells (MSCs), and it was additionally applied to DFs for comparative purposes. The panel comprises both the obligatory positive markers for MSCs as stipulated by ISCT, which include CD90, CD105, and CD73, as well as the essential MSC-negative markers encompassing CD34, CD11b, CD19, CD45, and HLA-DR (presented collectively as the negative panel). In addition to the ISCT-prescribed markers, supplementary markers associated with MSCs, though not necessarily typically expressed by DFs (with the exception of CD44), were integrated into the analysis. These supplementary markers include CD146, CD271, and CD106. The outcomes of this analysis are presented as follows: **A.** Illustrates DFs expressing the positive surface marker CD90, akin to MSCs. **B.** Depicts a subset of DFs displaying positivity for the surface marker CD105. **C.** Illustrates DFs exhibiting positivity for the surface marker CD73. **D.** Reveals DFs expressing CD44. **E.** Highlights DFs exhibiting negativity for the negative panel markers (CD34, CD11b, CD19, CD45, HLA-DR) in accordance with MSCs. **F.** Demonstrates DFs expressing negativity for the surface marker CD146, an MSC-associated marker. **G.** Depicts DFs expressing negativity for CD271, another MSC-associated marker. **H.** Illustrates DFs expressing negativity for CD106, which is another MSC-associated marker.

This analysis provides insights into the phenotypic profile of the examined dermal-derived fibroblasts, encompassing both ISCT-mandated criteria and additional markers associated with MSCs, thus facilitating comparative assessments.

B. Dermal Fibroblast Tri-lineage Differentiation

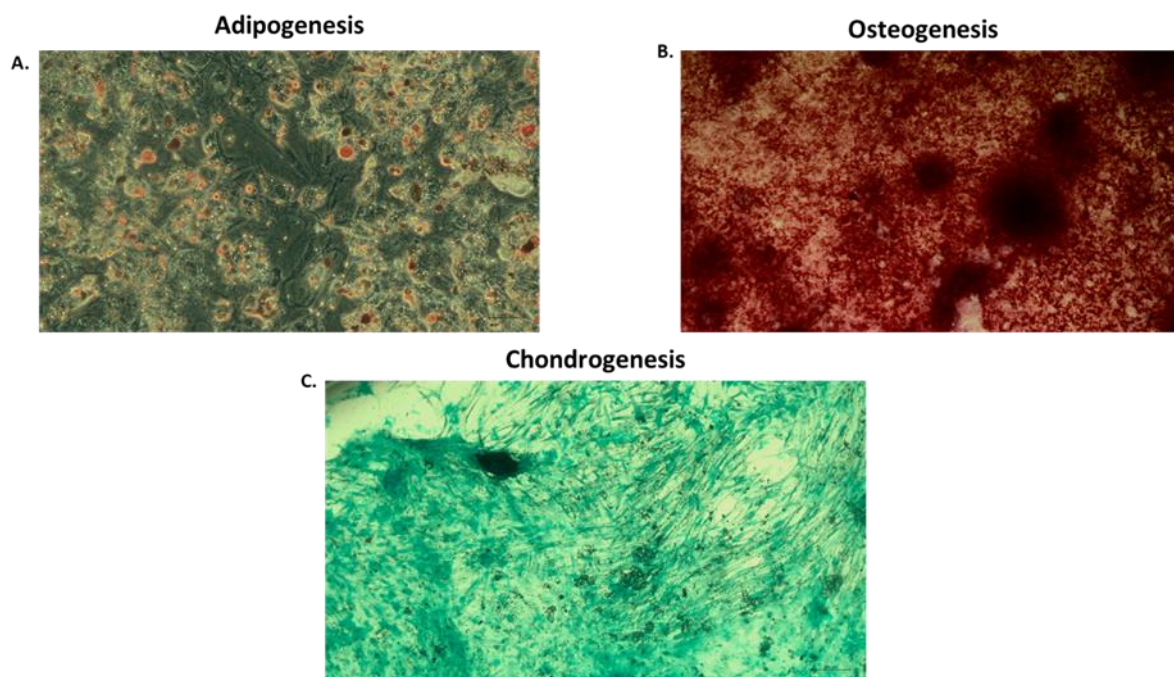


Figure 28. Tri-lineage Differentiation of Human Dermal Fibroblasts. **A.** Oil red staining of adipocyte vacuoles taken at x10 magnification. **B.** Alizarin Red staining of osteocyte calcium deposits taken at x5 magnification. **C.** Alcian blue staining of chondrocytes taken at x5 magnification.

To assess the potential of human dermal fibroblasts (DFs) to undergo differentiation into the three primary lineages associated with mesenchymal stromal cells (MSCs) and to evaluate the feasibility of the coculture hypothesis within the context of tissue-engineered trachea construction (with the assumption that dermal cells possess MSC-like differentiation capabilities), an experimental study involving eight samples of DFs was conducted. These DFs were subjected to differentiation induction protocols aimed at promoting their differentiation into osteocytes, chondrocytes, and adipocytes. Microscopic examination of the differentiated cells following appropriate staining procedures revealed that DFs indeed exhibited the capacity to differentiate into osteocytes, adipocytes, and chondrocytes. However, it was observed that the formation of three-dimensional chondrocyte spheres by DFs was less efficient in comparison to the differentiation capabilities exhibited by traditional MSCs.

3.1.5. DECELLULARISED PORCINE SCAFFOLDS

3.1.5.1. Handling of Porcine Trachea

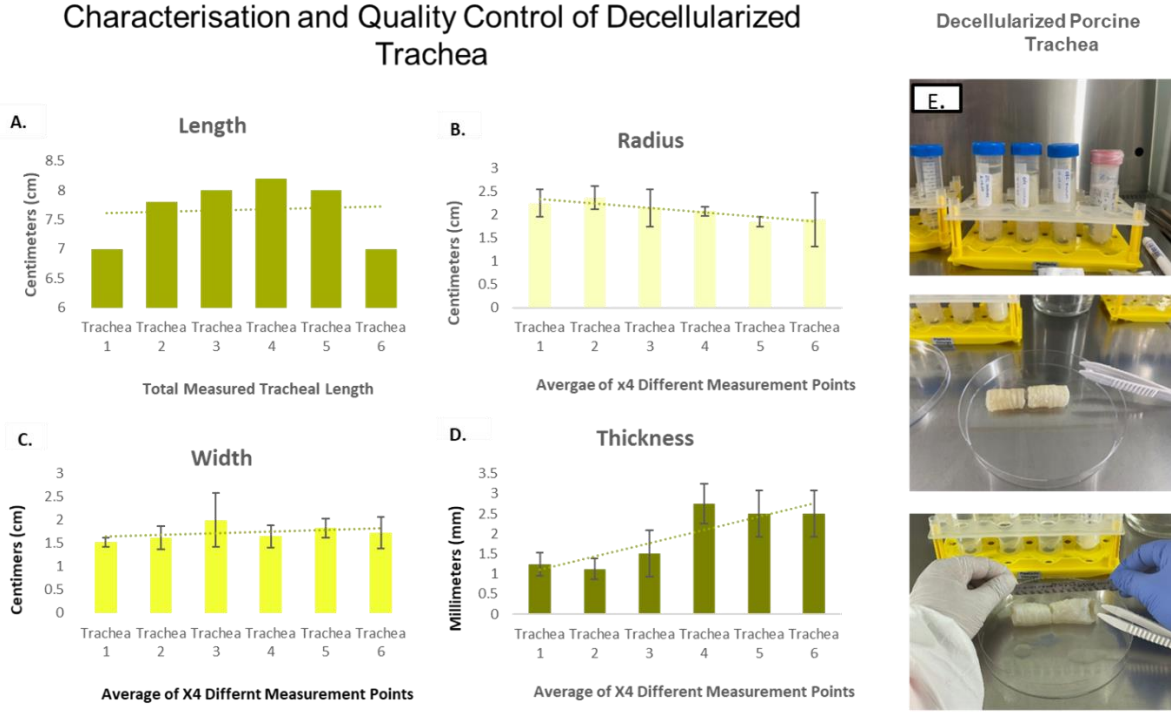


Figure 29. Measurement Metrics of Decellularized Porcine Trachea. **A.** Overall length of trachea. **B.** Inner tracheal lumen radius size (average of 4 measurements). **C.** The width/height of the trachea (average of 4 measurements). **D.** Thickness of the tracheal lumen wall (average of 4 measurements). **E.** Images of handling process.

Following the thawing process, each trachea was subjected to measurements, encompassing the assessment of various parameters, namely the overall length, inner lumen size (radius of the inner lumen), tracheal width (height), and the overall thickness of the lumen wall. These measurements served as crucial indicators for determining the subsequent seeding requirements. The calculation of the number of cells necessary for seeding was performed with the consideration of the cells per square centimetre (cells/cm²) seeding density, a pivotal factor in the tissue engineering process.

3.1.5.2. Sterilisation

Decellularized scaffolds, particularly those derived from xenogeneic sources, often pose a challenge due to the potential presence of tenacious and resilient bacteria [146, 148]. Upon identifying the existence of robust Gram-negative bacterial strains within the acquired scaffolds, including *Pseudomonas aeruginosa*, *Stenotrophomonas maltophilia*, *Escherichia coli*, and *Citrobacter braakii*, we employed four distinct sterilization protocols with the aim of eliminating bacterial contaminants while simultaneously maintaining the scaffold's suitability for subsequent cultivation endeavours.

A. Post Sterilisation Electron Microscopy Images of Tracheal Scaffold Post-Sterilisation

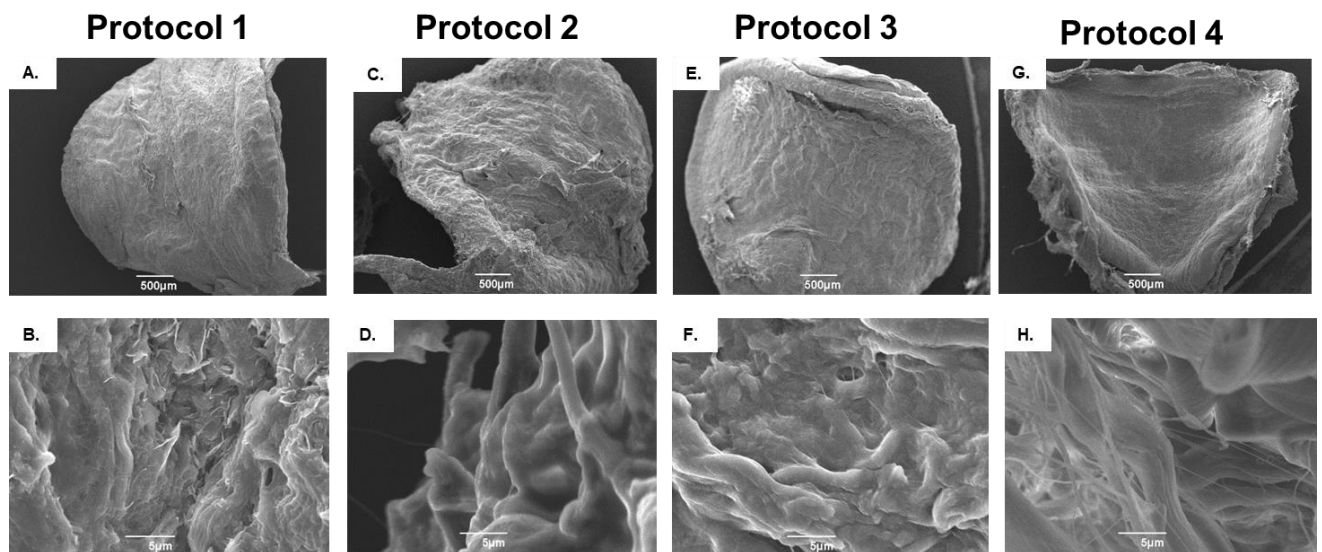


Figure 30. Scanning Electron Microscopy Images of Post-Sterilised Scaffolds. A. 30x magnification of tracheal scaffold post-sterilisation with Protocol 1. B. 4000x magnification of tracheal scaffold post-sterilisation with Protocol 1. C. 30x magnification of tracheal scaffold post-sterilisation with Protocol 2. D. 4000x magnification of tracheal scaffold post-sterilisation with Protocol 2. E. 30x magnification of tracheal scaffold post-sterilisation with Protocol 3. F. 4000x magnification of tracheal scaffold post-sterilisation with Protocol 3. G. 30x magnification of tracheal scaffold post-sterilisation with Protocol 4. H. 30x magnification of tracheal scaffold post-sterilisation with Protocol 4.

Following the application of the four distinct sterilization protocols detailed in the methods section, the tracheal biopsies underwent scanning via electron microscopy. Surface electron microscopy examination of the tracheal tissues did not yield any evidence of bacterial presence. Despite employing varying magnifications and capturing multiple images, no discernible bacterial presence was observed or identified.

B. Cultivation of Sterilised Scaffolds and Biocompatibility Assessment

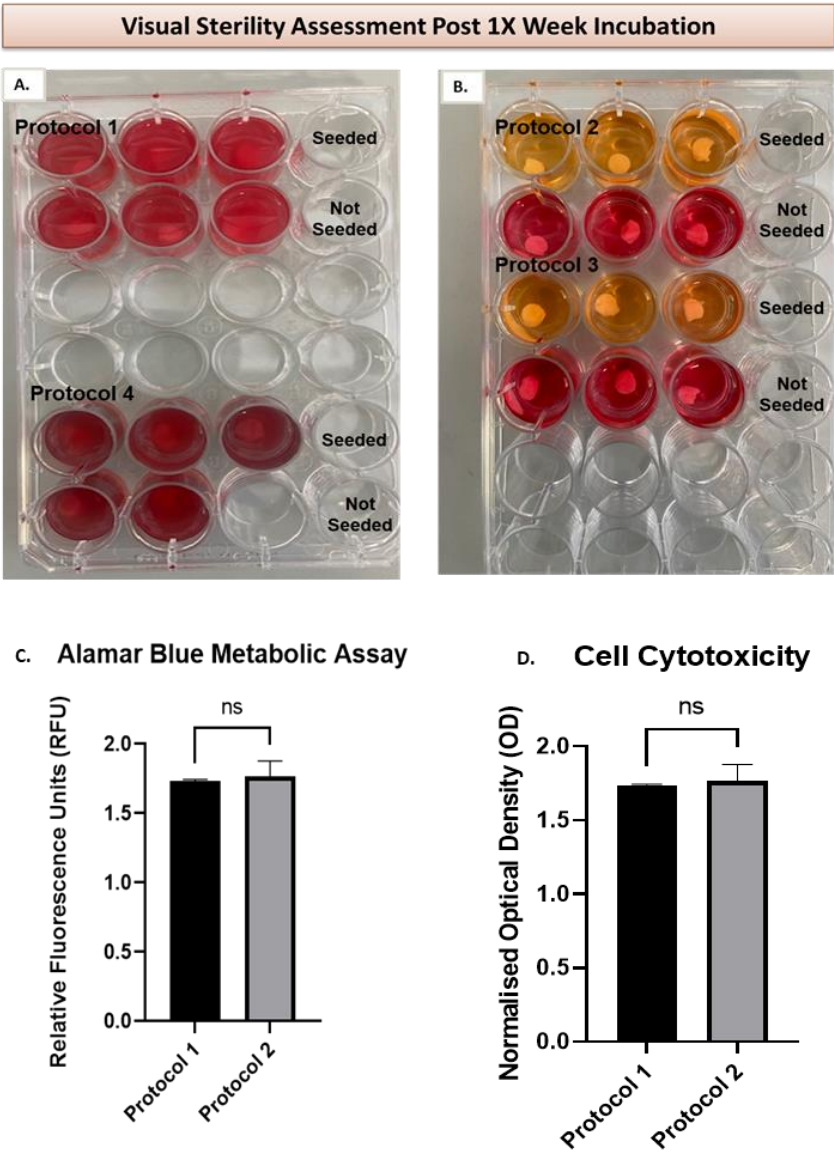


Figure 31. Post-Sterilisation Cultivation of Trachea. **A.** Cultivation of trachea both seeded with 3T3 Cells, and unseeded post sterilisation with Protocols 1 and 4. **B.** Cultivation of trachea both seeded with 3T3 Cells, and unseeded post sterilisation with Protocols 2 and 3. **C.** Measurement of cell viability and metabolic function with

Alamar blue metabolic assay **D.** Measurement of cell cytotoxicity post-treatment with protocols 3 and 3 with the LDH Cytotoxicity Assay

As part of the evaluation of sterilization protocols, tracheal scaffolds underwent cultivation under two conditions: one without cellular seeding using complete culture medium, and the other with the introduction of 3T3 mouse embryonic fibroblasts. After a five-day incubation at 37°C, scaffolds treated with protocols 1 (10% ab/am + washing) and 4 (1% triton-x + washing) exhibited clear signs of contamination, as evidenced by media turbidity, the presence of bacteria observed under bright-field microscopy, and the distinct grape-like odour emanating from Plate A (a distinct characteristic of *Pseudomonas aeruginosa*). In contrast, no bacterial contamination was observed in Plate B.

Subsequently, scaffolds seeded with cells following protocols 2 (ethanol + PAA + washing) and 3 (ab/am +PAA + washing) underwent comprehensive assessments that included Alamar blue metabolic profiling and LDH cytotoxicity evaluation, in order to discern potential differences in scaffold and cell biocompatibility between the two protocols. However, no significant disparities were observed. Although electron scanning microscopy did not reveal visible surface bacteria on the tracheal biopsies, paradoxically, the results of subsequent cultivation experiments were contradictory, confirming the persistent contamination of scaffolds treated with protocols 1 and 4.

3.2. COCULTURE OF DERMAL FIBROBLASTS WITH BONE MARROW DERIVED MSCS

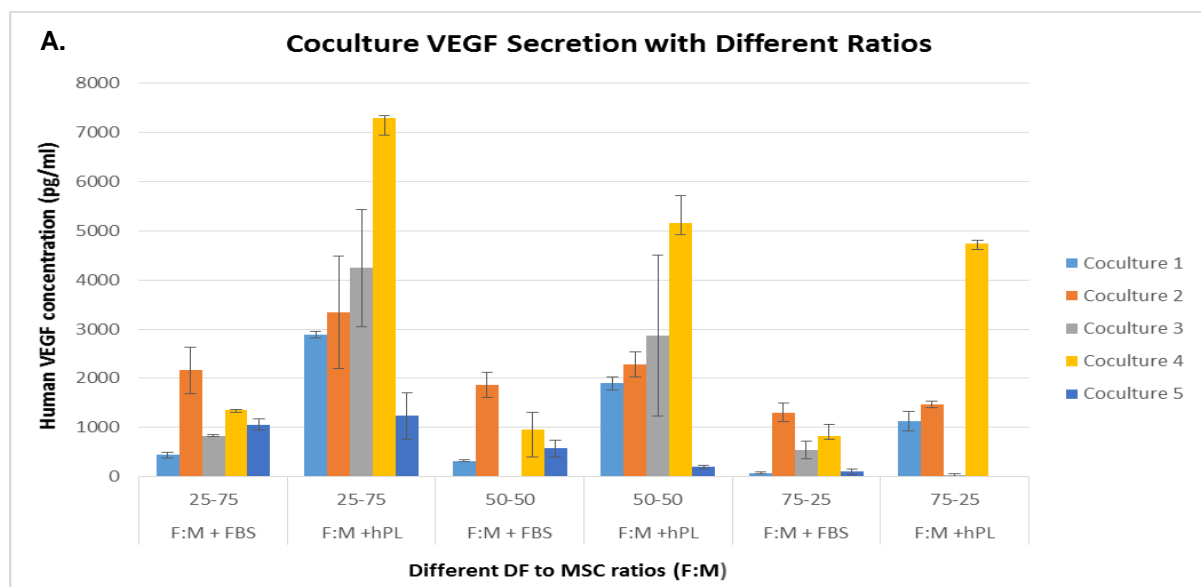


Figure 32. The impact of co-cultivating DFs with MSCs with varying ratios on the modulation of vascularization-stimulating growth factor expression, in the presence of distinct culture supplements (n=5). A. Outcome of cell co-culture on VEGF expression under various culture conditions.

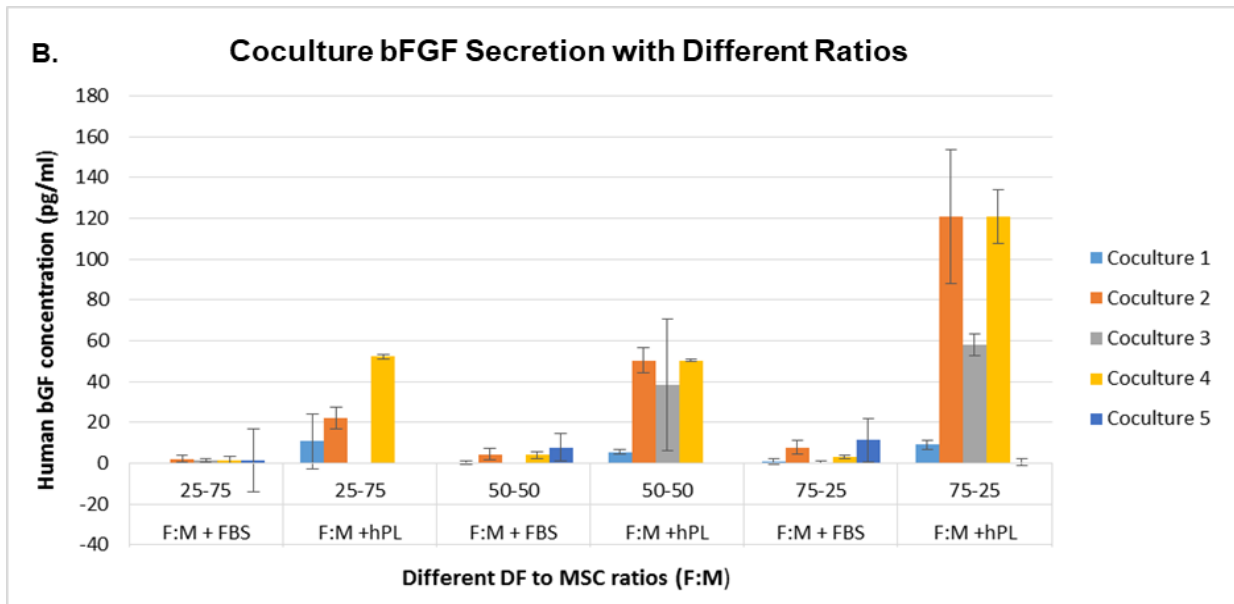


Figure 33. The impact of co-cultivating DF with MSCs at varying ratios on the modulation of vascularization-stimulating growth factor expression, in the presence of distinct culture supplements(n=5). B. Outcome of cell co-culture on bFGF expression under various culture conditions.

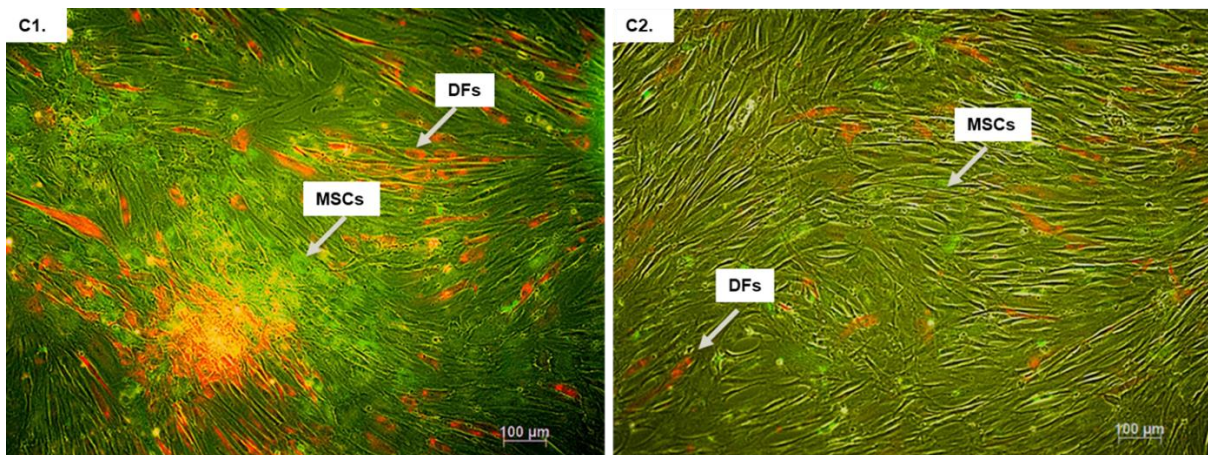


Figure 34. Coculture of DFs and MSCs at 50:50 ratio.

C1. Coculture of DFs (red) and MSCs (Green) in the presence of FBS supplementation.

C2. Coculture of DFs (red) and MSCs (green) in the presence of hPL supplementation.

In **Figure 11**, a series of co-culture experiments were conducted involving varying ratios of mesenchymal stromal cells (MSCs) and dermal fibroblasts (DFs), initially commencing with a ratio of 25:75, representing 25% DFs and 75% MSCs, in the presence of fetal bovine serum (FBS) supplementation. Subsequently, this identical cellular ratio was maintained, but the culture medium was supplemented with human platelet lysate (hPL). The subsequent experimental condition involved a 50:50 ratio of DFs to MSCs, equating to an equal representation of both cell types in the culture,

while FBS served as the culture supplement. This sequence was then repeated with the same cellular ratio but with hPL as the supplementation. The final co-culture condition entailed a 72:25 ratio, comprising 75% DFs and **25%** MSCs, in the presence of FBS. Subsequently, the identical ratio was maintained in the last co-culture condition, with hPL as the culture supplement. Each of these co-culture combinations was subsequently evaluated for its capacity to induce the expression of vascular endothelial growth factor (VEGF). The 25:75 ratio (25% DFs and 75% MSCs) with hPL supplementation yielded the highest observed results across five independent replicates. The second highest results were observed in the 50:50 ratio (50% DFs and 50% MSCs) also in the presence of hPL supplementation. The last ratio 75:25 (72% DFs and 20% MSC) had the lowest VEGF expression results and the comparison between FBS and hPL supplementation in this group yielded variable results.

In Figure 12, a series of co-culture experiments were also conducted involving varying ratios of mesenchymal stromal cells (MSCs) and dermal fibroblasts (DFs), initially commencing with a ratio of 25:75, representing 25% DFs and 75% MSCs, in the presence of fetal bovine serum (FBS) supplementation. Subsequently, this identical cellular ratio was maintained, but the culture medium was supplemented with human platelet lysate (hPL). The subsequent experimental condition involved a 50:50 ratio of DFs to MSCs, equating to an equal representation of both cell types in the culture, while FBS served as the culture supplement. This sequence was then repeated with the same cellular ratio but with hPL as the supplementation. The final co-culture condition entailed a 72:25 ratio, comprising 75% DFs and **25%** MSCs, in the presence of FBS. Subsequently, the identical ratio was maintained in the last co-culture condition, with hPL as the culture supplement. Each of these co-culture combinations was subsequently evaluated for its capacity to induce the expression of basic fibroblast growth factor (bFGF). In contrast, with basic fibroblast growth factor (bFGF), the highest levels of expression were observed within the final co-culture group, characterized by a 75:25 ratio of DFs to MSCs (comprising 75% DFs and 25% MSCs) and supplemented with hPL. Followed by, the co-culture group with the second-highest bFGF expression which consisted of a 50:50 ratio (50% DFs and 50% MSCs), also cultivated in the presence of hPL. Notably, across all co-culture combinations featuring varying DF to MSC ratios, elevated levels of bFGF expression were observed exclusively when hPL supplementation was employed. Conversely, the expression of bFGF in co-culture configurations with FBS supplementation remained nearly negligible.

Figure 13. illustrates the co-culture of dermal fibroblasts (DFs) and mesenchymal stem cells (MSCs) at an equimolar ratio of 1:1. In this depiction, DFs were stained with Mitotracker® Red CMXRos, rendering them in a red hue, while MSCs were stained with Mitotracker® Green FM, conferring a green coloration to these cells. Within Figure C1, the co-culture consists of DFs and MSCs at a 1:1 ratio, conducted in the presence of fetal bovine serum (FBS) supplementation. Conversely, Figure C2 portrays the co-culture of DFs and MSCs at a 1:1 ratio with human platelet lysate (hPL) supplementation.

Remarkably, in both Figure C1 and Figure C2, the ratio of red (representing DFs) to green (representing MSCs) fluorescence intensity, following a cultivation period of 5 days, appears to remain relatively unchanged. Image adjustment included only a decrease in brightness.

In assessing the most favourable combination of both bFGF and VEGF expression, based on the results of this experiment, the optimal selection would be the co-culture ratio of 50:50 (50% DFs and 50% MSCs) when cultivated in the presence of hPL supplementation. This configuration yielded the highest levels of both growth factors collaboratively, making it the most promising choice for the concurrent expression of bFGF and VEGF in this context.

3.3. GENETIC MODIFICATION OF CELLS: NUCLEOFECTION

3.3.1. 2D Experiments: Investigation of the impact of hPL on the nucleofection of Cells with pmax-GFP plasmid

3.3.1.1. Nucleofection output

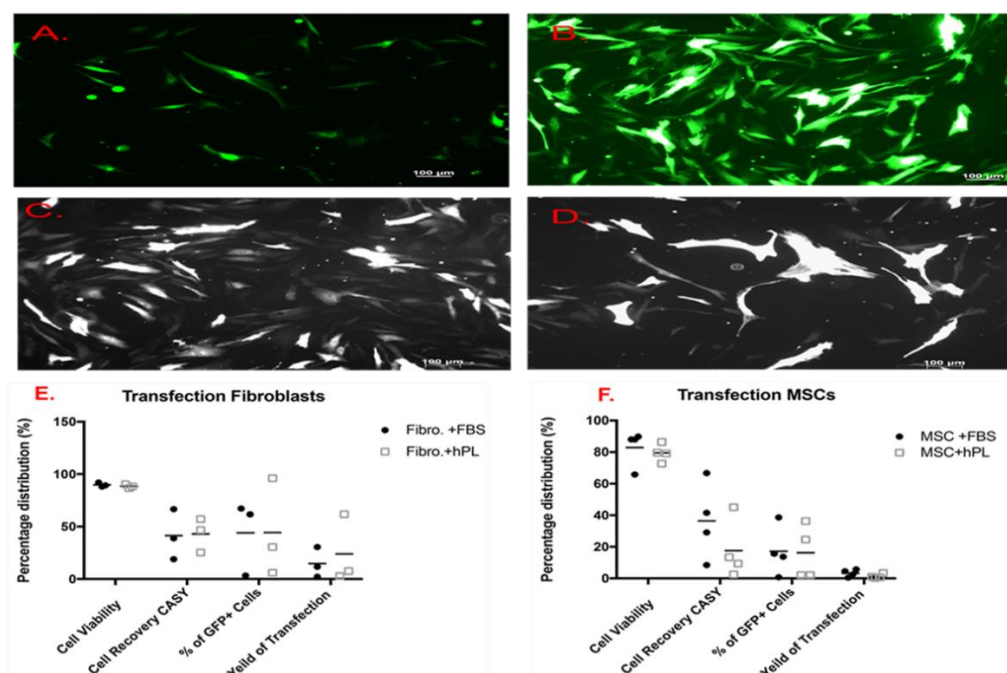


Figure 35. Transfection Studies: Assessed parameters post pmax-GFP nucleofection. A. Post-transfected fibroblasts cultivated with FBS. B. Post-transfected Fibroblasts cultivated with hPL. C. Post-transfected MSCs cultivated with FBS. D. Post-transfected MSCs cultivated with hPL. E. Assessed Parameters of transfected fibroblasts (n=3) with pmax-GFP plasmid cultured with FBS comparatively to hPL. F. Assessed parameters of transfected MSCs (n=4) with pmax-GFP+ plasmid cultured with FBS comparatively to hPL.

The previous results describe the different transfection parameters examined post: primary human bone marrow derived MSCs cultivated with hPL (n=4), human bone marrow derived MSCs cultivated with FBS (n=4), human dermal fibroblasts cultivated with FBS (n=3), and human dermal fibroblast cultivated with hPL nucleofection. Examined and compared parameters included: post-transfection viability percentage, the amount of cell recovery, the percentage of GFP+ Cells, and the yield of

transfection. In figures E & F, results indicate an analogy between outcomes of transfection (cell viability %, the amount of cell recovery from pre-transfected cells, the % of GFP+ expression, and the overall yield of transfection) when cultivating fibroblasts and MSCs with hPL versus FBS. No clear distinction is observed.

3.3.1.2. Cellular Metabolics Post-Transfection

A. Alamar Blue Metabolic Assay

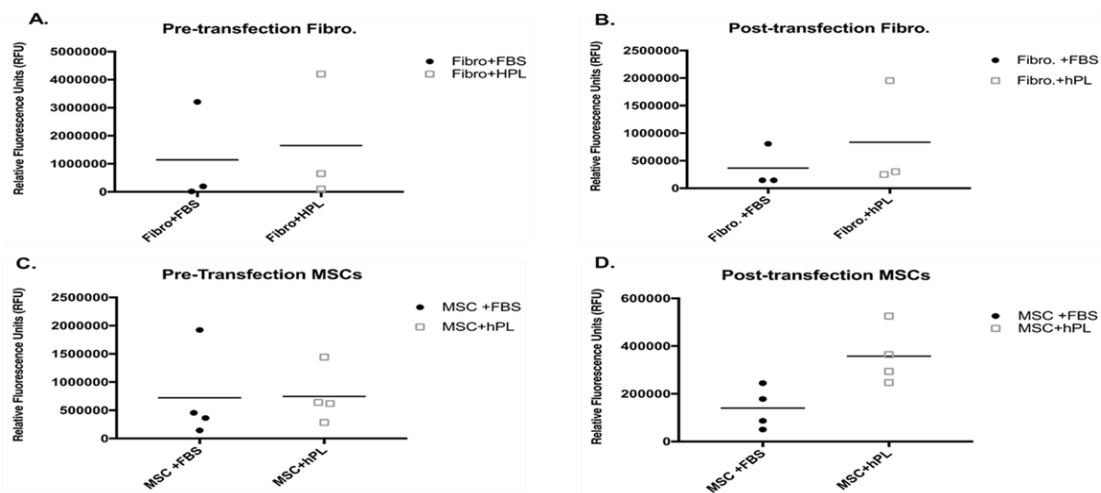


Figure 36. Alamar Blue Metabolic Assay results. **A.** Alamar blue assay results of fibroblast cultured with FBS in comparison to hPL (n=3) prior to transfection. **B.** Alamar blue assay results fibroblasts cultured with FBS in comparison to hPL (n=3) post-transfection. **C.** Alamar blue assay results of MSCs cultured with FBS in comparison to hPL (n=4) prior to transfection. **D.** Alamar blue assay results of MSCs cultured with FBS in comparison to hPL (n=4) post-transfection.

The previous results illustrate the impact of transfection on the metabolic condition of cells cultivated with two different media additives. **Figure A** depicts the metabolic condition of human dermal fibroblasts (n=3) cultivated with FBS in comparison to the same cells cultivated with hPL prior to transfection with no difference to be observed. **Figure B** depicts the condition of the same cells post-transfection (n=3) with a non-significant shift towards cells cultivated with hPL. **Figure C** does the same for human bone-marrow derived MCS (n=4); comparing the overall metabolic condition of the same cells cultivated with FBS versus hPL prior to transfection. **Figure D** on the other hand, indicates a bigger shift towards the same cells cultivated with hPL post-transfection. Here we observe that MSCs cultivated with hPL have higher metabolic activity than those cultivated with FBS post-transfection.

B. Cell Cytotoxicity Studies

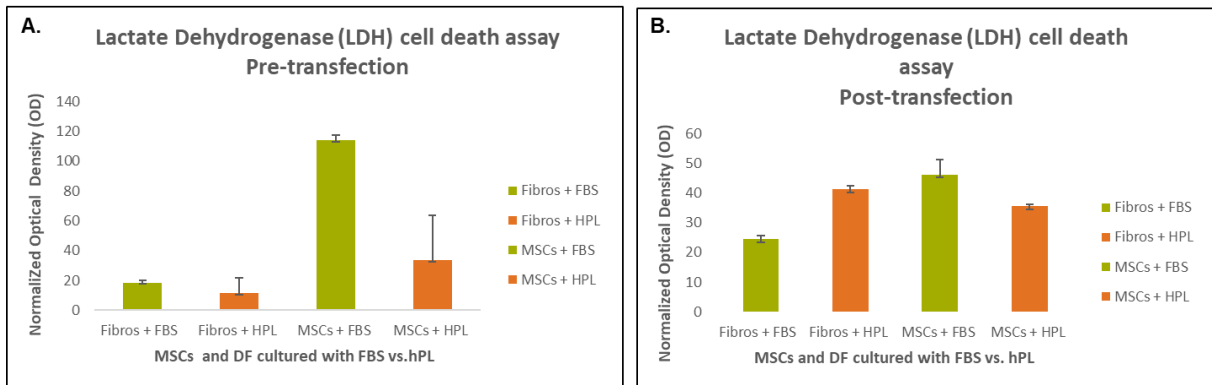


Figure 37. Cell Cytotoxicity Studies. Lactate Dehydrogenase (LDH) cell death assay optical density (OD) performed in conjunction with Alamar blue metabolic assay. A. Pre-transfection cell cytotoxicity levels Fibroblasts (n=3) and MSCs (n=4) cultivated with FBS versus hPL **B.** Post-transfection cell cytotoxicity levels Fibroblasts (n=3) and MSCs (n=4) cultivated with FBS versus hPL.

In the above figure a comparison is made between pre- and post-transfection cell cytotoxicity levels depicted by the LDH (lactate dehydrogenase) assay. **Figure A**, does not indicate much disparity between fibroblasts cultivated with FBS vs. hPL in terms of cytotoxicity levels pre-transfection. MSCs on the other hand are observed to have lower cell cytotoxicity levels when cultivated with hPL. **Figure B** describes the post-transfection results indicating slightly elevated toxicity results with fibroblasts cultivated with hPL in comparison to FBS, while maintaining lower cytotoxicity results for MSCs cultivated with hPL in comparison to FBS. The samples used in the above assay were taken from the same samples from which the alamar blue assays were conducted. ***Thus, when taken together, MSCs cultivated with hPL are observed to have a higher metabolic activity and a lower cell cytotoxicity post-transfection.***

3.3.1.3. Characterisation of GFP+ Nucleofected Cells

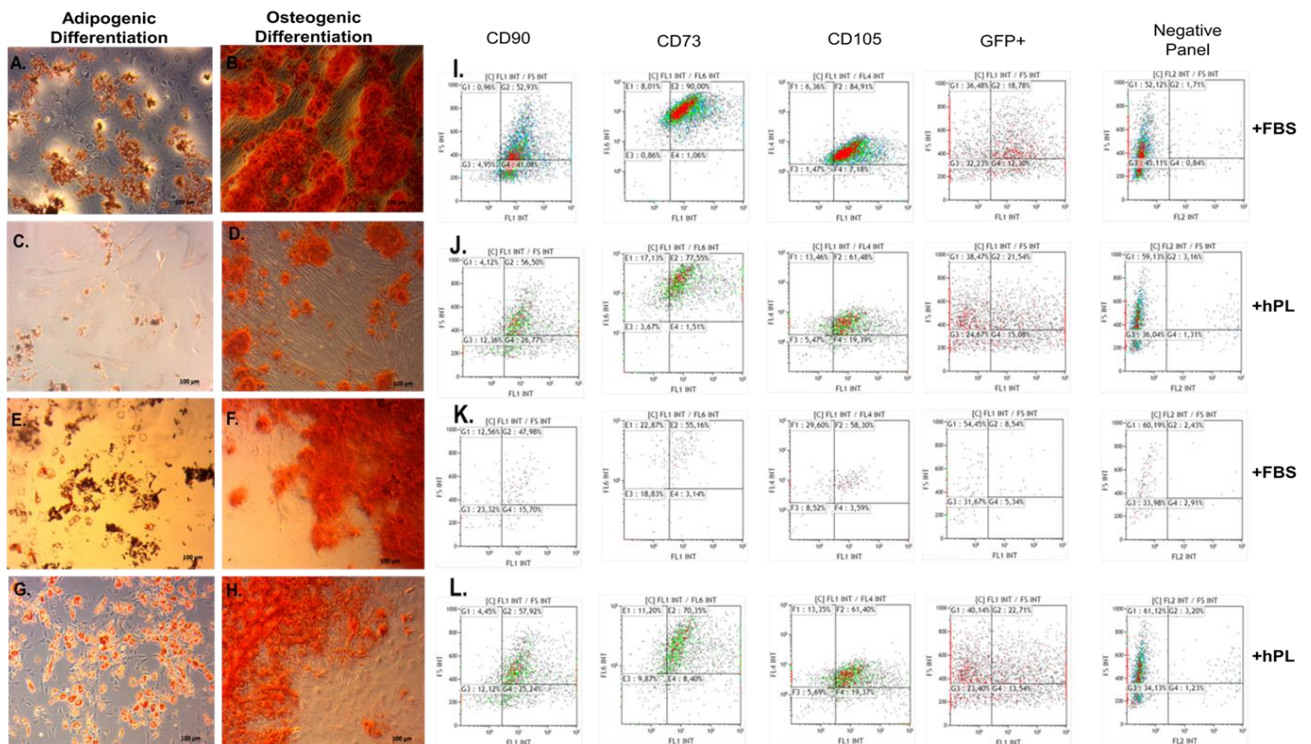


Figure 38. Cell Characterisation Assays. Differentiation and Flow Cytometry Analysis post-transfection. **A&B.** Differentiation of Fibroblasts cultivated with FBS. **C&D.** Differentiation of Fibroblasts cultivated with hPL. **E&F.** Differentiation of MSCs cultivated with FBS. **G&H.** Differentiation of MSCs cultivated with hPL. **I&J.** Flow cytometry characterisation of dermal fibroblasts cultivated with FBS and hPL. **K&L.** Flow cytometry characterisation of MSCs cultivated with FBS and hPL.

The above panel illustrates the ability of the human dermal fibroblasts (DFs) cultivated with FBS (n=3), the human dermal fibroblasts cultivated with hPL (n=3), the human mesenchymal stromal cells cultivated with FBS (n=4), and the human MSCs cultivated with hPL (n=4) to differentiate and express MSCs surface markers as previously defined by the ISCT minimum criteria for MSC identification both pre- and post-transfection with pmax-GFP plasmid. In these experiments, only osteogenesis and adipogenesis induction had taken place. **Figures A&B** illustrate DFs cultivated with FBS' ability to differentiate into adipocytes and osteocytes post-induction. **Figures C&D** illustrate DFs cultivated with hPL ability to differentiate into adipocytes and osteocytes post induction. **Figures E&F** illustrate MSCs cultivated with FBS' ability to differentiate into adipocytes and osteocytes post induction. While **figures G&H** illustrate MSCs cultivated with hPL's ability to differentiate into adipocytes and osteocytes post induction. No discernible difference in the differentiation capacity between MSCs cultivated with FBS and MSCs cultivated with hPL was observed. **Figure I**, illustrates the level of surface marker expression of CD90, CD73, CD105, GFP+, and the negative hematopoietic panel (CD34, CD11b, CD19, CD45, HLA-DR) expressed by fibroblasts cultivated with FBS by means of flow cytometry post-transfection. While **figure J**, illustrates the level of surface marker expression of CD90, CD73, CD105, GFP+, and the negative hematopoietic panel (CD34, CD11b, CD19, CD45, HLA-DR) expressed by fibroblasts cultivated with hPL by means of flow cytometry post-transfection. **Figure K** illustrates the level of surface marker

expression of CD90, CD73, CD105, GFP+, and the negative hematopoietic panel (CD34, CD11b, CD19, CD45, HLA-DR) expressed by MSCs cultivated with FBS by means of flow cytometry post-transfection. While **figure L** illustrates the level of surface marker expression of CD90, CD73, CD105, GFP+, and the negative hematopoietic panel (CD34, CD11b, CD19, CD45, HLA-DR) expressed by MSCs cultivated with hPL by means of flow cytometry post-transfection. No discernible difference in the surface marker expression of cells cultivated with FBS vs. hPL post-transfection was observed.

In summary, the nucleofection experiments endorse the use of hPL as a supplement for genetic modification via electroporation. No adverse effects were observed, and cells cultured with hPL exhibited higher metabolic activity and lower cytotoxicity compared to those cultured with FBS, indicating a potentially more favourable outcome with hPL supplementation.

3.4. 3D SCREENING EXPERIMENTS WITH INEGRA® MATRIX

3.4.1. Influence of Serum Additives (FBS Vs. hpl) on the Secretome Of Unaltered MSCs (Without Any Genetic Manipulation)

A. Assessment of VEGF and bFGF expression

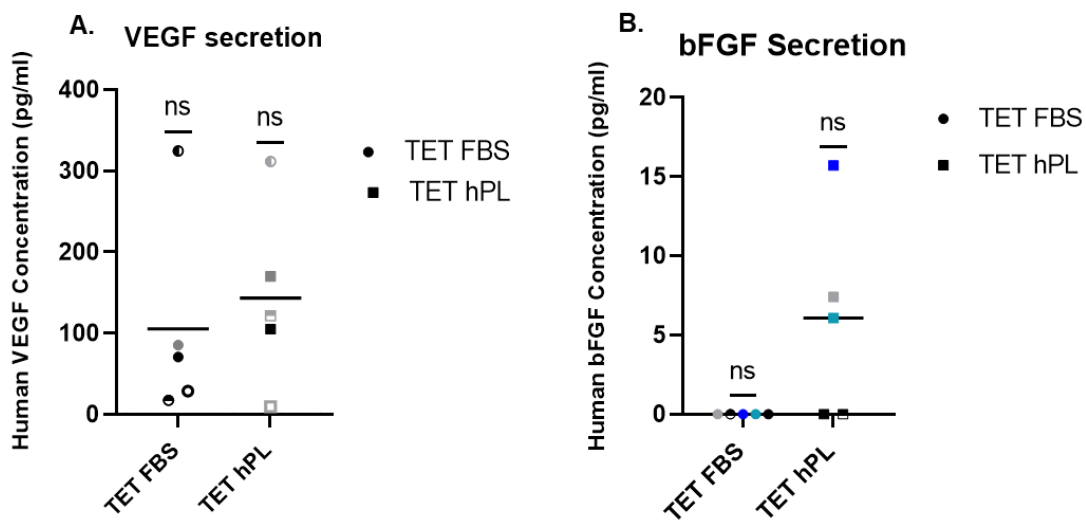


Figure 39. Comparison of natural secretions of human bone-marrow derived MSCs cultivated with FBS versus hPL (n=5). **A.** Natural Vascular Endothelial Growth Factor (VEGF) secretion. **B.** Natural basic Fibroblast Growth Factor (bFGF) secretion. TET = MSCs seeded onto integra scaffolds and incubated for *1 week in accordance. Statistical analysis: changing media additives has no significant effects on the natural secretion of VEGF and bFGF between different donors (Wilcoxon Signed Rank Test)

In the depicted figure, scaffolds made of Integra® Matrix were directly seeded with MSCs cultivated in two different conditions: one group with FBS (n=5) (TET+FBS), and the other with hPL (TET+hPL), following the original protocol provided by TETRA. The seeding density employed was 1.5×10^5 cells/cm². After one week of incubation at 37°C, just before in vivo implantation, we collected media samples to assess the expression of angiogenesis growth factors, specifically VEGF and bFGF. In Figure A, the data reveals no statistically significant difference between MSCs cultivated with FBS and those cultivated with hPL in terms of VEGF expression. Similarly, Figure B also demonstrates no statistical significance between the two groups in relation to bFGF expression. In the case of VEGF, all donors, whether treated with FBS or hPL, exhibited some level of VEGF expression. However, for bFGF expression, none of the five donors expressed bFGF in the presence of FBS, whereas in the presence of hPL, three out of the five donors displayed varying levels of bFGF expression. (All results were normalized against media containing either FBS or hPL, as appropriate).

B. Vascular Assessment: the CAM Assay

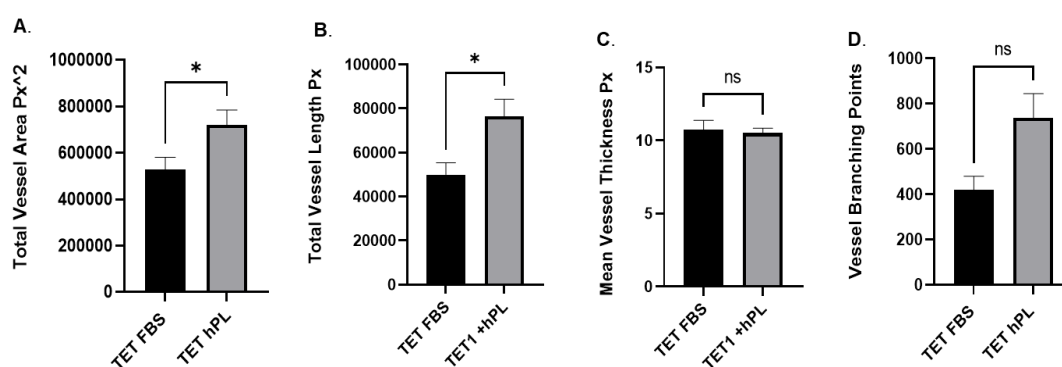


Figure 40. Enumeration of CAM Assay Blood Vessels. Comparison between protocols 1 & 2 output on the CAM (n=6). **A.** Effect of biopsies treated with protocols 1 (TET+FBS) & 2 (TET+hPL) on the total vessel area. **B.** Effect of biopsies treated with protocols 1&2 on the total vessel length. **C.** Effect of biopsies treated with protocols 1&2 on the mean vessel thickness. **D.** Effect of biopsies treated with protocols 1&2 on the number of vessels branching points.

In Figure B, scaffolds sourced from the same groups as those in Figure A were implanted in-ovo (n=6) to assess the capacity of MSC-seeded scaffolds to engraft and promote vascularization. A comparative analysis was conducted between scaffolds inoculated with cells cultivated in FBS (TET+FBS) and scaffolds inoculated with cells cultivated in hPL (TET+hPL), focusing on several parameters: the quantity of blood vessels within the overall area surrounding the scaffolds, the total length of vessels, the average vessel thickness, and the number of branching points in the vessels. Scaffolds seeded with MSCs cultivated in hPL exhibited better outcomes in terms of the number of vessels within the surrounding area compared to scaffolds seeded with MSCs cultivated in FBS. Additionally, the total vessel length in scaffolds seeded with MSCs cultivated in hPL was greater than those in scaffolds seeded with MSCs cultivated in FBS. ***These findings provide support for the cultivation of MSCs with hPL in the context of promoting vascular formation.***

3.4.2. Influence of alginate encapsulation on the secretome of unaltered MSCs following treatment with FBS

A. Assessment of VEGF and bFGF expression

Direct vs. Encapsulated MSC Protein Secretion

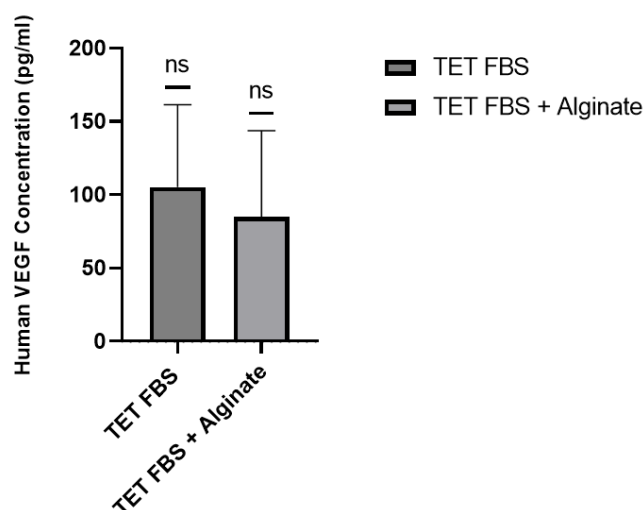


Figure 41. VEGF Release Under Different Conditions. Comparison between the amount of VEGF released from MSCs seeded directly onto Integra® scaffolds and MSCs encapsulated in Alginate then seeded onto the Scaffolds (n=5). Statistical analysis depicting the Mean and +/-SEM (One sample Wilcoxon test). bFGF was undetectable in media surrounding scaffolds with both direct and encapsulated + seeded MSCs.

In the depicted figure, scaffolds composed of Integra® Matrix were seeded in two different ways: one set with MSCs (n=5) directly cultivated with FBS, and another set with MSCs (n=5) initially encapsulated in alginate and then seeded onto the Integra® Matrix with FBS supplementation. The aim was to compare the expression of VEGF and bFGF. The analysis revealed that there was no statistically significant difference in VEGF expression between the scaffolds seeded directly with MSCs and those seeded with MSCs encapsulated in alginate. However, it is worth noting that the scaffolds seeded with alginate did exhibit a slightly lower level of VEGF expression (n=5). Regarding bFGF expression, no detectable levels were observed in either of the two groups (n=5 for each group) in the presence of FBS supplementation.

B. Vascular Assessment: the CAM Assay

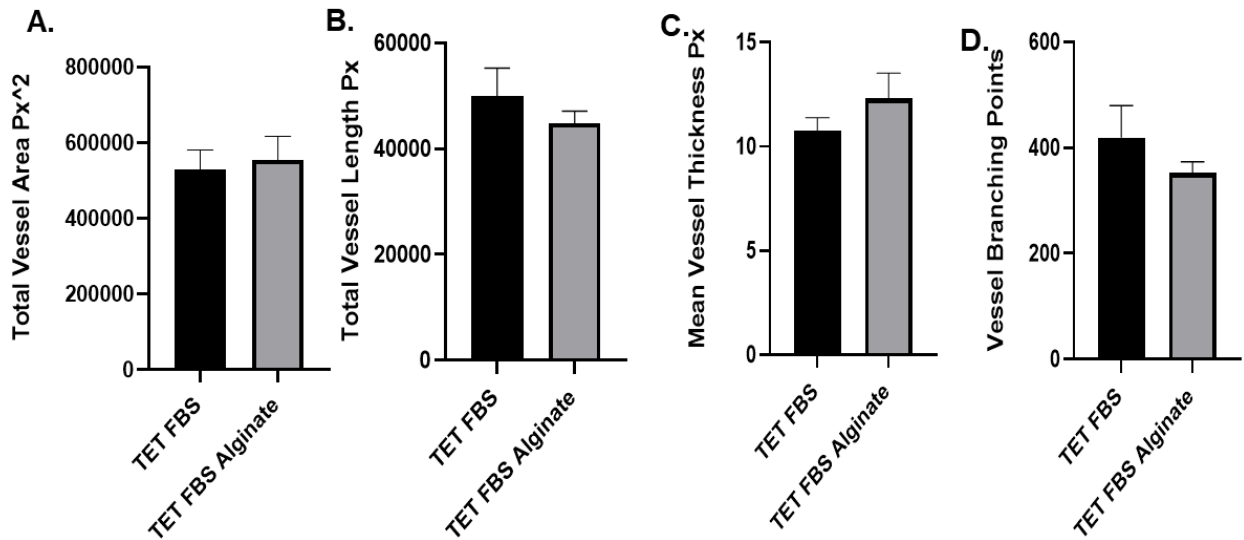


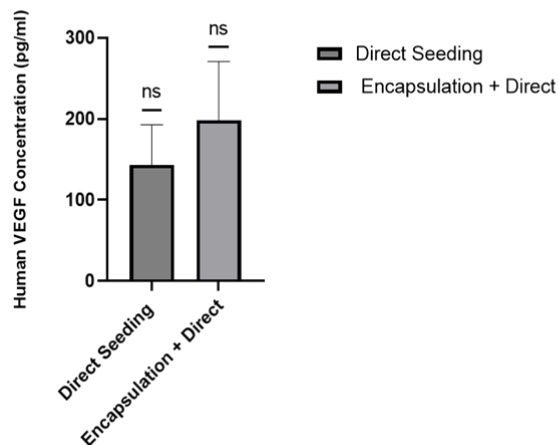
Figure 42. Enumeration CAM Assay Blood Vessels: comparison between protocols 1 (TET+FBS) & 3 (TET+ FBS+ Alginate). A. Effect of biopsies treated with protocols 1&3 on the total vessel area. B. Effect of biopsies treated with protocols 1&3 on the total vessel length. C. Effect of biopsies treated with protocols 1&3 on the mean vessel thickness. D. Effect of biopsies treated with protocols 1&3 on the number of vessels branching points (n=6).

In Figure B, scaffolds obtained from the same groups as those in Figure A were implanted in-ovo (n=6) to evaluate the ability of MSC-seeded scaffolds to engraft and facilitate vascularization. A comparative analysis was conducted between scaffolds inoculated with cells cultivated in FBS (TET+FBS) and seeded directly, and scaffolds inoculated with cells cultivated in FBS but encapsulated in alginate prior to seeding (TET+FBS +Alginate). This analysis focused on various parameters related to vascularization, including the quantity of blood vessels within the surrounding area, the total length of vessels, the average vessel thickness, and the number of branching points in the vessels. The results showed no discernible differences between both groups in any of the vascularization parameters assessed.

3.4.3. Influence of Alginate Encapsulation on The Secretome Of Unaltered MSCs Following Treatment With hPL

A. Assessment of VEGF and bFGF expression

A. MSC Protein Secretion + hPL



B. MSC bFGF Protein Secretion +hPL

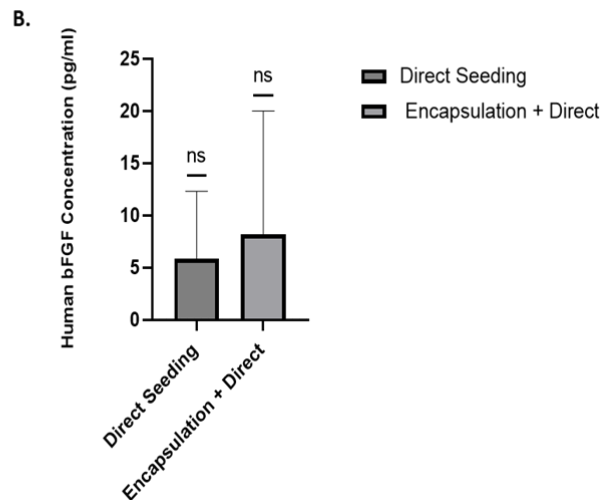


Figure 43. VEGF and bFGF Release Under Different Conditions. Comparison between the amount of protein released from MSCs seeded directly onto Integra® scaffolds and MSCs encapsulated in Alginate then seeded onto the Scaffolds (n=5). **A.** Comparison between the amount of VEGF secreted by seeded MSCs. **B.** Comparison between the amount of bFGF secreted by seeded MSCs. Statistical analysis depicting the Mean and +/-SEM (One sample Wilcoxon test).

In the depicted figure, scaffolds composed of Integra®Matrix were seeded in two different ways: one set with MSCs (n=5) directly cultivated with hPL (TET+hPL), and another set with MSCs (n=5) initially encapsulated in alginate and then seeded onto the Integra®Matrix with hPL supplementation (TET+hPL + Alginate). The aim was to compare the expression of VEGF and bFGF. The analysis revealed that there was no statistically significant difference in VEGF expression between the scaffolds seeded directly with MSCs and those seeded with MSCs encapsulated in alginate in the presence of hPL supplementation.

B. Vascular Assessment: the CAM Assay

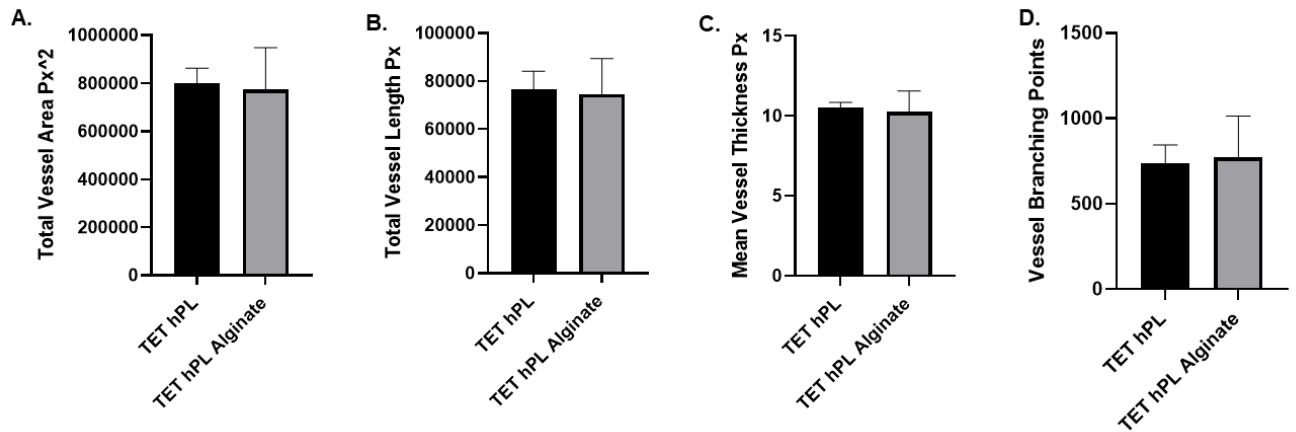


Figure 44. Enumeration of CAM Assay Blood Vessels: comparison between protocols 2 (TET+ hPL) & 4 (TET + hPL + Alginate). **A.** Effect of biopsies treated with protocols 2 & 4 on the total vessel area. **B.** Effect of biopsies treated with protocols 2 & 4 on the total vessel length. **C.** Effect of biopsies treated with protocols 2 & 4 on the mean vessel thickness. **D.** Effect of biopsies treated with protocols 2 & 4 on the number of vessels branching points (n=6).

In Figure B, scaffolds obtained from the same groups as those in Figure A were implanted in-ovo (n=6) to evaluate the ability of MSC-seeded scaffolds to engraft and facilitate vascularization. A comparative analysis was conducted between scaffolds inoculated with cells cultivated in hPL (TET+hPL) and seeded directly, and scaffolds inoculated with cells cultivated in hPL but encapsulated in alginate prior to seeding (TET+ hPL +Alginate). This analysis focused on various parameters related to vascularization, including the quantity of blood vessels within the surrounding area, the total length of vessels, the average vessel thickness, and the number of branching points in the vessels. The results showed no discernible differences between both groups in any of the vascularization parameters assessed.

3.4.4. **Impact of a fivefold increase in cell concentration on the secretome of unaltered MSCs after treatment with both FBS and hPL**

A. Assessment of VEGF and bFGF expression

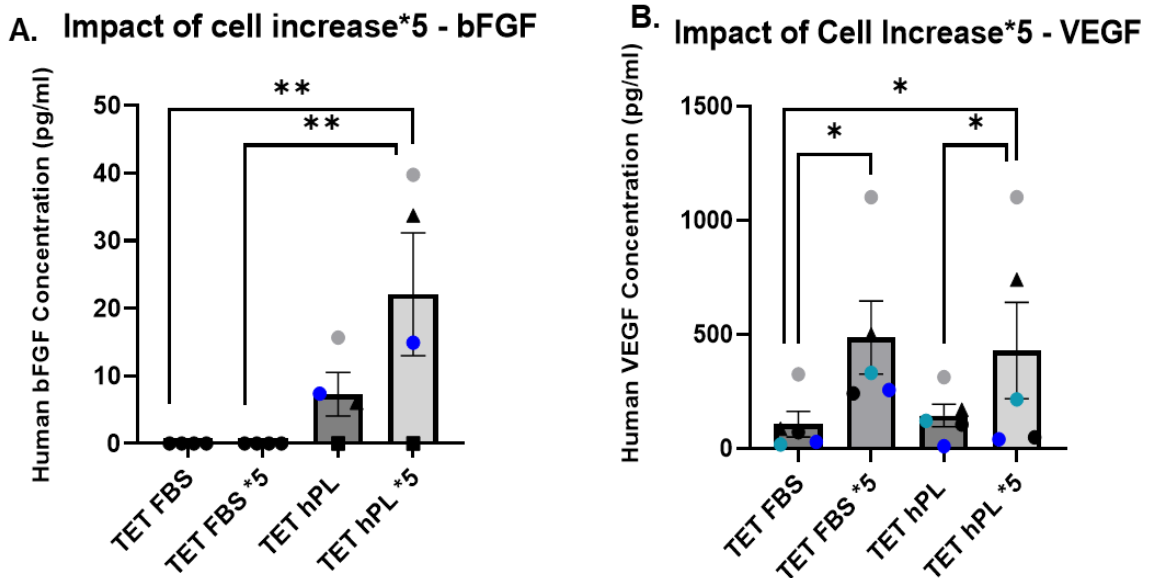


Figure 45. VEGF and bFGF Expression Under Different Conditions. **Comparison between the amount of protein released from MSCs seeded directly onto Integra® scaffolds, treated with FBS and hPL, and the MSCs encapsulated in Alginate then seeded onto the Scaffolds (n=5).** **A.** Comparison between the amount of VEGF secreted by seeded MSCs. **B.** Comparison between the amount of bFGF secreted by seeded MSCs. Statistical analysis depicting the Mean and +/-SEM.

In the presented figure, scaffolds made of Integra® Matrix were seeded using four distinct methods: 1. MSCs (n=5) cultured with FBS (TET+FBS) and seeded directly at an initial seeding density of 1.5×10^5 cells/cm². 2. MSCs (n=5) cultured with FBS (TET2+FBS) and seeded directly at an increased seeding density of 7.5×10^5 cells/cm². 3. MSCs (n=5) cultured with hPL (TET+hPL) and seeded directly at an initial seeding density of 1.5×10^5 cells/cm². 4. MSCs (n=5) cultured with hPL (TET2+hPL) and seeded directly at an increased seeding density of 7.5×10^5 cells/cm². The primary objective was to compare the expression of VEGF and bFGF. The analysis revealed that with the original cell concentration and FBS supplementation, bFGF expression was undetectable. However, when hPL was supplemented, a notable difference in bFGF expression was observed between the original seeding concentration and the fivefold higher concentration. As for VEGF, Figure B displayed a statistically significant difference between the original cell concentration and the fivefold higher concentration, irrespective of whether cells were cultivated with FBS or hPL.

B. Vascular Assessment: the CAM Assay + FBS

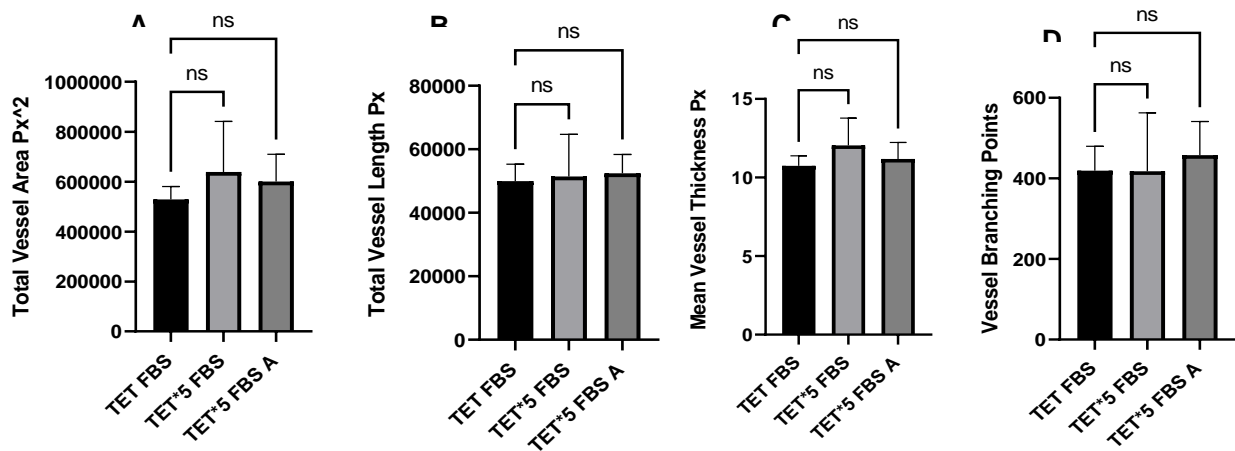


Figure 46. Enumeration of CAM Assay Blood Vessels: comparison between protocols 1 (TET+FBS), 3 (TET+FBS + alginate) & 5 (TET2 + FBS). A. Effect of biopsies treated with protocols 1,3 & 5 on the total vessel area. B. Effect of biopsies treated with protocols 1,3 & 5 on the total vessel length. C. Effect of biopsies treated with protocols 1,3 & 5 on the mean vessel thickness. D. Effect of biopsies treated with protocols 1,3 & 5 on the number of vessels branching points (n=6).

In Figure B, scaffolds obtained from the same groups as those in Figure A (with the addition of scaffolds seeded with cells directly and encapsulated with alginate) were implanted in-ovo (n=6) to evaluate the ability of MSC-seeded scaffolds to engraft and facilitate vascularization. A comparative analysis was conducted between scaffolds inoculated with cells cultivated in FBS (TET+FBS) and seeded directly at an initial seeding density of 1.5×10^5 cells/cm², scaffolds inoculated with MSCs (n=5) cultured with FBS (TET2+FBS) and seeded directly at an increased seeding density of 7.5×10^5 cells/cm², and scaffolds inoculated with cells cultivated in FBS (TET+FBS) and seeded directly at an initial seeding density of 1.5×10^5 cells/cm² with alginate encapsulation. This analysis focused on various parameters related to vascularization, including the quantity of blood vessels within the surrounding area, the total length of vessels, the average vessel thickness, and the number of branching points in the vessels. The results showed no discernible differences between the three groups in any of the vascularization parameters assessed.

C. Vascular Assessment: the CAM Assay + hPL and Alginate

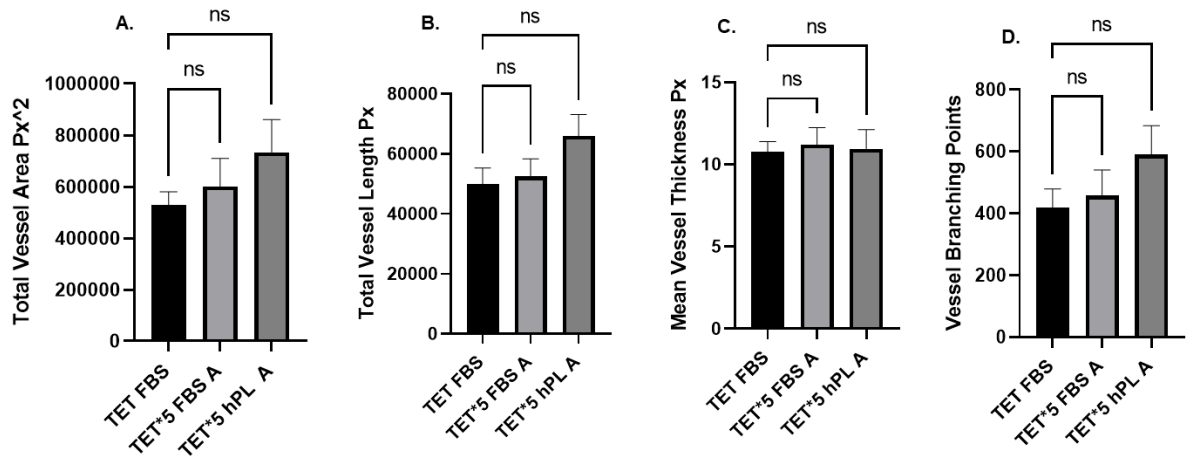


Figure. Enumeration of CAM Assay Blood Vessels: comparison between protocols 1 (TET+FBS),3 (TET+FBS+ Alginate) & 6 (TET2+hPL). **A.** Effect of biopsies treated with protocols 1,3 & 6 on the total vessel area. **B.** Effect of biopsies treated with protocols 1,3 & 6 on the total vessel length. **C.** Effect of biopsies treated with protocols 1,3 & 6 on the mean vessel thickness. **D.** Effect of biopsies treated with protocols 1,3 & 6 on the number of vessels branching points (n=6).

In Figure C, scaffolds inoculated with cells cultivated in FBS (TET+FBS) and seeded directly at an initial seeding density of 1.5×10^5 cells/cm², scaffolds inoculated with MSCs (n=5) cultured with FBS (TET2+FBS + alginate) and seeded directly at an increased seeding density of 7.5×10^5 cells/cm² with alginate encapsulation, and scaffolds inoculated with MSCs (n=5) cultured with hPL (TET2+ hPL+ alginate) and seeded directly at an increased seeding density of 7.5×10^5 cells/cm² with alginate encapsulation were implanted in-ovo (n=6) to evaluate the ability of MSC-seeded scaffolds to engraft and facilitate vascularization. A comparative analysis was conducted between scaffolds focused on various parameters related to vascularization, including the quantity of blood vessels within the surrounding area, the total length of vessels, the average vessel thickness, and the number of branching points in the vessels. The results showed no discernible differences between the three groups in any of the vascularization parameters assessed.

3.4.5. Influence of Coculturing MSCs with Dermal Fibroblasts in The Presence of FBS and hPL as Culture Supplementation

A. Assessment of VEGF and bFGF expression

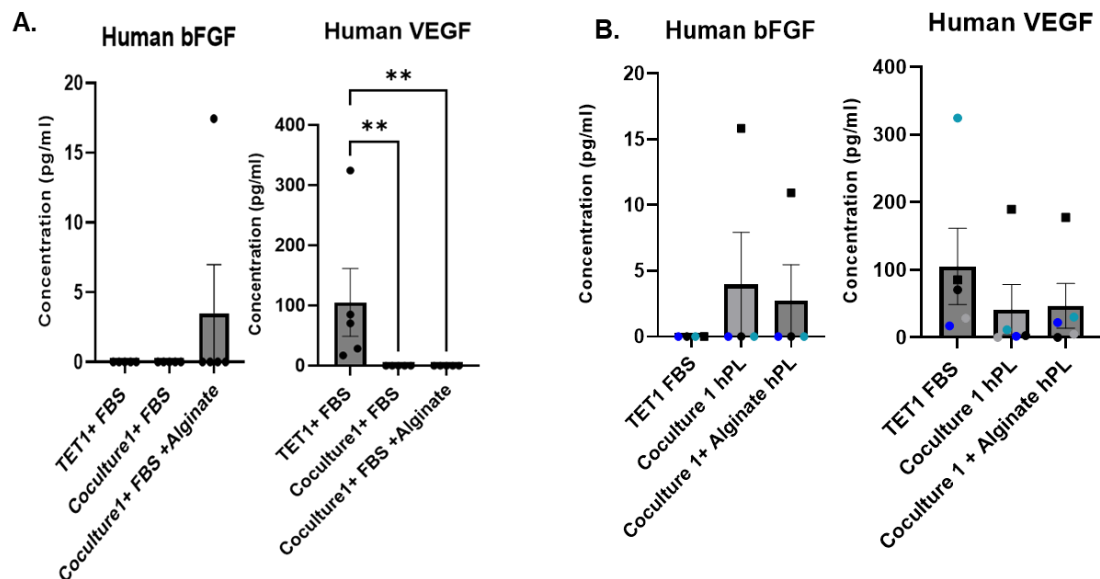


Figure 47. VEGF and bFGF Expression Under Different Conditions. Comparison between the amount of protein released from cocultured MSCs and Fibroblasts seeded directly onto Integra® scaffolds, treated with FBS and hPL, (n=5). **A.** Comparison between the amount of bFGF & VEGF secreted by directly, and encapsulated, seeded coculture of MSC with DFs in comparison to Protocol 1 with FBS supplementation. **B.** Comparison between the amount of bFGF & VEGF secreted by seeded the same cocultures in relation to protocol 1 with hPL supplementation. Statistical analysis depicting the Mean and +/-SEM.

In Figure A, scaffolds composed of Integra®Matrix were subjected to the following seeding protocols: MSCs (n=5) cultured with FBS (TET+FBS) and directly seeded. MSCs (n=5) co-cultured with human dermal fibroblasts (hDFs) at a 50:50 ratio (Coculture 1 + FBS) and directly seeded with FBS supplementation. MSCs (n=5) co-cultured with human dermal fibroblasts (hDFs) at a 50:50 ratio (Coculture 1 + FBS + Alginate) and directly seeded after alginate encapsulation with FBS supplementation.

The primary objective was to assess the expression of vascular endothelial growth factor (VEGF) and basic fibroblast growth factor (bFGF), particularly in comparison to the TETRA protocol (Protocol 1: TET+FBS). The analysis revealed that, in the presence of FBS supplementation, there was minimal bFGF expression observed across all three groups (n=5). However, with regards to VEGF, MSCs cultured solely with FBS supplementation (Protocol 1) demonstrated VEGF expression, whereas MSCs co-cultured with hDFs, with or without alginate encapsulation, did not exhibit VEGF expression. These findings provide additional support for the direct seeding of MSCs as opposed to their co-culture with hDFs and/or encapsulation with alginate in this experimental context.

In Figure B, scaffolds composed of Integra® Matrix underwent the following seeding procedures: MSCs (n=5) cultured with FBS (TET+FBS) and directly seeded. MSCs (n=5) co-cultured with human dermal fibroblasts (hDFs) at a 50:50 ratio (Coculture 1 + hPL) and directly seeded with hPL supplementation. MSCs (n=5) co-cultured with human dermal fibroblasts (hDFs) at a 50:50 ratio (Coculture 1 + hPL + Alginate) and directly seeded after alginate encapsulation with hPL supplementation.

The objective here was to evaluate the expression of VEGF and bFGF, specifically in reference to the TETRA protocol (Protocol 1: TET+FBS). The analysis revealed that, in the presence of hPL supplementation, there was minimal bFGF expression observed across all three groups (n=5). With regards to VEGF, the expression levels in Coculture 1 and Coculture 1+alginate were not statistically different but appeared to be lower in the co-culture groups when compared to the original protocol (Protocol 1 – MSCs + FBS). Consequently, these results further endorse the direct seeding approach while discouraging the unaltered co-culturing of MSCs and hDFs.

B. Vascular Assessment: the CAM Assay

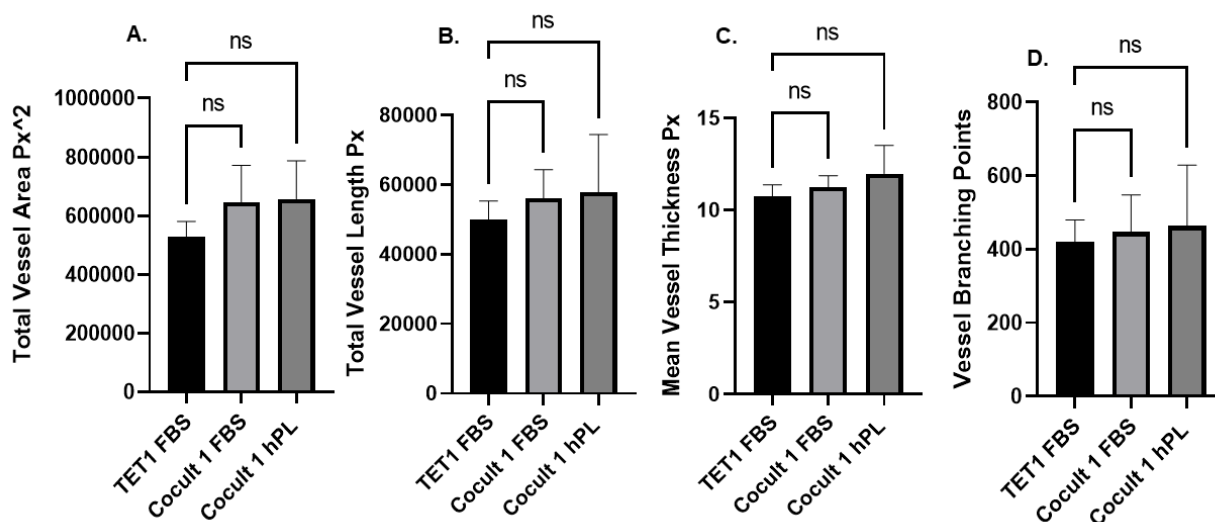


Figure 48. Enumeration of CAM Assay Blood Vessels: Comparison between protocols 1,7 & 9. **A.** Effect of biopsies treated with protocols 1,3 & 6 on the total vessel area. **B.** Effect of biopsies treated with protocols 1,7 & 9 on the total vessel length. **C.** Effect of biopsies treated with protocols 1,7 & 9 on the mean vessel thickness. **D.** Effect of biopsies treated with protocols 1,7 & 9 on the number of vessels branching points (n=6).

In the preceding figure, scaffolds were subjected to different seeding methods: Scaffolds inoculated with cells cultured in FBS (TET+FBS) and directly seeded (n=5). Scaffolds inoculated with a co-culture of MSCs (n=5) with dermal fibroblasts (DFs) cultured with FBS (Coculture 1 + FBS) and directly seeded. Scaffolds inoculated with a co-culture of MSCs (n=5) with DFs cultured with hPL (Coculture 1 + hPL) and directly seeded. Subsequently, these scaffolds were implanted in-ovo (n=6) to assess the capacity

of MSC-seeded scaffolds to engraft and promote vascularization. A comparative analysis was conducted, focusing on various parameters associated with vascularization, including the quantity of blood vessels in the surrounding area, total vessel length, average vessel thickness, and the number of vessels branching points. The results indicated that there were no observable differences between the three groups in any of the assessed vascularization parameters.

3.4.6. Impact of Combining Nucleofected MSCs With Unaltered MSCs on the Overall MSC Secretome

A. Assessment of VEGF and bFGF expression

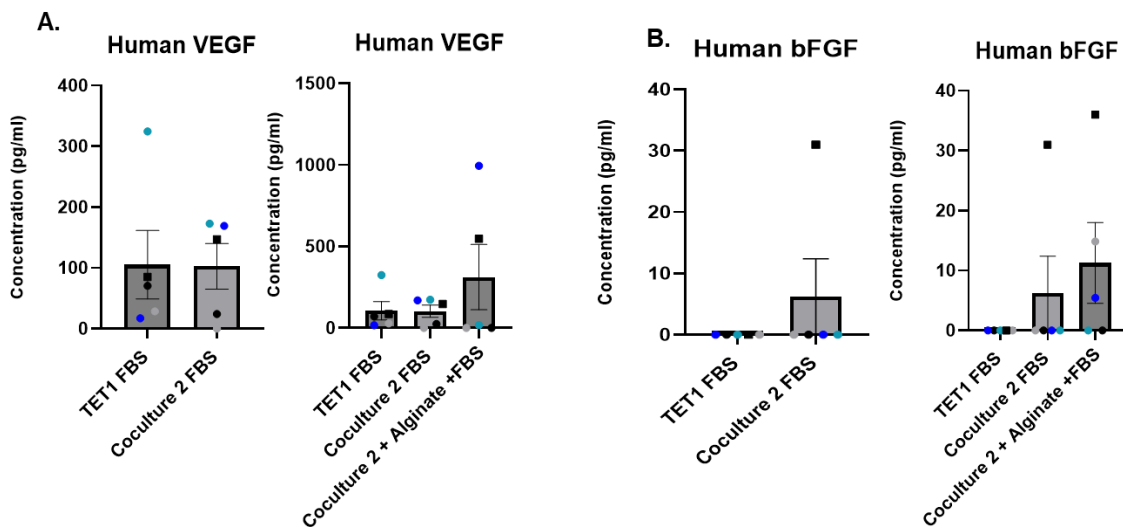


Figure 49. VEGF and bFGF Expression Under Different Conditions. Comparison between the amount of protein released from cocultured MSCs and nucleofected MSCs seeded directly onto Integra® scaffolds, treated with FBS, (n=5) and then encapsulated with alginate. A. Comparison between the amount of bFGF & VEGF secreted by seeded the coculture of MSC in comparison to Protocol 1 + Alginate. **B.** Comparison between the amount of bFGF & VEGF secreted by seeded the coculture in relation to protocol 1 + alginate. Statistical analysis depicting the Mean and +/-SEM.

In Figure A, Integra® Matrix scaffolds underwent the following seeding protocols: MSCs (n=5) cultured with FBS (TET+FBS) and directly seeded. Unmodified MSCs (n=5) co-cultured with nucleofected MSCs (n=5) at a 50:50 ratio (Coculture 2 + FBS) and directly seeded with FBS supplementation. Unmodified MSCs (n=5) co-cultured with nucleofected MSCs (n=5) at a 50:50 ratio (Coculture 2 + FBS + Alginate) and directly seeded after alginate encapsulation with FBS supplementation.

The primary objective was to assess the expression of human vascular endothelial growth factor (VEGF) expression, particularly in comparison to the TETRA protocol (Protocol 1: TET+FBS). The analysis revealed that, in the presence of FBS supplementation, there was no statistically significant difference observed among the three groups (n=5).

In Figure B, the same scaffolds were evaluated for basic fibroblast growth factor (bFGF) expression, specifically in comparison to the TETRA protocol (Protocol 1: TET+FBS). The analysis showed no statistically significant difference among the three groups (n=5) in the presence of FBS supplementation. However, in the scaffolds with alginate encapsulation, there was some bFGF expression observed, whereas there was minimal to no expression in the non-encapsulated groups.

B. Vascular Assessment: the CAM Assay

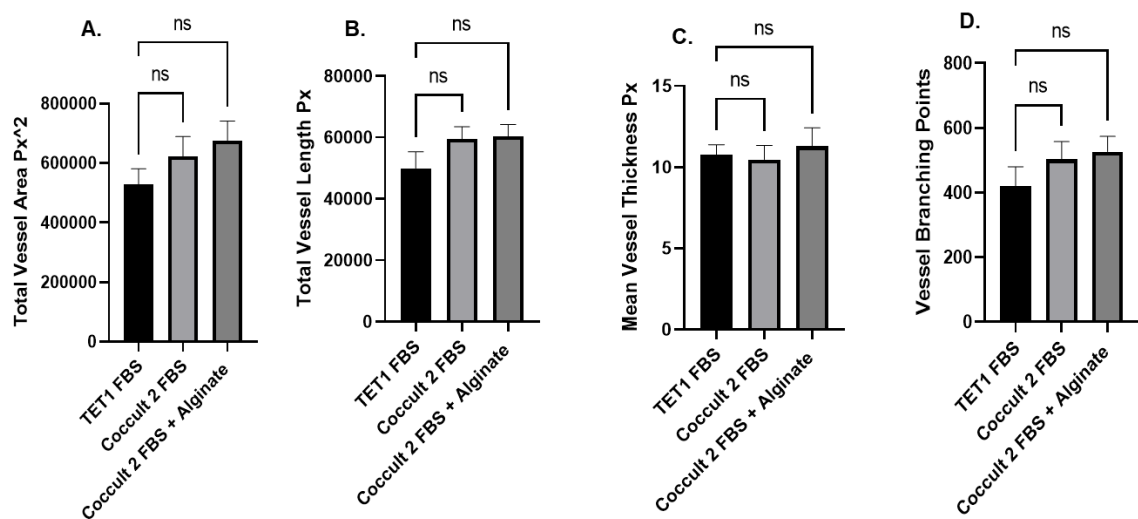


Figure 50. Enumeration of CAM Assay Blood Vessels: Comparison between protocols 1, 11 & 13. A. Effect of biopsies treated with protocols 1 (TET+FBS), 11 (Coculture 2 + FBS) & 13 (coculture 2 + FBS + Alginate) on the total vessel area. B. Effect of biopsies treated with protocols 1, 11 & 13 on the total vessel length. C. Effect of biopsies treated with protocols 1, 11 & 13 on the mean vessel thickness. D. Effect of biopsies treated with protocols 1, 11 & 13 on the number of vessels branching points (n=6).

In the preceding figure, scaffolds underwent different seeding procedures: Scaffolds were inoculated with cells cultured in FBS (TET+FBS) and directly seeded (n=5). Scaffolds were inoculated with a co-culture of unaltered MSCs (n=5) with genetically modified MSCs cultured with FBS (Coculture 2 + FBS) and directly seeded (n=5). Scaffolds were inoculated with a co-culture of unaltered MSCs (n=5) with genetically modified MSCs cultured with FBS (Coculture 2 + FBS + Alginate), encapsulated with alginate, and then directly seeded.

These scaffolds were subsequently implanted in-ovo (n=6) to assess the ability of MSC-seeded scaffolds to engraft and promote vascularization. A comparative analysis was conducted, focusing on various parameters associated with vascularization, including the quantity of blood vessels within the surrounding area, the total length of vessels, the average vessel thickness, and the number of branching points in the vessels. The results indicated no discernible differences between the three groups in any of the vascularization parameters assessed.

3.4.7. Impact of Combining Nucleofected MSCs With Unaltered MSCs on the Overall MSC Secretome

A. Assessment of VEGF and bFGF expression

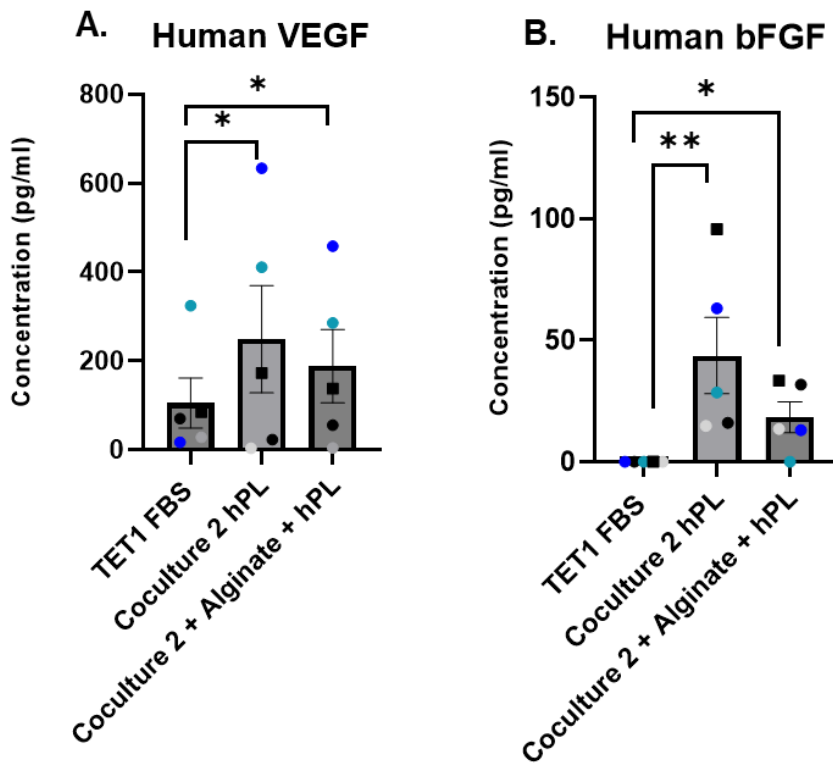


Figure 51. VEGF and bFGF Expression Under Different Conditions. Comparison between the amount of protein released from cocultured MSCs and nucleofected MSCs. The cells were seeded directly onto Integra® scaffolds, treated with hPL, (n=5) and then encapsulated with alginate. A. Comparison between the amount of VEGF secreted by seeded the coculture of MSC in comparison to Protocol 1+ Alginate. **B.** Comparison between the amount of bFGF secreted by seeded the coculture in relation to protocol 1 + alginate. Statistical analysis depicting the Mean and +/-SEM.

In Figure A, scaffolds consisting of Integra®Matrix were subjected to the following seeding methods: MSCs (n=5) cultured with FBS (TET+FBS) and directly seeded. Unmodified MSCs (n=5) co-cultured with nucleofected MSCs (n=5) at a 50:50 ratio (Coculture 2 + hPL) and directly seeded with hPL supplementation. Unmodified MSCs (n=5) co-cultured with nucleofected MSCs (n=5) at a 50:50 ratio (Coculture 2 + hPL + Alginate) and directly seeded after alginate encapsulation with hPL supplementation. The primary objective was to assess the expression of human vascular endothelial growth factor (VEGF) specifically, concerning the TETRA protocol, Protocol 1 (TET + FBS). The analysis revealed that in the presence of hPL supplementation, both Coculture 2 (direct seeding) and Coculture 2 + alginate (encapsulation followed by direct seeding) exhibited higher VEGF expression levels compared to the TETRA group (n=5).

In Figure B, the same scaffolds were evaluated for basic fibroblast growth factor (bFGF) expression, specifically in relation to the TETRA protocol, Protocol 1 (TET + FBS). The analysis indicated that in the presence of hPL supplementation, both Coculture 2 (direct seeding) and Coculture 2 + alginate (encapsulation followed by direct seeding) displayed higher bFGF expression levels compared to the TETRA group (n=5). However, it is noteworthy that the scaffolds seeded directly exhibited a higher level of bFGF expression than those seeded with alginate encapsulation in comparison to the TETRA protocol.

B. Vascular Assessment: the CAM Assay

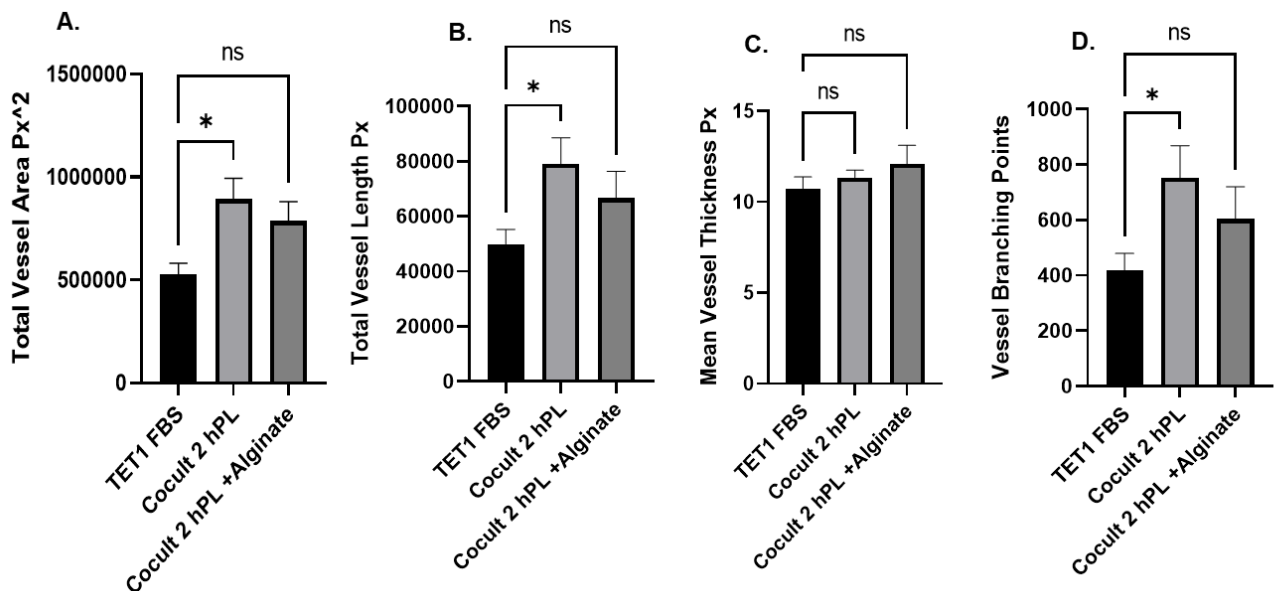


Figure 52. Enumeration of CAM Assay Blood Vessels: Comparison between protocols 1 ,12 & 14. A. Effect of biopsies treated with protocols 1 ,12 & 14 on the total vessel area. B. Effect of biopsies treated with protocols 1 ,12 & 14 on the total vessel length. C. Effect of biopsies treated with protocols 1 ,12 & 14 on the mean vessel thickness. D. Effect of biopsies treated with protocols 1 ,12 & 14 on the number of vessels branching points (n=6).

In the aforementioned Figure, scaffolds were implanted in-ovo (n=6) to assess the capacity of MSC-seeded scaffolds to engraft and promote vascularization. Three groups were compared, each subjected to different seeding procedures: Scaffolds inoculated with cells cultivated in FBS (TET+FBS) and directly seeded (n=5). Scaffolds inoculated with a coculture of unaltered MSCs (n=5) with genetically modified MSCs cultured with hPL (Coculture 2 + hPL) and directly seeded (n=5). Scaffolds inoculated with a coculture of unaltered MSCs (n=5) with genetically modified MSCs cultured with hPL (Coculture 2 + hPL + Alginate), encapsulated with alginate, and then directly seeded.

A comparative analysis focused on various parameters related to vascularization, including the quantity of blood vessels within the surrounding area, the total length of vessels, the average vessel thickness, and the number of branching points in the vessels. The results indicated that Coculture 2 (direct seeding) in the presence of hPL cultivation outperformed both the TETRA (TET+FBS) protocol

and the Coculture 2 + alginate protocol in terms of the total vessel area, total vessel length, and the number of vessels branching points. This supports the notion of direct seeding as a more favorable approach and lends credibility to the Coculture 2 protocol with hPL cultivation.

3.4.8. Impact of Combining Human Dermal Fibroblasts and Unmanipulated MSCS on the Overall Cell Secretome (FBS)

A. Assessment of VEGF and bFGF expression

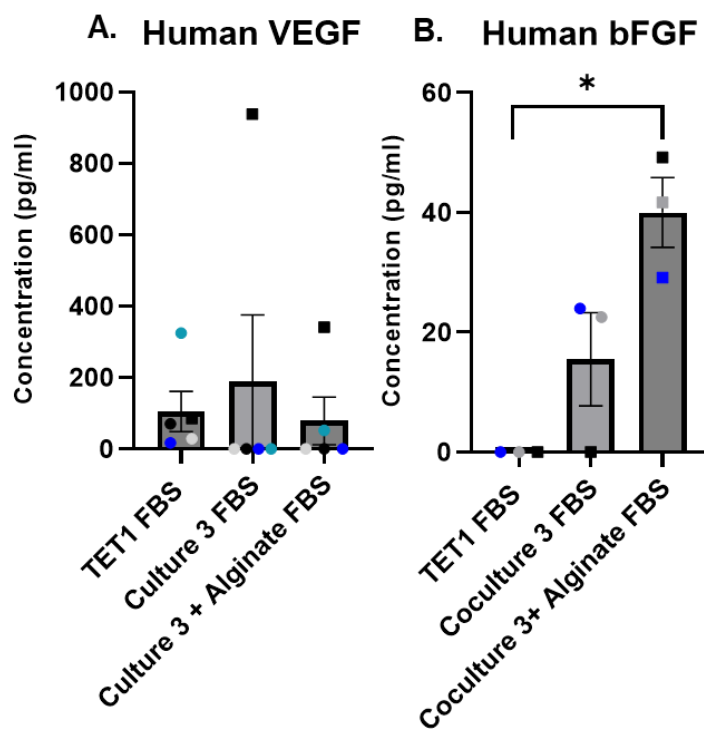


Figure 53. VEGF and bFGF Expression Under Different Conditions. Comparison between the amount of protein released from cocultured MSCs and Fibroblasts seeded directly onto Integra® scaffolds, treated with FBS, (n=5) and then encapsulated with alginate. A. Comparison between the amount of VEGF secreted by seeded the coculture of MSC in comparison to Protocol 1+ Alginate. **B.** Comparison between the amount of bFGF secreted by seeded the coculture in relation to protocol 1 + alginate. Statistical analysis depicting the Mean and +/-SEM.

In the previous Figure A, scaffolds composed of Integra®Matrix were subjected to different seeding approaches: MSCs (n=5) cultured with FBS (TET+FBS) and directly seeded. Unaltered MSCs (n=5) cocultured with nucleofected DFs (n=5) at a 50:50 ratio (Coculture 3 + FBS) and directly seeded in the presence of FBS supplementation. Unaltered MSCs cocultured with nucleofected DFs at a 50:50 ratio (Coculture 3 + FBS + Alginate) and seeded directly after alginate encapsulation in the presence of FBS supplementation. The objective was to assess the expression of human VEGF and bFGF in comparison to the TETRA protocol, specifically Protocol 1 (TET + FBS). The analysis indicated no significant difference in the VEGF group across the three groups. However, in the bFGF group, a disparity was observed between the Coculture 3 + Alginate group and the original TET + FBS group in the presence of FBS supplementation.

B. Vascular Assessment: the CAM Assay

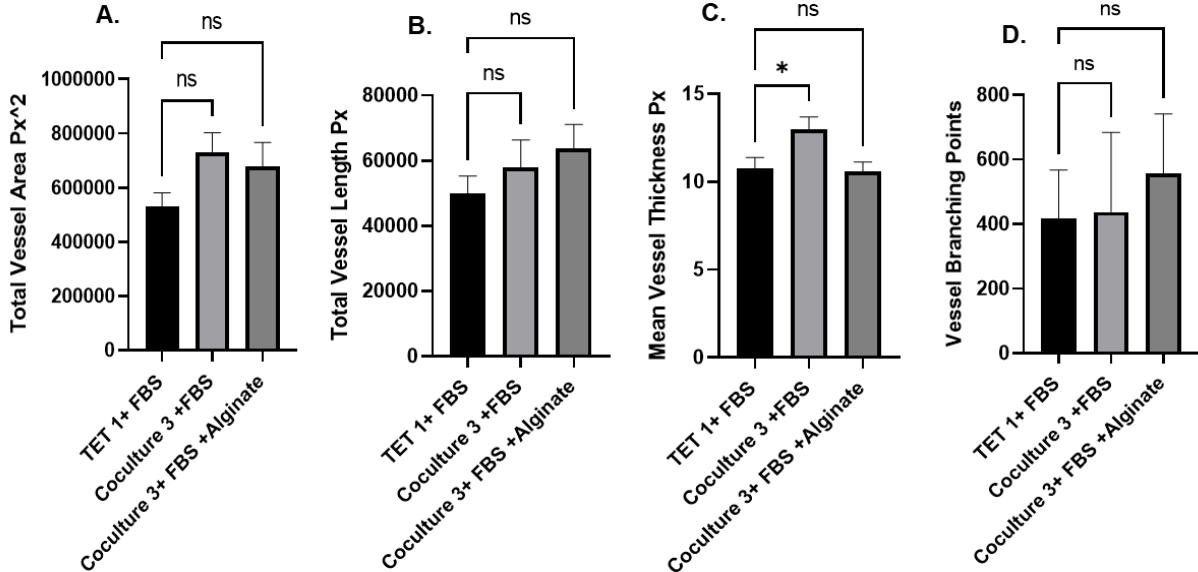


Figure 54. Enumeration of CAM Assay Blood Vessels: comparison between protocols 1,17 & 19. A. Effect of biopsies treated with protocols 1,11 & 13 on the total vessel area. **B.** Effect of biopsies treated with protocols 1,17 & 19 on the total vessel length. **C.** Effect of biopsies treated with protocols 1,17 & 19 on the mean vessel thickness. **D.** Effect of biopsies treated with protocols 1,17 & 19 on the number of vessels branching points (n=6).

In the preceding Figure, scaffolds inoculated with cells cultivated in FBS (TET+FBS) and seeded directly (n=5), scaffolds inoculated with a coculture of unaltered MSCs with genetically modified DFs cultured with FBS (coculture 3 + FBS) and seeded directly, and scaffolds inoculated with a coculture of unaltered MSCs (n=5) with genetically modified DFs cultured with FBS (coculture 3 + FBS + Alginate), encapsulated with alginate and then seeded directly, were implanted in-ovo (n=6) to evaluate the ability of MSC/DFs-seeded scaffolds to engraft and facilitate vascularization. A comparative analysis was conducted among scaffolds focusing on various parameters related to vascularization, including the quantity of blood vessels within the surrounding area, the total length of vessels, the average vessel thickness, and the number of branching points in the vessels. **The results showed a higher mean vessel thickness when comparing the direct seeding of unaltered MSCs in conjunction with genetically modified DFs in the presence of FBS, in comparison to the original TETRA (TET+FBS) protocol.**

3.4.9. Impact of Combining Human Dermal Fibroblasts and Unmanipulated MSCS on the Overall Cell Secretome (hPL)

A. Assessment of VEGF and bFGF expression

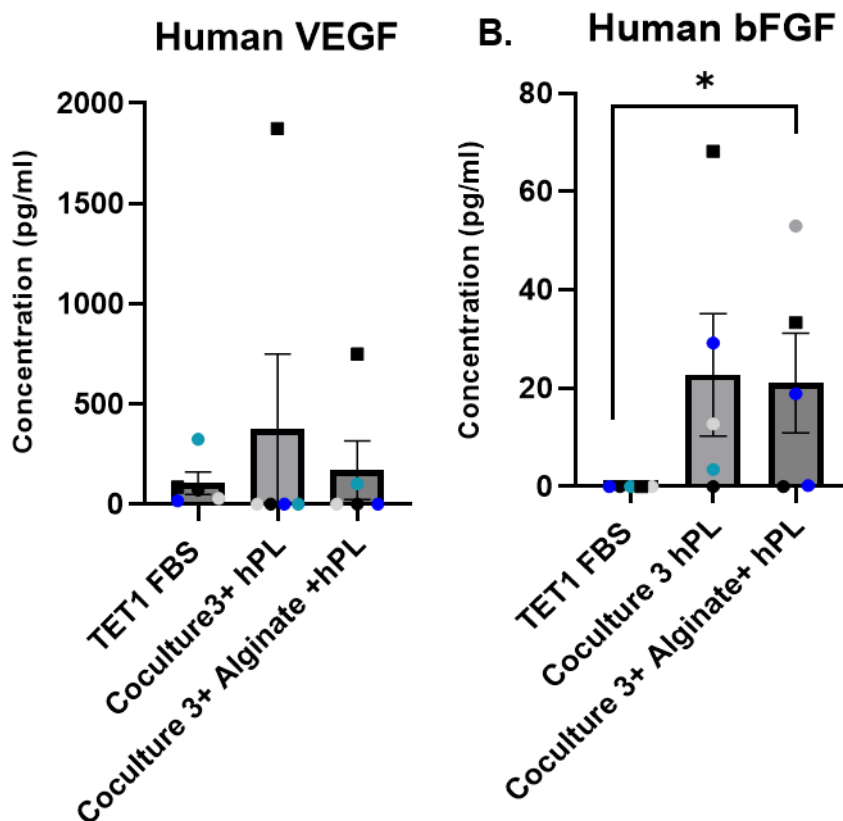


Figure 55. VEGF and bFGF Expression Under Different Conditions. Comparison between the amount of protein released from cocultured MSCs and Fibroblasts seeded directly onto Integra® scaffolds, treated with hPL, (n=5) and then encapsulated with alginate. A. Comparison between the amount of VEGF secreted by seeded the

coculture of MSC in comparison to Protocol 1+ Alginate. **B.** Comparison between the amount of bFGF secreted by seeded the coculture in relation to protocol 1 + alginate. Statistical analysis depicting the Mean and +/-SEM.

In the previous Figure, scaffolds composed of Integra®Matrix were seeded using the following methods: 1. MSCs (n=5) cultured with FBS (TET+FBS) and seeded directly. 2. Unaltered MSCs (n=5) cocultured with nucleofected DFs (n=5) at a ratio of 50:50 (Coculture 3 + hPL) and seeded directly in the presence of hPL supplementation. 3. Unaltered MSCs cocultured with nucleofected DFs at a ratio of 50:50 (Coculture 3 + hPL + Alginate) and seeded directly after alginate encapsulation in the presence of hPL supplementation. The aim was to compare the expression of human VEGF and bFGF, specifically in relation to the TETRA protocol, protocol 1 (TET + hPL). The analysis revealed that in the presence of hPL supplementation, no significant difference was observed in the VEGF group. However, in the bFGF group, a difference was observed between the Coculture 3 group and the original TET + FBS group.

B. Vascular Assessment: the CAM Assay

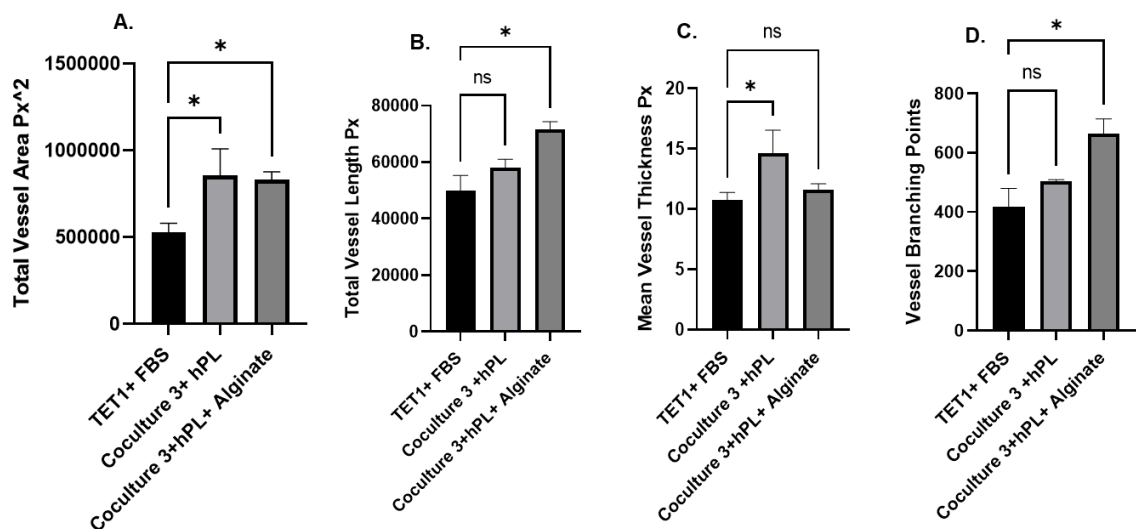


Figure 56. Enumeration of CAM Assay Blood Vessels: Comparison between protocols 1,18 & 20. **A.** Effect of biopsies treated with protocols 1,18 & 20 on the total vessel area. **B.** Effect of biopsies treated with protocols 1,18 & 20 on the total vessel length. **C.** Effect of biopsies treated with protocols 1,18 & 20 on the mean vessel thickness. **D.** Effect of biopsies treated with protocols 1,18 & 20 on the number of vessels branching points (n=6).

In the preceding figure, scaffolds that were seeded with cells cultured in FBS (TET+FBS) and directly seeded (n=5), scaffolds inoculated with a coculture of unaltered MSCs and genetically modified DFs cultured with hPL (coculture 3 + hPL) and directly seeded (n=5), and scaffolds inoculated with a coculture of unaltered MSCs (n=5) with genetically modified DFs, cultured with hPL (coculture 3 + hPL + Alginate), encapsulated with alginate, and then directly seeded were implanted in-ovo (n=6) to assess the potential of MSC/DF-seeded scaffolds to engraft and promote vascularization. An in-depth analysis compared these scaffolds based on various parameters related to vascularization, including the quantity of blood vessels within the surrounding area, the total length of vessels, the average vessel thickness, and the number of branching points in the vessels. The results indicated a higher outcome

in the total vessel area and the mean vessel thickness when comparing the direct seeding of unaltered MSCs in conjunction with genetically modified DFs (coculture 3) in the presence of hPL, in comparison to the original TETRA (TET+FBS) protocol. Additionally, they revealed a higher outcome in the total vessel area and the number of vessels branching points when comparing the direct seeding (after encapsulation) of unaltered MSCs in conjunction with genetically modified DFs (coculture 3 seeded directly) in the presence of hPL, in comparison to the original TETRA (TET+FBS) protocol.

In summary, the collective results from the screening experiments suggest that cultivation with hPL is more favourable compared to FBS cultivation. Furthermore, the results indicate that there is no significant advantage in encapsulating cells before seeding them onto the scaffolds; in fact, direct seeding often yielded better outcomes. Coculturing MSCs and DFs without genetic manipulation did not produce favourable results. Additionally, increasing the cell number led to higher levels of VEGF and bFGF expression. Among the tested protocols, coculture 2 and coculture 3 in the presence of hPL cultivation appear to be the most promising.

3.5.EXPRESSION OF ANGIOGENESIS FACTORS: SCREENING EXPERIMENTS

A. Angiogenesis Proteomic Profile: Heat Map

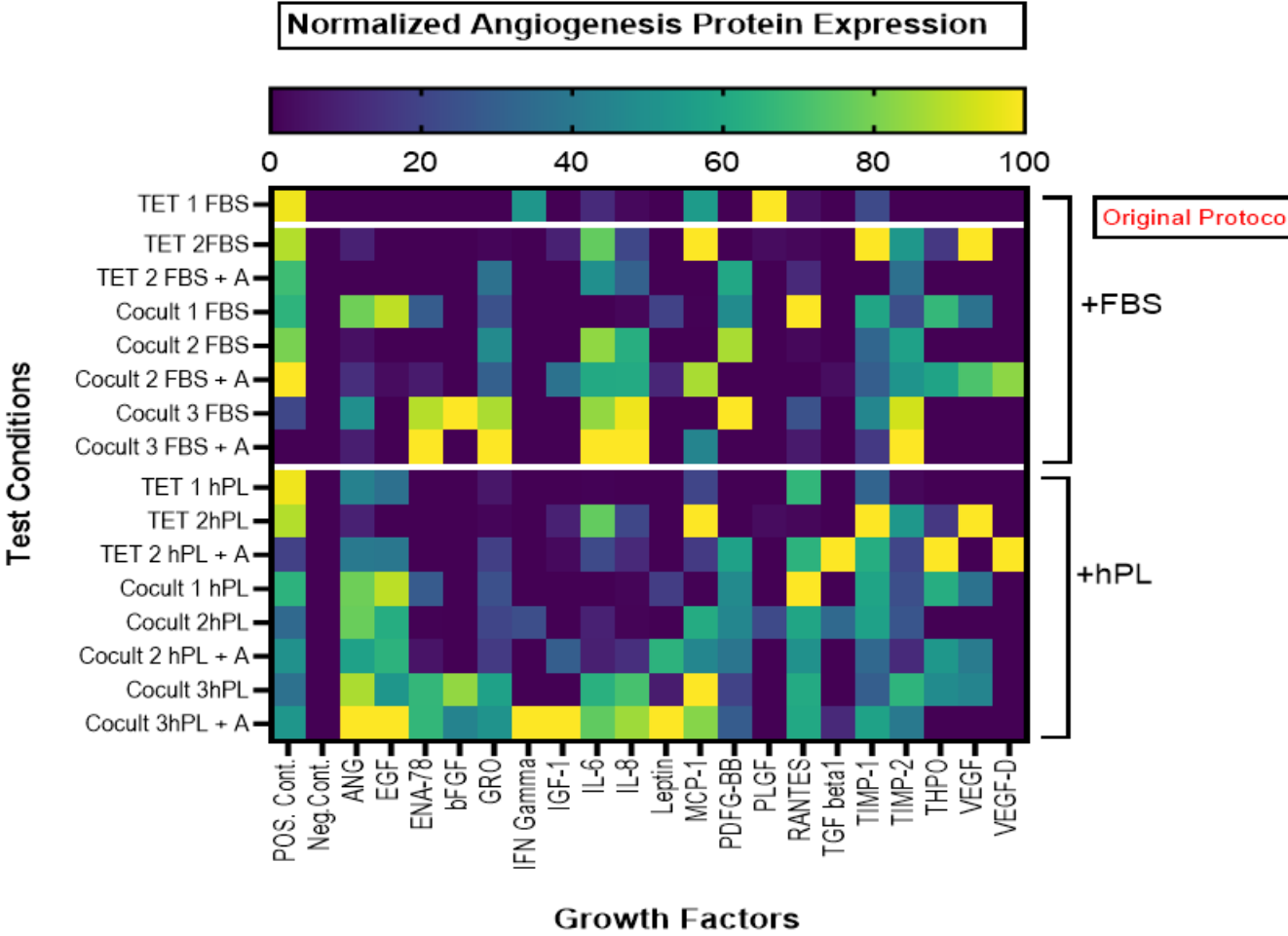
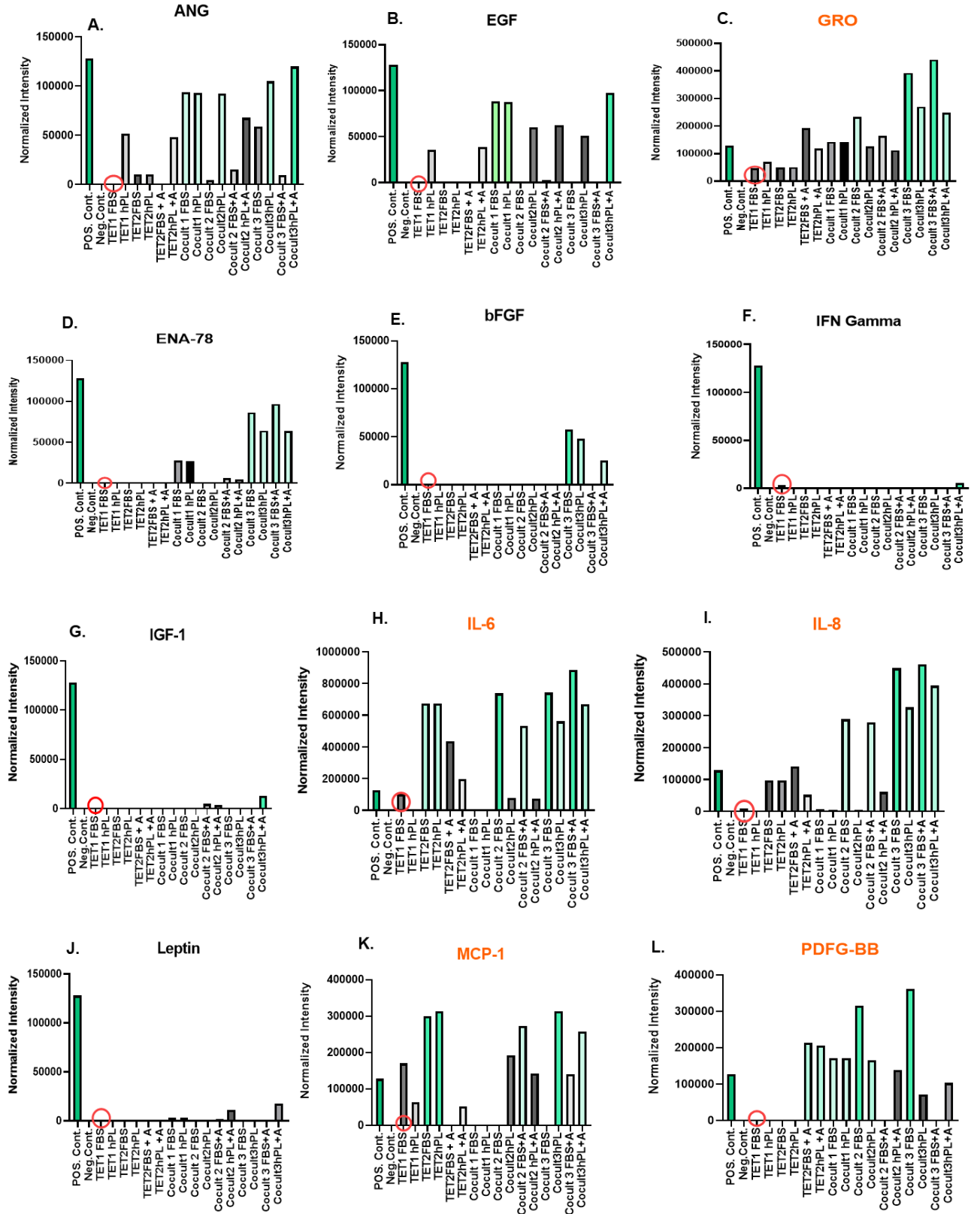


Figure 57. Heat Map: Engineering Protocols Angiogenesis Growth Factor Release.

In the provided heatmap, data from media samples collected from cultivated scaffolds under various protocols were aggregated from five independent runs (n=5) and are represented using a colour scale. Higher values are depicted in yellow, whereas lower values are shown in dark blue.

B. Angiogenesis Proteomic Profile: Individual Factors



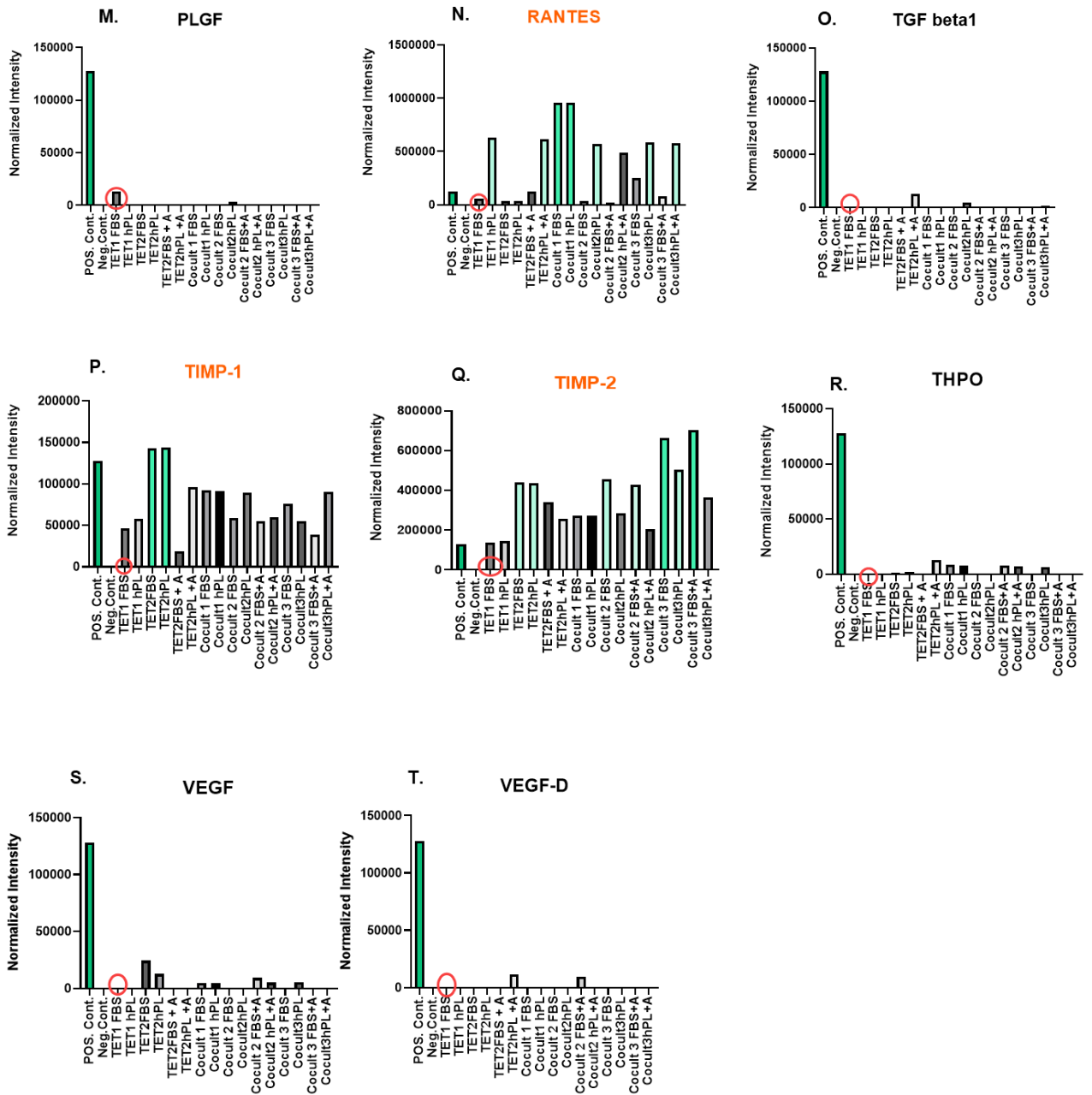


Figure 58. Angiogenic Proteome Profile: Individual Factors. A. Expression levels of Angiogenin. B. Expression levels of EGF. C. Expression levels of GRO. D. Expression levels of ENA-78. E. Expression levels of bFGF. F. Expression levels of IFN Gamma. G. Expression levels of IGF-1. H. Expression levels of IL-6. I. Expression levels of IL-8. J. Expression levels of Leptin. K. Expression levels of MCP-1. L. Expression levels of PDGF-BB. M. Expression levels of PLGF. N. Expression levels of RANTES. O. Expression levels of TGF beta 1. P. Expression levels of TIMP-1. Q. Expression levels of TIMP-2. R. Expression levels of THPO. S. Expression levels of VEGF. T. Expression levels of VEGF-D.

The presented figure illustrates the comparison of angiogenesis growth factor and cytokine expression levels among different protocols using pooled data. In relation to the original TETRA (TET1 + FBS) protocol, most of the tested protocols exhibited varying degrees of increased cytokine expression. However, when comparing these protocols to the TET + FBS protocol and the positive control set by the assay, several cytokines stood out for their significant overexpression. These cytokines include GRO, IL-6, IL-8, MCP-1, PDGF-BB, RANTES, TIMP-1, and TIMP-2.

3.6. 3D TESTING OF TRACHEAL BIOPSIES: IDENTIFICATION OF FINAL PROTOCOL

3.6.1. Seeded Scaffolds' VEGF and bFGF Expression Level Prior to Implantation

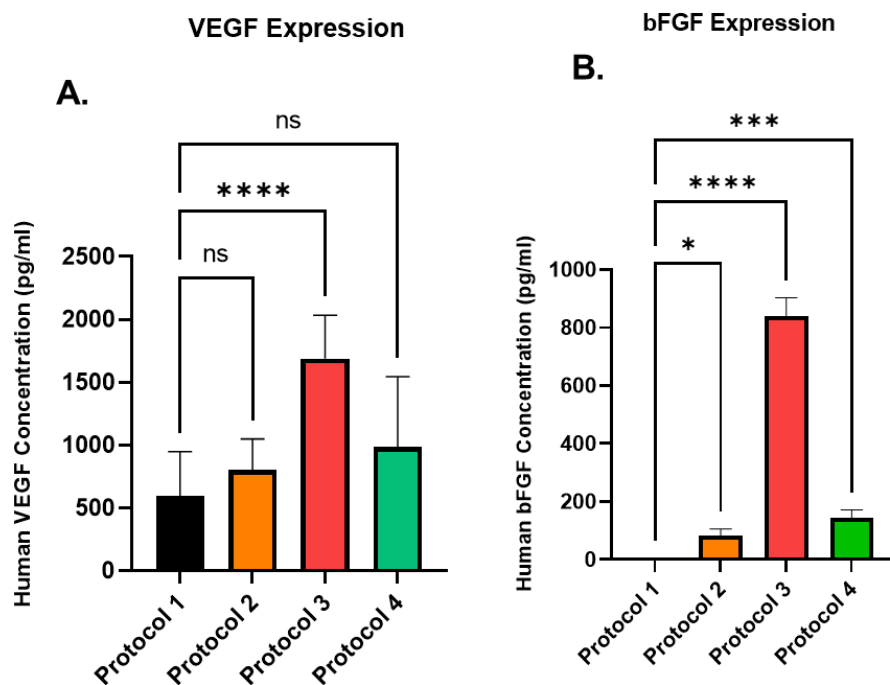


Figure 59. Tracheal Biopsies VEGF and bFGF Expression Levels. Comparison Between the Different Protocols (n=6 per protocol). A. VEGF expression variance between protocols (analysis performed using Kruskal-Wallis test). B. bFGF expression with a large variance between protocols 3 and 1 (analysis performed using an ordinary One-way ANOVA).

In the previous figure, the tracheal scaffolds were compared across four different protocols: Protocol 1 involving cells cultivated in FBS and seeded directly (n=6), Protocol 2 with cells cultivated in hPL and seeded directly (n=6), Protocol 3 featuring a coculture of unaltered MSCs with genetically modified MSCs cultivated with hPL (n=6), and Protocol 4 employing a coculture of unaltered MSCs with genetically modified DFs, also cultivated with hPL (n=6). The aim was to assess their ability to express human VEGF and bFGF in comparison to Protocol 1 (TET + hPL) as the reference. The analysis revealed a notable preference for Protocol 3 (involving unaltered MSCs + genetically manipulated MSCs) over Protocol 1 when examining VEGF expression and bFGF expression. Specifically, regarding bFGF

expression, all three protocols (Protocols 2, 3, and 4) exhibited higher levels compared to the reference Protocol 1.

3.6.2. Single Cell Isolation of Scaffolds Prior to Implantation and Flow Cytometry Staining

3.6.2.1. Comparison Between Different Single Cell Isolation Procedures

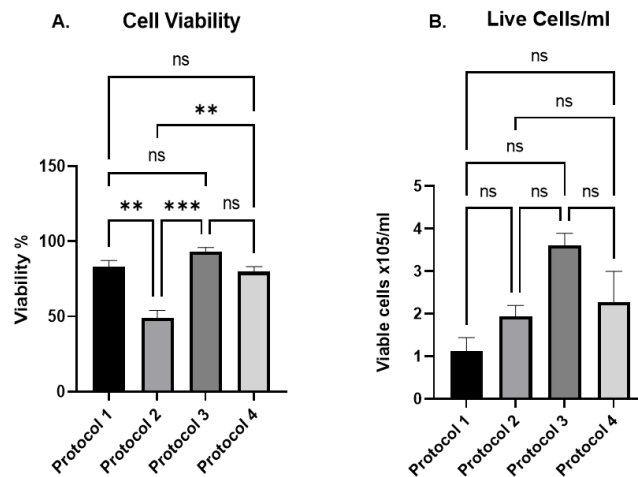


Figure 60. Single Cell Protocols: cellular outputs. **A.** Percentage of viable cells post-isolation as counted by the CASY® Counter. **B.** Number of viable cells/ml post-isolation as counted by the CASY® Counter.

In the previous figure, an evaluation of four distinct protocols was conducted to determine their suitability for the isolation of single cells from seeded scaffolds, with a focus on cellular viability and total cell count. These protocols included: Protocol 1, an in-house method relying on Collagenase A; Protocol 2, adapted from a study by Greaney AM et al. in 2020, utilizing Accutase; Protocol 3, also adapted from the same study but relying on Protease XIV; and Protocol 4, adapted from a study by Ravindran A et al. in 2018, and dependent on Collagenase II.

Figure A clearly indicates a preference for Protocol 3 among the four protocols, as it exhibited the highest percentage of cellular viability. On the other hand, Figure B demonstrates no statistically significant difference between the protocols, but it is worth noting that Protocol 3 resulted in the highest total cell count, indicating its potential advantage in cell isolation.

3.6.2.2. 3D cultivated cells on the trachea- in Process quality control, defining the cell state after seeding and incubation, and prior to implantation.

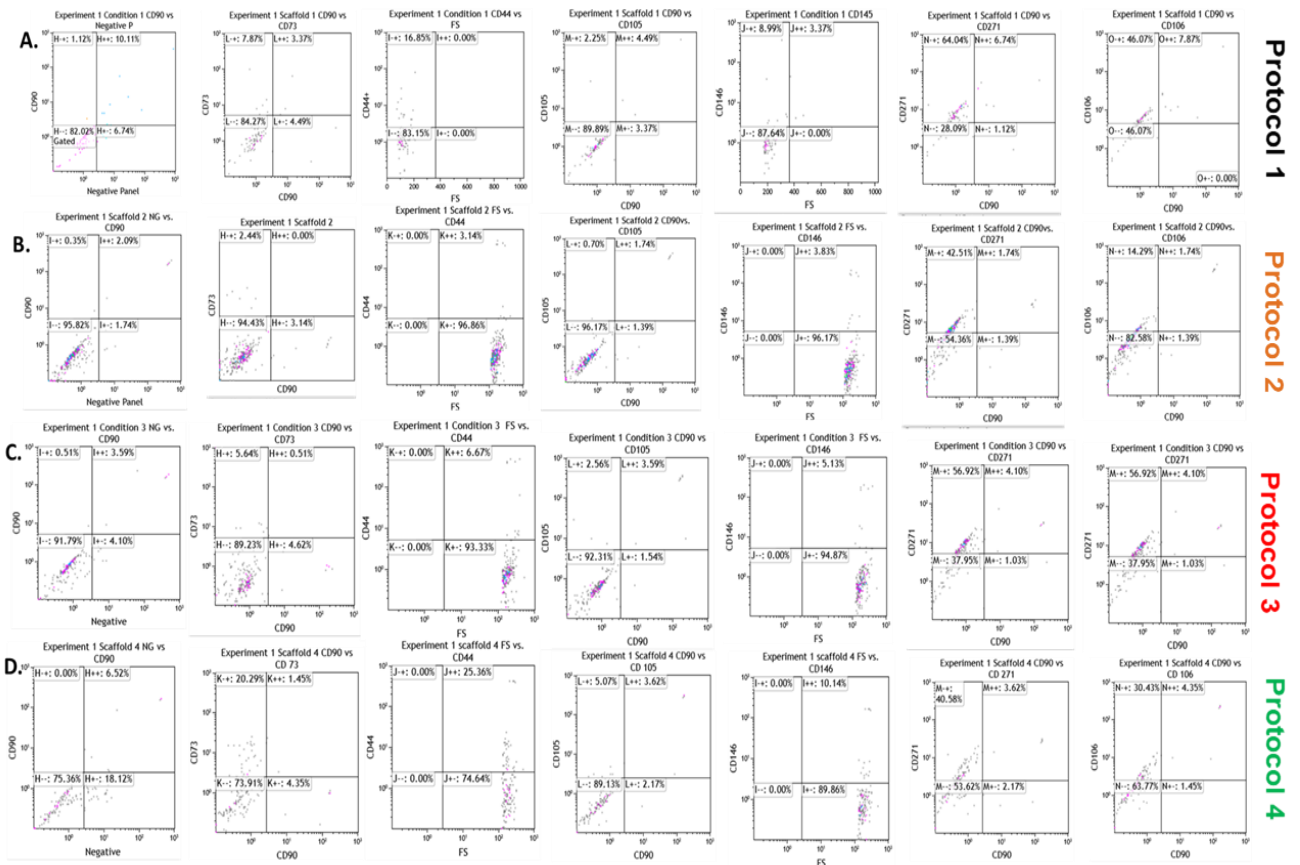


Figure 61. Flow Cytometry analysis of single cells isolated from seeded trachea prior to implantation. Analysed Markers: CD90, CD73, CD44, CD105, CD146, Negative haematopoietic panel, CD271, and CD106. A. Illustrates the outcome of Protocol 1. **B.** Illustrates the outcome of Protocol 2. **C.** Illustrates the outcome of Protocol 3. **D.** Illustrates the outcome of Protocol 4.

The previous panel of experiments was conducted on cells isolated from tracheal scaffolds seeded under various conditions, including protocol 1 (TET+FBS), protocol 2 (TET+hPL), protocol 3 (MSC coculture + hPL), and protocol 4 (MSC and DFs coculture + hPL). Normal cultured cells with FBS and hPL were used as compensation controls. The results of the panel staining revealed an overall reduction in the expression of surface markers associated with MSCs, particularly those defined by the ISCT's minimal criteria (CD90, CD105, and CD73), as well as CD44 and CD146 when compared to the compensation controls. However, it was noteworthy that the cells still exhibited the expression of CD271 and CD106, especially in the context of protocol 4, which involved a mixture of MSCs and DFs.

3.6.2.3. Statistical Analysis of the Flow Cytometry Results

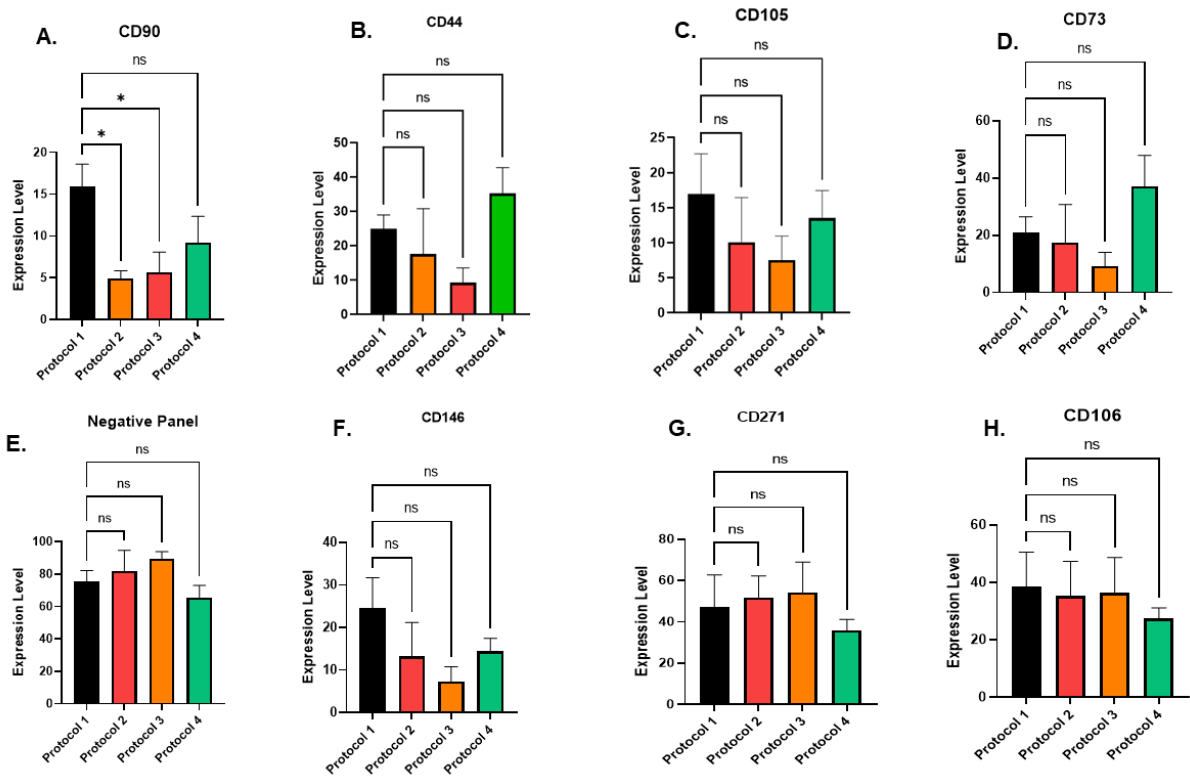


Figure 62. Statistical Analysis of Surface Marker Expression of Isolated Seeded Cells. A. A comparison between cells isolated from the four protocols and their ability to express **CD90**. B. A comparison between cells isolated from the four protocols and their ability to express **CD44**. C. A comparison between cells isolated from the four protocols and their ability to express **CD105**. D. A comparison between cells isolated from the four protocols and their ability to express **CD73**. E. A comparison between cells isolated from the four protocols and their ability to express the negative panel. F. A comparison between cells isolated from the four protocols and their ability to express **CD146**. G. A comparison between cells isolated from the four protocols and their ability to express **CD271**. H. A comparison between cells isolated from the four protocols and their ability to express **CD106**.

The presented figure illustrates the results of a statistical analysis of surface marker expression in cells isolated from various engineering protocols (1, 2, 3, 4) conducted under different combinations and conditions. Graph A reveals a reduction in CD90 surface marker expression, while for other surface markers, no significant differences were observed except for CD90. Of particular interest is protocol 4, which involves a 50:50 coculture of MSCs and DFs. This protocol exhibited surface marker expression for CD146, CD271, and CD106, which are typically associated with MSCs and not commonly expressed by DFs.

3.7. 3D IMPLANTATION OF TRACHEAL BIOPSIES: IDENTIFICATION OF FINAL PROTOCOL

3.7.1. CAM Assay: Blood Vessel Enumeration

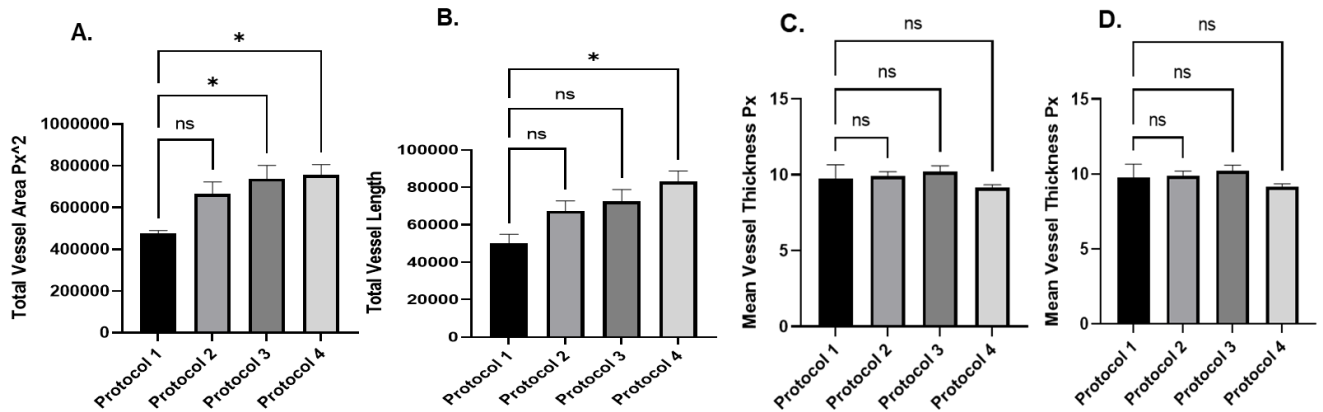


Figure 63. Enumeration of CAM Assay Blood Vessels: comparison between protocols 1,2,3, and 4. **A.** Effect of biopsies treated with protocols **1,2,3, and 4** on the total vessel area. **B.** Effect of biopsies treated with protocols **1,2,3, and 4** on the total vessel length. **C.** Effect of biopsies treated with protocols 1&3 on the mean vessel thickness. **D.** Effect of biopsies treated with protocols **1,2,3, and 4** on the number of vessels branching points (n=6).

In the previous figure, tracheal scaffolds that were inoculated with cells cultured in FBS (Protocol 1) and seeded directly (n=6), tracheal scaffolds inoculated with cells cultured in hPL (Protocol 2) and seeded directly (n=6), tracheal scaffolds inoculated with a coculture of unaltered MSCs with genetically modified MSCs and cultured with hPL (Protocol 3), and tracheal scaffolds inoculated with a coculture of unaltered MSCs (n=6) with genetically modified DFs, cultured with hPL (Protocol 4) were implanted in-ovo (n=6). This implantation aimed to assess the ability of the seeded scaffolds to engraft and promote vascularization. A comparative analysis was conducted, focusing on various parameters related to vascularization, including the quantity of blood vessels within the surrounding area, the total length of vessels, the average vessel thickness, and the number of branching points in the vessels. The results indicated a higher total vessel area in protocols 3 and 4 compared to protocol 1, as well as an increase in total vessel length in protocol 4 compared to protocol 1.

3.7.2. MicroCT: Assessment of Vascularity

3.7.2.1. Enumeration Process

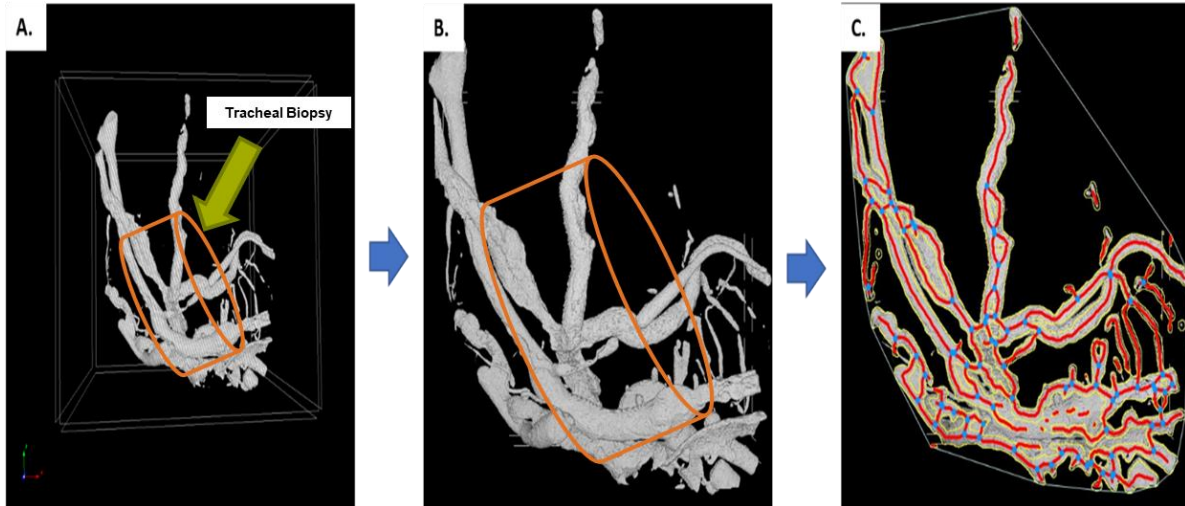


Figure 64. MicroCT Image analysis steps. **A.** Original image with grid. **B.** Image processed with Fiji/Image J Version 1.53t. (removal of the grid and converting image to JPG). **C.** Enumeration using AngioTool 64. Version 0.6a (02.18.14). The orange cylinder is a depiction of what the images would look like with Scaffolds

The previous image illustrates the process of analyzing tracheal scaffolds after MicroCT imaging. The orange disk represents a tracheal punch biopsy, which is not visible through MicroCT imaging but is an integral part of the analysis process.

3.7.2.2. Enumeration of MicroCT Images: Experiment 1

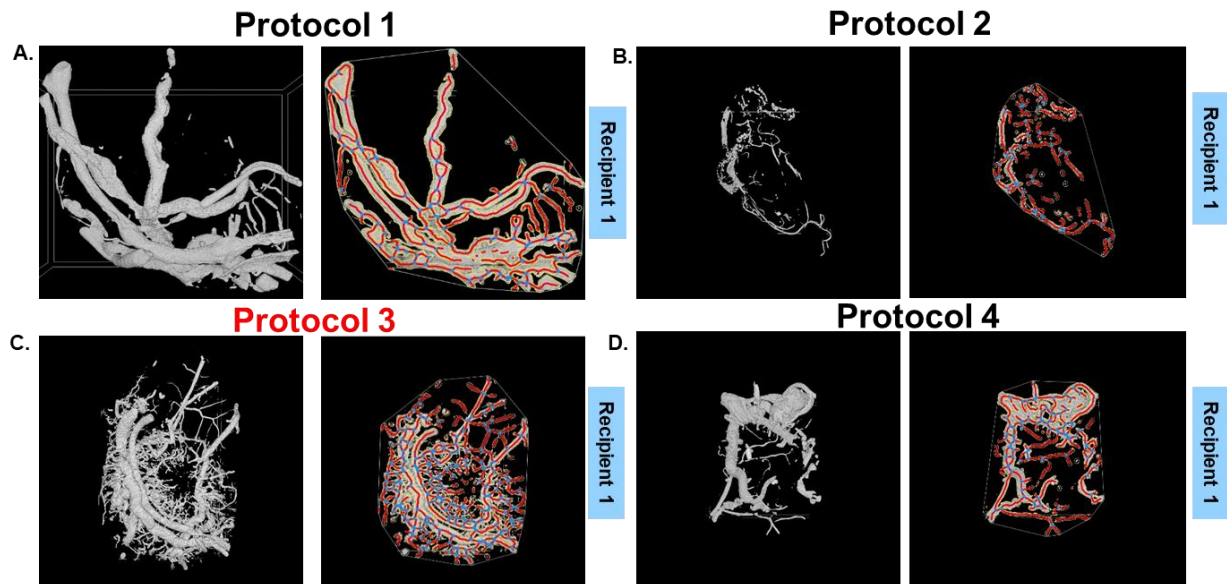


Figure 65. MicroCT imaging and Quantification with AngioTool®: Experiment 1. A. Before and after quantification images of biopsies engineered with Protocol 1. B. Before and after quantification images of biopsies engineered with Protocol 2. C. Before and after quantification images of biopsies engineered with Protocol 3. D. Before and after quantification images of biopsies engineered with Protocol 4.

The preceding figure presents the results of experiment number 1, where tracheal biopsies were engineered using the four previously mentioned protocols and then implanted in-ovo to assess vascularization and engraftment outcomes. The displayed images are MicroCT scans depicting the extent of vasculature infiltration into the engrafted tracheal biopsies. The objective is to identify the protocol yielding the most favorable vascularity outcomes.

In **Image A**, we observe the vascularization of tracheal biopsies seeded with MSCs cultivated with FBS. The blood vessels in this image are notably large and thick. However, the absence of micro blood vessels suggests that the observed vascularization may be limited to the vicinity of the tracheal biopsy rather than true invasion into the scaffold.

Image B represents a tracheal biopsy seeded with MSCs cultivated with hPL. In this image, the blood vessels are thinner, and there is evidence of the beginning of microvasculature formation. This suggests a potential for inter-tracheal vascular invasion.

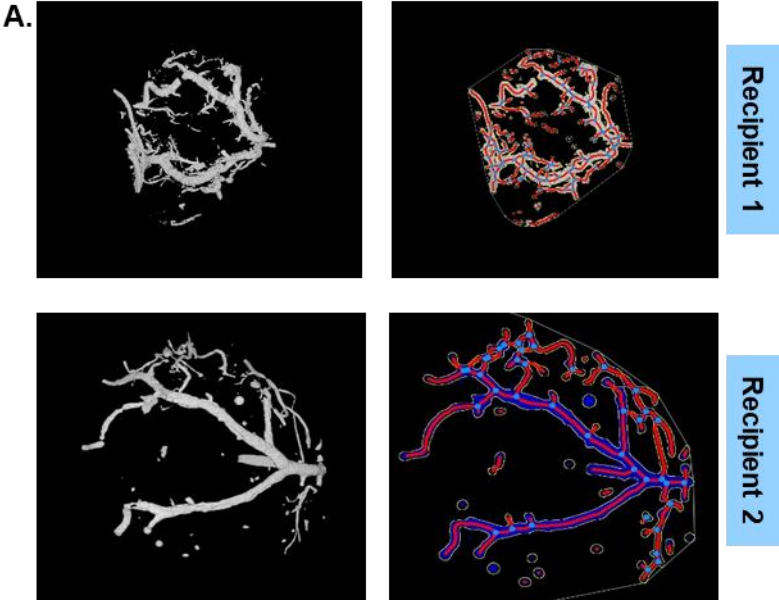
Image C showcases a tracheal biopsy seeded with a coculture of unmodified MSCs and modified MSCs engineered to overexpress VEGF and bFGF. This image supports the hypothesis that this condition can enhance vascularization and overall graft survival. Here, both large and small blood vessels are observed, and the cylindrical shape of the scaffold biopsy is mostly maintained, indicating the occurrence of vascular invasion and microinvasion into the scaffold.

Finally, in **Image D**, we see a tracheal biopsy seeded with a coculture of unmodified MSCs and modified dermal fibroblasts (DFs) engineered to overexpress VEGF and bFGF. The majority of blood vessels in this image are large, although there is some evidence of microvasculature formation and potential scaffold invasion.

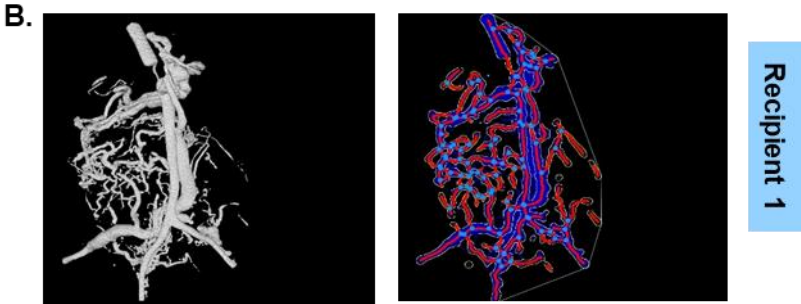
These observations provide insights into the varying degrees of vascularization achieved with each protocol and may inform the selection of the most effective approach for future experiments.

3.7.2.3. Enumeration of MicroCT Images: Experiment 2

Protocol 1



Protocol 2



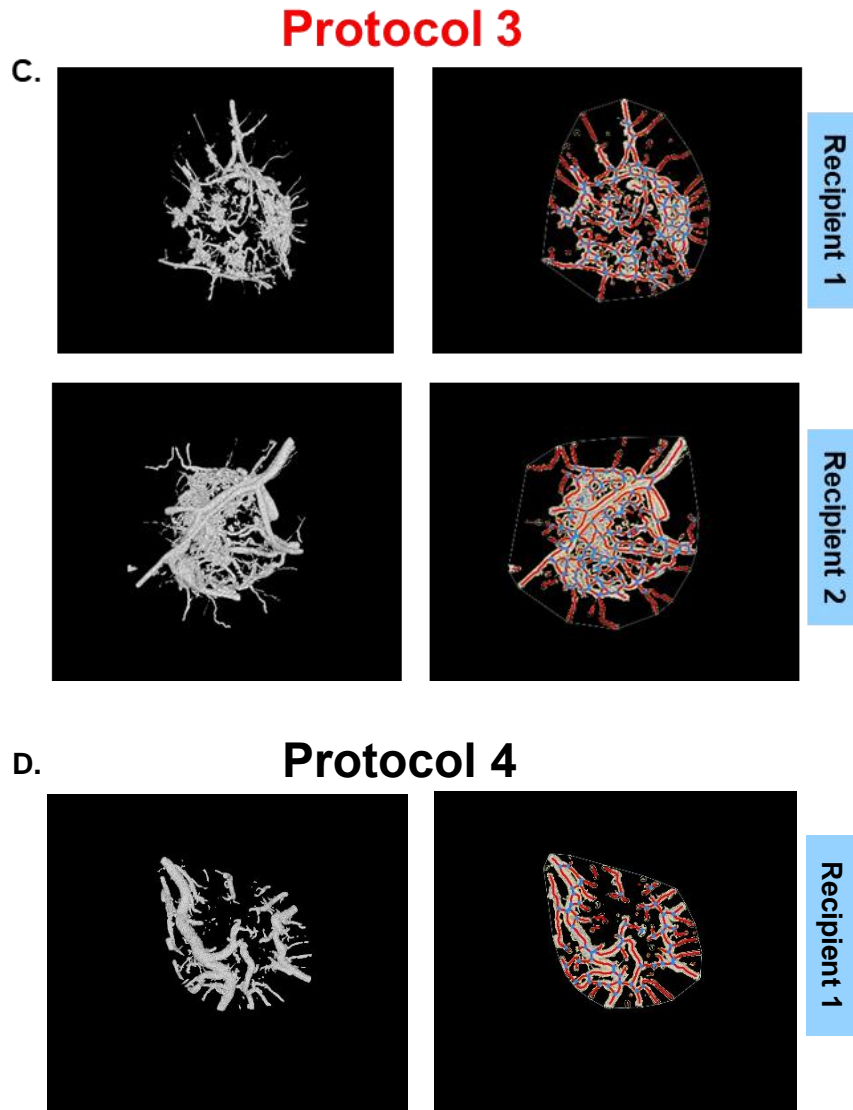


Figure 66. MicroCT imaging and Quantification with AngioTool®: Experiment 2. A. Before and after quantification images of biopsies engineered with Protocol 1. B. Before and after quantification images of biopsies engineered with Protocol 2. C. Before and after quantification images of biopsies engineered with Protocol 3. D. Before and after quantification images of biopsies engineered with Protocol 4.

The provided figure illustrates the outcomes of experiment number 2, wherein tracheal biopsies were engineered using the four previously mentioned protocols and subsequently implanted in-ovo to evaluate vascularization and engraftment. The MicroCT images presented here allow for a comparison aimed at identifying the protocol that yields the most favorable vascularity outcomes.

In **Image A**, we observe vascularization in two tracheal biopsies seeded with MSCs cultivated with FBS, which were implanted into two different recipient eggs. Similar to the previous experiment, the blood vessels in this image are notably large and thick. However, the first image suggests the possible initiation of micro blood vessel formation. Nonetheless, the overall vascularization appears to be concentrated around the scaffolds rather than penetrating them.

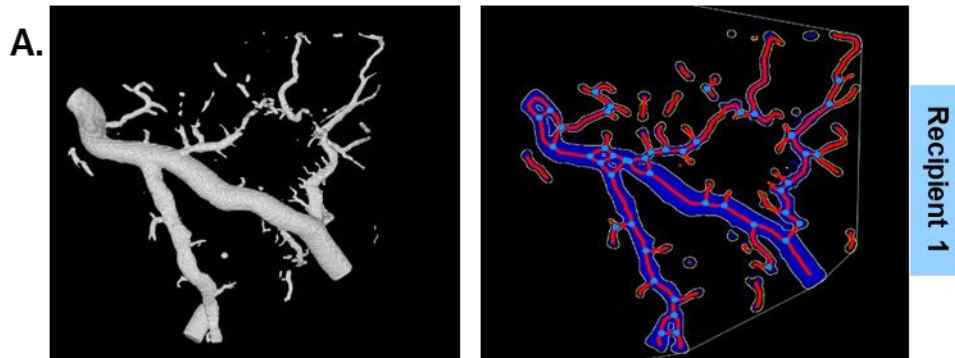
Image B displays a tracheal biopsy seeded with MSCs cultivated with hPL. In this image, the blood vessels are somewhat thinner compared to those in Image A. However, they exhibit a more extensive branching pattern, hinting at possible infiltration of tracheal blood vessels into the scaffold.

Image C presents two tracheal biopsies seeded with a coculture of unmodified MSCs and modified MSCs engineered to overexpress VEGF and bFGF. Once again, these images support the hypothesis that this condition can enhance vascularization and overall graft survival. Large and small blood vessels are observable, and the cylindrical shape of the scaffold biopsy is largely maintained. These findings suggest the occurrence of both vascular invasion and microinvasion into the scaffold.

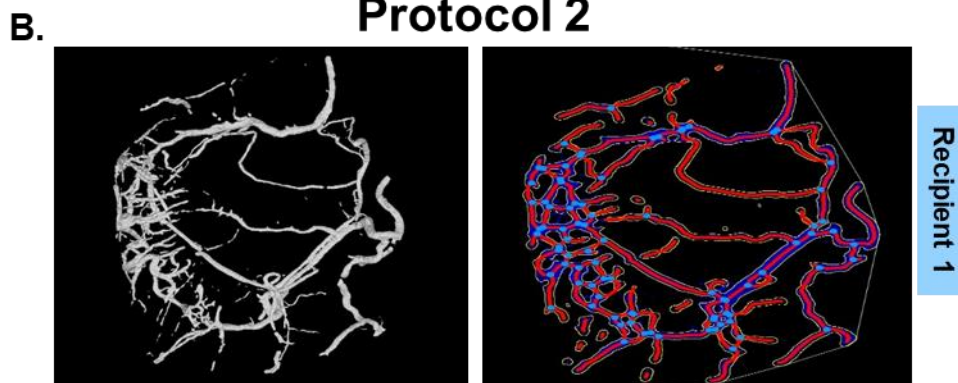
Finally, **Image D** shows a tracheal biopsy seeded with a coculture of unmodified MSCs and modified dermal fibroblasts (DFs) engineered to overexpress VEGF and bFGF. The majority of blood vessels in this image are large, but there is some evidence of microvasculature formation and the potential beginning of invasion into the scaffold.

3.7.2.4. Enumeration of MicroCT Images: Experiment 3

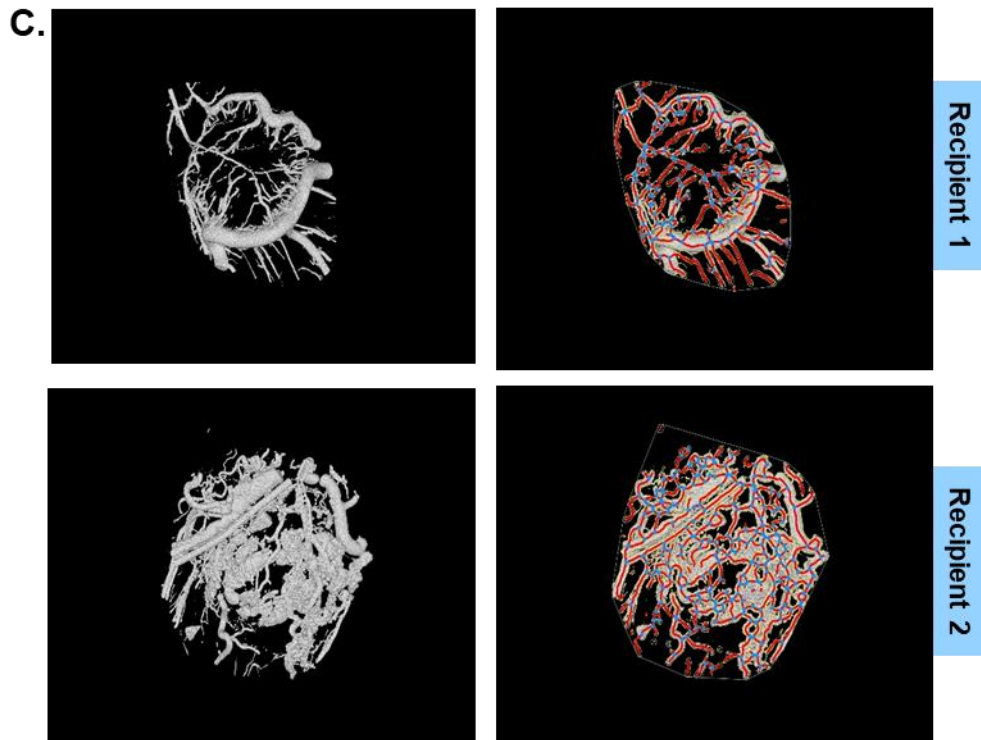
Protocol 1



Protocol 2



Protocol 3



Protocol 4

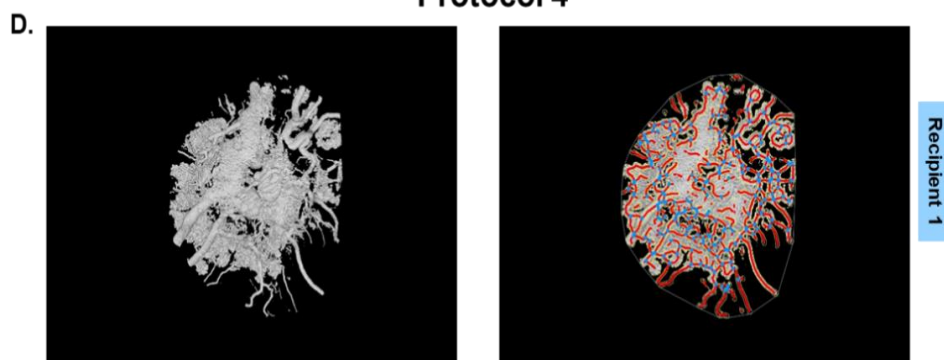


Figure 67. MicroCT imaging and Quantification with AngioTool®: Experiment 3. A. Before and after quantification images of biopsies engineered with Protocol 1. B. Before and after quantification images of biopsies engineered with Protocol 2. C. Before and after quantification images of biopsies engineered with Protocol 3. D. Before and after quantification images of biopsies engineered with Protocol 4.

The provided figure illustrates the outcomes of experiment number 3, wherein tracheal biopsies were engineered using the four different protocols previously mentioned and subsequently implanted in-ovo to assess vascularization and engraftment. The MicroCT images presented here facilitate a comparative analysis aimed at identifying the protocol that yields the most favourable vascularity outcomes.

Image A depicts the vascularization of tracheal biopsies seeded with MSCs cultivated with FBS. In this image, the blood vessels appear large and thick. However, no micro blood vessels are observable,

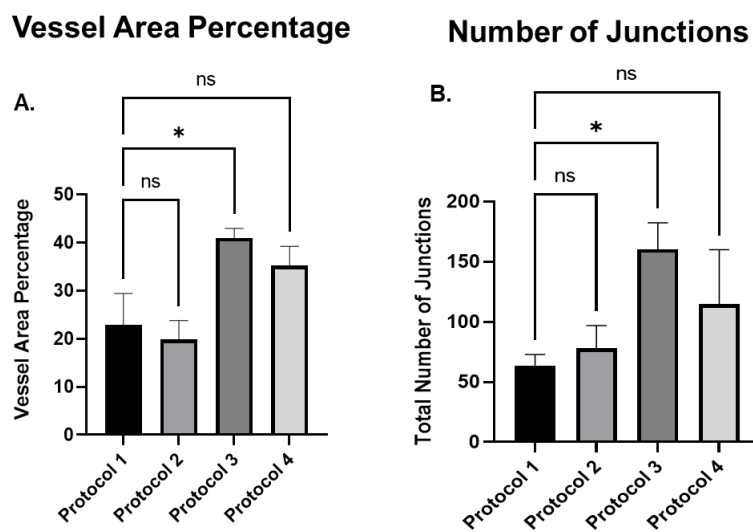
suggesting that the vascularization observed is likely concentrated around the tracheal biopsy rather than penetrating it.

Image B portrays a tracheal biopsy seeded with MSCs cultivated with hPL. The blood vessels in this image are somewhat thinner than those in Image A, but they exhibit a more extensive branching pattern. This indicates a potential infiltration of tracheal blood vessels into the scaffold, supporting the notion of improved vascularization.

In Image C, two tracheal biopsies seeded with a coculture of unmodified MSCs and modified MSCs engineered to overexpress VEGF and bFGF are displayed. Once again, these images provide support for the hypothesis that this condition can enhance vascularization and overall graft survival. Large and small blood vessels are observable, and the cylindrical shape of the scaffold biopsy is largely maintained, suggesting both vascular invasion and microinvasion into the scaffold.

Finally, **Image D** shows a tracheal biopsy seeded with a coculture of unmodified MSCs and modified dermal fibroblasts (DFs) engineered to overexpress VEGF and bFGF. While the majority of blood vessels in this image are large, there appear to be ruptures in the blood vessels, resulting in a cauliflower-like morphology surrounding the blood vessels.

3.7.2.5. MicroCT Analysis: Vascular Assessment



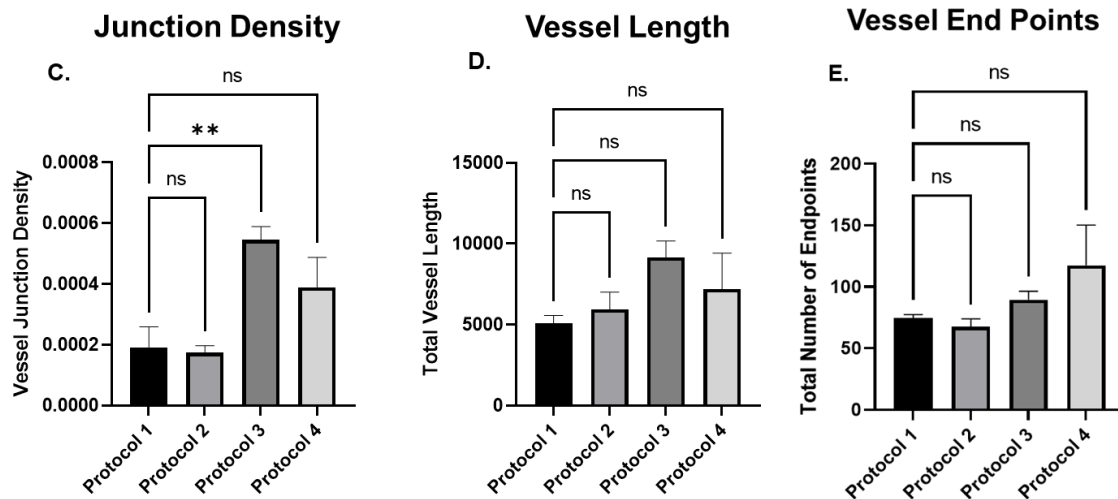


Figure 68. Statistical Analysis of MicroCT imaging and Quantification with AngioTool®. **A.** Comparison between the 4 protocols in terms of vessel Area Percentage. **B.** Comparison between the 4 protocols in terms of enumerated number of junctions. **C.** Comparison between the 4 protocols in terms of Junction Density. **D.** Comparison between the 4 protocols in terms of enumerated Total Vessel Length.

After the analysis of the MicroCT images obtained from four different protocols across three separate experiments, AngioTool was employed to enumeration the blood vessels so that a comparative analysis based on various parameters related to vascularization could be conducted. These parameters included the quantity of blood vessels within the surrounding area, the number of junctions, the junction density, and the number of vessel endpoints. The results of this analysis consistently favored protocol 3, which involves a combination of unmodified MSCs and genetically modified MSCs engineered to overexpress VEGF and bFGF. This finding further supports the hypothesis that the overexpression of growth factors associated with angiogenesis can significantly enhance blood vessel formation. Specifically, protocol 3 exhibited a larger vessel area, a higher number of blood vessel junctions, and a greater junction density.

In summary, the collective results of these experiments suggest the following key findings:

- 1. The substitution of FBS with hPL for the cultivation of MSCs has a positive impact on the MSCs' capacity to secrete angiogenic factors.***
- 2. The use of hPL instead of FBS in MSC cultivation contributes to overall improved MSC health following transfection or other manipulation.***
- 3. The incorporation of alginate into the tracheal engineering process does not appear to yield specific benefits in terms of vascularization.***
- 4. A coculture of unaltered MSCs and genetically manipulated MSCs demonstrates superior vascular outcomes compared to a coculture of unaltered MSCs and genetically manipulated dermal fibroblasts (DFs), with the latter still showing substantial vascularization capacity as the second most favourable option.***

These findings collectively provide valuable insights into optimizing protocols for enhanced vascularization in future experiments.

4. CHAPTER VI: DISSCUSSION

4.1. VASCULARISATION

The development of functional vascular networks within engineered tissue remains a critical challenge in the field of tissue engineering and regenerative medicine. It is a bottleneck that obstructs the progression towards more advanced constructs, limiting their viability and therapeutic potential especially in the context of tissue engineered trachea.

The successful growth of engineered tissues relies on the establishment of functional vascular networks to ensure proper nutrient and oxygen supply, and waste removal. The absence of efficient vascular beds in tissues thicker than 100-250 μ m can lead to central necrosis [180-182]. Therefore, the survival of engineered tissue constructs during the initial phase after their implantation depends on the rapid development of an adequate vascularization.

The formation of new blood vessels is a critical process essential for physiological development, organ growth, and tissue repair. This multifaceted phenomenon involves different modes of vascular assembly, including vasculogenesis and angiogenesis[183, 184]. Understanding these processes and their regulation is vital for comprehending their roles in various physiological and pathological conditions. Vasculogenesis and angiogenesis are fundamental processes underlying blood vessel formation. Vasculogenesis involves the de novo formation of vascular structures from aggregated endothelial precursors, while angiogenesis encompasses the development of new vessels from existing ones [182, 183]. Both processes are crucial in embryonic development and tissue repair[183, 184].

Angiogenesis encompasses different modes, including sprouting angiogenesis, intussusceptive angiogenesis, and coalescent angiogenesis[182, 184]. Sprouting angiogenesis involves the outgrowth of new vessels from existing ones, driven by specialized endothelial tip cells[182, 183]. In contrast, intussusceptive angiogenesis, or splitting angiogenesis, involves the division of existing vessels by forming transluminal endothelial pillars[182-184]. Coalescent angiogenesis is a newly proposed mechanism involving the transformation of an isotropic capillary network into hierarchical vessel trees through the fusion of capillaries and elimination of tissue islands[182, 183]. These processes allow the rapid expansion of vascular beds while maintaining perfusion and tissue function[182-184]. Understanding the modes of blood vessel formation is crucial for various physiological and pathological conditions. Developmental sprouting angiogenesis contributes to the formation of initial vessels, while reactive sprouting angiogenesis responds to events such as wound healing, inflammation, cancer, and muscle training [4, 5]. Intussusceptive angiogenesis plays a role in expanding vascular networks efficiently, and its regulation is likely influenced by local hemodynamics [4]. Coalescent angiogenesis, a novel mode, transforms capillary networks into functional vascular trees [4]. The choice of angiogenic mode depends on the specific requirements of the tissue and the nature of the stimulus [4, 5].

Early tissue engineering efforts relied on extrinsic vascularisation, where nearby host capillaries would grow into the implanted tissue construct. However, this process is slow (taking up to several weeks depending on the size of the construct) and often resulted in tissue ischemia, and cell death before complete vascularisation [185]. In 2010, a study by Tilkorn, et.al. established that the survival of implanted cells in vivo was directly related to the vascular volume of the recipient site capillary bed [185, 186]. In 2002, a new approach called *intrinsic vascularization* was developed by Tanaka, et.al., involving the isolation of a macrovascular pedicle in a plastic chamber[185, 187]. This pedicle

underwent significant angiogenic sprouting to create an arteriovenous capillary network within the chamber, supporting the survival of implanted tissue-specific cells [185]. More recently, a growing emphasis has been placed on pre-vascularisation techniques [185], first evidenced by the work of Erol OO and Sira M., who pioneered the “vascular loop model” [188]. This model successfully demonstrated the induction of neovascularisation within dermal tissue by establishing an arteriovenous fistula [188]. The concept of pre-vascularisation is centred on the creation of a pre-existing microvasculature within tissue constructs before implantation, with the goal of mitigating the period during which the constructs remain avascular and endure hypoxic conditions [180, 189]. Pre-vascularization strategies can be broadly categorized into two principal approaches: in-vitro techniques (such as cell seeding, coculturing, spheroid formation, and cell sheet technologies) and in-vivo/in-situ methods (involving flaps, arteriovenous (AV)-loop techniques, or leveraging the host body as a bioreactor to induce vascularization through angiogenic growth) [185, 189]. The most efficient strategy for vascularizing voluminous three-dimensional tissue constructs is considered to be the combination of pre-vascularization with angiogenic sprouting from a vascular pedicle [185]. However, the successful implementation of this combination remains relatively infrequent [185].

In the same context, adequate vascularisation is one of the major challenges facing the translation of tissue engineered trachea into the clinic. In the following pages, we dissect the outcomes of our study and their relevance to the broader context of the tracheal engineering, elucidating the potential of our findings to influence the vascularisation capabilities of implanted tracheal constructs.

4.2. CELLS AND SCAFFOLDS

Pre-vascularization stands as a pivotal imperative within the realm of tissue engineering, with the selection of suitable cell types holding paramount importance in realizing this objective. Among the prospective candidates contributing to the advancement of tissue-engineered tracheal constructs, particularly with regard to vascular development, are Mesenchymal Stromal Cells (MSCs) and Dermal Fibroblasts (DFs). These cell types are categorically designated as perivascular cells, underscoring their intrinsic involvement in the intricate processes associated with vascular development [180].

The nomenclature and characterization of the cell population now commonly referred to as Mesenchymal Stromal Cells (MSCs) have evolved since their initial designation as “mesenchymal stem cells” by Arnold Caplan in 1991 [190]. Subsequently, the International Society for Cellular Therapy and Gene Therapy (ISCT) provided a more encompassing definition, leading to the widely accepted term “mesenchymal stromal cells” (MSCs) [191]. These cells, also known as multipotential stromal cells or mesenchymal progenitor cells, represent a diverse and heterogeneous population [137, 192, 193]. They can be sourced from various tissues throughout the body, including adipose tissue stromal vascular fraction, skin/dermal tissue, muscle tissue, synovial membrane, skeletal muscle, dental pulp, as well as extra-embryonic tissues such as the placenta, umbilical Wharton's Jelly, umbilical cord stroma, umbilical cord blood, amniotic membrane, and amniotic fluid, all of which serve as rich reservoirs of MSCs [56, 137, 192, 193]. Additionally, bone marrow (BM) remains a quintessential source for the isolation of MSCs [137, 192, 193]. It is noteworthy that cell populations sharing remarkable similarities with MSCs, often referred to as tissue-specific MSCs, have been successfully extracted from various organs, including the kidney, liver, and others [56, 194, 195]. This widespread occurrence across connective tissues within diverse organs has sparked a compelling debate concerning the ubiquity of MSC-like populations in the body [56]. MSCs, while displaying the capacity to differentiate into osteocytes, chondrocytes, and adipocytes, have encountered controversy in their potential trans-differentiation into endothelial cells. Nevertheless, their role as perivascular precursor cells is well-

established, as they contribute to the stabilization of nascent blood vessels [196]. Despite their potential, the integration of MSCs into newly formed vasculature remains limited. Consequently, their other attributes, particularly their secretome, have garnered attention as potentially more advantageous for therapeutic angiogenesis [196]. The MSC secretome, encompassing factors released by these cells, has emerged as a potent tool for enhancing vascularization [197], exhibiting beneficial angiogenic effects in various pathologies related to tissue injury [197].

Fibroblasts, recognized as the primary contributors to the synthesis of extracellular matrix collagen, assume a crucial role in processes such as angiogenesis and wound healing [180]. In tissue engineering, fibroblasts have found utility in co-cultures alongside endothelial cell lines to create pre-vascularized substitutes for a spectrum of tissues, including skin [180]. These fibroblasts can be isolated from diverse anatomical sites, encompassing skin, mucosal membranes, and soft tissues. It is noteworthy that the method and source of isolation exert notable influences on the angiogenic potential of fibroblasts [180]. In a pivotal study conducted in 2015 by Costa-Almeida et al., it was observed that the formation of capillary-like networks occurred exclusively in cultures involving endothelial lineage cells co-cultured with human dermal fibroblasts, as opposed to cultures involving neonatal human foreskin fibroblasts (hFF-1) [180, 198]. This observation underscores the significance of fibroblast heterogeneity influenced by their tissue of origin. Advancements in single-cell RNA sequencing techniques in recent years have unveiled the marked diversity among fibroblasts across various tissues [199]. These fibroblasts assume a central role in the maintenance of tissue homeostasis and are implicated in an array of pathological conditions [199].

In research involving self-isolated primary cells for developmental studies, it is imperative to ensure the correct cell type is used, necessitating thorough characterization of the cells [1]. Therefore, prior to the utilisation of MSCs in subsequent experiments, in accordance to the International Society for Cellular Therapy and Gene Therapy (ISCT) minimal criteria for the identification of mesenchymal stem cells [82], the plastic adhering MSCs used in this study were characterised phenotypically for positivity of markers CD90, CD73, and CD105, and negativity of CD34, CD11, CD19, CD45, and HLA-DR (represented in the negative panel staining). Furthermore, in addition to the phenotypic assessment, the MSCs underwent induction towards differentiation along three distinct lineages, leading to their transformation into chondrocytes, osteocytes, and adipocytes. These rigorous characterization steps serve as a foundational assurance of the identity and functionality of the MSCs employed in our subsequent experiments.

The human dermal fibroblasts employed in this study were procured from a commercial source and had previously undergone characterization. Nonetheless, in the interest of ensuring congruence in experimental procedures and evaluating whether they exhibit comparable functionality to the mesenchymal stem cells (MSCs) throughout the tracheal tissue engineering process, these fibroblasts were subjected to an identical battery of assays, commencing with their characterization process. This approach was undertaken to streamline the experimental workflow and to ascertain any potential distinctions or parallels in their behaviour with respect to the MSCs during the course of this study.

Distinguishing between mesenchymal stem cells (MSCs) and fibroblasts presents a notable challenge due to their shared expression of certain cell surface markers. While both cell types express markers such as CD11, CD44, CD73, CD90, CD105, and CD166, distinctions arise in the level of expression or the presence of markers like CD106, integrin alpha 1, IGF-2, MMP1, MMP-3, and CD146 [180, 200]. Notably, fibroblasts also possess the capacity to undergo differentiation into osteocytes, adipocytes, and chondrocytes when induced [154, 201]. In light of these challenges and to facilitate accurate discrimination, our study encompassed additional marker staining beyond the standard markers

stipulated by the International Society for Cellular Therapy and Gene Therapy (ISCT). Specifically, both MSCs and dermal fibroblasts (DFs) were subjected to staining for the expression of CD106, CD146, and CD271. CD271, in particular, is of significance as it is expressed in human bone marrow-derived MSCs and is associated with cell proliferation and differentiation, while typically remaining unexpressed in dermal fibroblasts [202, 203].

Our results confirmed the ability of human MSCs and DFs donor cells used in this study, to differentiate into three lineages post-induction (result section 3.1.2 -B & 3.1.3-B). Furthermore, our investigations established the capacity of these cells to both express and abstain from the recommended surface markers delineated by the International Society for Cellular Therapy and Gene Therapy (ISCT), as expounded in the result section (result section 3.1.2-A). Specifically concerning dermal fibroblasts, our findings were consistent with established expectations and previous literature [180, 200]. Notably, DFs exhibited a negative staining profile for CD271 and CD106, aligning with established characteristics. Moreover, the expression levels of CD146 in DFs were either partial or notably diminished, in accordance with anticipated outcomes (result section 3.1.3-A).

Mesenchymal stem cells (MSCs) play a pivotal role in tissue regeneration and repair among adults, primarily by means of paracrine regulatory mechanisms. However, it is imperative to acknowledge that the aging process exerts significant influence on tissue homeostasis, including the intricate process of neovascularization [139]. In the context of angiogenesis, multiple studies have underscored a noteworthy decline in the angiogenic potential of senescent adipose stromal/stem cells (ASCs) or MSCs derived from adipose tissue [138, 139, 204]. Clinical challenges that arise in conjunction with MSC-based therapy encompass suboptimal cell engraftment and variability in stem cell potency [137, 205, 206]. This variability in cell potency can predominantly be attributed to factors such as donor or source disparities, variations in culture conditions, and the occurrence of cellular senescence [137, 206]. While the prospects of MSCs for therapeutic angiogenesis are buoyed by their inherent capacities, particularly paracrine signalling, it is crucial to emphasize that the effectiveness of harnessing their therapeutic potential is contingent upon the initial condition of these cells. Suboptimal starting conditions can significantly compromise their utility.

A principal technical impediment in MSC-based cell therapy lies in the challenges associated with isolating MSCs from tissues where their abundance is limited and cultivating these cells in sufficient quantity and quality [207]. Bone marrow-derived human mesenchymal stromal/stem cells (BM-hMSCs) in particular, represent a minuscule fraction, accounting for as little as 0.01-0.001% of a bone marrow mononucleated cell population [208]. To obtain a sufficient quantity of BM-hMSCs for therapeutic purposes, extensive in vitro expansion is an imperative requirement [209, 210]. Regrettably, prolonged in vitro culture and expansion of these cells are associated with an accelerated aging phenomenon and a gradual diminishment of their differentiation potential. Therefore, the overarching objective is to efficiently generate a substantial population of healthy cells within the shortest possible timeframe [211].

In clinical applications necessitating the expansion of mesenchymal stem cells (MSCs), the ability to achieve substantial ex vivo growth is paramount [207] and successful isolation and rapid expansion of MSCs necessitate a substantial volume of complete media supplemented with bioactive additives [207]. Empirical evidence substantiates a positive dose-response relationship between platelet concentrations and MSC proliferation, indicating a direct correlation between PL supplementation and the augmentation of MSC activities [207].

Platelet lysate (PL) is a bioactive medium enriched with a profusion of growth factors, endowing it with considerable potential to enhance cellular growth and function [207]. In physiological contexts, platelets serve a multifaceted role encompassing primary haemostasis, wound healing, and tissue

regeneration. This is achieved through the release of an array of growth factors when platelets are activated[207]. Artificial generation of platelet lysates via freeze/thaw lysis represents an avenue to harness these growth factors for therapeutic purposes[207]. Key constituents of PL include basic fibroblast growth factor (bFGF), platelet-derived growth factor (PDGF), insulin-like growth factor (IGF), basic epidermal growth factor (EGF), and transforming growth factor- β (TGF- β), soluble CD40L (sCD40L), vascular cell adhesion molecule-1 (VCAM-1), intercellular adhesion molecule-1 (ICAM-1), chemokine (C-C) ligand 5 (CCL5; RANTES) transforming growth factor- β 1 (TGF- β 1), chemokine (C-X-C) ligand 1/2/3 (GRO), and vascular endothelial growth factor (VEGF) [113, 207, 212]. The presence of these growth factors within PL is known to confer beneficial effects on cell proliferation, chemotaxis, and extracellular matrix production [207, 212] without adversely affecting the MSC immunophenotype, immunomodulatory potential, differentiation potential, and relative telomere length [209].

This phenomenon was directly observed through a comparative analysis with foetal bovine serum (FBS) during the initial isolation of mesenchymal stem cells (MSCs) from bone marrow (results: Figures 3.1) and amid the growth kinetic assessments (results, Figures 3.1). Cells isolated from the same donor were divided into two equal portions at Passage 0, which corresponds to the mononuclear harvest stage. One portion was cultured in the presence of human platelet lysate (hPL), while the other was cultured with Foetal Bovine Serum (FBS). The results revealed an increase in cell yield at Passage 1 (MSC harvest passage), when hPL was used as a supplement in comparison to FBS (Results: Figure 3.1.C). Furthermore, cells cultivated with hPL exhibited a morphology characterized by a fibroblast-spindle-like appearance (Results: Figure 3.1), while those cultured with FBS displayed a mixed morphology, including a fibroblast-like appearance along with a more flattened and ovoid-like formation typical of FBS supplementation (Results: Figure 3.1). These differences in cell morphology align with previously reported observations. Notably, MSCs cultured in FBS have been reported to exhibit lower proliferative capacity [142] and a propensity to assume a senescent phenotype more rapidly, characterized by enlarged, flattened cells [143]. In contrast, hPL appears to favour the development of MSC populations with a healthier and spindle-shaped morphology, in line with the aforementioned observations.

The underlying mechanisms governing these morphological disparities can be attributed to the upregulation of gene expression associated with cell cycle inhibition in the presence of FBS [142], as well as epigenetic modifications that accelerate senescence, including DNA methylation [213, 214]. Remarkably, despite these morphological differences at the cellular level, molecular-level distinctions were not as pronounced as initially expected, and they demonstrated reversibility. This implies that transitioning the culture medium to one supplemented with hPL can result in the reacquisition of the characteristic spindle-shaped morphology, as documented in the scientific literature[214].

In the context of our investigation into the growth kinetics of Mesenchymal Stem Cells (MSCs), as previously mentioned, the initial cell isolates were bifurcated into two groups, where one was cultivated with Foetal Bovine Serum (FBS) and the other with Human Platelet Lysate (hPL). These cultures were subsequently expanded to reach passage 3, as expounded upon in the results section 3.1.1.2. Subsequent assessments undertaken encompassed the quantification of cell yield at the conclusion of passage 3, analysis of population doubling levels, and an evaluation of cumulative doubling levels. Our findings revealed a pronounced exponential proliferation of MSCs when cultivated in the presence of hPL, as compared to those subjected to FBS supplementation. This observed outcome is consistent with the existing body of published literature [178, 179, 215].

The same growth kinetics assessment parameters were measured during human dermal fibroblast expansion from passage 0 to passage 3, comparing the effects of FBS and hPL as culture supplements (results section 3.1.3). The findings revealed no significant disparities in growth kinetics between hDFs cultivated with FBS and those cultured with hPL.

While there exists a dearth of information regarding the growth rates of dermal fibroblasts treated with hPL as opposed to FBS, several studies have explored the effects of hPL on the proliferation of MSCs as previously mentioned. One such investigation demonstrated a marked increase in ASC proliferation when treated with 5% PLTMax, a commercial hPL product, in comparison to cells exposed to 10% FBS[216]. This observation suggests that hPL may exert a growth-promoting influence on different cell types, including dermal fibroblasts.

A separate study assessed the feasibility of using in-house produced hPL solutions as supplements for in vitro fibroblast culture and concluded that hPL constitutes a viable candidate to replace FBS as a growth supplement in clinical settings[217]. It is noteworthy, however, that these studies did not directly compare the growth rate of fibroblasts under hPL versus FBS supplementation. Furthermore, the utilization of hPL under Good Manufacturing Practice (GMP) conditions for dermal fibroblasts has been validated and reported to yield congruent results. Research involving in-house produced GMP-HPL demonstrated its capacity to support fibroblast growth at levels akin to FBS and commercial hPL products. Cells cultivated in hPL maintained characteristic fibroblast features, extracellular matrix generation capabilities, and exhibited genomic stability. Notably, gene expression profiling revealed certain alterations linked to cell metabolism, adhesion, and cellular senescence. The GMP-compliant manufacturing process for hPL was validated, and the solution exhibited stability at -80°C and -20°C for a duration of 2 years. Dermal fibroblasts expanded in vitro with hPL preserved a normal karyotype and the expression of fibroblast markers, with only minor alterations in their global gene expression profile. The in-house produced GMP-HPL emerged as an efficient, safe, and cost-effective cell culture supplement, with potential implications for enhancing the operational efficiency of blood transfusion centres by reusing transfusional plasma and platelets nearing their expiration date [217].

Overall, while there is limited information available on the growth rate of dermal fibroblasts treated with hPL compared to FBS, the available studies suggest that hPL may have a growth-promoting effect on other cell types, including ASCs, and may be a good candidate to replace FBS as a growth supplement for fibroblast culture in a clinical context.

Decellularized extracellular matrices (dECM) have garnered significant attention in biomaterial research due to their complex composition, close resemblance to natural tissues, commendable biocompatibility, and low immunogenicity [43]. They have enabled advancements in regenerative medicine, notably in tracheal transplantation, where decellularized allogeneic human cadaveric tracheal segments have been clinically used for transplantation without the requirement for immunosuppression [59]. The decellularization process involves the transformation of grafts into biological scaffolds composed of organ-specific ECM, known to guide cellular migration and differentiation [59]. These matrices result from the removal of cells, which can be accomplished through enzymatic, chemical, or physical methods while preserving the native three-dimensional extracellular matrix (ECM) structure [43, 54]. They retain crucial ECM components, such as collagen, elastin, proteoglycan, and hyaluronic acid, in addition to bioactive molecules including growth factors. These matrices have found applications in various tissue types, encompassing decellularized pericardium[218], blood vessels [219, 220], corneas[221], bones [222], lungs [223, 224], nerves [225], and trachea][43, 226-228]. Decellularized matrices offer several advantages, including facilitating perfusion, vascularization, and cellular differentiation while preventing immunological reactions and

preserving the original tissue's mechanical properties[54, 228]. Most importantly, they provide a pre-established vascular network suitable for in vitro pre-vascularization.

Following the acquisition of decellularized porcine tracheas from Griffin's Clinic (NHSBT, London, UK), decellularized porcine tracheal scaffolds underwent thorough washing and treatment with PBS and a 1% antibiotic/antimycotic (ab/am) solution over a four-hour period with continuous media changes. Despite these efforts, subsequent testing revealed the presence of resilient gram-negative bacteria, including *Pseudomonas aeruginosa*, *Stenotrophomonas maltophilia*, *Escherichia coli*, and *Citrobacter braakii*. To address this concern, four distinct sterilization protocols were implemented, and their efficacy was assessed through electron microscopy (results section 3.1.5.2-A) and cultivation, both with and without cells in the presence of complete media (results section 3.1.5.2-B). Surprisingly, electron microscopy examinations did not reveal any evidence of bacterial presence on the surfaces of the scaffolds (results section 3.1.5.2-A). However, upon subsequent cultivation, two of the four protocols (protocol 1 involving treatment with 10% ab/am, and protocol 4 involving treatment with 1% Triton-X) were found to still harbour bacteria (results section 3.1.5.2-B). This suggests that the bacteria had penetrated the pores of the decellularized matrices and exhibited such resilience that neither the 10% ab/am treatment nor the 1% Triton-X treatment could eradicate them.

Decellularization, while effective in eliminating certain contaminants, does not provide terminal sterilization, leaving the scaffold susceptible to viruses and bacterial spores. Thus, it is imperative to perform a final sterilization protocol before in vivo implantation [148]. Although the use of decellularized matrices in tissue engineering is highly promising, the challenge of sterilizing decellularized grafts remains a subject of debate. Traditional sterilization methods like autoclaving, ethylene oxide treatment, and gamma irradiation may adversely affect the graft's microstructure, chemical composition, and biomechanical properties, leading to complications such as macromolecular chain breakage and collagen cross-linking [229].

Irradiation, which is a physical sterilization method involves gamma rays from a ^{60}Co device and electron beams from electron accelerators. While it can effectively destroy microbial nucleic acids, proteins, and enzymes due to its penetration capability, it may also lead to changes in the physical, chemical, and biological properties of the decellularized extracellular matrix (dECM) [229-231]. Ethylene oxide (EO) sterilization, is a well-established method that inactivates microbial proteins and nucleic acids. It can be performed at room temperature without material damage but leaves toxic residues post-sterilization [229, 232, 233]. Antibiotic disinfection, can inhibit bacterial growth by disrupting cell walls and essential cellular processes. However, their effectiveness is limited to specific microbial targets and does not extend to viruses and spores [229, 234, 235]. Peracetic acid (PAA) sterilization, PAA is a chemical detergent, can achieve bactericidal effects under certain conditions. It does not produce toxic decomposition products, but its strong oxidation can alter scaffold properties and its effects, both positive and negative are dependent on its concentration and the type of tissue being sterilized[229]. A recent study investigated the efficiency of a two-step sterilization method involving an antibiotics/antimycotic (AA) cocktail and peracetic acid (PAA) on porcine and bovine decellularized pericardium. This approach not only achieved sterility but also preserved the structural integrity and biocompatibility of the decellularized tissues, albeit with slight effects on surface properties and cellular adhesion in the case of porcine pericardium [148].

In light of these considerations, addressing limitations such as the risk of microbial contamination and adapting protocols for different tissue types is crucial. These challenges may require

supplementation with antibiotics, UV sterilization, and tissue-specific adjustments to ensure the production of ideal scaffolds for tissue engineering purposes [236]. Thus, the choice of sterilization method for dECM scaffolds in tissue engineering is a critical consideration, given its potential impact on both microorganisms and scaffold properties. Continued research and innovative approaches are essential to develop sterilization methods that meet the stringent requirements of tissue engineering and regenerative medicine.

4.3. 2D COCULTURE OF MSCS AND DERMAL FIBROBLASTS

Unmanipulated Mesenchymal Stem Cells (MSCs) and Dermal Fibroblasts (DFs) were co-cultured in various ratios, supplemented with both foetal bovine serum (FBS) and human platelet lysate (hPL). The primary objective was to assess the efficacy of this co-cultivation in terms of its impact on the expression of key growth factors, namely vascular endothelial growth factor (VEGF) and basic fibroblast growth factor (bFGF), with a focus on their relevance to angiogenesis. Notably, the highest level of VEGF expression, as observed across five independent experiments, was found in co-cultures with a dermal fibroblast to mesenchymal stem/stromal cell ratio of 25:75, indicating a prevalence of MSCs over DFs respectively (results section 3.2-A). The second-highest VEGF expression levels were observed in a 50:50 cell ratio (results section 3.2-A). Remarkably, these findings were exclusive to hPL supplementation, as there were no discernible differences in VEGF expression between varying cell ratios when cultivated in the presence of FBS supplementation.

Conversely, bFGF expression exhibited different trends, with the highest levels observed in co-cultures containing more DFs than MSCs (75:25, wherein 75% were DFs and 25% were MSCs) (results section 3.2-B), and the second-highest levels were noted in a 50:50 cell ratio (results section 3.2-B). These results were also specific to hPL supplementation, as co-cultures cultivated with FBS supplementation displayed minimal bFGF expression, irrespective of the cell ratios.

It is crucial to consider that the ratio or concentration of different cell types seeded onto a scaffold can significantly influence the developmental outcomes of the scaffold. Variations in cell ratios can impact cell characteristics, behaviour, and viability [90, 237], consequently affecting the desired outcomes.

Both MSCs and human dermal fibroblasts possess the capacity to secrete an array of growth factors and cytokines, particularly in the context of angiogenesis and wound healing [238-241]. Notably, MSCs tend to express higher levels of VEGF [238, 242]. This observation aligns with a 2008 study by Chen L, et al., which compared the paracrine factors released by bone marrow-derived MSCs and human dermal fibroblasts in the context of angiogenesis and wound healing. The study highlighted significant disparities between the two cell types, with MSCs exhibiting notably higher VEGF expression than DFs [238]. In contrast, DFs tend to express higher levels of bFGF [238, 241], corroborating our findings (results section 3.2). Several other studies have also supported the notion that MSCs secrete substantial quantities of VEGF, a potent angiogenesis factor that promotes the formation of new blood vessels by mediating the differentiation of endothelial progenitor cells into endothelial cells [239, 240, 242-245]. While, bFGF expressed by fibroblasts plays a pivotal role in cell migration, wound healing, and tissue repair [246, 247].

The differential effects observed with hPL and FBS supplementation can be attributed to the composition of these supplements. Human platelet lysate (hPL) comprises a diverse array of growth factors, including VEGF and bFGF, which can stimulate both MSCs and hDFs. In contrast, FBS lacks such factors, which may explain the variations in expression observed depending on the cell ratios, primarily in the presence of hPL cultivation but not with FBS.

4.4. GENETIC MODIFICATION

Nucleofection, a transfection technique based on electroporation, allows for the efficient delivery of nucleic acids, such as DNA and RNA, into eukaryotic cells through the application of specific voltage parameters and associated reagents [248, 249]. Developed by Amaxa (now Lonza), this method, also referred to as nucleofector technology, employs a device known as the Nucleofector. By combining electrical parameters generated by this device with cell-specific reagents, nucleofection enables the direct transfer of nucleic acid substrates (including DNA, RNA, proteins, and small molecules) into the cell nucleus [249, 250]. by creating transient pores in the cell membrane through the application of pulsed electrical fields [250]. This technique has proven highly effective in transfecting cells that have historically been challenging to modify via traditional electroporation or other non-viral methods [3][4]. Nucleofection has been widely employed in various applications, including CRISPR/Cas9-mediated gene editing in specific immune cells and the transfection of distinct cell lines [248, 249]. Notably, nucleofection exhibits exceptional efficiency when applied to primary human keratinocytes[131]. Its advantages lie in its ability to introduce nucleic acids directly into the nucleus, minimizing cytotoxicity and preserving cellular functionality [131].

Efforts to enhance non-viral gene delivery to challenging cell types like human mesenchymal stem cells (hMSCs) have been hampered by limitations in gene delivery techniques [251]. Viral methods, while highly efficient, present safety and cost concerns [251]. Non-viral methods, though safer and cost-effective, generally exhibit lower transfection efficiencies[251]. hMSCs, in particular, pose challenges due to their therapeutic potential and safety requirements[251]. The majority of non-viral gene delivery techniques applied to human mesenchymal stem cells (hMSCs) typically yield transfection efficiencies ranging from 1% to 10%, as documented in various studies, [251-255]. However, there have been reports of transfection efficiencies reaching as high as 20%, but these higher rates were observed primarily in cells at early passages, typically between one and two[252-255]. It is important to note that achieving efficient gene delivery to hMSCs remains a challenging endeavor, and researchers continue to explore strategies to improve transfection efficiency while maintaining cell viability and safety. Strategies to improve non-viral gene delivery to hMSCs have included chemical modifications of existing vectors and de novo synthesis, yet these approaches have yielded only modest improvements in transfection efficiency [251-253]. An alternative approach involves priming cells with pharmacological agents to temporarily overcome barriers to gene delivery and enhance transfection [255].

Transient nucleofection was performed on human bone marrow-derived mesenchymal stem cells (BM-MSCs) and human dermal fibroblasts (DFs) using pmax-GFP plasmids, and a good manufacturing practice (GMP)nucleofection protocol. Evaluations were conducted both before and after transfection under two different culture conditions: one with supplementation of human platelet lysate (hPL) and

the other with supplementation of foetal bovine serum (FBS). Various parameters were assessed, including cell viability and recovery, phenotypic characterization, GFP positivity, transfection yield, metabolic capacity, and cytotoxicity (as detailed in the results section 3.3.1.1). Statistical analysis of post-transfection results, including cellular viability of fibroblasts and MSCs, cellular recovery, the percentage of GFP-positive cells, and transfection yield, indicated no significant differences between the hPL and FBS cultivation conditions for MSCs. In both conditions, MSC identification markers were preserved, and the cells exhibited the ability to differentiate into osteocytes and adipocytes, demonstrating their phenotypic stability and multilineage potential (as detailed in the results section 3.3.1.3). However, it is noteworthy that cells cultured in the presence of hPL displayed a higher metabolic rate and lower cytotoxicity levels post-transfection compared to cells cultured with FBS supplementation. These findings suggest an overall better post-transfection cellular health (especially for MSCs) under the hPL culture condition (as detailed in the results section 3.3.1.2). These results partially align with a study by Agostini et al. conducted in 2021, where adipose tissue mesenchymal stem cells (ASCs) were nucleofected with a pmax-GFP plasmid in the presence of FBS and supernatant rich in growth factors (SRGF) derived from platelets, which is similar to hPL[128]. In the study by Agostini et al., cells cultivated in the presence of SRGF exhibited increased nucleofection efficiency, enhanced post-transfection viability, and an increase in vesicle endocytosis. However, they also showed a decrease in phagocytosis properties. These observations were hypothesized to be due to potential changes in membrane structure and alterations in intracellular actin content induced by SRGF supplementation[128].

4.5. SCREENING STUDIES

To initially investigate the impact of various hypotheses on angiogenesis and blood vessel formation, we employed the chorioallantoic membrane (CAM) assay in conjunction with the Integra® Matrix as a surrogate scaffold in place of the trachea.

The Integra® Matrix is a versatile synthetic acellular dermal regeneration template initially developed for wound healing and the reconstruction of full-thickness skin defects [256]. Comprising a bilayer structure, it consists of a porous matrix crafted from cross-linked bovine tendon collagen and glycosaminoglycan, coupled with an epidermal-like layer composed of synthetic polysiloxane polymer. Over a span of 2 to 3 weeks, the dermal layer undergoes vascularization, ultimately serving as a platform for an ultrathin autograft following the removal of the artificial epidermal layer [257]. Originally designed with soft tissue reconstruction in mind, the Integra® Matrix, particularly the Integra dermal regeneration template, has found extensive utility in addressing thermal injuries and various reconstructive surgical scenarios, even those involving exposed joints, tendons, and bones [257]. Its composition features a bi-laminate sheet incorporating cross-linked bovine tendon collagen and shark glycosaminoglycans, complemented by a silicone sheet cover, which not only closes the wound but also prevents fluid leakage [257, 258]. The mechanism of action in dermal regeneration involves several sequential phases: imbibition, fibroblast migration, neovascularization, and remodelling and maturation. Imbibition occurs rapidly, facilitated by the presence of fibrin in the wound exudate, while fibroblasts commence migration into the matrix around the seventh day. By the third week, myofibroblasts arrive and contribute to the deposition of native collagen within the matrix. As time progresses, native collagen gradually replaces the matrix collagen, leading to a thickened yet increasingly pliable neodermis. Typically, full vascularization of the neodermis is achieved by the fourth

week, marked by a shift in colour from pink to pale yellow to peach. It is essential to note that the neodermis lacks adnexa, nerve endings, or elastic fibres. Following complete vascularization, the neodermis is prepared to receive a graft, and the dermal-epidermal junction starts developing rete ridges [257]. Hence, the Integra® Matrix is a synthetic dermal regeneration template known for its versatility and effectiveness in wound healing and reconstructive surgery [256]. Composed of two layers (can be purchased as a single layer as well), it fosters vascularization and tissue growth, making it a valuable tool in various medical applications

The Chorioallantoic Membrane Assay (CAM) is a well-established and versatile *in vivo* model used for various scientific applications. It has been validated and employed in a wide range of studies, including vascular research, toxicity assessment, biocompatibility evaluation, cancer investigations, immunological studies, bone studies, gene therapy approaches, and more recently, engineering studies [160, 162, 259-264]. The CAM offers several advantages, including an immune-tolerant environment up to embryonic day 15, which allows for xenogeneic transplant studies without the need for immune suppression, making it a valuable tool for establishing engineering protocols. Additionally, its relatively quick, cost-effective, and equipment-independent nature makes it an attractive choice for various experiments [160, 162, 259-264]. The CAM assay involves using fertilized chicken eggs, which serve as an *in vivo* angiogenesis-supporting environment to assess the formation of new blood vessels. It closely mimics certain aspects of mammalian vascular development and provides a platform for studying developmental angiogenesis. The assay is typically conducted between embryonic days 3 to 15, with the immune system beginning to function around day 15 [160, 162, 259-264]. The CAM provides a transparent, two-dimensional layout for studying angiogenesis and vascular adaptation, making it particularly suitable for optical observations over extended periods. It develops through the fusion of the allantois and chorion from day 3 to day 13 of embryonic development and shares functional similarities with the human lung, allowing the study of the pulmonary system [182]. In addition, intravital microscopy of the CAM over a 33-hour period revealed a previously unrecognized mode of angiogenesis termed "coalescent angiogenesis." This mode is distinct from intussusception and plays a role in the formation of mature vessel trees [182]. The CAM assay is a valuable tool in scientific research, offering a wide range of applications and advantages, such as its immune-tolerant environment, cost-effectiveness, and simplicity [182, 265].

We hypothesized that a potential synergistic effect can be achieved through the co-culturing of Mesenchymal Stem Cells (MSCs) and Dermal Fibroblasts (DFs), with the aim of enhancing factor secretion from both cell types and subsequently promoting vascularization. However, the results obtained from Human basic Fibroblast Growth Factor (bFGF) enzyme-linked immunosorbent assay (ELISA) assays, conducted on co-cultures of MSCs and DFs at a 50:50 ratio in the presence of Foetal Bovine Serum (FBS), did not reveal any significant differences when compared to MSCs cultured alone (Results section 3.4.5.A.). These results corroborate with the coculture studies performed earlier. In fact, the co-cultures of MSCs and DFs exhibited a decrease in the expression of Vascular Endothelial Growth Factor (VEGF) compared to MSCs cultivated alone in the presence of FBS supplementation. This decline in VEGF expression can be attributed to a dilution effect caused by the co-cultivation of MSCs with DFs (Results section 3.4.5.-A). Conversely, in the presence of Human Platelet Lysate (hPL), the expression levels of human VEGF were not as low as observed in the presence of FBS. This difference can be attributed to the stimulation of a fraction of MSCs within the coculture to express higher levels of VEGF in response to hPL [238, 242]. Additionally, no significant angiogenic response, in terms of blood vessel growth or branching, was observed when comparing MSCs cultivated alone with those co-cultivated with DFs in the presence of either FBS or hPL. Consequently, there was no discernible difference in the overall expression of VEGF or bFGF between MSCs cultivated alone and those co-cultivated with DFs in this context.

Our hypothesis also posited that encapsulating cells within alginate and subsequently seeding this hydrogel onto our scaffold would enhance cell retention on the substrate, mitigating cell dispersion. Consequently, this approach would potentially lead to an increased secretion of growth factors and paracrine factors by the augmented cell population, ultimately yielding improved outcomes in terms of angiogenesis-related processes.

Alginate, a biocompatible and biodegradable polymer derived from brown seaweed, possesses unique properties that make it an ideal material for cell encapsulation purposes. It is a natural polysaccharide that is characterised by its biocompatibility and biodegradability, rendering it suitable for a wide range of applications in regenerative medicine and drug delivery [266-268]. Alginate encapsulation serves various purposes, including shielding cells from the immune system, providing a three-dimensional cell culture environment, and targeted cell delivery [266, 267, 269, 270]. Its characteristics, such as its molecular weight, degree of polymerization, and guluronic acid content, can be tailored to suit different cell types and applications [266, 267]. Alginate encapsulation of cells protect both allo- and xenogeneic cells while maintaining isolation from the immune system [267]. Therefore, it is very applicable in regenerative medicine, tissue engineering, and cell therapies. In addition, the encapsulation of cells with alginate serves as a reliable material for controlled drug delivery systems. It can encapsulate drugs or growth factors within its matrix and releases them in a controlled and sustained manner [271]. Alginate has been particularly effective in delivering growth factors, including Vascular Endothelial Growth Factor (VEGF), Bone Morphogenetic Protein-2 (BMP-2), and Basic Fibroblast Growth Factor (bFGF) [272-274], and has demonstrated the ability to enhance the biological activity of VEGF, by efficiently incorporating and releasing VEGF at a controlled rate, making it more potent in stimulating endothelial cells than direct VEGF addition [272]. It has also been employed for BMP-2 delivery to promote bone regeneration [272] and as a delivery system for bFGF to facilitate wound healing [274, 275]. Alginate has the capability to encapsulate both antibiotics and growth factors, thus enabling their dual release to enhance wound healing [274, 275].

Based on the outcomes of our investigation, a notable disparity in Vascular Endothelial Growth Factor (VEGF) expression levels between unmodified Mesenchymal Stem Cells (MSCs) and encapsulated MSCs did not emerge as a significant finding. In fact, encapsulated MSCs exhibited a marginally reduced expression of VEGF at the single time-point at which VEGF measurements were conducted (as detailed in Section 3.4.2.-A) during cultivation with Fetal Bovine Serum (FBS). Notably, there was an absence of detectable basic Fibroblast Growth Factor (bFGF) expression from the seeded Integra® matrix scaffolds, irrespective of alginate encapsulation, under FBS cultivation conditions.

Upon an examination of the effects of alginate encapsulation followed by seeding onto Integra® matrix scaffolds, in contrast to direct seeding without encapsulation, no discernible distinctions were observable in the parameters pertaining to vascular growth on the Chorioallantoic Membrane (CAM) during in-ovo experimentation (as elucidated in Section 3.4.2.-B). Furthermore, under human Platelet Lysate (hPL) cultivation conditions, a slight elevation in both VEGF and bFGF expression levels was observed in scaffolds harbouring encapsulated MSCs when compared to those directly seeded without encapsulation (Section 3.4.3-A). However, these variations did not attain statistical significance within this population, and no disparities manifested in the vascular assessment outcomes of the CAM assay (Section 3.4.3-B).

Upon elevating the cell population to five times the original seeding density, nearly identical results were discerned in the vascular assessment of the CAM assay during FBS cultivation (Section 3.4.4.-B).

Likewise, during hPL cultivation, equivalent or marginally elevated (though statistically insignificant within this population) results were noted when cells were encapsulated, as observed in the vascular assessment of the CAM assay (Section 3.4.4.-C).

In the context of co-culturing unaltered MSCs with Dermal Fibroblasts (DFs), alginate encapsulation yielded decreased VEGF and bFGF expression results under both FBS and hPL supplementation conditions (Section 3.4.5-A). In a comparative analysis of seeded, encapsulated, and cultured manipulated MSCs (partially transfected and non-transfected) with non-encapsulated MSCs under identical conditions, the presence of alginate encapsulation appeared to result in slightly higher VEGF and bFGF expression levels during FBS supplementation, with comparable blood vessel growth observed in the CAM assay (Section 3.4.6.-A). However, under hPL supplementation, alginate encapsulation led to lower levels of VEGF and bFGF expression in comparison to direct seeding (Section 3.4.7-A), along with slightly diminished blood vessel formation parameters on the CAM assay (Section 3.4.7-B).

Concerning the co-cultivation of MSCs with genetically modified DFs, in the presence of FBS cultivation, human VEGF expression exhibited a minor reduction with alginate encapsulation, while human bFGF expression showed an increase compared to non-encapsulated cells (Section 3.4.8-A). No discernible differences emerged in the parameters associated with vessel growth in the CAM assay (Section 3.4.8-B). Under hPL supplementation, alginate encapsulation once again yielded marginally lower (though statistically insignificant) VEGF and bFGF expression levels (Section 3.4.9-A) but did exhibit improved vascular responses in certain parameters of blood vessel development assessed in the CAM assay (Section 3.4.9-B).

In summary, encapsulating cells with alginate yielded conflicting outcomes in terms of VEGF and bFGF expression, media supplementation, and their impact on the CAM assay. Notably, no substantial disparity in the incorporation of alginate into the manufacturing protocol was observed. This observation can be attributed to several factors, including the controlled and gradual release of VEGF and bFGF by alginate, as previously documented [271, 272], in comparison to the duration of implantation in the CAM assay (which spans 5 days). Directly seeded scaffolds have the capacity to release VEGF and bFGF more rapidly, aligning better with the brief timeframe of the CAM assay. Furthermore, the characteristics of alginate itself in comparison to the cell type and media additives may contribute to this variance; for example, some studies have indicated that maximal secretion of VEGF occurs when MSCs are cultured on substrates with optimal stiffness [243], whereas alginate is less rigid. Additionally, fibroblasts' mechanotransduction response can be influenced by the type of surface on which they are cultivated [276-278], potentially resulting in differing responses compared to MSCs.

Given the absence of substantial differences observed with alginate encapsulation and considering the principles of advanced therapeutic medicinal product (ATMP) “design with the intention to translate”, as supported by the European Medicines Agency (EMA) [279-281], the addition of an extra step, coupled with the requisite quality control measures, appears unwarranted.

Our primary hypothesis centred on the transient genetic modification of human bone marrow-derived Mesenchymal Stem Cells (MSCs) and/or human dermal fibroblasts to induce overexpression of Vascular Endothelial Growth Factor (VEGF) and basic Fibroblast Growth Factor (bFGF), and its consequential impact on vascularization, with the ultimate goal of optimizing the tissue-engineered graft. In this context, Integra® matrix scaffolds were employed for the seeding of a coculture system consisting of genetically modified MSCs overexpressing VEGF and bFGF, in conjunction with unaltered

MSCs (referred to as "coculture 2" at a 50:50 ratio). Additionally, Integra® matrix scaffolds were seeded with a coculture of genetically modified fibroblasts overexpressing VEGF and bFGF, along with unaltered MSCs (referred to as "coculture 3" at a 50:50 ratio). These cocultures were cultured in the presence of Fetal Bovine Serum (FBS) and human Platelet Lysate (hPL) supplementation.

The outcomes of coculture 2 experiments revealed a modest elevation in VEGF and bFGF expression levels, albeit without statistical significance when compared to the control protocol with FBS supplementation (as detailed in Section 3.4.6.-A). Additionally, no observable differences were noted in the parameters associated with blood vessel development on the Chorioallantoic Membrane (CAM) assay (Section 3.4.6.-A). Conversely, in the presence of hPL supplementation, both human VEGF and bFGF expression levels exhibited statistically significant increases, indicative of enhanced functionality, aligning with the results obtained from the Green Fluorescent Protein (GFP) experiments (Section 3.3). The augmented VEGF and bFGF expression levels also corresponded with heightened values in blood vessel parameters, including total vessel area, total vessel length, and the number of branching points, as observed in the CAM assay.

Regarding coculture 3, under FBS cultivation conditions and direct seeding, no statistically significant differences were observed in the expression levels of VEGF and bFGF (as delineated in Section 3.4.8.-A), with only an increase noted in the mean vessel thickness parameter on the CAM assay (Section 3.4.8.-B). With hPL supplementation, an elevation was observed solely in the levels of bFGF (Section 3.4.9.-A); however, discernible differences emerged in the CAM model, particularly in total vessel area, mean vessel thickness, and the number of branching points (Section 3.4.9.-B). These findings hold promise in substantiating our hypothesis, given that both VEGF and bFGF are potent stimulators of angiogenesis [73-75, 282]. This potency is readily observable in the CAM assay, where the utilization of VEGF and bFGF treatments has been instrumental in studying angiogenesis and assessing the impact of diverse agents on vascular development.

VEGF treatment within the CAM assay has been well-documented for its significant angiogenic effects, exemplified by an increase in both total vessel number and total vessel length, underscoring its potent angiogenic properties [283, 284]. Modifications to the CAM assay have facilitated the quantitative measurement of vascular density, enabling VEGF treatment to serve as a stimulus for evaluating alterations in vascular density, thereby providing a more precise and objective means of assessing the effects of VEGF and other substances on blood vessel formation [285].

Furthermore, bFGF is also widely recognized for its angiogenic effects, eliciting neovascularization in various *in vivo* and *in vitro* assays, including the CAM assay [286]. It plays a pivotal role in promoting blood vessel proliferation and serves as a potent inducer of angiogenesis [287]. Comparative studies have highlighted significant distinctions in the angiogenic capacities of bFGF when compared to other growth factors, such as VEGF, emphasizing the complex and distinct roles of different growth factors in the regulation of blood vessel formation [288].

Our final hypothesis centred on the replacement of Foetal Bovine Serum (FBS) with Human Platelet Lysate (hPL) as a suitable and Good Manufacturing Practice (GMP) compliant substitute to facilitate cellular expansion and enhance viability. The transition from FBS to hPL not only proved to be suitable but also yielded superior outcomes, particularly in terms of Mesenchymal Stem Cell (MSC) expression of basic Fibroblast Growth Factor (bFGF) in the majority of our experiments (as detailed in Results

Section 3.4.4.-A, 3.4.7-A, and 3.4.9-A). Furthermore, this transition also resulted in increased Vascular Endothelial Growth Factor (VEGF) expression in coculture 2 (as indicated in Results Section 3.4.7-A). These enhanced expressions of growth factors correlated with notable improvements in various blood vessel parameters, including total vessel length, total vessel area, and total branching points, observed in the Chorioallantoic Membrane (CAM) assay (detailed in Results Section 3.4.7-B). Similar enhancements in blood vessel parameters, encompassing total vessel area, total vessel length, mean vessel thickness, and total branching points, were also evident in coculture 3 scaffolds when implanted in-ovo onto the CAM (as described in Results Section 3.4.9-B). These favourable outcomes can plausibly be attributed to the higher concentration of growth factors present in hPL [113, 207, 212], which can act as priming or pre-conditioning agents, thereby stimulating improved cellular outcomes.

Media samples containing the secretome of various experimental conditions was assessed with a focus on angiogenesis-related growth factors. In comparison to the reference protocol (TET + FBS), nearly all the growth factors exhibited increased levels. Nevertheless, it is noteworthy that, in contrast to the positive control, the growth factor known as GRO demonstrated elevated expression, specifically within the scaffolds of coculture 3, and its overall expression was more pronounced in scaffolds cultivated in the presence of Foetal Bovine Serum (FBS) as opposed to human Platelet Lysate (hPL). Furthermore, Interleukin-6 (IL-6), Interleukin-8 (IL-8), and Monocyte Chemoattractant Protein-1 (MCP-1) also exhibited heightened expression under these same conditions.

Conversely, Platelet-Derived Growth Factor-BB (PDGF-BB) was found to be more prominently elevated in the scaffolds seeded with coculture 2. On the other hand, Regulated on Activation, Normal T Cell Expressed and Secreted (RANTES) exhibited the highest expression levels within the unmodified coculture 1 of Mesenchymal Stem Cells (MSCs) and fibroblasts. Interestingly, Tissue Inhibitor of Metalloproteinase-2 (TIMP-2) demonstrated the most substantial elevation in coculture 3, once again in the context of FBS supplementation.

GRO, or growth-regulated oncogene, represents a chemokine family integral to angiogenesis [289]. Key facets of GRO's role in angiogenesis encompass its function as an angiogenic inducer, stimulating the genesis of new blood vessels [289]. GRO operates as a chemoattractant for endothelial cells, the foundational components of blood vessels, enhancing their migration and proliferation [289]. Furthermore, GRO is produced by diverse cell types, including endothelial cells, fibroblasts, and immune cells, in response to inflammatory stimuli [289]. It intricately contributes to the interplay between inflammation and angiogenesis by recruiting immune cells to sites of inflammation and facilitating the generation of new blood vessels to support tissue repair and remodelling [289]. GRO also emerges as a key player in tumour angiogenesis, facilitating the formation of new blood vessels to nourish tumour growth and metastasis [290]. A comprehension of GRO's involvement in angiogenesis offers insights into the intricate processes governing tissue development, repair, and disease progression. Consequently, targeting GRO and other angiogenic factors holds therapeutic promise for addressing angiogenesis-related disorders, including cancer and cardiovascular diseases [291, 292].

IL-6, or interleukin-6, represents a cytokine pivotal in angiogenesis [293]. IL-6 exerts a direct stimulus on angiogenesis by fostering vessel sprouting, endothelial cell proliferation, and migration [293]. These effects are observed with a potency akin to that of VEGF (vascular endothelial growth factor) [293]. The role of IL-6 in tumorigenesis remains multifaceted, thus, its potential as an angiogenic agent has garnered scrutiny [293]. IL-6 has been shown to stimulate vessel sprouting in the ex vivo aortic ring

model and promote endothelial cell behaviours, albeit with compromised pericyte coverage compared to VEGF-stimulated vessels [293]. The underlying mechanism of IL-6's actions on pericytes encompasses the induction of the Notch ligand Jagged1 and Angiopoietin2 (Ang2)[293]. In pertinent applications, the administration of an anti-IL-6 antibody restored pericyte coverage in peritoneal xenografts of ovarian cancer [293]. This observation is further corroborated by findings associating IL-6 mRNA levels, Jagged1, and Ang2 in human ovarian cancer biopsies [293]. This underscores the significance of IL-6 in angiogenesis and its potential implications for therapeutic strategies targeting VEGF or IL-6 [293].

IL-8, or interleukin-8, emerges as a pro-angiogenic factor pivotal in the process of angiogenesis, [294-298]. IL-8 exercises a direct influence on endothelial cells, fostering their survival, proliferation, and the production of matrix metalloproteinases (MMPs), integral to angiogenesis [295]. IL-8's multifaceted role extends to both autocrine and paracrine pathways, where it is secreted by various solid tumour types and associated inflammatory cells, exuding a potent angiogenic impact in tumorigenesis [296]. Importantly, IL-8's actions have been implicated in cancer metastasis, bolstering angiogenesis to support tumour expansion and dissemination [296]. The mediation of IL-8's angiogenic effects is realized through its interaction with the CXCR2 receptor on endothelial cells, activating signalling cascades conducive to angiogenesis[297]. Furthermore, IL-8 also exhibits therapeutic potential in promoting angiogenesis, as exemplified in a study utilizing FGF2-primed 3D spheroids [298]. These spheroids, through IL-8 production, facilitated angiogenesis and muscle regeneration in a mouse hindlimb ischemia model, thereby underscoring IL-8's candidacy as a target for therapeutic agents aimed at addressing ischemic conditions [298].

MCP-1, or monocyte chemoattractant protein-1, assumes a significant role in angiogenesis, [299, 300]. A central facet of MCP-1's involvement in angiogenesis is its direct induction of this process through the stimulation of endothelial cell migration, sprouting, and the formation of in vivo blood vessels[300]. Importantly, this suggests that MCP-1 can catalyse the growth and organization of new blood vessels independently of an inflammatory response [300]. MCP-1's interaction with CCR2 receptors on endothelial cells initiates signalling pathways conducive to angiogenesis[300]. Additionally, MCP-1 has been identified as a TGF- β target gene in endothelial cells, functioning as a mediator of TGF- β -induced angiogenesis by facilitating vascular smooth muscle cell migration [301]. Thus, MCP-1 collaborates with other angiogenic factors to promote blood vessel growth [301]. The implications of MCP-1's role in angiogenesis extend to a spectrum of diseases and tumour progression [300, 302]. Dysregulation of MCP-1 has been linked to inflammatory diseases and its involvement in tumour angiogenesis and progression [300, 302].

PDGF-BB, or platelet-derived growth factor-BB, is a pivotal player in angiogenesis, orchestrating the intricate process of new blood vessel formation [303-308]. PDGF-BB's foremost role during development centres on promoting perivascular cell recruitment, a process integral to angiogenesis [303]. Furthermore, PDGF-BB modulates endothelial proliferation and angiogenesis in vitro through PDGF beta-receptors, directly contributing to angiogenesis by fostering endothelial cell migration, sprouting, and cord/tube formation [304]. Notably, PDGF-BB's involvement also extends to various diseases and tumour angiogenesis, where it functions as a growth factor, initiating cell division via β -receptors [305]. Excessive secretion of PDGF-BB has also been associated with aberrant angiogenesis-dependent bone formation, contributing to osteoarthritis pathogenesis [306]. PDGF-BB exerts its angiogenic effects through its interaction with PDGFR- β , mediating pericyte coverage crucial for blood vessel stability and maturation [308]. This underscores the role of the PDGF-BB/PDGFR- β axis in

orchestrating the complex process of angiogenesis by regulating the interplay between endothelial cells and pericytes [308].

RANTES, or regulated upon activation, normal T-cell expressed and secreted, also known as CCL5 (CC chemokine ligand 5), occupies a significant niche in angiogenesis, the dynamic process governing new blood vessel formation [309-311]. A central facet of RANTES's role in angiogenesis is its capacity to induce the expression of growth factors such as VEGF (vascular endothelial growth factor), a pivotal regulator of angiogenesis [309, 311]. This suggests that RANTES may promote angiogenesis by stimulating VEGF production, which, in turn, fuels the growth of new blood vessels [311]. Furthermore, RANTES engages in intricate interactions with GPCRs (G-protein-coupled receptors) and GAG (glycosaminoglycan) chains anchored to HSPGs (heparan sulphate proteoglycans)[309]. Specific receptors of RANTES, including CCR1 and CCR5, and heparan sulphate proteoglycans such as SDC-1, SDC-4, or CD-44, have been recognized as pivotal components governing RANTES-induced angiogenic effects [310]. The success of RANTES in promoting angiogenesis hinges on chemokine oligomerization and binding to GAGs, processes that are fundamental to its angiogenic effects [310]. Understanding these intricate mechanisms has driven the exploration of RANTES as a therapeutic target for neo-angiogenesis in vascular injury scenarios [310]. RANTES-loaded microparticles have demonstrated a pro-angiogenic effect in a mouse ischemia therapy model, further underscoring the therapeutic potential of RANTES for angiogenesis-related disorders [311].

TIMP-2, or tissue inhibitor of metalloproteinase-2, assumes a multifaceted role in angiogenesis [312-316]. At its core, TIMP-2 operates by inhibiting matrix metalloproteinases (MMPs), enzymes pivotal in extracellular matrix degradation and, consequently, angiogenesis [312, 313, 316]. TIMP-2's unique characteristic is its selective interaction with membrane type 1-MMP (MT1-MMP) at the cell membrane [315]. This interaction is integral to the activation of pro-MMP-2, which regulates the sprouting of newly formed blood vessels [315]. The MT1-MMP/TIMP-2 complex plays a pivotal role in activating pro-MMP-2, thereby facilitating the release of cytokines and growth factors that influence angiogenesis [315]. TIMP-2 exhibits a dual role in angiogenesis, sometimes promoting it by facilitating pro-MMP-2 activation and the release of angiogenic factors, while at other times inhibiting it through direct binding to angiogenic factors or blocking the activity of other pro-angiogenic molecules [312, 314]. TIMP-2's interactions extend to other molecules involved in angiogenesis, such as integrins and growth factors, further modulating the intricate angiogenic process [312, 314]. Dysregulation of TIMP-2 has been linked to various diseases and tumour angiogenesis due to its potential to disrupt the equilibrium between MMPs and TIMPs, resulting in aberrant angiogenesis [314]. A comprehensive understanding of TIMP-2's complex role in angiogenesis holds the promise of targeted therapies for these conditions [314].

In summary, the growth factors delineated in the preceding discussion exhibit multifaceted roles, and their expression or overexpression can exert differential effects on angiogenesis, contingent upon the specific cellular milieu. Notably, cells cultured in the presence of Foetal Bovine Serum (FBS) appeared to exhibit a diminished quality compared to those cultivated with human Platelet Lysate (hPL) supplementation. This discrepancy in quality may account for the potential upregulation of inflammatory markers, thereby contributing to the observed absence of favourable outcomes in terms of vessel growth on the Chorioallantoic Membrane (CAM) assay. However, a comprehensive interpretation necessitates a more exhaustive evaluation of each distinct condition.

Conclusively, the unaltered coculture of Mesenchymal Stem Cells (MSCs) and Dermal Fibroblasts (DFs), coupled with the incorporation of alginate encapsulation, did not yield favourable results in our preliminary screening investigations. Consequently, this approach has been excluded from further consideration in our manufacturing process. Furthermore, it is noteworthy that human Platelet Lysate (hPL) supplementation demonstrated superior performance compared to Foetal Bovine Serum (FBS) supplementation in terms of basic outcomes. As a result, hPL has replaced FBS as the preferred choice for the cultivation of trachea, with the exception of the reference TETRA protocol.

4.6. TRACHEAL STUDIES

In accordance with previous findings, a comparison of four distinct engineering protocols within the framework of three separate manufacturing experiments was conducted. Tracheal biopsies were employed as scaffolds, subsequently implanted in-ovo into the Chick Chorioallantoic Membrane (CAM) assay. The protocols under investigation included:

Protocol 1 (TETRA + FBS): Mesenchymal Stem Cells (MSCs) cultivated with Fetal Bovine Serum (FBS) supplementation. **Protocol 2:** MSCs cultivated in the presence of human Platelet Lysate (hPL) supplementation. **Protocol 3:** A coculture consisting of unmodified MSCs and transiently genetically modified MSCs, engineered to overexpress Vascular Endothelial Growth Factor (VEGF) and Basic Fibroblast Growth Factor (bFGF) in the presence of hPL cultivation. **Protocol 4:** A combination of unaltered MSCs and transiently genetically modified dermal fibroblasts, engineered to overexpress VEGF and bFGF.

Results pertaining to the expression levels of VEGF and bFGF, obtained from the culture media of the scaffolds on the day of implantation (results section 3.6.1), revealed a significantly higher expression of both growth factors in Protocol 3 (MSC coculture) compared to all other protocols. Protocol 4 also exhibited notably elevated levels of bFGF (although not to the extent of Protocol 3), with no statistically significant difference in VEGF expression compared to the TET + FBS control in this context. Furthermore, MSCs cultivated in the presence of hPL displayed higher growth factor levels in comparison to MSCs cultivated with FBS, with statistically significant differences observed for bFGF expression, aligning with previously documented outcomes.

Before implantation, scaffolds engineered under each condition underwent single-cell isolation and subsequent staining with recognized Mesenchymal Stem Cells (MSCs) surface markers, following the International Society for Cellular Therapy (ISCT) recommendations (results section 3.6.2.2). Additional markers included CD44, CD146, CD271, and CD106. Most of the tested conditions exhibited a reduction in the expression of MSCs surface markers, except for CD271 and CD106. Notably, Protocol 4, comprising a blend of MSCs and dermal fibroblasts, displayed nearly equivalent levels of CD271 and CD106 as compared to the protocols consisting solely of MSCs. However, the most pronounced and statistically significant decline in surface marker expression was observed with CD90 in all protocols cultivated with hPL in comparison to the TET + FBS (MSC + FBS) protocol.

Cluster of Differentiation 90 (CD90), also known as Thy-1 (Thymocyte Differentiation Antigen-1), is a glycosylphosphatidylinositol (GPI)-anchored glycoprotein with a molecular weight ranging from 25 to 37 kDa. It is expressed predominantly in leukocytes and plays a pivotal role in mediating cell–cell and cell–matrix interactions [317]. Furthermore, CD90, or Thy-1, is expressed in diverse cell types, encompassing leukocytes, neurons, thymocytes, fibroblasts, endothelial cells, mesangial cells, hematopoietic and mesenchymal stem cells[317]. CD90 influences a wide array of cellular processes, including T cell activation, neurite outgrowth, migration, cell death, and tumour growth[317]. Notably,

it serves as a counterreceptor for the leukocyte integrin Mac-1 (CD11b/CD18) on activated endothelial cells[318]. Moreover, CD90 has garnered attention as a candidate marker for cancer stem cells (CSCs) in primary high-grade gliomas, demonstrating a broader applicability than the established stem cell marker CD133[319]. Studies on cardiosphere-derived cells (CDCs) have revealed the involvement of CD90 in their regenerative efficacy in the context of human and mouse models of myocardial infarction, alongside c-Kit [320]. Nevertheless, the expression of c-Kit does not exhibit a direct correlation with the therapeutic effectiveness of CDCs in human subjects [4]. CD90 is capable of manifesting in a soluble form, which may carry distinct functionalities distinct from its membrane-bound counterpart [321].

Within the realm of human mesenchymal stem or stromal cells (MSCs), CD90 exerts significant control over the process of MSC differentiation. Notably, a decrease in CD90 expression is associated with augmented differentiation of MSCs, underscoring its role as a regulatory obstacle in the pathway of differentiation commitment[322]. Furthermore, a study conducted by Wiesmann et al. in 2006 postulated that the transient expression of CD90 in MSCs during differentiation into osteoblast-like cells in culture contributes to the observed loss of CD90 expression post mechanical stimulation [323]. CD90 serves as one of the defining markers for the identification of MSCs, alongside CD73 and CD105[324]. Moreover, it functions as a discriminative surface marker for an adventitial mesenchymal population located in adult human medium- and large-sized arteries [325]. The transient expression of CD90 in MSCs during early differentiation towards osteogenic cells highlights its utility as a marker in the differentiation process [323]. In the context of glioma-associated MSCs, the presence of two distinct subpopulations based on CD90 expression (CD90+ and CD90-) is noteworthy. These subpopulations exhibit divergent roles in tumour progression, with CD90^{high} MSCs promoting proliferation and/or tumorigenesis of U87 cells, while CD90^{low} MSCs contribute to angiogenesis and tube formation [326]. The varying levels of CD90 expression influence the growth and adhesion properties of MSCs, with CD90^{low} MSCs demonstrating enhanced in vitro growth and angiogenic potential, contributing to the formation of new tubular structures [326]. In a mouse model, the implantation of U87 cells with CD90^{high} conditioned medium (CM) resulted in larger tumour size, indicating increased proliferation and/or tumorigenesis, while CD90^{low} CM induced the formation of more capillary-like endothelial cell structures and CD31-expressing vessels [326]. Research conducted by Moraes et al. in 2016 reinforced the notion that reduced CD90 (THY-1) MSC expression is linked to increased mesenchymal stromal cell differentiation in vitro, alongside a decrease in CD44 and CD166 expression[322]. This finding underscored the role of CD90 as an impediment in the pathway of differentiation commitment within MSCs[322].

As MSCs undergo differentiation, the expression of CD90 undergoes changes that are closely associated with the differentiation process. The reduction in CD90 expression has been shown to enhance the osteogenic and adipogenic differentiation of MSCs in vitro, supporting the role of CD90 in regulating MSC differentiation[322]. CD90 also exhibits a direct relationship with CD44, another cell surface receptor, wherein reduced CD90 expression reduces CD44 expression and increases cell differentiation, suggesting that CD44, in association with CD90, may influence the stemness state of MSCs [323, 327]. Notably, mechanical stimulation can decrease CD90 expression in human MSCs, indicating that external cues and the microenvironment have the capacity to influence the expression of CD90 during MSC differentiation.

CD90's involvement in oncogenesis and its potential role as a marker for cancer stem cells (CSCs) underscore the intricate nature of its involvement in cellular processes[322]. In the realm of human dermal fibroblasts, CD90 plays a crucial role in tissue homeostasis, wound healing, scar formation, the prevention of tissue fibrosis, and tumour progression [328]. CD90 acts to inhibit the expression of adipogenic markers, such as PPAR γ and Src, in dermal fibroblasts, suggesting a role in balancing

fibroblast proliferation, differentiation, and apoptosis, critical for tissue homeostasis and physiological wound healing [329]. CD90+ fibroblasts have been observed to hinder the differentiation of lung fibroblasts into myofibroblasts, contributing to the prevention of tissue fibrosis and the regulation of inflammatory processes [328]. These CD90+ fibroblasts have been implicated in a range of pathological processes, including pulmonary fibrosis, inflammatory arthritis, inflammatory skin diseases, and skin scar formation, serving as biomarkers for related cancers [328]. While the precise molecular mechanisms of CD90+ fibroblasts in these processes remain unclear, the location and lineage identity of fibroblasts within the dermis influence the role of CD90, with expression predominantly in the lower dermis and rare presence in the superficial dermis [330]. The decreased expression of CD90 in human dermal fibroblasts can have several implications for tissue homeostasis, wound healing, and disease processes. It is considered a defining fibroblastic marker, and its reduced expression may indicate a shift in the phenotype of dermal fibroblasts, which, in turn, could affect the balance between fibroblast proliferation, differentiation, and apoptosis, thus influencing tissue regeneration and repair processes[328].

In conjunction with CD90, several other markers are frequently co-expressed in mesenchymal stem cells (MSCs), collectively aiding in their identification and characterization. MSCs are typically identified by their concurrent expression of CD73, CD90, and CD105[324]. CD73 is an ecto-5'-nucleotidase enzyme that participates in purine metabolism [324]. While also known as endoglin, CD105 is a transmembrane glycoprotein with roles in TGF- β signalling and angiogenesis[324]. Other markers that aid in the identification of MSCs include:

PDGFR α : In the context of adventitial mesenchymal progenitor cells found in the medium- and large-sized arteries of adult humans, CD90 is co-expressed with PDGFR α , CD44, CD73, and CD105[9]. PDGFR α serves as a receptor for platelet-derived growth factors and plays critical roles in cell proliferation and migration[325]. Another marker, CD44 is a cell adhesion molecule involved in mediating cell-cell and cell-matrix interactions[325]. It is recognized as a marker that co-expresses with CD90 in adventitial mesenchymal progenitor cells located in adult human medium- and large-sized arteries[325]. CD146, also known as melanoma cell adhesion molecule (MCAM), CD146 is a cell surface glycoprotein contributing to cell adhesion and migration[331]. It is co-expressed with CD90 and CD73 in human MSCs[331]. CD29 on the other hand, is referred to as integrin β 1, is a cell surface glycoprotein that forms heterodimers with various integrin α subunits and plays pivotal roles in cell adhesion and migration [331]. CD29 is commonly co-expressed with CD90 and CD73 in human MSCs [331]. Known as activated leukocyte cell adhesion molecule (ALCAM), CD166 is a cell surface glycoprotein with functions related to cell adhesion and migration[331]. It has been identified as a co-expressed marker with CD90 and CD73 in human MSCs[331]. When co-expressed with CD90, these markers collectively provide a robust molecular signature for identifying and characterizing MSCs.

CD73, also recognized as ecto-5'-nucleotidase, serves as an ectoenzyme responsible for the extracellular adenosine production through the hydrolysis of adenosine monophosphate (AMP). This enzymatic process enables CD73 to play a pivotal role in modulating the inflammatory response and immune suppression by converting AMP into adenosine. Adenosine, in its capacity as a product generated by CD73, subsequently exerts control over immune cell function and serves as a regulator of inflammatory processes [332, 333]. Furthermore, adenosine, as facilitated by CD73, contributes to the promotion of dermal fibrosis via the activation of adenosine receptor A2AR (A2A receptor). This signifies its involvement in tissue remodelling processes [334]. It is noteworthy that CD73 engages in interactions with other proteins, such as emmprin, to orchestrate the production of matrix metalloproteinase-2 (MMP-2) within the context of co-cultured sarcoma cells and fibroblasts. This interplay is of considerable importance in the remodelling of the extracellular matrix during interactions within the tumour-stromal milieu [335]. Moreover, the expression of CD73 has been

associated with various malignancies, and its presence within the tumour microenvironment has been correlated with unfavourable prognostic outcomes and resistance to therapeutic interventions. This strongly implies a contributory role in tumour progression and therapeutic responses [333]. Within the domain of mesenchymal stromal cells (MSCs), the expression of CD73 has been found to be linked to the regulatory phenotypes exhibited by T and natural killer (NK) cells, thus signifying its involvement in the modulation of immune responses [336]. MSCs expressing CD73 have exhibited their potential to ameliorate myocardial infarction through their capability to promote angiogenesis. This angiogenic effect is mediated through the hydrolysis of 5'-adenosine monophosphate (AMP) into adenosine, which subsequently interacts with cell surface adenosine receptors [337]. CD73 expression is also closely associated with heightened stemness in MSCs. MSCs characterized by the presence of CD73 have demonstrated heightened proliferative capabilities compared to their CD73-negative counterparts and have exhibited a heightened ability for colony formation. This observation underscores the pivotal role of CD73 in the preservation of the stem cell characteristics within the MSC population [338]. Furthermore, investigations have revealed that in ovarian cancer-initiating cells, CD73 is instrumental in the promotion of the expression of genes related to stemness and the epithelial-mesenchymal transition (EMT), thus shedding light on its role in the regulatory mechanisms governing these processes [339]. It is noteworthy that the proportion of CD73-positive cells may exhibit variations contingent upon the specific tissue source. For instance, subcutaneous fat has demonstrated a higher prevalence of CD73-positive cells as compared to visceral fat, thereby underscoring the importance of accounting for the potential diversity in the characteristics of MSCs based on their tissue origin [340].

CD105, also recognized as endoglin, is a type I membrane glycoprotein expressed in mesenchymal stromal cells (MSCs), contributing to a spectrum of biological functions. CD105 serves as an accessory receptor for members of the transforming growth factor-beta (TGF- β) superfamily ligands and thereby assumes a pivotal role in modulating the TGF- β signalling cascade within MSCs [341]. Its effects on the responsiveness of MSCs to TGF- β 1 and TGF- β 3 are context-dependent and can either augment or diminish this responsiveness [342]. In practical terms, CD105 has been employed as a marker to facilitate the isolation of multipotent human MSCs [343]. Notably, its expression correlates with the undifferentiated state of MSCs, and the diminishment of CD105 expression has been observed concomitant with the process of MSC differentiation [342]. CD105's association with the chondrogenic potential of MSCs is recognized; however, it is noteworthy that its predictive capacity for chondrogenic potential may vary based on the specific subset of MSCs, as evidenced by a study on bone marrow-derived MSCs [344].

Moreover, CD105 also exerts an influence on angiogenesis and participates in the modulation of migration, survival, and cytoskeletal organization of endothelial cells [341]. This multifaceted role renders CD105-expressing MSCs a potential focus for cancer therapy [343]. Their inherent immunomodulatory properties and the propensity of MSCs to home in on tumours render them compelling candidates for cell-based interventions in cancer treatment. Conversely, the precise role of CD105 in human dermal fibroblasts has yet to be comprehensively elucidated. CD105 has been identified as a potential marker associated with a subset of dermal fibroblasts characterized by multipotency [345]. This distinct subset, marked by CD73(-) CD105(+) fibroblasts, exhibits a fibroblast phenotype and lacks the expression of antigens commonly attributed to MSCs. In a noteworthy discovery, the expression of CD105 has been linked to the enhancement of osteogenic differentiation in human dermal-derived CD105+ fibroblast cells, primarily mediated through the Smad and MAPK pathways [346]. This suggests an active role for CD105 in regulating the differentiation potential of dermal fibroblasts.

Furthermore, CD105 expression has emerged as a biomarker for bone metastasis in early-stage invasive ductal breast cancer patients in the context of cancer-associated fibroblasts [347]. Intriguingly, CD105-positive pancreatic fibroblasts have been characterized as permissive for tumour growth *in vivo*, whereas their CD105-negative counterparts exhibit a pronounced tumour-suppressive phenotype [348]. These observations collectively imply that CD105 may potentially influence tumour-stromal interactions, further underscoring its significance in the context of the tumour microenvironment.

CD44, a widely expressed cell-surface glycoprotein, assumes a pivotal role in the biological functions of mesenchymal stromal/stem cells (MSCs) primarily concerning adhesion, migration, and homing [349]. The influence of CD44 on MSCs is observed during exposure to nicotine, where it contributes to their migration [350]. Notably, CD44's interaction with hyaluronic acid (HA) in the extracellular matrix holds relevance in the context of MSC migration [35]. CD44, in conjunction with hyaluronic acid, also enhances the potency of mesenchymal stem cell extracellular vesicles, which can be observed in the context of severe pneumonia [349]. Within the tumour microenvironment, the expression of CD44 by MSCs is associated with the acquisition of an activated fibroblast phenotype, a process mediated by TWIST activation [350].

CD44's relevance transcends MSCs, as it is overexpressed in various cell types, including cancer stem cells, and is often marked by alternative spliced variants, which are implicated in cancer development and progression [327, 351]. The CD44/CD44v axis assumes a critical role in the regulation of cancer stemness [36]. CD44 functions as a signalling platform, effectively integrating cues from the cellular microenvironment with signals from growth factors and cytokines. These integrated signals are subsequently transduced to membrane-associated cytoskeletal proteins and to the nucleus, thereby regulating a multitude of gene expression patterns associated with cell-matrix adhesion, cell migration, proliferation, differentiation, and survival [351].

In the realm of dermal fibroblasts, the primary contributors to the synthesis and remodelling of the extracellular matrix (ECM) during wound healing, CD44 plays a noteworthy role. It influences fibrillar collagen accumulation and wound healing within the context of the injury response [352]. CD44-mediated processes, encompassing inflammation, fibrogenesis, and collagenolysis, serve as pivotal regulators of ECM remodelling and tensile strength during cutaneous wound healing [352]. In this context, CD44 is instrumental in modulating the expression of the α -SMA gene in primary murine dermal fibroblasts. It exerts control over actin cytoskeleton, thereby inhibiting α -SMA gene expression through a novel G-actin/MRTF-mediated pathway that intersects with TGF β R/p38MAPK signalling [353]. CD44's impact extends to influencing fibroblast behaviours through the modulation of cell-cell and cell-matrix interactions, affecting the survivin and Hippo pathways [354]. Within dermal fibroblasts, CD44 assumes critical roles in regulating cell adhesion, proliferation, and migration/invasion by modulating adherens junctional processes [354]. As in MSCs, CD44 serves as a signalling platform in dermal fibroblasts, translating environmental cues, growth factor signals, and cytokine inputs into responses that encompass cell-matrix adhesion, migration, proliferation, differentiation, and survival [355]. While the role of CD44 in dermal fibroblasts is intricate and multifaceted, it remains an area that necessitates further in-depth investigation to fully unravel its implications.

CD271, also known as the low-affinity nerve growth factor receptor (LNGFR), serves as a cell surface marker that has garnered significant attention for its utility in the characterization and purification of human bone marrow mesenchymal stem cells (MSCs) [202]. It has been recognized as a versatile marker with the capacity to selectively isolate and expand multipotent MSCs, thereby encompassing immunosuppressive and lymphohematopoietic engraftment-promoting properties [202, 356].

CD271's specificity lies in its expression by MSCs derived from bone marrow, and it has been widely employed for the identification and purification of MSCs from various sources prior to culture initiation [202]. Consequently, CD271 emerges as a marker denoting a subset of bone marrow-derived MSCs characterized by an enhanced differentiation capacity tailored for applications in bone or cartilage repair [349]. Notably, CD271-selected MSCs derived from adipose tissue have exhibited properties conducive to cartilage repair while displaying a reduced angiogenic profile in contrast to their plastic-adherent MSC counterparts [349].

A comprehensive study has explored the potential effects of CD271 on human MSC proliferation and differentiation and has established an association between CD271 expression and the heightened proliferation and differentiation potential of MSCs [203]. Nonetheless, the precise role of CD271 in governing the intricate processes of MSC proliferation and differentiation remains a subject of ongoing investigation.

Turning attention to its role within human dermal fibroblasts, it is evident that the comprehension of CD271's function within this context is presently limited, and the available information is scarce. Notwithstanding this, a study conducted by Vaculik et al. has made efforts to distinguish dermal MSCs from their differentiated fibroblast counterparts by the selection of CD271+ and SSEA-4+ cells from adherent dermal cells and subsequently assessing their differentiation capacity [202]. The findings of this investigation have suggested that the CD271+ dermal subpopulation exhibits a heightened potential for adipogenic, osteogenic, and chondrogenic differentiation, thereby implying that CD271 may play a role in governing the differentiation potential of dermal fibroblasts. It is crucial to underscore, however, that additional research endeavours are essential to provide a comprehensive understanding of CD271's contributions within the domain of dermal fibroblasts.

Therefore, CD271 emerges as a valuable marker employed in the characterization and purification of human bone marrow MSCs. It is associated with enhanced differentiation potential for bone or cartilage repair and with augmented proliferation and differentiation capabilities in MSCs. Nevertheless, it is imperative to recognize that CD271 should not be regarded as a universal marker for identifying MSCs from diverse sources before the initiation of culture, as its utility may be context-specific [202, 331].

CD146, a transmembrane protein, fulfils a pivotal role in mediating cell-cell and cell-extracellular matrix adhesion. It is prominently expressed on the surface of various mesenchymal stem cells (MSCs) [357]. Notably, CD146-positive (CD146+) MSCs have been demonstrated to exhibit superior cellular properties, encompassing heightened proliferation, enhanced differentiation capacity, augmented migration, and enhanced immune regulation capabilities when compared to their CD146-negative (CD146-) or unsorted MSC counterparts [357, 358]. Within this context, CD146+ bone marrow-derived MSCs play integral roles within the perivascular niche, contribute to skeletogenesis, and exert influence over haematopoiesis [358]. While CD146 has been implicated in mediating a diverse array of cellular signalling pathways, further exploration is necessary to determine its precise role within the domain of MSCs [357].

Moreover, CD146+ MSCs have exhibited substantial therapeutic potential, particularly in the context of treating collagen-induced arthritis in murine models. Their enrichment has been established as a strategy to promote cartilage regeneration when combined with articular cartilage extracellular matrix scaffolds [357]. CD146 defines a distinct subpopulation of mesenchymal stromal cells, characterized by enhanced suppressive properties, thereby regulating the intricate cross-talk between MSCs and myeloid cells [359]. This distinctive attribute has also been harnessed to ensure the quality of clinical-grade MSCs derived from human dental pulp [360]. Consequently, CD146 emerges as a promising

marker for the identification and purification of MSCs characterized by their exceptional cellular properties, therapeutic potential, and suppressive capabilities.

It is essential to underscore that CD146 expression is particularly distinctive in MSCs derived from bone marrow and dental pulp, and its application within the realm of specific diseases has yielded notable outcomes. Nevertheless, the precise role of CD146 within MSCs remains an area of ongoing investigation.

CD106, also known as vascular cell adhesion molecule-1 (VCAM-1), serves as a cell adhesion molecule found on the surface of various mesenchymal stem cells (MSCs) [361-363]. It plays a pivotal role in identifying a distinct subset of MSCs distinguished by their unique immunomodulatory properties [361]. CD106, through its mediation of cell-cell adhesion, emerges as a critical factor in T cell activation and the recruitment of leukocytes to sites of inflammation [361]. Notably, CD106 is expressed on MSCs prior to osteogenic induction, but its expression is downregulated after approximately two weeks of osteogenic differentiation, highlighting its involvement in the regulation of osteogenic differentiation [363]. Thus, CD106 holds promise as a valuable surface marker for bone marrow-derived MSCs (BMMSCs) with an intricate link to the regulation of osteogenic differentiation [363]. Moreover, it also emerges as a novel mediator of bone marrow MSCs, particularly through its interaction with NF- κ B, in the context of bone marrow failure, as observed in acquired aplastic anaemia [364]. Furthermore, CD106 has been recognized as a marker of MSCs characterized by their differentiation potential [362]. A comprehensive analysis of 13 CD antigens revealed a clear correlation between CD106 expression and the differentiation potential of individual MSC clones [362]. CD106 is distinctly associated with MSCs and has not been found to be expressed by dermal fibroblasts.

In summary, the downregulation of cell surface marker expression, notably CD90, can be interpreted as a reflection of the loss of the stem cell or stromal cell phenotype and a transition toward a more differentiated state.

Enumeration of blood vessels on the CAM assay revealed an increase in the total vessel area for Protocols 3 and 4 when compared to the reference Protocol 1 (TET + FBS), and an increase in the total vessel length when comparing Protocol 4 to Protocol 1 (results section 3.7.1).

Subsequent intravascular fluorescent staining with Microfil[®] dye followed by MicroCT analysis provided further insights (results section 3.7.2). Scaffolds engineered under Protocol 1 (MSCs + FBS) exhibited the lowest quantity of blood vessels but larger vessels surrounding the scaffolds without significant infiltration. In contrast, Protocol 2 resulted in thinner blood vessels with the initiation of smaller infiltrating vessels across different experiments. Protocol 3 demonstrated the most favourable outcome, with the presence of small, large, infiltrating, and dense blood vessels in the images. Protocol 4 also exhibited some small and large infiltrating blood vessels, although not as densely as Protocol 3.

Statistical analysis of the enumeration of 3D images utilizing AngioTool software revealed higher values for total vessel area, number of junctions, and vessel junction density in Protocol 3 compared to the other protocols. These findings conclusively support the main hypothesis that the overexpression of VEGF and bFGF can enhance blood vessel formation and contribute to the vascularization of the trachea.

Angiogenesis, the process of generating new blood vessels from pre-existing ones, encompasses various contexts such as developmental, wound healing, and tumour growth. It comprises five key events: (1) initiation driven primarily by pro-angiogenic factors, notably Vascular Endothelial Growth Factor (VEGF), and NOTCH signalling; (2) induction of endothelial tip cells guided by high VEGFA signalling; (3) formation of adjacent endothelial stalk cells through NOTCH-mediated lateral inhibition; (4) vessel outgrowth directed perpendicularly to the parent vessel via soluble FLT1 production; and (5)

vessel fusion or anastomosis facilitated by macrophages. VEGF family members, including VEGFA isoforms, play pivotal roles in angiogenesis, alongside factors such as Fibroblast Growth Factor 2 (FGF2). VEGF gradients govern vessel growth, while macrophages may aid in vessel fusion by releasing VEGFC and activating FLT4 in endothelial tip cells. However, the precise macrophage role remains ambiguous [183]. Hence, the intermittent presence of a heightened concentration of vascular endothelial growth factor (VEGF) and basic fibroblast growth factor (bFGF) is expected to facilitate the initiation of the angiogenic process.

Mesenchymal Stem Cells (MSCs) can be primed with VEGF, a potent inducer of new blood vessel growth. Hypoxic priming, for instance, increases hypoxia-inducible factor 1-alpha (HIF-1 α) in MSCs, leading to the production of a conditioned medium enriched with VEGF that promotes angiogenesis. In another approach, MSCs were genetically engineered to overexpress VEGF, demonstrating their angiogenic potential. This priming enhances MSCs' vasculogenic and therapeutic potential for various applications, including cardiac repair [244, 365, 366]. Additionally, other growth factors, such as Basic Fibroblast Growth Factor (bFGF), can also influence MSCs' behaviour and be considered as priming agents. bFGF stimulation for example, can upregulate Hepatocyte Growth Factor (HGF) expression in MSCs via the JNK signalling pathway, contributing to tissue repair and fibrogenesis suppression [367, 368].

Furthermore, the secretome of MSCs can be modulated through preconditioning with hypoxia, cytokine treatments, and specific culture systems like three-dimensional (3D) conditions. MSC "priming" shifts the secreted factors towards an anti-inflammatory and pro-trophic phenotype, regulating tissue regeneration and repair. The efficacy of MSC therapies is often attributed to the production of paracrine factors, including cytokines, growth factors, and exosomes. These factors transiently and paracrinely influence tissue injury responses, orchestrating tissue repair processes [244].

BM-MSCs secrete various growth factors, including Epidermal Growth Factor (EGF), Keratinocyte Growth Factor (KGF), Insulin-Like Growth Factor-1 (IGF-1), VEGF- α , Erythropoietin (EPO), and Stromal Cell-Derived Factor-1 (SDF-1), which play roles in tissue regeneration. BM-MSCs also express higher levels of VEGF- α compared to dermal fibroblasts. They can enhance the proliferation and migration of target cells, impacting tissue repair in a paracrine manner. The composition of the MSC secretome can be affected by culture conditions and stimuli, ultimately influencing tissue regeneration and repair [238].

MSCs support angiogenesis not only through direct differentiation but also through paracrine communication, secreting pro-angiogenic factors such as bFGF, VEGF, Placental Growth Factor (PGF), Transforming Growth Factor- β (TGF- β), Platelet-Derived Growth Factor (PDGF), Angiopoietin-1, Interleukin-6 (IL-6), and Monocyte Chemoattractant Protein-1 (MCP-1). These factors induce angiogenesis in vivo and can be neutralized with antibodies. IL-6 and MCP-1 exhibit proangiogenic properties, while VEGF regulates endothelial cell migration, differentiation, and recruitment for angiogenesis. VEGFR2 activates multiple signalling pathways, including MAPK, PI3K/AKT, Src, and Rac, promoting endothelial cell survival, proliferation, and migration. IGF-1 secreted by MSCs enhances endothelial progenitor cell proliferation via the PI3K/Akt signalling pathway. HGF secreted by MSCs stimulates angiogenesis, tissue regeneration, and ECM remodelling. Moreover, MSCs support skin cell differentiation and exhibit anti-fibrotic properties in wound tissue repair. They also increase ECM components production, promoting tissue repair after vascular damage [238, 245]

In summary, the modulation of MSCs' secretome through priming with factors like VEGF and their inherent paracrine effects significantly influences angiogenesis and tissue regeneration.

Consequently, it is entirely plausible to ascribe the augmented angiogenesis observed in protocol 3 not solely to the overexpression of genetically manipulated subpopulation of MSCs in coculture, but also to the priming effect on the unmanipulated MSC subpopulation induced by the growth factor overexpression in the manipulated subset. This results in a compounded and synergistic enhancement of angiogenesis, as evidenced by the emergence of numerous smaller blood vessels sprouting from larger ones in the images from protocol 3. The effect of human platelet lysate cultivation can also be explained in the same manner albeit in a subtler manner.

Furthermore, beyond their recognized role as proangiogenic stimulatory cells, investigations have also demonstrated that MSCs exhibit greater efficacy in wound healing attributed to their secretory profile when compared to human dermal fibroblasts [197, 369-372]. This distinction provides a plausible explanation for the superior outcome observed in protocol 3 relative to protocol 4.

5. THE CONCLUSION

In summary, inadequate vascularization poses a significant challenge in tissue repair, particularly in cases involving critical-sized injuries and post-radiation therapy scenarios, thereby impeding both clinical outcomes and the application of tissue engineering techniques. This deficiency in vascularization can result in issues related to graft integration and the viability of cells, primarily due to factors such as hypoxia and inadequate nutrient supply. The demand for organ transplantation remains high, but the limitations of donor availability and the complications associated with allogeneic transplantation, particularly in the context of tracheal transplantation, present formidable hurdles.

The fundamental research undertaken in this study seeks to initiate and facilitate the vascularization process with the ultimate goal of enhancing tissue or graft integration and post-transplant survival. It represents a “from bed back to the bench-side” reverse translational endeavour.

Within the framework of our experimental model, we have demonstrated that co-culturing unaltered mesenchymal stem cells (MSCs) with genetically modified MSCs is effective in vascularizing tracheal biopsies. Additionally, we have observed that cultivating MSCs in the presence of human platelet lysate (hPL) supplementation yields superior results compared to foetal bovine serum (FBS) supplementation in terms of potential angiogenic cellular benefits.

While regulatory authorities, such as the European Medicines Agency (EMA), advocate for the design of basic science experiments with translational intent, practical challenges related to resource constraints, time limitations, and procedural complexities often hinder this process, especially when conducting proof-of-concept studies. Nevertheless, it is important to highlight that our contribution to this foundational scientific project has included the substitution of FBS with hPL, the implementation of a Good Manufacturing Practice (GMP)-compatible nucleofection protocol using GMP-compliant bacterial plasmids, and the selection of materials with GMP-compatible counterparts. This strategic choice ensures that revalidation is not required, even as we transition from initial proof-of-concept experimentation to more advanced stages.

However, it is important to acknowledge that the chorioallantoic membrane (CAM) assay utilized in this study does have certain limitations, such as interspecies variations between chicken and human systems, particularly with regard to species-specific immune responses. Consequently, further investigations should explore alternative models that closely mimic the human system to provide more accurate insights.

BIBLIOGRAPHY

1. Chiang, T., et al., *Clinical translation of tissue engineered trachea grafts*. Annals of Otolaryngology, Rhinology & Laryngology, 2016. **125**(11): p. 873-885.
2. Friedel, G., et al. *Long-term results after 110 tracheal resections*. in *Zurück in die Zukunft: 120. Kongress der Deutschen Gesellschaft für Chirurgie 29. April—2. Mai 2003, München*. 2003. Springer.
3. Hamilton, N., et al., *Tissue-engineered tracheal replacement in a child: A 4-year follow-up study*. American Journal of Transplantation, 2015. **15**(10): p. 2750-2757.
4. Etienne, H., et al., *Tracheal replacement*. European Respiratory Journal, 2018. **51**(2).
5. Crowley C, B.M., Seifalian AM., *Trachea transplantation: from laboratory to patient*, in *J Tissue Eng Regen Med*. 2015. p. 357-67.
6. Delaere, P., & Van Raemdonck, D., *Tracheal replacement*. Journal of thoracic disease, 2016. **8**(Suppl 2): p. S186.
7. Chiang, T., et al, *Clinical translation of tissue engineered trachea grafts*. Annals of Otolaryngology, Rhinology & Laryngology, 2016. **125**(11): p. 873-885.
8. Fabre, D., et al, *Successful tracheal replacement in humans using autologous tissues: an 8-year experience*. 2013. p. 1146-1155.
9. Hung, S.H., et al, *Preliminary experiences in trachea scaffold tissue engineering with segmental organ decellularization*. The Laryngoscope, 2016. **126**(11): p. 2520-2527.
10. Jia Xian Law, L.L.L., Bin Saim Aminuddin, et al, *Tissue-engineered trachea: A review*. International Journal of Pediatric Otorhinolaryngology, 2016. **91**: p. 55- 63.
11. Mark Weidenbecher, H.M.T., David A. Gilpin, and James E. Dennis, *Tissue-engineered trachea for airway reconstruction*. Laryngoscope, 2009. **119**(11): p. 2118–2123.
12. Kuttan, J.C., et al., *Decellularized tracheal extracellular matrix supports epithelial migration, differentiation, and function*. Tissue Engineering Part A, 2014. **21**(1-2): p. 75-84.
13. Virk, J.S., Zhang, H., Nouraei, R., & Sandhu, G., *Prosthetic reconstruction of the trachea: A historical perspective*. World Journal of Clinical Cases, 2017. **5**(4): p. 128.
14. Rose, K.-G., K. Sesterhenn, and F. Wustrow, *Tracheal allotransplantation in man*. The Lancet, 1979. **313**(8113): p. 433.
15. Batioglu-Karaaltin, A., et al., *In vivo tissue-engineered allogenic trachea transplantation in rabbits: a preliminary report*. Stem Cell Reviews and Reports, 2015. **11**(2): p. 347-356.
16. Haykal, S., et al, *The effect of decellularization of tracheal allografts on leukocyte infiltration and of recellularization on regulatory T cell recruitment*. Biomaterials, 2013. **34**(23): p. 5821-5832.
17. Fabre, D., et al., *Successful tracheal replacement in humans using autologous tissues: an 8-year experience*. The Annals of thoracic surgery, 2013. **96**(4): p. 1146-1155.
18. Saksena, R., et al, *Tubular organ epithelialisation*. Journal of tissue engineering, 2016. **7**.
19. Kojima, K., and Charles A. Vacanti, *Tissue engineering in the trachea*. The Anatomical Record, 2014. **297**(1): p. 44-50.
20. Abouarab, A.A., et al., *Current solutions for long-segment tracheal reconstruction*. Annals of thoracic and cardiovascular surgery, 2017: p. ra. 16-00251.
21. Grillo, H.C., *Surgery of the Trachea and Bronchi*. 2004: PMPH USA.
22. Belsey, R., *Resection and reconstruction of the intrathoracic trachea*. British journal of surgery, 1950. **38**(150): p. 200-205.
23. Abouarab, A.A., Elsayed, H. H., Elkhayat, H., Mostafa, A., Cleveland, D. C., & El Nori, A, *Current Solutions for Long-Segment Tracheal Reconstruction*. Annals of Thoracic and Cardiovascular Surgery, 2017. **23**(2): p. 66-75.

24. Walles, T., *Bioartificial tracheal grafts: can tissue engineering keep its promise?* Expert review of medical devices, 2004. **1**(2): p. 241-250.
25. Law, J.X., Liau, L.L., Aminuddin, B.S. and Ruszymah, B.H.I., *Tissue-engineered trachea: A review.* International journal of pediatric otorhinolaryngology, 2016. **91**: p. 55-63.
26. Law, J.X., et al., *Tissue-engineered trachea: A review.* International journal of pediatric otorhinolaryngology, 2016. **91**: p. 55-63.
27. Delaere, P. and D. Van Raemdonck, *Tracheal replacement.* Journal of Thoracic Disease, 2016. **8**(Suppl 2): p. S186.
28. Furlow, P.W. and D.J. Mathisen, *Surgical anatomy of the trachea.* Annals of cardiothoracic surgery, 2018. **7**(2): p. 255.
29. Mieczkowski, B. and B.F. Seavey, *Anatomy, Head and Neck, Trachea.* 2017.
30. Kim, H., et al., *Improved chondrogenic performance with protective tracheal design of Chitosan membrane surrounding 3D-printed trachea.* Scientific reports, 2021. **11**(1): p. 1-8.
31. Downey, R.P. and N.S. Samra, *Anatomy, Thorax, Tracheobronchial Tree.* 2020.
32. Downey, R.P. and N.S. Samra, *Anatomy, Thorax, Tracheobronchial Tree*, in *StatPearls [Internet]*. 2021, StatPearls Publishing.
33. Dimou, Z., et al., *Evaluation of a decellularization protocol for the development of a decellularized tracheal scaffold.* Anticancer research, 2019. **39**(1): p. 145-150.
34. Adamo, D., et al., *The Growing Medical Need for Tracheal Replacement: Reconstructive Strategies Should Overcome Their Limits.* Frontiers in Bioengineering and Biotechnology, 2022. **10**.
35. Kamel, K.S., G. Lau, and M.D. Stringer, *In vivo and in vitro morphometry of the human trachea.* Clinical Anatomy: The Official Journal of the American Association of Clinical Anatomists and the British Association of Clinical Anatomists, 2009. **22**(5): p. 571-579.
36. Brand-Saber, B.E. and T. Schäfer, *Trachea: anatomy and physiology.* Thoracic surgery clinics, 2014. **24**(1): p. 1-5.
37. Hennel, M., et al., *Structure of vagal afferent nerve terminal fibers in the mouse trachea.* Respiratory physiology & neurobiology, 2018. **249**: p. 35-46.
38. Canning, B. and D. Spina, *Sensory nerves and airway irritability.* Sensory Nerves, 2009: p. 139-183.
39. Audrit, K.J., et al., *The nervous system of airways and its remodeling in inflammatory lung diseases.* Cell and tissue research, 2017. **367**(3): p. 571-590.
40. Lawrence, D.A., et al., *The wonderful world of the windpipe: a review of central airway anatomy and pathology.* Canadian Association of Radiologists Journal, 2015. **66**(1): p. 30-43.
41. Allen, W.E., *diFiore's Atlas of Histology with Functional Correlations.* Journal of Anatomy, 2008. **213**(3): p. 357.
42. Nahumi, A., et al., *Tracheal Anatomy and Factors Contributing to Tissue Engineering.* Gene, Cell and Tissue, 2022(In Press).
43. Tao, M., et al., *Sterilization and disinfection methods for decellularized matrix materials: Review, consideration and proposal.* Bioactive Materials, 2021. **6**(9): p. 2927-2945.
44. Grillo, H.C., *Tracheal replacement: a critical review.* The Annals of thoracic surgery, 2002. **73**(6): p. 1995-2004.
45. George, C.E., et al., *COVID-19 symptoms are reduced by targeted hydration of the nose, larynx and trachea.* Scientific reports, 2022. **12**(1): p. 4599.
46. Bi, Y., et al., *Long-term outcomes of tracheal stents removal under fluoroscopy guidance: comparison of tracheal fistulas and tracheal stenosis.* BMC Pulmonary Medicine, 2021. **21**(1): p. 1-8.
47. Bibas, B.J., P.F.G. Cardoso, and K. Hoetzenecker, *The burden of tracheal stenosis and tracheal diseases health-care costs in the 21st century.* Translational Cancer Research, 2020. **9**(3): p. 2095.
48. Yao, Z.-Y., et al., *The Application of a Bone Marrow Mesenchymal Stem Cell Membrane in the Vascularization of a Decellularized Tracheal Scaffold.* Stem Cells International, 2021. **2021**.

49. Gao, M., et al., *Tissue-engineered trachea from a 3D-printed scaffold enhances whole-segment tracheal repair*. Scientific reports, 2017. **7**(1): p. 5246.
50. Zagalo, C., et al., *Morphology of trachea in benign human tracheal stenosis: a clinicopathological study of 20 patients undergoing surgery*. Surgical and Radiologic Anatomy, 2002. **24**(3/4): p. 160-168.
51. Mostafa, B.E., C. Chaouch-Mberek, and A. El Halafawi, *Tracheal stenosis: diagnosis and treatment*. 2012: Faculty of Medicine, Ain Shams University.
52. Hamilton, N.J., et al., *Tissue-Engineered Tracheal Replacement in a Child: A 4-Year Follow-Up Study*. Am J Transplant, 2015. **15**(10): p. 2750-7.
53. Fiacchini, G., et al., *Evaluation of the incidence and potential mechanisms of tracheal complications in patients with COVID-19*. JAMA Otolaryngology–Head & Neck Surgery, 2021. **147**(1): p. 70-76.
54. Damiano, G., et al., *Current Strategies for Tracheal Replacement: A Review*. Life, 2021. **11**(7): p. 618.
55. Fang, Y., et al., *Distinct stem/progenitor cells proliferate to regenerate the trachea, intrapulmonary airways and alveoli in COVID-19 patients*. Cell research, 2020. **30**(8): p. 705-707.
56. de Wit, R., et al., *Isolation of multipotent progenitor cells from pleura and pericardium for tracheal tissue engineering purposes*. Journal of Cellular and Molecular Medicine, 2021. **25**(23): p. 10869-10878.
57. Aoki, F.G., et al., *De-epithelialization of porcine tracheal allografts as an approach for tracheal tissue engineering*. Scientific reports, 2019. **9**(1): p. 1-12.
58. Gonfiotti, A., et al., *The first tissue-engineered airway transplantation: 5-year follow-up results*. The Lancet, 2014. **383**(9913): p. 238-244.
59. Johnson, C.M., et al., *The feasibility of gamma radiation sterilization for decellularized tracheal grafts*. The Laryngoscope, 2017. **127**(8): p. E258-E264.
60. Huang, H.-F., J.-J. Hwang, and P.-M. Huang, *Tracheal reconstruction with nail grafts: a novel approach*. JTCVS techniques, 2021. **10**: p. 554-560.
61. Pennarossa, G., et al., *Tracheal In Vitro Reconstruction Using a Decellularized Bio-Scaffold in Combination with a Rotating Bioreactor*, in *Bioreactors in Stem Cell Biology: Methods and Protocols*. 2021, Springer. p. 157-165.
62. Fayzullin, A., et al., *A defined road to tracheal reconstruction: laser structuring and cell support for rapid clinic translation*. Stem cell research & therapy, 2022. **13**(1): p. 1-22.
63. Vacanti, J.P. and R. Langer, *Tissue engineering: the design and fabrication of living replacement devices for surgical reconstruction and transplantation*. The lancet, 1999. **354**: p. S32-S34.
64. Merckx, G., et al., *Chorioallantoic membrane assay as model for angiogenesis in tissue engineering: Focus on stem cells*. Tissue Engineering Part B: Reviews, 2020. **26**(6): p. 519-539.
65. Pellegata, A.F., A.M. Tedeschi, and P. De Coppi, *Whole organ tissue vascularization: engineering the tree to develop the fruits*. Frontiers in bioengineering and biotechnology, 2018. **6**: p. 56.
66. Barbulescu, G.I., et al., *Decellularized extracellular matrix scaffolds for cardiovascular tissue engineering: Current techniques and challenges*. International journal of molecular sciences, 2022. **23**(21): p. 13040.
67. Gilpin, A. and Y. Yang, *Decellularization strategies for regenerative medicine: from processing techniques to applications*. BioMed research international, 2017. **2017**.
68. Hagmann, S., et al., *Different culture media affect growth characteristics, surface marker distribution and chondrogenic differentiation of human bone marrow-derived mesenchymal stromal cells*. BMC musculoskeletal disorders, 2013. **14**(1): p. 1-11.
69. de Sá Schiavo Matias, G., et al., *In vivo biocompatibility analysis of the recellularized canine tracheal scaffolds with canine epithelial and endothelial progenitor cells*. Bioengineered, 2022. **13**(2): p. 3551-3565.

70. Tsao, C.-K., et al., *An ectopic approach for engineering a vascularized tracheal substitute*. *Biomaterials*, 2014. **35**(4): p. 1163-1175.
71. Jungebluth, P., et al., *Tracheal tissue engineering in rats*. *Nature protocols*, 2014. **9**(9): p. 2164-2179.
72. Elliott, M.J., et al., *Tracheal replacement therapy with a stem cell-seeded graft: lessons from compassionate use application of a GMP-compliant tissue-engineered medicine*. *Stem cells translational medicine*, 2017. **6**(6): p. 1458-1464.
73. Samura, M., Hosoyama, T., Takeuchi, Y., et.al, *Therapeutic strategies for cell-based neovascularization in critical limb ischemia*. *Journal of translational medicine*, 2017. **15**(1): p. 49.
74. Sun, X.T., Ding, Y. T., Yan, X. G., Wu, L. Y., Li, Q., Cheng, N., ... & Zhang, M. Y., *Angiogenic synergistic effect of basic fibroblast growth factor and vascular endothelial growth factor in an in vitro quantitative microcarrier-based three-dimensional fibrin angiogenesis system.*, in *World journal of gastroenterology: WJG*. 2004. p. 2524.
75. Gao, J., Huang, Y., Li, M., Zhao, H., Zhao, Y., Li, R., ... & Qiao, J., *Effect of local basic fibroblast growth factor and vascular endothelial growth factor on subcutaneously allotransplanted ovarian tissue in ovariectomized mice.*, in *PloS one*. 2015. p. e0134035.
76. Zhang, Z., Slobodianski, A., Ito, W. D., Arnold, A., Nehlsen, J., Weng, S., ... & Müller, D. F., *Enhanced collateral growth by double transplantation of gene-nucleofected fibroblasts in ischemic hindlimb of rats.*, in *PloS one*. 2011. p. e19192.
77. Agnieszka Jazwa, P.K., Justyna Leja, et.al, *Combined vascular endothelial growth factor-A and fibroblast growth factor 4 gene transfer improves wound healing in diabetic mice*. *Genet Vaccines Ther*, 2010. **6**.
78. Zhang H, K.A., Lay YE, Fierro FA, Chen H, Lane NE, Yao W, *Acceleration of Fracture Healing by Overexpression of Basic Fibroblast Growth Factor in the Mesenchymal Stromal Cells*, in *Stem Cells Transl Med*. 2017. p. 1880-1893.
79. Makoto Komura, H.K., Kenichi Ikebukuro, Atsuhiko Hikita, Kazuto Hoshi, and Tsuyoshi Takato, *Tracheal cartilage growth by intratracheal injection of basic fibroblast growth factor*, in *Journal of Pediatric Surgery*. 2017. p. 235-238.
80. Caplan, A.I., *Mesenchymal Stem Cells: Time to Change the Name!*, in *Stem cells translational medicine*. 2017. p. 1445-1451.
81. Wuchter, P., et al., *Standardization of Good Manufacturing Practice-compliant production of bone marrow-derived human mesenchymal stromal cells for immunotherapeutic applications*. *Cytotherapy*, 2015. **17**(2): p. 128-139.
82. Dominici, M., et al., *Minimal criteria for defining multipotent mesenchymal stromal cells. The International Society for Cellular Therapy position statement*. *Cytotherapy*, 2006. **8**(4): p. 315-317.
83. Secunda, R., Vennila, R., Mohanashankar, A. M., Rajasundari, M., Jeswanth, S., & Surendran, R., *Isolation, expansion and characterisation of mesenchymal stem cells from human bone marrow, adipose tissue, umbilical cord blood and matrix: a comparative study.*, in *Cytotechnology*. 2015. p. 793-807.
84. Pelekanos, R.A., Sardesai, V. S., Futrega, K., Lott, W. B., Kuhn, M., & Doran, M. R., *Isolation and expansion of mesenchymal stem/stromal cells derived from human placenta tissue.*, in *ournal of visualized experiments: JoVE*. 2016. p. 112.
85. Talwadekar, M.D., Kale, V. P., & Limaye, L. S., *Placenta-derived mesenchymal stem cells possess better immunoregulatory properties compared to their cord-derived counterparts-a paired sample study.* , in *Scientific reports*. 2015. p. 5.
86. Tsai, A.I., Hong, H. H., Lin, W. R., Fu, J. F., Chang, C. C., Wang, I., ... & Yen, T. H., *Isolation of Mesenchymal Stem Cells from Human Deciduous Teeth Pulp*, in *BioMed research international*. 2017.
87. Spees, J.L., Lee, R. H., & Gregory, C. A., *Mechanisms of mesenchymal stem/stromal cell function*, in *Stem cell research & therapy*. 2016. p. 125.

88. Watt, S.M., Gullo, F., van der Garde, M., Markeson, D., Camicia, R., Khoo, C. P., & Zwaginga, J. J., *The angiogenic properties of mesenchymal stem/stromal cells and their therapeutic potential*, in *British medical bulletin*. 2013. p. 25-53.
89. Fierro, F.A., Kalomoiris, S., Sondergaard, C. S., & Nolte, J. A., *Effects on proliferation and differentiation of multipotent bone marrow stromal cells engineered to express growth factors for combined cell and gene therapy*, in *Stem Cells*. 2011. p. 1727-1737.
90. Laco, F., et al., *The dose effect of human bone marrow-derived mesenchymal stem cells on epidermal development in organotypic co-culture*. *Journal of dermatological science*, 2009. **55**(3): p. 150-160.
91. Yates, C.C., Rodrigues, M., Nuschke, A., Johnson, Z. I., Whaley, D., Stolz, D., ... & Wells, A., *Multipotent stromal cells/mesenchymal stem cells and fibroblasts combine to minimize skin hypertrophic scarring.*, in *Stem cell research & therapy*. 2017. p. 193.
92. Smith, A.N., Willis, E., Chan, V. T., Muffley, L. A., Isik, F. F., Gibran, N. S., & Hocking, A. M., *Mesenchymal stem cells induce dermal fibroblast responses to injury*, in *Experimental cell research*. 2010. p. 48-54.
93. Fan, H., Liu, H., Toh, S. L., & Goh, J. C., *Enhanced differentiation of mesenchymal stem cells co-cultured with ligament fibroblasts on gelatin/silk fibroin hybrid scaffold.*, in *Biomaterials*. 2008. p. 1017-1027.
94. Yuval Rinkevich, G.G.W., Michael S. Hu, Zeshaan N. Maan, Aaron M. Newman, Micha Drukker, Michael Januszyk, Geoffrey W. Krampitz, Geoffrey C. Gurtner, H. Peter Lorenz, Irving L. Weissman, and Michael T. Longaker, *Identification and isolation of a dermal lineage with intrinsic fibrogenic potential*, in *Science*. 2016.
95. Alberts B, J.A., Lewis J, et al, *Molecular Biology of the Cell-Fibroblasts and Their Transformations: The Connective-Tissue Cell Family*. 2002, New York: Garland Science.
96. Marcos Perez-Basterrechea, M.M.E., Maria Alvarez-Viejo, Tania Fontanil, Santiago Cal, Marta Sanchez Pitiot, Jesus Otero, and Alvaro Jesus Obaya, *Fibroblasts accelerate islet revascularization and improve long-term graft survival in a mouse model of subcutaneous islet transplantation* in *PLOS one*. 2017.
97. Kühbacher, A., Henkel, H., Stevens, P., Grumaz, C., Finkelmeier, D., Burger-Kentischer, A., ... & Rupp, S., *Central Role for Dermal Fibroblasts in Skin Model Protection against Candida albicans*. *The Journal of infectious diseases*, 2017. **215**(11): p. 1742-1752.
98. Bautista-Hernández, L.A., Gómez-Olivares, J. L., Buentello-Volante, B., & Bautista-de Lucio, V. M., *Fibroblasts: the unknown sentinels eliciting immune responses against microorganisms*. *European Journal of Microbiology and Immunology*, 2017. **7**(3): p. 151-157.
99. Tigges, J., Krutmann, J., Fritsche, E., Haendeler, J., Schaal, H., Fischer, J. W., ... & Ventura, N., *The hallmarks of fibroblast ageing*. *The hallmarks of fibroblast ageing*, 2014. **138**: p. 26-44.
100. Tracy, L.E., Minasian, R. A., & Caterson, E. J., *Extracellular matrix and dermal fibroblast function in the healing wound*. *Advances in wound care*, 2016. **5**(3): p. 119-136.
101. Newman, A.C., Nakatsu, M. N., Chou, W., Gershon, P. D., & Hughes, C. C., *The requirement for fibroblasts in angiogenesis: fibroblast-derived matrix proteins are essential for endothelial cell lumen formation*. *Molecular biology of the cell*, 2011. **22**(20): p. 3791-3800.
102. Nakatsu, M.N., Sainson, R. C., Aoto, J. N., Taylor, K. L., Aitkenhead, M., Pérez-del-Pulgar, S., ... & Hughes, C. C., *Angiogenic sprouting and capillary lumen formation modeled by human umbilical vein endothelial cells (HUVEC) in fibrin gels: the role of fibroblasts and Angiopoietin-1*. *Microvascular research*, 2003. **66**(2): p. 102-112.
103. Sukmana, I., & Vermette, P., *The effects of co-culture with fibroblasts and angiogenic growth factors on microvascular maturation and multi-cellular lumen formation in HUVEC-oriented polymer fibre constructs*. *Biomaterials*, 2010. **31**(19): p. 5091-5099.
104. Maughan, E.F., Hynds, R. E., Proctor, T. J., Janes, S. M., Elliott, M., Birchall, M. A., ... & De Coppi, P., *Autologous Cell Seeding in Tracheal Tissue Engineering.*, in *Current stem cell reports*. 2017. p. 279-289.

105. Kobayashi, K., et al, *Effect of fibroblasts on tracheal epithelial regeneration in vitro*. Tissue engineering, 2006. **12**(9): p. 2619-2628.
106. Nomoto, Y., et al., *Effect of fibroblasts on epithelial regeneration on the surface of a bioengineered trachea*. Annals of Otology, Rhinology & Laryngology, 2008. **117**(1): p. 59-64.
107. Burnouf T, S.D., Koh MB, and Schallmoser K, *Human platelet lysate: Replacing fetal bovine serum as a gold standard for human cell propagation?* Biomaterials. , 2016. **76**: p. 371-87.
108. Pilgrim, C.R., et al., *A review of fetal bovine serum in the culture of mesenchymal stromal cells and potential alternatives for veterinary medicine*. Frontiers in Veterinary Science, 2022. **9**: p. 859025.
109. Van der Valk, J., et al., *Fetal bovine serum (FBS): past–present–future*. Altex, 2018. **35**(1): p. 1-20.
110. Minonzio, G. and E. Linetsky, *The Use of fetal bovine serum in cellular products for clinical applications: commentary*. CellR4, 2014. **2**(6): p. e1307.
111. Astori, G., et al, *Platelet lysate as a substitute for animal serum for the ex-vivo expansion of mesenchymal stem/stromal cells: present and future*. Stem cell research & therapy, 2016. **7**(1): p. 93.
112. Chelladurai, K.S., et al., *Alternative to FBS in animal cell culture-An overview and future perspective*. Heliyon, 2021. **7**(8).
113. Guiotto, M., et al., *Human platelet lysate to substitute fetal bovine serum in hMSC expansion for translational applications: a systematic review*. Journal of Translational Medicine, 2020. **18**(1): p. 1-14.
114. de Wildt, B.W., K. Ito, and S. Hofmann, *Human platelet lysate as alternative of fetal bovine serum for enhanced human in vitro bone resorption and remodeling*. Frontiers in immunology, 2022. **13**: p. 915277.
115. Seidelmann, N., et al., *Human platelet lysate as a replacement for fetal bovine serum in human corneal stromal keratocyte and fibroblast culture*. Journal of Cellular and Molecular Medicine, 2021. **25**(20): p. 9647-9659.
116. Gstraunthaler, G., et al, *Preparation of Platelet Lysates for Mesenchymal Stem Cell Culture Media*. J Stem Cells Res. Rev & Rep, 2015. **2**(1): p. 1021.
117. Patrick Wuchter, K.B., Hubert Schrezenmeier, Martin Bornhäuser, Lutz P. Müller, Halvard Bönig, Wolfgang Wagner, Roland Meisel, Petra Pavel, Torsten Tonn, Peter Lang, Ingo Müller, Matthias Renner, Georg Malcherek, Rainer Saffrich,et.al., *Standardization of Good Manufacturing Practice–compliant production of bone marrow–derived human mesenchymal stromal cells for immunotherapeutic applications*. Cytotherapy, 2015. **17**(2): p. 128-139.
118. Wu, R.X., et al, *Platelet lysate supports the in vitro expansion of human periodontal ligament stem cells for cytotherapeutic use*. Journal of tissue engineering and regenerative medicine, 2017. **11**(8): p. 2261-2275.
119. Del Bue, M., et al, *Platelet lysate promotes in vitro proliferation of equine mesenchymal stem cells and tenocytes*. Veterinary research communications, 2007. **31**: p. 289-292.
120. Chevallier, N., et al, *Osteoblastic differentiation of human mesenchymal stem cells with platelet lysate*. Biomaterials, 2010. **31**(2): p. 270-278.
121. Barsotti, M.C., et al, *Effect of platelet lysate on human cells involved in different phases of wound healing*. PLoS One, 2013. **8**(12): p. e84753.
122. Hildner, F., et al, *Human platelet lysate successfully promotes proliferation and subsequent chondrogenic differentiation of adipose-derived stem cells: a comparison with articular chondrocytes*. Journal of tissue engineering and regenerative medicine, 2015. **9**(7): p. 808-818.
123. Fortunato, T.M., et al, *Platelet lysate gel and endothelial progenitors stimulate microvascular network formation in vitro: tissue engineering implications*. Scientific reports, 2016. **6**: p. 25326.
124. Masoudi, E.A., et al, *Platelet-rich blood derivatives for stem cell-based tissue engineering and regeneration*. Current stem cell reports, 2016. **2**(1): p. 33-42.

125. Kølle, S.-F.T., et al, *Pooled human platelet lysate versus fetal bovine serum—investigating the proliferation rate, chromosome stability and angiogenic potential of human adipose tissue-derived stem cells intended for clinical use*. *Cytotherapy*, 2013. **15**(9): p. 1086-1097.
126. Zhang, Z., et al., *Enhanced collateral growth by double transplantation of gene-nucleofected fibroblasts in ischemic hindlimb of rats*. *PLoS one*, 2011. **6**(4): p. e19192.
127. May, R.D., et al., *Efficient nonviral transfection of primary intervertebral disc cells by electroporation for tissue engineering application*. *Tissue Engineering Part C: Methods*, 2017. **23**(1): p. 30-37.
128. Agostini, F., et al., *Nucleofection of Adipose Mesenchymal Stem/Stromal Cells: Improved Transfection Efficiency for GMP Grade Applications*. *Cells*, 2021. **10**(12): p. 3412.
129. Kelly, A.M., et al., *Glucocorticoid Cell Priming Enhances Transfection Outcomes in Adult Human Mesenchymal Stem Cells*. *Mol Ther*, 2016. **24**(2): p. 331-341.
130. Mellott, A.J., et al., *Improving viability and transfection efficiency with human umbilical cord wharton's jelly cells through use of a ROCK inhibitor*. *Cellular reprogramming*, 2014. **16**(2): p. 91-97.
131. Distler, J.H., et al., *Nucleofection: a new, highly efficient transfection method for primary human keratinocytes*. *Experimental dermatology*, 2005. **14**(4): p. 315-320.
132. Hosseini, S., et al., *Comparative evaluation of autologous platelet-rich plasma and platelet lysate in patients with knee osteoarthritis*. *Growth Factors*, 2023: p. 1-13.
133. Guiotto, M., et al., *Is human platelet lysate (hPL) the ideal candidate to substitute the foetal bovine serum for cell-therapy translational research?* *Journal of Translational Medicine*, 2021. **19**: p. 1-3.
134. Masoudi, E.A., et al., *Platelet-rich blood derivatives for stem cell-based tissue engineering and regeneration*. *Current stem cell reports*, 2016. **2**: p. 33-42.
135. Berndt, S., et al., *Angiogenesis is differentially modulated by platelet-derived products*. *Biomedicine*, 2021. **9**(3): p. 251.
136. Kim, M.K., et al., *Human platelet-rich plasma facilitates angiogenesis to restore impaired uterine environments with Asherman's syndrome for embryo implantation and following pregnancy in mice*. *Cells*, 2022. **11**(9): p. 1549.
137. Wright, A., M.L. Arthaud-Day, and M.L. Weiss, *Therapeutic use of mesenchymal stromal cells: the need for inclusive characterization guidelines to accommodate all tissue sources and species*. *Frontiers in cell and developmental biology*, 2021. **9**: p. 632717.
138. Suvakov, S., et al., *Targeting senescence improves angiogenic potential of adipose-derived mesenchymal stem cells in patients with preeclampsia*. *Biology of sex differences*, 2019. **10**(1): p. 1-13.
139. Ratushnyy, A., M. Ezdakova, and L. Buravkova, *Secretome of senescent adipose-derived mesenchymal stem cells negatively regulates angiogenesis*. *International Journal of Molecular Sciences*, 2020. **21**(5): p. 1802.
140. Spohn, G., et al., *More Human BM-MSC With Similar Subpopulation Composition and Functional Characteristics Can Be Produced With a GMP-Compatible Fabric Filter System Compared to Density Gradient Technique*. *Frontiers in cell and developmental biology*, 2021. **9**: p. 638798.
141. Lindström, H.J.G. and R. Friedman, *Inferring time-dependent population growth rates in cell cultures undergoing adaptation*. *BMC bioinformatics*, 2020. **21**(1): p. 1-13.
142. Sareen, N., et al., *Early passaging of mesenchymal stem cells does not instigate significant modifications in their immunological behavior*. *Stem Cell Research & Therapy*, 2018. **9**(1): p. 1-11.
143. Fernandez-Rebollo, E., et al., *Human Platelet Lysate versus Fetal Calf Serum: These Supplements Do Not Select for Different Mesenchymal Stromal Cells*. *Sci Rep*, 2017. **7**(1): p. 5132.
144. Longhin, E.M., et al., *The alamar blue assay in the context of safety testing of nanomaterials*. *Frontiers in Toxicology*, 2022. **4**: p. 981701.

145. Kaja, S., et al., *Quantification of lactate dehydrogenase for cell viability testing using cell lines and primary cultured astrocytes*. Current protocols in toxicology, 2017. **72**(1): p. 2.26. 1-2.26. 10.
146. Hennessy, R.S., et al., *Supercritical carbon dioxide–based sterilization of decellularized heart valves*. Basic to translational science, 2017. **2**(1): p. 71-84.
147. Dohmen, P.M., et al., *Histological evaluation of tissue-engineered heart valves implanted in the juvenile sheep model: is there a need for in-vitro seeding?* The Journal of heart valve disease, 2006. **15**(6): p. 823-829.
148. Fidalgo, C., et al., *A sterilization method for decellularized xenogeneic cardiovascular scaffolds*. Acta Biomaterialia, 2018. **67**: p. 282-294.
149. Soundararajan, M. and S. Kannan, *Fibroblasts and mesenchymal stem cells: Two sides of the same coin?* Journal of cellular physiology, 2018. **233**(12): p. 9099-9109.
150. Brohem, C., et al., *Comparison between fibroblasts and mesenchymal stem cells derived from dermal and adipose tissue*. International journal of cosmetic science, 2013. **35**(5): p. 448-457.
151. Denu, R.A., et al., *Fibroblasts and mesenchymal stromal/stem cells are phenotypically indistinguishable*. Acta haematologica, 2016. **136**(2): p. 85-97.
152. Vaculik, C., et al., *Human dermis harbors distinct mesenchymal stromal cell subsets*. Journal of Investigative Dermatology, 2012. **132**(3): p. 563-574.
153. Jääger, K. and T. Neuman, *Human dermal fibroblasts exhibit delayed adipogenic differentiation compared with mesenchymal stem cells*. Stem cells and development, 2011. **20**(8): p. 1327-1336.
154. Ichim, T.E., P. O’Heeron, and S. Kesari, *Fibroblasts as a practical alternative to mesenchymal stem cells*. Journal of translational medicine, 2018. **16**(1): p. 1-9.
155. Xiao, B., et al., *Flow cytometry-based assessment of mitophagy using MitoTracker*. 2016, Frontiers Media SA. p. 76.
156. Zhang, Z., et al., *High efficiency low cost fibroblast nucleofection for GMP compatible cell-based gene therapy*. International Journal of Medical Sciences, 2017. **14**(9): p. 798.
157. Nakamichi, M., et al., *Basic fibroblast growth factor induces angiogenic properties of fibrocytes to stimulate vascular formation during wound healing*. The American journal of pathology, 2016. **186**(12): p. 3203-3216.
158. Holmes, D.I. and I. Zachary, *The vascular endothelial growth factor (VEGF) family: angiogenic factors in health and disease*. Genome biology, 2005. **6**(2): p. 1-10.
159. Al Belushi, H., *Development and characterisation of MSC-seeded decellularised airway scaffolds for regenerative bioengineering*. 2020, UCL (University College London).
160. Moreno-Jiménez, I., et al., *The chorioallantoic membrane (CAM) assay for the study of human bone regeneration: a refinement animal model for tissue engineering*. Scientific reports, 2016. **6**(1): p. 1-12.
161. Ribatti, D., *The chick embryo chorioallantoic membrane (CAM) assay*. Reproductive toxicology, 2017. **70**: p. 97-101.
162. Naik, M., P. Brahma, and M. Dixit, *A cost-effective and efficient chick ex-ovo CAM assay protocol to assess angiogenesis*. Methods and protocols, 2018. **1**(2): p. 19.
163. Schmitd, L.B., et al., *The chick chorioallantoic membrane in vivo model to assess perineural invasion in head and neck cancer*. JoVE (Journal of Visualized Experiments), 2019(148): p. e59296.
164. Sys, G.M., et al., *The in ovo CAM-assay as a xenograft model for sarcoma*. JoVE (Journal of Visualized Experiments), 2013(77): p. e50522.
165. Greaney, A.M., et al., *Platform effects on regeneration by pulmonary basal cells as evaluated by single-cell RNA sequencing*. Cell reports, 2020. **30**(12): p. 4250-4265. e6.
166. Ravindran, A., et al., *An optimized protocol for the isolation and functional analysis of human lung mast cells*. Frontiers in immunology, 2018. **9**: p. 2193.

167. Woloszyk, A. and T.A. Mitsiadis, *Angiogenesis within stem cell–seeded silk scaffolds cultured on the chorioallantoic membrane and visualized by 3D imaging*. *Current Protocols in Stem Cell Biology*, 2017. **41**(1): p. 1F. 19.1-1F. 19.9.
168. Woloszyk, A., et al., *Novel multimodal MRI and MicroCT imaging approach to quantify angiogenesis and 3D vascular architecture of biomaterials*. *Scientific reports*, 2019. **9**(1): p. 1-14.
169. Ames, J.J., et al., *Methods for analyzing tumor angiogenesis in the chick chorioallantoic membrane model*, in *Breast Cancer*. 2016, Springer. p. 255-269.
170. Woloszyk, A., D. Liccardo, and T.A. Mitsiadis, *Three-dimensional imaging of the developing vasculature within stem cell-seeded scaffolds cultured in ovo*. *Frontiers in Physiology*, 2016. **7**: p. 146.
171. Zhang, W., et al., *VEGF and BMP-2 promote bone regeneration by facilitating bone marrow stem cell homing and differentiation*. *Eur Cell Mater*, 2014. **27**(12): p. 1-11.
172. Gu, J., et al., *Construction of nanofibrous scaffolds with interconnected perfusable microchannel networks for engineering of vascularized bone tissue*. *Bioactive materials*, 2021. **6**(10): p. 3254-3268.
173. Royet, A., et al., *Ephrin-B3 supports glioblastoma growth by inhibiting apoptosis induced by the dependence receptor EphA4*. *Oncotarget*, 2017. **8**(14): p. 23750.
174. Baudino, T.A., et al., *c-Myc is essential for vasculogenesis and angiogenesis during development and tumor progression*. *Genes & development*, 2002. **16**(19): p. 2530-2543.
175. Woloszyk, A., D. Liccardo, and T.A. Mitsiadis, *Three-Dimensional Imaging of the Developing Vasculature within Stem Cell-Seeded Scaffolds Cultured in ovo*. *Front Physiol*, 2016. **7**: p. 146.
176. Annese, T., R. Tamma, and D. Ribatti, *IKOSA® CAM Assay Application to Quantify Blood Vessels on Chick Chorioallantoic Membrane (CAM)*, in *Tumor Angiogenesis Assays: Methods and Protocols*. 2022, Springer. p. 129-139.
177. Pamies, D., et al., *Guidance document on good cell and tissue culture practice 2.0 (GCCP 2.0)*. 2022.
178. Schallmoser, K., et al., *Human platelet lysate can replace fetal bovine serum for clinical-scale expansion of functional mesenchymal stromal cells*. *Transfusion*, 2007. **47**(8): p. 1436-46.
179. Azouna, N.B., et al., *Phenotypical and functional characteristics of mesenchymal stem cells from bone marrow: comparison of culture using different media supplemented with human platelet lysate or fetal bovine serum*. *Stem cell research & therapy*, 2012. **3**: p. 1-14.
180. Shafiee, S., et al., *Recent Advances on Cell-Based Co-Culture Strategies for Prevascularization in Tissue Engineering*. *Frontiers in Bioengineering and Biotechnology*, 2021. **9**.
181. Brennan, M.A., J.-M. Davaine, and P. Layrolle, *Pre-vascularization of bone tissue-engineered constructs*. *Stem cell research & therapy*, 2013. **4**(4): p. 1-3.
182. Nitzsche, B., et al., *Coalescent angiogenesis—evidence for a novel concept of vascular network maturation*. *Angiogenesis*, 2022. **25**(1): p. 35-45.
183. Udan, R.S., J.C. Culver, and M.E. Dickinson, *Understanding vascular development*. *Wiley Interdisciplinary Reviews: Developmental Biology*, 2013. **2**(3): p. 327-346.
184. Ruger, B.M., et al., *De novo vessel formation through cross-talk of blood-derived cells and mesenchymal stromal cells in the absence of pre-existing vascular structures*. *Frontiers in bioengineering and biotechnology*, 2020. **8**: p. 602210.
185. Mitchell, G.M. and W.A. Morrison, *In Vitro and In Vivo Approaches for Prevascularization of Three-Dimensional Engineered Tissues*. *Vascularization for Tissue Engineering and Regenerative Medicine*, 2021: p. 449-474.
186. Tilkorn, D.J., et al., *Implanted myoblast survival is dependent on the degree of vascularization in a novel delayed implantation/prevascularization tissue engineering model*. *Tissue Engineering Part A*, 2010. **16**(1): p. 165-178.
187. Tanaka, Y., et al., *Generation of an autologous tissue (matrix) flap by combining an arteriovenous shunt loop with artificial skin in rats: preliminary report*. *British journal of plastic surgery*, 2000. **53**(1): p. 51-57.

188. Erol, Ö.O. and M. Spira, *New capillary bed formation with a surgically constructed arteriovenous fistula*. Plastic and reconstructive surgery, 1980. **66**(1): p. 109-115.
189. Laschke, M.W. and M.D. Menger, *Prevascularization in tissue engineering: current concepts and future directions*. Biotechnology advances, 2016. **34**(2): p. 112-121.
190. Caplan, A.I., *Mesenchymal stem cells*. Journal of orthopaedic research, 1991. **9**(5): p. 641-650.
191. Horwitz, E., et al., *Clarification of the nomenclature for MSC: The International Society for Cellular Therapy position statement*. Cytotherapy, 2005. **7**(5): p. 393-395.
192. Fazzina, R., et al., *Potency testing of mesenchymal stromal cell growth expanded in human platelet lysate from different human tissues*. Stem cell research & therapy, 2016. **7**(1): p. 1-16.
193. Pittenger, M.F., et al., *Mesenchymal stem cell perspective: cell biology to clinical progress*. NPJ Regenerative medicine, 2019. **4**(1): p. 22.
194. Leuning, D.G., et al., *Clinical-grade isolated human kidney perivascular stromal cells as an organotypic cell source for kidney regenerative medicine*. Stem Cells Translational Medicine, 2017. **6**(2): p. 405-418.
195. Leuning, D.G., et al., *A novel clinical grade isolation method for human kidney perivascular stromal cells*. JoVE (Journal of Visualized Experiments), 2017(126): p. e55841.
196. Kim, H.K., et al., *A subset of paracrine factors as efficient biomarkers for predicting vascular regenerative efficacy of mesenchymal stromal/stem cells*. Stem Cells, 2019. **37**(1): p. 77-88.
197. Maacha, S., et al., *Paracrine mechanisms of mesenchymal stromal cells in angiogenesis*. Stem cells international, 2020. **2020**.
198. Costa-Almeida, R., et al., *Fibroblast-endothelial partners for vascularization strategies in tissue engineering*. Tissue Engineering Part A, 2015. **21**(5-6): p. 1055-1065.
199. Buechler, M.B., et al., *Cross-tissue organization of the fibroblast lineage*. Nature, 2021. **593**(7860): p. 575-579.
200. Costa-Almeida, R., R. Soares, and P.L. Granja, *Fibroblasts as maestros orchestrating tissue regeneration*. Journal of tissue engineering and regenerative medicine, 2018. **12**(1): p. 240-251.
201. Lysy, P.A., et al., *Human skin fibroblasts: From mesodermal to hepatocyte-like differentiation*. Hepatology, 2007. **46**(5): p. 1574-1585.
202. Álvarez-Viejo, M., Y. Menéndez-Menéndez, and J. Otero-Hernández, *CD271 as a marker to identify mesenchymal stem cells from diverse sources before culture*. World journal of stem cells, 2015. **7**(2): p. 470.
203. Calabrese, G., et al., *Potential effect of CD271 on human mesenchymal stromal cell proliferation and differentiation*. International journal of molecular sciences, 2015. **16**(7): p. 15609-15624.
204. De Barros, S., et al., *Aging-related decrease of human ASC angiogenic potential is reversed by hypoxia preconditioning through ROS production*. Molecular Therapy, 2013. **21**(2): p. 399-408.
205. Kim, H.-K., et al., *A subset of paracrine factors as efficient biomarkers for predicting vascular regenerative efficacy of mesenchymal stromal/stem cells*. Stem Cells, 2019. **37**(1): p. 77-88.
206. Neri, S., *Genetic stability of mesenchymal stromal cells for regenerative medicine applications: a fundamental biosafety aspect*. International journal of molecular sciences, 2019. **20**(10): p. 2406.
207. Yan, L., et al., *Growth factors-based beneficial effects of platelet lysate on umbilical cord-derived stem cells and their synergistic use in osteoarthritis treatment*. Cell death & disease, 2020. **11**(10): p. 857.
208. Wilson, A., et al., *Multiplicity of mesenchymal stromal cells: finding the right route to therapy*. Frontiers in immunology, 2019. **10**: p. 1112.
209. Becherucci, V., et al., *Human platelet lysate in mesenchymal stromal cell expansion according to a GMP grade protocol: a cell factory experience*. Stem cell research & therapy, 2018. **9**(1): p. 1-10.
210. Xu, L. and G. Li, *Circulating mesenchymal stem cells and their clinical implications*. Journal of Orthopaedic Translation, 2014. **2**(1): p. 1-7.

211. Bhat, S., et al., *Expansion and characterization of bone marrow derived human mesenchymal stromal cells in serum-free conditions*. Scientific Reports, 2021. **11**(1): p. 3403.
212. Fekete, N., et al., *Platelet lysate from whole blood-derived pooled platelet concentrates and apheresis-derived platelet concentrates for the isolation and expansion of human bone marrow mesenchymal stromal cells: production process, content and identification of active components*. Cytotherapy, 2012.
213. Reis, M., et al., *Global phenotypic characterisation of human platelet lysate expanded MSCs by high-throughput flow cytometry*. Scientific reports, 2018. **8**(1): p. 3907.
214. Fernandez-Rebollo, E., et al., *Human platelet lysate versus fetal calf serum: these supplements do not select for different mesenchymal stromal cells*. Scientific reports, 2017. **7**(1): p. 5132.
215. Henschler, R., et al., *Human platelet lysate current standards and future developments*. Transfusion, 2019. **59**(4): p. 1407-1413.
216. Kakudo, N., et al., *Differences between the proliferative effects of human platelet lysate and fetal bovine serum on human adipose-derived stem cells*. Cells, 2019. **8**(10): p. 1218.
217. Fernandez Munoz, B., et al., *A proprietary GMP human platelet lysate for the expansion of dermal fibroblasts for clinical applications*. Platelets, 2022. **33**(1): p. 98-109.
218. Wollmann, L., et al., *Characterization of decellularized human pericardium for tissue engineering and regenerative medicine applications*. Arquivos brasileiros de cardiologia, 2019. **113**: p. 11-17.
219. Niklason, L.E. and J.H. Lawson, *Bioengineered human blood vessels*. Science, 2020. **370**(6513): p. eaaw8682.
220. Wang, X., V. Chan, and P.R. Corridon, *Decellularized blood vessel development: Current state-of-the-art and future directions*. Frontiers in Bioengineering and Biotechnology, 2022. **10**: p. 951644.
221. Poliseti, N., et al., *A decellularized human corneal scaffold for anterior corneal surface reconstruction*. Scientific reports, 2021. **11**(1): p. 2992.
222. Pereira, A.R., M. Rudert, and M. Herrmann, *Decellularized human bone as a 3D model to study skeletal progenitor cells in a natural environment*, in *Methods in Cell Biology*. 2020, Elsevier. p. 123-141.
223. Ren, X., et al., *Engineering pulmonary vasculature in decellularized rat and human lungs*. Nature biotechnology, 2015. **33**(10): p. 1097-1102.
224. Wagner, D.E., et al., *Comparative decellularization and recellularization of normal versus emphysematous human lungs*. Biomaterials, 2014. **35**(10): p. 3281-3297.
225. Han, G.-H., et al., *Therapeutic strategies for peripheral nerve injury: decellularized nerve conduits and Schwann cell transplantation*. Neural regeneration research, 2019. **14**(8): p. 1343.
226. Baiguera, S., et al., *Long-term changes to in vitro preserved bioengineered human trachea and their implications for decellularized tissues*. Biomaterials, 2012. **33**(14): p. 3662-3672.
227. Ogunlade, O., et al., *Monitoring neovascularization and integration of decellularized human scaffolds using photoacoustic imaging*. Photoacoustics, 2019. **13**: p. 76-84.
228. Butler, C.R., et al., *Vacuum-assisted decellularization: an accelerated protocol to generate tissue-engineered human tracheal scaffolds*. Biomaterials, 2017. **124**: p. 95-105.
229. Zhang, X., et al., *Decellularized extracellular matrix scaffolds: Recent trends and emerging strategies in tissue engineering*. Bioactive materials, 2022. **10**: p. 15-31.
230. Goecke, T., et al., *In vivo performance of freeze-dried decellularized pulmonary heart valve allo- and xenografts orthotopically implanted into juvenile sheep*. Acta biomaterialia, 2018. **68**: p. 41-52.
231. Qiu, S., et al., *Decellularized nerve matrix hydrogel and glial-derived neurotrophic factor modifications assisted nerve repair with decellularized nerve matrix scaffolds*. Journal of tissue engineering and regenerative medicine, 2020. **14**(7): p. 931-943.
232. Zhou, C., et al., *Kidney extracellular matrix hydrogel enhances therapeutic potential of adipose-derived mesenchymal stem cells for renal ischemia reperfusion injury*. Acta biomaterialia, 2020. **115**: p. 250-263.

233. Qing, Q., et al., *Effects of hydrogen peroxide on biological characteristics and osteoinductivity of decellularized and demineralized bone matrices*. Journal of Biomedical Materials Research Part A, 2019. **107**(7): p. 1476-1490.
234. Wang, W., S. Itoh, and K. Takakuda, *Comparative study of the efficacy of decellularization treatment of allogenic and xenogeneic nerves as nerve conduits*. Journal of biomedical materials research Part A, 2016. **104**(2): p. 445-454.
235. Bombelli, S., et al., *Nephrosphere-derived cells are induced to multilineage differentiation when cultured on human decellularized kidney scaffolds*. The American journal of pathology, 2018. **188**(1): p. 184-195.
236. Belviso, I., et al., *Cardiac-derived extracellular matrix: A decellularization protocol for heart regeneration*. Plos one, 2022. **17**(10): p. e0276224.
237. Baldwin, J., et al., *In vitro pre-vascularisation of tissue-engineered constructs A co-culture perspective*. Vascular cell, 2014. **6**: p. 1-16.
238. Chen, L., et al., *Paracrine factors of mesenchymal stem cells recruit macrophages and endothelial lineage cells and enhance wound healing*. PloS one, 2008. **3**(4): p. e1886.
239. Ge, Q., et al., *VEGF secreted by mesenchymal stem cells mediates the differentiation of endothelial progenitor cells into endothelial cells via paracrine mechanisms*. Molecular medicine reports, 2018. **17**(1): p. 1667-1675.
240. Lee, D.E., N. Ayoub, and D.K. Agrawal, *Mesenchymal stem cells and cutaneous wound healing: novel methods to increase cell delivery and therapeutic efficacy*. Stem cell research & therapy, 2016. **7**(1): p. 1-8.
241. Root, L.L. and G.D. Shipley, *Human dermal fibroblasts express multiple bFGF and aFGF proteins*. In Vitro Cellular & Developmental Biology-Animal, 1991. **27**: p. 815-822.
242. Ruan, Q., et al., *Prevascularization techniques for dental pulp regeneration: potential cell sources, intercellular communication and construction strategies*. Frontiers in Bioengineering and Biotechnology, 2023. **11**: p. 1186030.
243. Nasser, M., et al., *Engineering microenvironments towards harnessing pro-angiogenic potential of mesenchymal stem cells*. Materials Science and Engineering: C, 2019. **102**: p. 75-84.
244. Beckermann, B., et al., *VEGF expression by mesenchymal stem cells contributes to angiogenesis in pancreatic carcinoma*. British journal of cancer, 2008. **99**(4): p. 622-631.
245. Bian, D., et al., *The application of mesenchymal stromal cells (MSCs) and their derivative exosome in skin wound healing: a comprehensive review*. Stem Cell Research & Therapy, 2022. **13**(1): p. 24.
246. Shi, H., et al., *bFGF promotes the migration of human dermal fibroblasts under diabetic conditions through reactive oxygen species production via the PI3K/Akt-Rac1-JNK pathways*. International Journal of Biological Sciences, 2015. **11**(7): p. 845.
247. Gomes, R.N., F. Manuel, and D.S. Nascimento, *The bright side of fibroblasts: molecular signature and regenerative cues in major organs*. NPJ Regenerative Medicine, 2021. **6**(1): p. 43.
248. Hu, B., et al., *Nucleofection with plasmid DNA for CRISPR/Cas9-mediated inactivation of programmed cell death protein 1 in CD133-specific CAR T cells*. Human gene therapy, 2019. **30**(4): p. 446-458.
249. Đorđević, M., et al., *Nucleofection as an efficient method for alpha Tc1-6 cell line transfection*. Applied Sciences, 2022. **12**(15): p. 7938.
250. Ferreira, E., et al., *Optimization of a gene electrotransfer method for mesenchymal stem cell transfection*. Gene Therapy, 2008. **15**(7): p. 537-544.
251. Peng, L., et al., *The effectiveness, cytotoxicity, and intracellular trafficking of nonviral vectors for gene delivery to bone mesenchymal stem cells*. Journal of bioactive and compatible polymers, 2013. **28**(3): p. 204-217.

252. King, W.J., et al., *Environmental parameters influence non-viral transfection of human mesenchymal stem cells for tissue engineering applications*. Cell and tissue research, 2012. **347**: p. 689-699.
253. Madeira, C., et al., *Nonviral gene delivery to mesenchymal stem cells using cationic liposomes for gene and cell therapy*. Journal of Biomedicine and Biotechnology, 2010. **2010**.
254. Wang, W., et al., *Polyethylenimine-mediated gene delivery into human bone marrow mesenchymal stem cells from patients*. Journal of cellular and molecular medicine, 2011. **15**(9): p. 1989-1998.
255. Kelly, A.M., et al., *Glucocorticoid cell priming enhances transfection outcomes in adult human mesenchymal stem cells*. Molecular Therapy, 2016. **24**(2): p. 331-341.
256. Später, T., et al., *In vivo biocompatibility, vascularization, and incorporation of Integra® dermal regenerative template and flowable wound matrix*. Journal of Biomedical Materials Research Part B: Applied Biomaterials, 2018. **106**(1): p. 52-60.
257. Thinda, S., H.V. Wright, and L.A. Mawn, *Integra bilayer matrix wound dressing closure of large periorbital traumatic wound*. Archives of Ophthalmology, 2012. **130**(2): p. 217-219.
258. Chang, D.K., et al. *The basics of integra dermal regeneration template and its expanding clinical applications*. in *Seminars in Plastic Surgery*. 2019. Thieme Medical Publishers.
259. Mangir, N.i., et al., *Using ex ovo chick chorioallantoic membrane (CAM) assay to evaluate the biocompatibility and angiogenic response to biomaterials*. ACS Biomaterials Science & Engineering, 2019. **5**(7): p. 3190-3200.
260. Janser, F.A., et al., *The Chick Chorioallantoic Membrane (CAM) assay as a three-dimensional model to study autophagy in cancer cells*. Bio-protocol, 2019. **9**(13): p. e3290-e3290.
261. Eckrich, J., et al., *Monitoring of tumor growth and vascularization with repetitive ultrasonography in the chicken chorioallantoic-membrane-assay*. Scientific reports, 2020. **10**(1): p. 1-14.
262. Power, E.A., et al., *Chorioallantoic membrane (CAM) assay to study treatment effects in diffuse intrinsic pontine glioma*. Plos one, 2022. **17**(2): p. e0263822.
263. Elberskirch, L., et al., *A HET-CAM based vascularized intestine tumor model as a screening platform for nano-formulated photosensitizers*. European Journal of Pharmaceutical Sciences, 2022. **168**: p. 106046.
264. Kunz, P., et al., *Optimization of the chicken chorioallantoic membrane assay as reliable in vivo model for the analysis of osteosarcoma*. PLoS One, 2019. **14**(4): p. e0215312.
265. Moreno-Jimenez, I., et al., *The chorioallantoic membrane (CAM) assay for the study of human bone regeneration: a refinement animal model for tissue engineering*. Sci Rep, 2016. **6**: p. 32168.
266. Ashimova, A., et al., *Cell encapsulation within alginate microcapsules: immunological challenges and outlook*. Frontiers in Bioengineering and Biotechnology, 2019. **7**: p. 380.
267. Ghidoni, I., et al., *Alginate cell encapsulation: new advances in reproduction and cartilage regenerative medicine*. Cytotechnology, 2008. **58**: p. 49-56.
268. Zimmermann, H., S.G. Shirley, and U. Zimmermann, *Alginate-based encapsulation of cells: past, present, and future*. Current diabetes reports, 2007. **7**(4): p. 314-320.
269. Kang, S.-M., et al., *Alginate microencapsulation for three-dimensional in vitro cell culture*. ACS biomaterials science & engineering, 2020. **7**(7): p. 2864-2879.
270. Tran, N.-M., et al., *Alginate hydrogel protects encapsulated hepatic HuH-7 cells against hepatitis C virus and other viral infections*. PloS one, 2014. **9**(10): p. e109969.
271. Raus, R.A., W.M.F.W. Nawawi, and R.R. Nasaruddin, *Alginate and alginate composites for biomedical applications*. Asian Journal of Pharmaceutical Sciences, 2021. **16**(3): p. 280-306.
272. Peters, M.C., et al., *Release from alginate enhances the biological activity of vascular endothelial growth factor*. Journal of Biomaterials Science, Polymer Edition, 1998. **9**(12): p. 1267-1278.

273. Song, J., et al., *Controllable release of vascular endothelial growth factor (VEGF) by wheel spinning alginate/silk fibroin fibers for wound healing*. *Materials & Design*, 2021. **212**: p. 110231.
274. Shi, M., et al., *Sustainable dual release of antibiotic and growth factor from pH-responsive uniform alginate composite microparticles to enhance wound healing*. *ACS applied materials & interfaces*, 2019. **11**(25): p. 22730-22744.
275. Grulova, I., et al., *Delivery of alginate scaffold releasing two trophic factors for spinal cord injury repair*. *Scientific reports*, 2015. **5**(1): p. 13702.
276. D'Urso, M. and N.A. Kurniawan, *Mechanical and physical regulation of fibroblast–myofibroblast transition: from cellular mechanoreponse to tissue pathology*. *Frontiers in bioengineering and biotechnology*, 2020. **8**: p. 609653.
277. Dikici, S., F. Claeysens, and S. MacNeil, *Pre-seeding of simple electrospun scaffolds with a combination of endothelial cells and fibroblasts strongly promotes angiogenesis*. *Tissue Engineering and Regenerative Medicine*, 2020. **17**: p. 445-458.
278. Sapudom, J., et al., *Collagen Fibril Orientation Instructs Fibroblast Differentiation Via Cell Contractility*. *Advanced Science*, 2023: p. 2301353.
279. Hines, P.A., et al., *The European Medicines Agency's goals for regulatory science to 2025*. *Nature reviews Drug discovery*, 2019. **18**(6): p. 403-404.
280. Hines, P.A., et al., *A future for regulatory science in the European Union: the European Medicines Agency's strategy*. *Nature Reviews Drug Discovery*, 2020. **19**(5): p. 293-294.
281. Saesen, R., et al., *Involvement of the European Medicines Agency in multi-stakeholder regulatory science research projects: experiences of staff members and project coordinators*. *Frontiers in Medicine*, 2023. **10**: p. 1181702.
282. Samura, M., et al., *Therapeutic strategies for cell-based neovascularization in critical limb ischemia*. *Journal of Translational Medicine*, 2017. **15**(1): p. 49.
283. Guerra, A., et al., *Simulation of the process of angiogenesis: quantification and assessment of vascular patterning in the chicken chorioallantoic membrane*. *Computers in Biology and Medicine*, 2021. **136**: p. 104647.
284. Maugeri, A., et al., *The chorioallantoic membrane: A novel approach to extrapolate data from a well-established method*. *Journal of Applied Toxicology*, 2022. **42**(6): p. 995-1003.
285. Miller, W.J., et al., *A novel technique for quantifying changes in vascular density, endothelial cell proliferation and protein expression in response to modulators of angiogenesis using the chick chorioallantoic membrane (CAM) assay*. *Journal of translational medicine*, 2004. **2**(1): p. 1-12.
286. Ribatti, D., et al., *Endogenous basic fibroblast growth factor is implicated in the vascularization of the chick embryo chorioallantoic membrane*. *Developmental biology*, 1995. **170**(1): p. 39-49.
287. Nurhasanah, D., et al., *Antiangiogenic Activity of n-hexane Insoluble Fraction and Its Tylophorine Component from Ficus septica Leaves in Chicken Chorioallantoic Membrane Induced by bFGF*. *Asian Pacific Journal of Cancer Prevention: APJCP*, 2023. **24**(1): p. 75.
288. Bastaki, M., et al., *Basic fibroblast growth factor–induced angiogenic phenotype in mouse endothelium: a study of aortic and microvascular endothelial cell lines*. *Arteriosclerosis, thrombosis, and vascular biology*, 1997. **17**(3): p. 454-464.
289. Crivellato, E., *The role of angiogenic growth factors in organogenesis*. *International Journal of Developmental Biology*, 2011. **55**(4-5): p. 365-375.
290. Folkman, J. *Role of angiogenesis in tumor growth and metastasis*. in *Seminars in oncology*. 2002. Elsevier.
291. Ferrara, N., *Role of vascular endothelial growth factor in the regulation of angiogenesis*. *Kidney international*, 1999. **56**(3): p. 794-814.
292. Hicklin, D.J. and L.M. Ellis, *Role of the vascular endothelial growth factor pathway in tumor growth and angiogenesis*. *Journal of clinical oncology*, 2005. **23**(5): p. 1011-1027.

293. Gopinathan, G., et al., *Interleukin-6 stimulates defective angiogenesis*. *Cancer research*, 2015. **75**(15): p. 3098-3107.
294. Shi, J. and P.K. Wei, *Interleukin-8: A potent promoter of angiogenesis in gastric cancer*. *Oncology letters*, 2016. **11**(2): p. 1043-1050.
295. Li, A., et al., *IL-8 directly enhanced endothelial cell survival, proliferation, and matrix metalloproteinases production and regulated angiogenesis*. *The Journal of Immunology*, 2003. **170**(6): p. 3369-3376.
296. Martin, T.A., *Interleukin-8 and angiogenesis*. *Growth factors and their receptors in cancer metastasis*, 2001: p. 51-65.
297. Heidemann, J., et al., *Angiogenic effects of interleukin 8 (CXCL8) in human intestinal microvascular endothelial cells are mediated by CXCR2*. *Journal of Biological Chemistry*, 2003. **278**(10): p. 8508-8515.
298. Choi, J., et al., *FGF2-primed 3D spheroids producing IL-8 promote therapeutic angiogenesis in murine hindlimb ischemia*. *NPJ Regenerative Medicine*, 2021. **6**(1): p. 48.
299. Niu, J., et al., *Monocyte chemotactic protein (MCP)-1 promotes angiogenesis via a novel transcription factor, MCP-1-induced protein (MCPIP)*. *Journal of Biological Chemistry*, 2008. **283**(21): p. 14542-14551.
300. Salcedo, R., et al., *Human endothelial cells express CCR2 and respond to MCP-1: direct role of MCP-1 in angiogenesis and tumor progression*. *Blood, The Journal of the American Society of Hematology*, 2000. **96**(1): p. 34-40.
301. Ma, J., et al., *MCP-1 mediates TGF- β -induced angiogenesis by stimulating vascular smooth muscle cell migration*. *Blood*, 2007. **109**(3): p. 987-994.
302. Singh, S., D. Anshita, and V. Ravichandiran, *MCP-1: Function, regulation, and involvement in disease*. *International immunopharmacology*, 2021. **101**: p. 107598.
303. Raica, M. and A.M. Cimpian, *Platelet-derived growth factor (PDGF)/PDGF receptors (PDGFR) axis as target for antitumor and antiangiogenic therapy*. *pharmaceuticals*, 2010. **3**(3): p. 572-599.
304. Battegay, E.J., et al., *PDGF-BB modulates endothelial proliferation and angiogenesis in vitro via PDGF beta-receptors*. *The Journal of cell biology*, 1994. **125**(4): p. 917-928.
305. Krupinski, J., et al., *A putative role for platelet-derived growth factor in angiogenesis and neuroprotection after ischemic stroke in humans*. *Stroke*, 1997. **28**(3): p. 564-573.
306. Cui, Z., et al., *Endothelial PDGF-BB/PDGFR- β signaling promotes osteoarthritis by enhancing angiogenesis-dependent abnormal subchondral bone formation*. *Bone research*, 2022. **10**(1): p. 58.
307. Clarke, J., *PDGF-BB is the key to unlocking pathological angiogenesis in OA*. *Nature Reviews Rheumatology*, 2020. **16**(6): p. 298-298.
308. Mao, Y., et al., *VEGF-A/VEGFR-2 and FGF-2/FGFR-1 but not PDGF-BB/PDGFR- β play important roles in promoting immature and inflammatory intraplaque angiogenesis*. *PLoS One*, 2018. **13**(8): p. e0201395.
309. Suffee, N., et al., *Angiogenic properties of the chemokine RANTES/CCL5*. *Biochemical Society Transactions*, 2011. **39**(6): p. 1649-1653.
310. Suffee, N., et al., *RANTES/CCL5-induced pro-angiogenic effects depend on CCR1, CCR5 and glycosaminoglycans*. *Angiogenesis*, 2012. **15**: p. 727-744.
311. Suffee, N., et al., *Pro-angiogenic effect of RANTES-loaded polysaccharide-based microparticles for a mouse ischemia therapy*. *Scientific Reports*, 2017. **7**(1): p. 13294.
312. Costanzo, L., et al., *The Biology and Function of Tissue Inhibitor of Metalloproteinase 2 in the Lungs*. *Pulmonary Medicine*, 2022. **2022**.
313. Quintero-Fabián, S., et al., *Role of matrix metalloproteinases in angiogenesis and cancer*. *Frontiers in oncology*, 2019. **9**: p. 1370.
314. Cabral-Pacheco, G.A., et al., *The roles of matrix metalloproteinases and their inhibitors in human diseases*. *International journal of molecular sciences*, 2020. **21**(24): p. 9739.

315. Löffek, S., O. Schilling, and C.-W. Franzke, *Biological role of matrix metalloproteinases: a critical balance*. European Respiratory Journal, 2011. **38**(1): p. 191-208.
316. Visse, R. and H. Nagase, *Matrix metalloproteinases and tissue inhibitors of metalloproteinases: structure, function, and biochemistry*. Circulation research, 2003. **92**(8): p. 827-839.
317. Koike, N., *The Role of Stem Cells in the Hepatobiliary System and in Cancer Development: a Surgeon's Perspective*, in *Stem Cells and Cancer in Hepatology*. 2018, Elsevier. p. 211-253.
318. Wetzelschödt, A., et al., *Human Thy-1 (CD90) on activated endothelial cells is a counterreceptor for the leukocyte integrin Mac-1 (CD11b/CD18)*. The Journal of Immunology, 2004. **172**(6): p. 3850-3859.
319. He, J., et al., *CD90 is identified as a candidate marker for cancer stem cells in primary high-grade gliomas using tissue microarrays*. Molecular & Cellular Proteomics, 2012. **11**(6).
320. Cheng, K., et al., *Relative Roles of CD 90 and c-Kit to the Regenerative Efficacy of Cardiosphere-Derived Cells in Humans and in a Mouse Model of Myocardial Infarction*. Journal of the American Heart Association, 2014. **3**(5): p. e001260.
321. Wu, L., et al., *Urinary soluble CD90 predicts renal prognosis in patients with diabetic kidney disease*. Annals of Translational Medicine, 2021. **9**(4).
322. Moraes, D.A., et al., *A reduction in CD90 (THY-1) expression results in increased differentiation of mesenchymal stromal cells*. Stem cell research & therapy, 2016. **7**: p. 1-14.
323. Wiesmann, A., et al., *Decreased CD90 expression in human mesenchymal stem cells by applying mechanical stimulation*. Head & face medicine, 2006. **2**: p. 1-6.
324. Galipeau, J., *Mesenchymal stromal cells*, in *Hematology*. 2018, Elsevier. p. 1559-1567.
325. Michelis, K.C., et al., *CD90 identifies adventitial mesenchymal progenitor cells in adult human medium-and large-sized arteries*. Stem Cell Reports, 2018. **11**(1): p. 242-257.
326. Zhang, Q., et al., *CD90 determined two subpopulations of glioma-associated mesenchymal stem cells with different roles in tumour progression*. Cell Death & Disease, 2018. **9**(11): p. 1101.
327. Moraes, D., *What the relationship between CD90 e CD44 in Mesenchymal Stem Cells?* Cytotherapy, 2018. **20**(5): p. S47.
328. Zeng, F., et al., *Role and mechanism of CD90+ fibroblasts in inflammatory diseases and malignant tumors*. Molecular Medicine, 2023. **29**(1): p. 20.
329. Jiang, D. and Y. Rinkevich, *Defining skin fibroblastic cell types beyond CD90*. Frontiers in Cell and Developmental Biology, 2018. **6**: p. 133.
330. Korosec, A., et al., *Lineage identity and location within the dermis determine the function of papillary and reticular fibroblasts in human skin*. Journal of Investigative Dermatology, 2019. **139**(2): p. 342-351.
331. Lv, F.-J., et al., *Concise review: the surface markers and identity of human mesenchymal stem cells*. Stem cells, 2014. **32**(6): p. 1408-1419.
332. Eichin, D., et al., *CD73 contributes to anti-inflammatory properties of afferent lymphatic endothelial cells in humans and mice*. European Journal of Immunology, 2021. **51**(1): p. 231-246.
333. Tang, K., et al., *Identification of CD73 as a Novel Biomarker Encompassing the Tumor Microenvironment, Prognosis, and Therapeutic Responses in Various Cancers*. Cancers, 2022. **14**(22): p. 5663.
334. Fernández, P., et al., *Extracellular generation of adenosine by the ectonucleotidases CD39 and CD73 promotes dermal fibrosis*. The American journal of pathology, 2013. **183**(6): p. 1740-1746.
335. Aoki, M., et al., *CD73 complexes with emmprin to regulate MMP-2 production from co-cultured sarcoma cells and fibroblasts*. BMC cancer, 2019. **19**(1): p. 1-13.
336. Monguió-Tortajada, M., et al., *Mesenchymal stem cells induce expression of CD73 in human monocytes in vitro and in a swine model of myocardial infarction in vivo*. Frontiers in Immunology, 2017. **8**: p. 1577.

337. Li, Q., et al., *CD73+ mesenchymal stem cells ameliorate myocardial infarction by promoting angiogenesis*. *Frontiers in Cell and Developmental Biology*, 2021. **9**: p. 637239.
338. Kimura, K., et al., *Bone marrow CD73+ mesenchymal stem cells display increased stemness in vitro and promote fracture healing in vivo*. *Bone Reports*, 2021. **15**: p. 101133.
339. Lupia, M., et al., *CD73 regulates stemness and epithelial-mesenchymal transition in ovarian cancer-initiating cells*. *Stem cell reports*, 2018. **10**(4): p. 1412-1425.
340. Suto, E.G., et al., *Advantage of fat-derived CD73 positive cells from multiple human tissues, prospective isolated mesenchymal stromal cells*. *Scientific Reports*, 2020. **10**(1): p. 15073.
341. Lin, C.-S., et al., *Commonly used mesenchymal stem cell markers and tracking labels: Limitations and challenges*. *Histology and histopathology*, 2013. **28**(9): p. 1109.
342. Anderson, P., et al., *CD105 (endoglin)-negative murine mesenchymal stromal cells define a new multipotent subpopulation with distinct differentiation and immunomodulatory capacities*. *PLoS one*, 2013. **8**(10): p. e76979.
343. Lan, T., M. Luo, and X. Wei, *Mesenchymal stem/stromal cells in cancer therapy*. *Journal of Hematology & Oncology*, 2021. **14**(1): p. 1-16.
344. Cleary, M., et al., *Expression of CD105 on expanded mesenchymal stem cells does not predict their chondrogenic potential*. *Osteoarthritis and cartilage*, 2016. **24**(5): p. 868-872.
345. Lee, S.B., et al., *Identification of a distinct subpopulation of fibroblasts from murine dermis: CD73- CD105+ as potential marker of dermal fibroblasts subset with multipotency*. *Cell biology international*, 2016. **40**(9): p. 1008-1016.
346. Chen, F., et al., *Bone morphogenetic protein 7 enhances the osteogenic differentiation of human dermal-derived CD105+ fibroblast cells through the Smad and MAPK pathways*. *International journal of molecular medicine*, 2019. **43**(1): p. 37-46.
347. Giorello, M.B., et al., *CD105 expression in cancer-associated fibroblasts: a biomarker for bone metastasis in early invasive ductal breast cancer patients*. *Frontiers in Cell and Developmental Biology*, 2023. **11**.
348. Hutton, C., et al., *Single-cell analysis defines a pancreatic fibroblast lineage that supports anti-tumor immunity*. *Cancer cell*, 2021. **39**(9): p. 1227-1244. e20.
349. Zhou, L., et al., *Role of CD44 in increasing the potency of mesenchymal stem cell extracellular vesicles by hyaluronic acid in severe pneumonia*. *Stem cell research & therapy*, 2021. **12**(1): p. 1-12.
350. Ouhtit, A., et al., *CD44 mediates stem cell mobilization to damaged lung via its novel transcriptional targets, Cortactin and Survivin*. *International journal of medical sciences*, 2020. **17**(1): p. 103.
351. Isono, M., et al., *Effect of CD44 signal axis in the gain of mesenchymal stem cell surface antigens from synovial fibroblasts in vitro*. *Heliyon*, 2022. **8**(10).
352. Govindaraju, P., et al., *CD44-dependent inflammation, fibrogenesis, and collagenolysis regulates extracellular matrix remodeling and tensile strength during cutaneous wound healing*. *Matrix Biology*, 2019. **75**: p. 314-330.
353. Wang, Y., J.A. Mack, and E.V. Maytin, *CD44 inhibits α -SMA gene expression via a novel G-actin/MRTF-mediated pathway that intersects with TGF β R/p38MAPK signaling in murine skin fibroblasts*. *Journal of Biological Chemistry*, 2019. **294**(34): p. 12779-12794.
354. Tsuneki, M. and J.A. Madri, *CD44 influences fibroblast behaviors via modulation of cell-cell and cell-matrix interactions, affecting survivin and hippo pathways*. *Journal of Cellular Physiology*, 2016. **231**(3): p. 731-743.
355. Jordan, A.R., et al., *The role of CD44 in disease pathophysiology and targeted treatment*. *Frontiers in immunology*, 2015. **6**: p. 182.
356. Kuçi, S., et al., *CD271 antigen defines a subset of multipotent stromal cells with immunosuppressive and lymphohematopoietic engraftment-promoting properties*. *haematologica*, 2010. **95**(4): p. 651.

357. Zha, K., et al., *The role of CD146 in mesenchymal stem cells*. Zhongguo xiu fu Chong Jian wai ke za zhi= Zhongguo Xiufu Chongjian Waike Zazhi= Chinese Journal of Reparative and Reconstructive Surgery, 2021. **35**(2): p. 227-233.
358. Bowles, A.C., et al., *Signature quality attributes of CD146+ mesenchymal stem/stromal cells correlate with high therapeutic and secretory potency*. Stem Cells, 2020. **38**(8): p. 1034-1049.
359. Bikorimana, J.-P., et al., *CD146 Defines a Mesenchymal Stromal Cell Subpopulation with Enhanced Suppressive Properties*. Cells, 2022. **11**(15): p. 2263.
360. Ma, L., et al., *CD146 controls the quality of clinical grade mesenchymal stem cells from human dental pulp*. Stem Cell Research & Therapy, 2021. **12**(1): p. 1-16.
361. Yang, Z.X., et al., *CD106 identifies a subpopulation of mesenchymal stem cells with unique immunomodulatory properties*. PloS one, 2013. **8**(3): p. e59354.
362. Fukiage, K., et al., *Expression of vascular cell adhesion molecule-1 indicates the differentiation potential of human bone marrow stromal cells*. Biochemical and Biophysical Research Communications, 2008. **365**(3): p. 406-412.
363. Liu, F., et al., *Changes in the expression of CD106, osteogenic genes, and transcription factors involved in the osteogenic differentiation of human bone marrow mesenchymal stem cells*. Journal of bone and mineral metabolism, 2008. **26**: p. 312-320.
364. Lu, S., et al., *CD106 is a novel mediator of bone marrow mesenchymal stem cells via NF- κ B in the bone marrow failure of acquired aplastic anemia*. Stem Cell Research & Therapy, 2017. **8**(1): p. 1-14.
365. Noronha, N.d.C., et al., *Priming approaches to improve the efficacy of mesenchymal stromal cell-based therapies*. Stem cell research & therapy, 2019. **10**(1): p. 1-21.
366. Miceli, V., et al., *Therapeutic properties of mesenchymal stromal/stem cells: the need of cell priming for cell-free therapies in regenerative medicine*. International Journal of Molecular Sciences, 2021. **22**(2): p. 763.
367. Suga, H., et al., *IFATS collection: Fibroblast growth factor-2-induced hepatocyte growth factor secretion by adipose-derived stromal cells inhibits postinjury fibrogenesis through a c-Jun N-terminal kinase-dependent mechanism*. Stem cells, 2009. **27**(1): p. 238-249.
368. Han, Y., et al., *The secretion profile of mesenchymal stem cells and potential applications in treating human diseases*. Signal Transduction and Targeted Therapy, 2022. **7**(1): p. 92.
369. Jung, J.A., et al., *Comparison of human umbilical cord blood-derived mesenchymal stem cells with healthy fibroblasts on wound-healing activity of diabetic fibroblasts*. International wound journal, 2018. **15**(1): p. 133-139.
370. Hendrawan, S., et al., *Wound healing potential of human umbilical cord mesenchymal stem cell conditioned medium: An in vitro and in vivo study in diabetes-induced rats*. Veterinary world, 2021. **14**(8): p. 2109.
371. Liu, X., et al., *Direct comparison of the potency of human mesenchymal stem cells derived from amnion tissue, bone marrow and adipose tissue at inducing dermal fibroblast responses to cutaneous wounds*. International journal of molecular medicine, 2013. **31**(2): p. 407-415.
372. Tao, H., et al., *Proangiogenic features of mesenchymal stem cells and their therapeutic applications*. Stem cells international, 2016. **2016**.